PB85-197341

REPORT NO.
UCB/EERC-84/13
AUGUST 1984

EARTHQUAKE ENGINEERING RESEARCH CENTER

EARTHQUAKE ENGINEERING RESEARCH AT BERKELEY – 1984

Papers presented by faculty participants and research personnel associated with the Earthquake Engineering Research Center at the Eighth World Conference on Earthquake Engineering, San Francisco, California, U.S.A., July 1984.

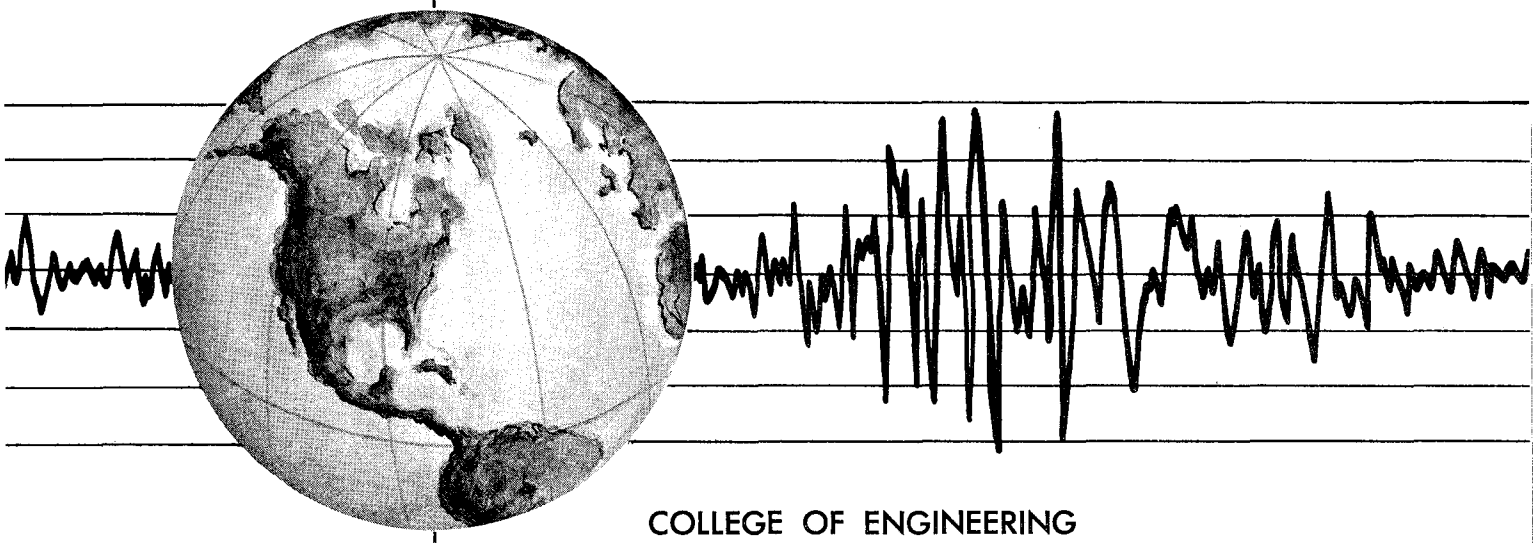

COLLEGE OF ENGINEERING

UNIVERSITY OF CALIFORNIA · Berkeley, California

REPRODUCED BY
NATIONAL TECHNICAL
INFORMATION SERVICE
U.S. DEPARTMENT OF COMMERCE
SPRINGFIELD, VA. 22161

For sale by the National Technical Information Service, U.S. Department of Commerce, Springfield, Virginia 22161.

See back of report for up to date listing of EERC reports.

DISCLAIMER

Any opinions, findings, and conclusions or recommendations expressed in this publication are those of the authors and do not necessarily reflect the views of the Sponsors or the Earthquake Engineering Research Center, University of California, Berkeley

50272-101

REPORT DOCUMENTATION PAGE	1. REPORT NO. NSF/CEE-84024	2.	3. Recipient's Accession No. PB85 197341/AS

4. Title and Subtitle
Earthquake Engineering Research at Berkeley - 1984

5. Report Date
August 1984

6.

7. Author(s)

8. Performing Organization Rept. No.
UCB/EERC-84/13

9. Performing Organization Name and Address
Earthquake Engineering Research Center
University of California, Berkeley
1301 So. 46th Street
Richmond, Calif. 94804

10. Project/Task/Work Unit No.

11. Contract(C) or Grant(G) No.
(C)
(G) CEE80-09478

12. Sponsoring Organization Name and Address
National Science Foundation
1800 G Street, N.W.
Washington, D.C. 20550

13. Type of Report & Period Covered

14.

15. Supplementary Notes

16. Abstract (Limit: 200 words)

At the Eighth World Conference on Earthquake Engineering held in San Francisco, California, U.S.A., July 21-28, 1984, twenty four papers were presented by faculty participants and research personnel associated with the Earthquake Engineering Research Center, University of California, Berkeley. The papers have been compiled in this report to illustrate some of the research work in earthquake engineering being conducted at the University of California, Berkeley. The research work described in the papers has been sponsored by the following agencies; National Science Foundation; Department of Housing and Urban Development; American Iron and Steel Institute.

17. Document Analysis a. Descriptors

b. Identifiers/Open-Ended Terms

c. COSATI Field/Group

18. Availability Statement: Release Unlimited	19. Security Class (This Report)	21. No. of Pages 211
	20. Security Class (This Page)	22. Price

(See ANSI-Z39.18) *See Instructions on Reverse*

OPTIONAL FORM 272 (4-77)
(Formerly NTIS-35)
Department of Commerce

EARTHQUAKE ENGINEERING RESEARC

EARTHQUAKE ENGINEERING RESE
AT BERKELEY - 1984

Papers presented by faculty parti
research personnel associated
Earthquake Engineering Research C
Eighth World Conference on Earthqua
San Francisco, California,
July 1984

Report No. UCB/EERC-8
College of Engineeri
University of Californi
Berkeley, Californi

7/8/1
0977167 PB83-176032
Earthquake Engineering Research - 1982
Descriptors: *Engineering; *Earthquakes; Research projects; Seismology;
Soil mechanics; Structural engineering
Identifiers: NTISNSFC
Section Headings: 8K (Earth Sciences and Oceanography--Seismology); 48
(Behavioral and Social Sciences--Administration and Management); 70
(Natural Resources and Earth Sciences--Geology and Geophysics);
(Administration and Management--Public Administration and Government)

August 1984

i.a

FOREWORD

At the Eighth World Conference on Earthquake Engineering held in San Francisco, California, U.S.A., July 21-28, 1984, twenty four papers were presented by faculty participants and research personnel associated with the Earthquake Engineering Research Center, University of California, Berkeley. The papers have been compiled in this report to illustrate some of the research work in earthquake engineering being conducted at the University of California, Berkeley. The research work described in the papers has been sponsored by the following agencies: National Science Foundation; Department of Housing and Urban Development; American Iron and Steel Institute.

TABLE OF CONTENTS

Paper No.		Page
1.	"Earthquake Response of a 1/5th-Scale Model of a 7-Story Reinforced Concrete Frame-Wall Structural System" by A. E. Aktan and V. V. Bertero.	1
2.	"Optimization-Based Computer-Aided Design of Earthquake Resistant Steel Structures" by M. A. Austin and K. S. Pister	9
3.	"Solution of the Three Dimensional Soil-Structure Interaction Problem in the Time Domain" by E. Bayo and E. L. Wilson	17
4.	"State of the Art and Practice in Seismic Resistant Design of R/C Frame-Wall Structural Systems" by V. V. Bertero.	25
5.	"The Variation of Strong Ground Motion over Short Distances" by B. A. Bolt, N. Abrahamson and Y. T. Yeh. . . .	33
6.	"Performance of School Canopies during the 10th October 1980 El-Asnam, Algeria Earthquake" by J. F. Cartin	41
7.	"Evaluation of Simplified Earthquake Analysis Procedures for Intake-Outlet Towers" by A. K. Chopra and K.-L. Fok. . .	49
8.	"Vibration Behavior of Xiang Hong Dian Dam" by R. W. Clough, K. T. Chang, R. M. Stephen, H.-Q. Chen and G. P. Lu	57
9.	"An Evaluation of the Response Spectrum Method for Lateral Analysis of Buildings" by E. Cruz and A. K. Chopra	65
10.	"Mathematical Modeling of a Frame with Joint Rotation" by J. S. Dimsdale and H. D. McNiven	73
11.	"A Mixed Finite Element Method for Dynamic Analysis of Seismically-Loaded Structures - Application to Coupled Shear Walls" by F. M. El-Kamshoshy and K. S. Pister.	81
12.	"Hysteretic Behavior of Reinforced Concrete Beams and Joints" by F. C. Filippou and E. P. Popov.	89
13.	"On Seismic Design of Eccentrically Braced Steel Frames" by K. Kasai and E. P. Popov.	97
14.	"Urban Design Vulnerability Components" by H. J. Lagorio . .	105
15.	"Identification of Wave Types, Directions, and Velocities using SMART-1 Strong Motion Array Data" by C. H. Loh and J. Penzien	113

TABLE OF CONTENTS (CONT'D)

Paper No.		Page
16.	"A Three Component Shaking Table Study of the Dynamic Response of a Single Story Masonry House" by G. C. Manos, R. W. Clough and R. L. Mayes	121
17.	"Experimental Study of a Flat-Plate Building Model" by J. P. Moehle, J. W. Diebold and H. L. Zee	129
18.	"Shaking Table Tests of Wet Jointed Precast Panel Walls" by M. G. Oliva and B. M. Shahrooz	137
19.	"Coupled Lateral-Torsional Response of Base-Isolated Structures" by T.-C. Pan and J. M. Kelly.	145
20.	"The Performance of Stairways in Earthquakes" by C. Roha. .	153
21.	"Evaluation of On-Line Computer Control Methods for Seismic Performance Testing" by P. B. Shing, S. A. Mahin and S. N. Dermitzakis	161
22.	"Determining Monetary Losses and Casualties for use in Earthquake Mitigation and Disaster Response Planning" by K. V. Steinbrugge, S. T. Algermissen and H. J. Lagorio. . .	169
23.	"Earthquake Response of Buildings on Winkler Foundation allowed to Uplift" by S. C. S. Yim and A. K. Chopra	177
24.	"Implications of Damages to the Imperial County Services Building for Earthquake-Resistant Design" by C. A. Zeris and R. Altmann.	185
List of EERC Reports.		193

EARTHQUAKE RESPONSE OF A 1/5th-SCALE MODEL OF A 7-STORY REINFORCED CONCRETE FRAME-WALL STRUCTURAL SYSTEM

A. E. Aktan (I)
V. V. Bertero (II)
Presenting Author: A. E. Aktan

SUMMARY

A 1/5th-scale model of a seven-story frame-wall structure was fabricated and tested on the earthquake simulator at the University of California, Berkeley. The experimental responses and associated studies led to assessments regarding significant inadequacies of the states-of-the-art of experimental and analytical response prediction, as well as an understanding of serviceability and ultimate limit state response characteristics of a conceptually designed, detailed, and well-constructed frame-wall structure. Significant overstrengths over the code-specified values of base shear and overturning moment were observed. Because of the low levels of axial and shear stress in all the critical regions of the structure at all limit states, the response was of a desirable nature.

INTRODUCTION

The U.S.-Japan Cooperative Research Program (Ref. 1) includes the construction and pseudo-dynamic testing (Ref. 2) of a full-scale seven-story reinforced concrete frame-wall structure in Japan, fabrication and testing, on the earthquake simulator, of a 1/5th-scale replica at the University of California, Berkeley (Ref. 3) as well as other experimental and analytical investigations related to the seven-story structure in collaborating institutions in the United States and Japan.

The seven-story test structure (Fig. 1) was selected to reflect good (conceptual) design, and to be tested along only one horizontal direction with fixed-base conditions. Its proportioning and reinforcement detailing led to low levels of axial and shear stress. Hence, favorable response characteristics were expected although the design did not strictly satisfy the Uniform Building Code (UBC) mainly because the boundary elements of the main wall did not possess as much flexural reinforcement as required by this code (Ref. 4).

The objectives of this paper are: (1) to describe the design, fabrication, instrumentation, and earthquake simulator testing of the 1/5th-scale model; (2) to discuss the degree of correlation obtained between the experimental responses of the full- and 1/5th-scale models; (3) to assess the state-of-the-art of experimental analyses of the response of reinforced concrete structures to earthquakes; and (4) to discuss the implications of the earthquake response characteristics of the model regarding the state-of-the-practice in seismic design of reinforced concrete frame-wall structures.

DESIGN, FABRICATION, AND INSTRUMENTATION OF 1/5th-SCALE MODEL

The model scale of 1 to 5 was selected in accordance with the capabilities of the earthquake simulator and in order to be able to excite an undistorted direct model to its collapse limit state (Ref. 3). In design and fabrication it was intended to have true simulation of: (1) the geometry; (2) the stress-strain relationship for constitutive materials; (3) reactive mass and gravity force; and (4) initial and boundary conditions (Ref. 3 & 5).

Geometric Similitude. This was satisfied by attaining in the 1/5th scale a geometric replica of the full-scale superstructure to within a 0.06 in. (1.5 mm) tolerance. Each reinforcing bar was also modeled individually, satisfying similitude in cross-sectional area as well as surface characteristics of the bar.

Similitude in the Mechanical Characteristics of the Model Materials. This condition required that the stress-strain constitutive relations of the constituent model materials be identical to

(I) Associate Research Engineer, University of California, Berkeley
(II) Professor of Civil Engineering, University of California, Berkeley

their counterparts in the prototype. This requirement proved to be exceptionally difficult to satisfy throughout the complete spectrum of stress and strain levels, histories, states, gradients, and rates that were expected to occur throughout the structure. Analyses were conducted to identify the critical regions of the structure and the material stress-strain characteristics which particularly affected the response of critical regions. The first story of the main wall and end regions of the frame beams were found to be critical regions of the structure, and similitude in the stress-strain responses of the main flexural reinforcement at these regions was predicted to be exceptionally important in order to minimize distortions in modeling for the ultimate limit states. The stress-strain characteristics of concrete, particularly under plane stress conditions in the panel of the wall, were expected to control the serviceability and initial damageability responses of the structure.

The correlation between the stress-strain characteristics of the full-scale and model wall flexural reinforcement is illustrated in Fig. 2. Heat treatments of the model reinforcement led to the observed level of similitude (Ref. 5). Response characteristics of reinforcing steel under inelastic strain reversals could not be incorporated in the studies.

The full-scale concrete was modeled by microconcrete, which was designed to attain similitude between uniaxial compressive stress-strain relations measured from cylinder tests. The microconcrete stress-strain characteristics changed significantly with age and this led to a poor correlation between stress-strain characteristics of the full-scale and microconcretes (Fig. 3.) at the time of testing. The tensile strength of the microconcrete was also twice that of the full-scale concrete. The use of microconcrete in the fabrication of a complete model of the size involved in this study to achieve a desirable level of similitude between the general constitutive relations of this material and full-scale concrete proved to be a difficult task if at all possible (Ref. 5). In fact, the state-of-the-art of the experimental evaluation of general constitutive relations and failure criteria of concrete was found to be inadequate to verify similitude between the stress-strain responses of the two concretes.

The bond characteristics of the model reinforcement and concrete were tested and observed to be superior to the corresponding characteristics of the full-scale materials.

Similitude in Reactive Mass and Gravity Forces. This similitude requirement was satisfied by complementing the weight of the model by lead ballast distributed at each floor (Ref. 3). The model time scale was compressed by the square root of five for acceleration similitude.

Similitude in Boundary and Initial Conditions. This was considered during design and fabrication of the model. The foundations of both models were adequately rigid and were constrained to represent fixed-base conditions. The initial mechanical characteristics of both models were measured and were similar (Ref. 3). The initial forces in the models were different, however, the difference caused by volumetric change characteristic of full-scale and microconcretes (Ref. 3).

Similitude in Loading. Despite efforts to minimize the distortions in experimental analysis, the different loading procedures used for the two models led to considerable differences in their loading rate and history. Furthermore, the strain gradient in the 1/5th-scale model was normally five times larger than in the full-scale, and this introduced an inherent distortion in experimental analysis since strain gradient is known to affect the inelastic response of reinforced concrete significantly.

Instrumentation. The model was instrumented by weldable strain gages installed on the reinforcement, paper gages installed on the concrete, and by displacement transducers and accelerometers, to measure global accelerations and displacements, and local distortions and strains. At the midheight of the first-story columns, special force transducers were inserted to monitor the internal force responses. In this manner, the distribution of internal forces at the first story could be measured. Figure 4 shows the model on the earthquake simulator during testing.

EARTHQUAKE SIMULATOR TESTS

In the earthquake simulator test program (Ref. 6) the model was successively excited to its serviceability and damageability limit states. Two input signals were used. These were modified versions of ground accelerations recorded at Miyagi-Ken-Oki (MO), Japan in 1978 and at Taft (T), California in 1952. The modifications (mainly filtering of the high-frequency components) were made to make these records suitable for pseudo-dynamic testing of the full-scale structure. The same records were used as source inputs by institutions participating in the cooperative research program. The pseudo-velocity response spectra corresponding to these two records, obtained after the time scales were compressed by $\sqrt{5}$ and the peak accelerations scaled to 0.28g, are compared in Fig. 5 for a damping coefficient of 0.05.

A total of sixty-two tests was conducted on the earthquake simulator. The initial forty-two tests were diagnostic, including harmonic motions as well as free vibration tests, in addition to low-level serviceability excitations. During ten subsequent tests, the model was excited to progressively higher levels of damage until a complete flexural failure occurred at the base of the main wall. Ten further tests were conducted on the model after the damaged base region of the wall had been repaired.

A brief summary of the test results is provided in Table 1 in which some of the significant global responses of the model during selected tests are listed. These tests included four conducted with the MO signal with peak accelerations of 9.7, 14.7, 24.7, and 28.3 percent of g, respectively, followed by two tests conducted with the T signal with 39.6 and 46.3 percent of g peak acceleration. Tests MO14.7 to T39.6 (rows 2 through 5, Table 1) were conducted in succession, and constitute the damageability level tests conducted after the seviceability excitations. Service level tests are represented in Table 1 by the MO9.7 (row 1) test. The wall was repaired after the T39.6 (row 5) test. The T46.3 test (row 6) was the final test of the program, leading to the highest level of distortion and damage.

The base shear-roof drift dynamic response envelope attained for the 1/5th-scale model is shown in Fig. 6 and is compared with the response envelope for the full-scale model (Ref. 7) and the minimum stiffness and strength required by the 1979 UBC Code, and ATC 3-06 Tentative Provisions, for the structure. The crack patterns observed in the wall-frames of both models after testing are shown in Fig. 7. The comparison between the responses of the two models will be discussed subsequently.

IMPLICATIONS OF RESULTS: STATE OF THE PRACTICE

Based on the information provided in Table 1 and Figs. 6 and 7 and the observed earthquake response characteristics of the model, the following observations can be made regarding the state-of-the-practice of seismic design of reinforced concrete frame-wall structures:

(1) The model exhibited excellent response characteristics. Its stiffness, strength, and capacity to dissipate energy exceeded the minimum requirements of the 1979 UBC or ATC 3-06 provisions by several times. It maintained its shear and overturning strength at roof drift levels exceeding 1.8% (the maximum interstory drift was 2.4% at the first story). Its energy dissipation capacity was maintained after over 50 cycles of full displacement reversals. It did not exhibit any appreciable nonrecoverable deformation and was appraised as reparable at the end of the test program. Its seismic performance was appraised to have exceeded the performance criteria of both the 1979 UBC and the ATC 3-06.

(2) The excellent response characteristics of the structure were attained through conceptual design. The layout of the structure in plan was symmetric, the wall was restrained by an outriggering system of frames in both main directions, and the wall was continuous in elevation. The intensity of the shear and axial stresses at the critical regions, mainly at the beam end regions and the first story of the wall, were controlled by proper proportioning and reinforcement detailing. The shear stress at first flexural yielding of the wall was only $3.60\sqrt{f'_c(psi)}$ and the axial force was only 12% of the force at balanced conditions. All framing elements were detailed to provide large deformability. The proportioning and reinforcement detailing of

the frames and wall led to a proper balance in the stiffness and strength of these components, such that when the wall resistance began to decrease and its stiffness to deteriorate at drift levels exceeding 1%, the frame strength and stiffness were adequate to sustain the overall stiffness, strength, and energy dissipation of the structure through higher drift levels.

(3) The outriggering system of the frame (including the transverse frames) and the diaphragm (R/C slab) were observed to provide significant energy dissipation after complete yielding of the wall at the base, and after it exhibited a rocking mode of response. The outriggering system also restrained the axial growth of the wall, and the compression induced in the wall due to this restraint enhanced and sustained its shear strength even after extensive yielding and damage at its base.

(4) The structure did not conform to the 1979 UBC mainly because the wall flexural reinforcement was considerably less than that demanded by the code. Providing the amount of reinforcement which was required by the code, however, would have increased the shear stress associated with the yielding of the wall and the response might not have been in accordance with the performance criteria envisioned by the code.

(5) The span lengths and height of the structure were such that the minimum stiffness and strength requirements of the 1979 UBC could have been satisfied by only the frame obtained by deleting the panel of the wall, rather than by the frame-wall system. Such a frame, however, would not have had the superior nonstructural damage resistance of the frame-wall system. Furthermore, analyses indicated that due to the very significant contribution of the slab reinforcement to the negative beam end moments, only a partial mechanism was likely to occur at the ultimate limit state if the structure was constructed as a frame without the wall, which would have significantly impaired its energy dissipation capacity.

PSEUDO-DYNAMIC RESPONSES OF FULL-SCALE STRUCTURE

The full-scale structure was tested in Japan by a pseudo-dynamic technique, maintaining a triangular force distribution along the structure and representing the structure as a single-degree-of-freedom system in the analytical idealization for computer control purposes. The test program is summarized in Table 2 (Ref. 7) and the base shear-roof drift envelope response is shown in Fig. 6. The crack pattern of the wall-frame is observed in Fig. 7 (Ref. 7). Based on comparisons between the crack patterns and response envelopes of the 1/5th-scale and full-scale models, the following observations pertaining to the similitude of response are made:

(1) The crack patterns and resulting damage mechanisms of the two models differed considerably. Cracks were fewer and relative crack widths were wider in the 1/5th-scale model (Fig. 7). In the 1/5th-scale model only the first story of the wall was cracked during the tests and the main damage and failure mechanisms were concentrated at the crack that developed at the interface of the wall and the foundation, while no such damage was apparent in the full-scale model. The difference in the crack and damage patterns was assessed to have been caused by the higher concrete tensile strength (twice), higher strain gradient (five times), and higher strain rate (over 13000 times) in the 1/5th-scale model (Ref. 5) and this result was despite the better bond characteristics of materials in the smaller model.

(2) Although the initial mechanical characteristics of the two models were similar (the initial frequencies of the 1/5th-scale and full-scale models were 2.1 Hz and 2.3 Hz, respectively, in real time), after cracking had begun in the full-scale model it was observed to lose a progressively higher portion of its stiffness than the 1/5th-scale model such that the maximum force resisted by the full-scale model was relatively only 73% of the force resisted by the 1/5th-scale model. The significantly higher reduction in the stiffness of the full-scale model was despite the considerably lesser number of displacement reversals and energy dissipation demands imposed on this structure: the full-scale structure was subjected to the equivalent of a total of 17.8 secs. of base excitation during the PSD-2 to PSD-4 tests (Fig. 6) while the 1/5th-scale model was subjected to an equivalent of approximately 180 secs. of excitation with amplitudes comparable to PSD-2 and PSD-4.

(3) The reasons for the lack of correlation in the envelope responses were: (a) The cracking and damage mechanisms differed, the reasons for which are discussed above; (b) The yield and ultimate strengths of the main reinforcement in the two models differed. Although the coupon test strength characteristics of the prototype and model reinforcement were generally similar, the hyper-, or statistical, strength of the model reinforcement was considerably higher than that of the corresponding prototype reinforcement. The strengths of concrete and steel were expected to increase further in the 1/5th-scale model due to the strain-rate effects; (c) The full-scale model was loaded under an inverted triangular force distribution which maintained a constant ratio of overturning moment to shear at the base. In the dynamic testing of the 1/5th-scale model, the base shear associated with the maximum overturning moment and the base overturning moment associated with the maximum base shear demand were less than those which would have occurred under the inverted triangular loading.

CONCLUSIONS

Two primary conclusions in addition to those specific points reached in the previous discussion are: (1) The state-of-the-practice (codes) of seismic resistant design of medium-rise buildings should be improved by emphasizing conceptual design. By limiting the levels of shear stress and axial stress at the critical regions of the structure through proper proportioning and detailing of reinforcement in addition to the selection of the structural system based on conceptual principles, designs capable of excellent seismic performance can be realized, even though these designs may not conform in some respects to present code requirements; (2) For a reliable experimental analysis of the earthquake response of reinforced concrete buildings, the complete structure rather than its components should be considered and similitude of: geometry; all relevant mechanical characteristics of materials in critical regions; gravity forces as well as initial stress and boundary conditions; and loading (rate and history) conditions is necessary. The pseudo-dynamic test procedure was assessed to be limited in its usefulness due to the significance of strain rate in the behavior of reinforced concrete. To incorporate the actual three-dimensional nature of earthquake motions and structural response in testing, as well as the realistic simulation of structure-foundation-soil interaction, was observed to be necessary if the state-of-the-art of experimental analysis is to be improved.

ACKNOWLEDGMENTS

The research was supported by the National Science Foundation, Grant Number CEE-8009478. The contributions of Messrs. F. A. Charney, R. Sause, A. A. Chowdhury, T. Nagashima, and D. Clyde are deeply appreciated. Illustrations by Richard Steele

REFERENCES

(1) U.S.-Japan Planning Group, Cooperative Research Program Utilizing Large-Scale Testing Facilities, "Recommendations for a U.S.-Japan Cooperative Research Program Utilizing Large-Scale Testing Facilities," *Report No. UCB/EERC-79/26*, Earthquake Engrg. Res. Ctr., Univ. of Calif., Berkeley (1979).

(2) S. Okamoto, "Characteristics of BRI Facilities," *Proceedings*, First Joint Technical Coordinating Committee Meeting, U.S.-Japan Cooperative Research Program, BRI, Tsukuba, Japan (1981).

(3) A. E. Aktan *et al.*, "Experimental and Analytical Predictions of the Mechanical Characteristics of a 7-Story 1/5 Scale Model R/C Frame-Wall Building Structure," *Report No. UCB/EERC-83/13*, Earthquake Engrg. Res. Ctr., Univ. of Calif., Berkeley (1983).

(4) F. A. Charney and V. V. Bertero, "An Evaluation of the Design and Analytical Seismic Response of a Seven-Story Reinforced Concrete Frame-Wall Structure," *Report No. UCB/EERC-82/08*, Earthquake Engrg. Res. Ctr., Univ. of Calif., Berkeley (1982).

(5) V. V. Bertero *et al.*, "Mechanical Characteristics of Materials Used in a 1/5 Scale Model of a 7-Story Reinforced Concrete Test Structure," *Report No. UCB/EERC-83/21*, Earthquake Engrg. Res. Ctr., Univ. of Calif., Berkeley (1983).

(6) V. V. Bertero *et al.*, "Earthquake Simulator Tests and Associated Experimental, Analytical and Correlation Studies of 1/5 Scale Model," paper to be published in a Special Publication by ACI on the U.S.-Japan Joint Cooperative Earthquake Research Program.

(7) S. Okamoto *et al.*, "A Progress Report on the Full-Scale Seismic Experiment of a Seven Story Reinforced Concrete Building—Part of the U.S.-Japan Cooperative Program," *Proceedings,* Third Joint Technical Committee Meeting, U.S.-Japan Cooperative Research Program, BRI, Tsukuba, Japan (1982).

TABLE 1 SUMMARY OF EARTHQUAKE SIMULATOR TEST RESULTS ON 1/5th-SCALE MODEL

ROW	TEST	INPUT SIGNAL* AND PEAK ACCELERATION	FREQUENCY** AND DAMPING		MAXIMUM ROOF DRIFT % H	MAXIMUM FORCE RESPONSE			
						MAX. SHEAR % W		MAX. OVM % WH	
			Before	After		Struc.	Wall	Struc.	Wall
1	MO 9.7	Miyagi-Oki 9.7%g	4.75 Hz 1.44%	--	0.09	17.5	14.0	11.5	6.4
2	MO 14.7	Miyagi-Oki 14.7%g	3.41 Hz 3.70%	--	0.20	27.3	21.0	18.2	8.8
3	MO 24.7	Miyagi-Oki 24.7%g	--	2.63 Hz 6.90%	0.61	41.7	29.6	27.1	11.5
4	MO 28.3	Miyagi-Oki 28.3%g	2.63 Hz 6.90%	2.50 Hz 7.50%	0.93	46.8	31.4	30.9	11.5
5	T 39.6	Taft 39.6%g	2.56 Hz 7.50%	2.33 Hz 7.70%	1.47	50.8	33.7	33.7	9.0
6	T 46.3	Taft 46.3%g	1.96 Hz 8.30%	--	1.83	47.8	28.4	30.5	6.7

* The durations of the Miyagi-Oki and Taft input signals were 45 and 30 sec. of real time.

** As obtained from free-vibration test; to convert to full-scale, multiply by $\sqrt{5}$.

TABLE 2 SUMMARY OF FULL-SCALE MODEL RESPONSES

ROW	TEST	INPUT	FREQ. & DAMPING*		MAXIMUM RESPONSE		
			Before Test	After Test	Roof Drift % H	Base Shear % W	OVM % WH
1	PSD-1	Miyagi-Oki 1.3 sec. 2.4%g	2.33 Hz 2.1%	2.33 Hz	0.01	2.67	1.78
2	PSD-2	Miyagi-Oki 1.3 sec. 10.7%g	2.33 Hz	1.82 Hz	0.15	19.14	12.76
3	PSD-3	Taft 10 sec. 32.7%g	1.82 Hz	0.86 Hz	1.10	34.81	23.21
4	PSD-4	Hachinohe 6.5 sec. 35.7%g	0.86 Hz	0.68Hz 2.5%	1.56	37.18	24.79

* As obtained from free-vibration tests.

Nomenclature: H and W are height and weight of the superstructure; OVM is base overturning moment.

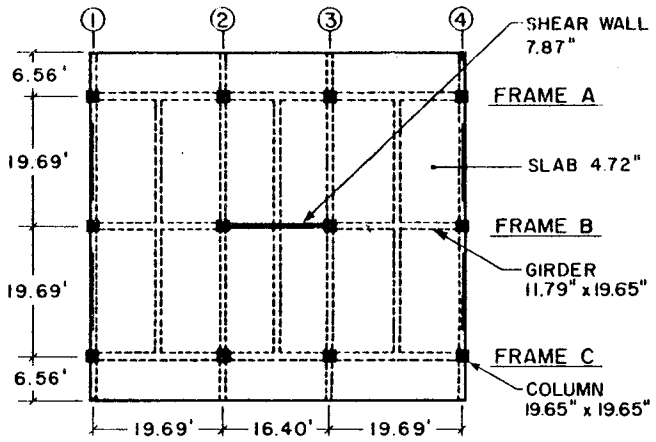

(a) PLAN OF PROTOTYPE

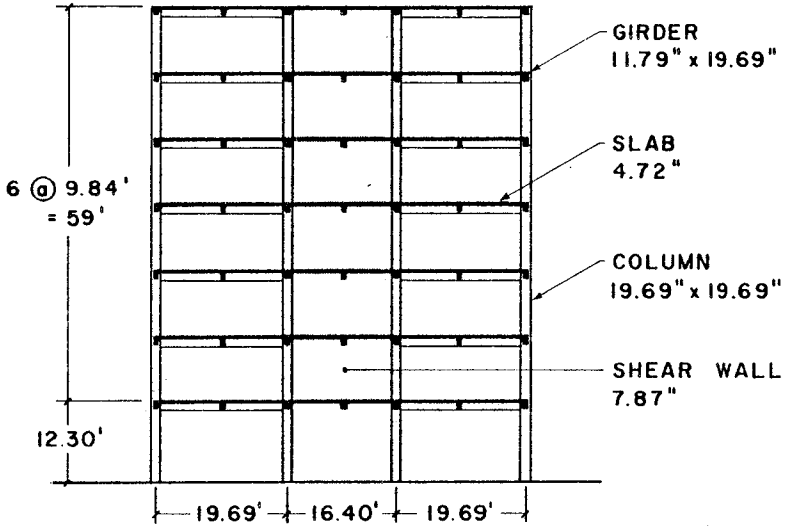

(b) SECTION OF PROTOTYPE

FIG. 1 PLAN & FRAME B OF TEST BUILDING

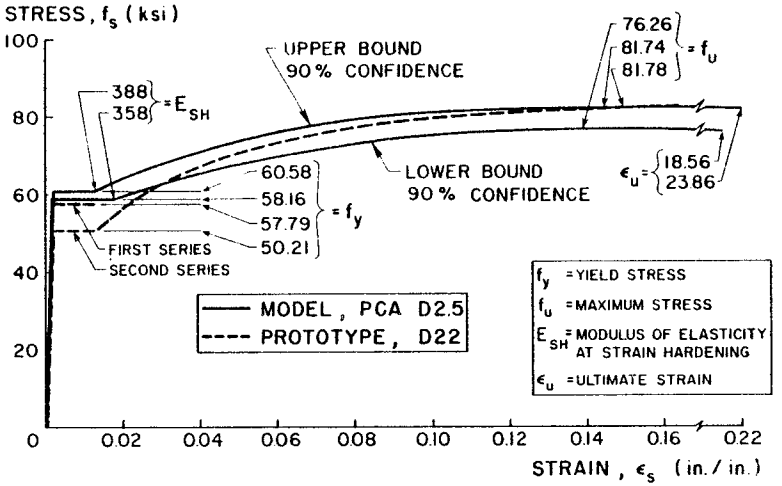

FIG. 2 STRESS-STRAIN RELATIONS FOR COLUMN REINFORCEMENT

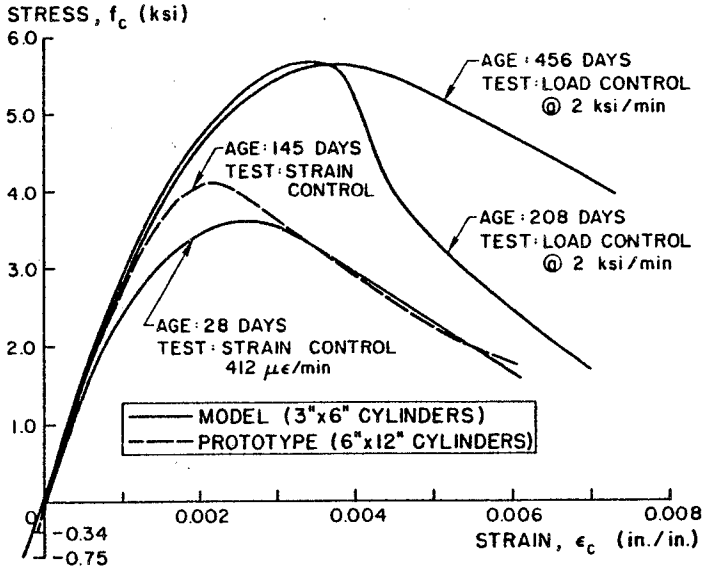

FIG. 3 STRESS-STRAIN RELATIONS OF CONCRETE IN 1st STORY OF 1/5th & FULL-SCALE MODELS

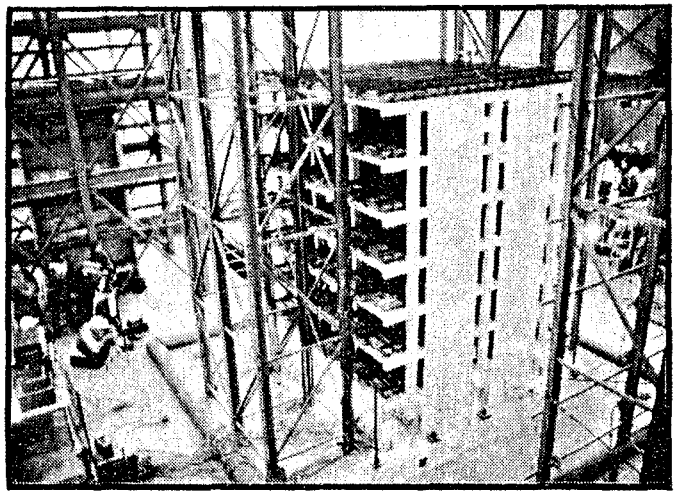

FIG. 4 1/5th SCALE MODEL DURING TESTING

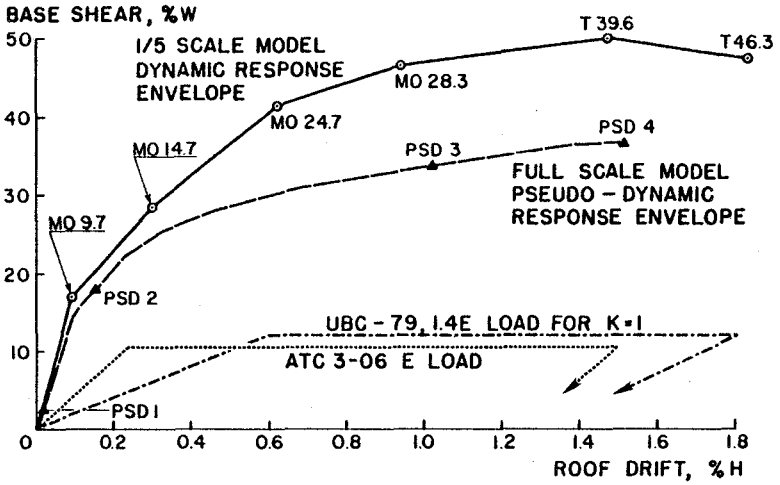

FIG. 6 BASE SHEAR-ROOF DRIFT RESPONSE ENVELOPES FOR MODELS & MINIMUM STIFFNESS & STRENGTH REQUIREMENTS OF DESIGN DOCUMENTS

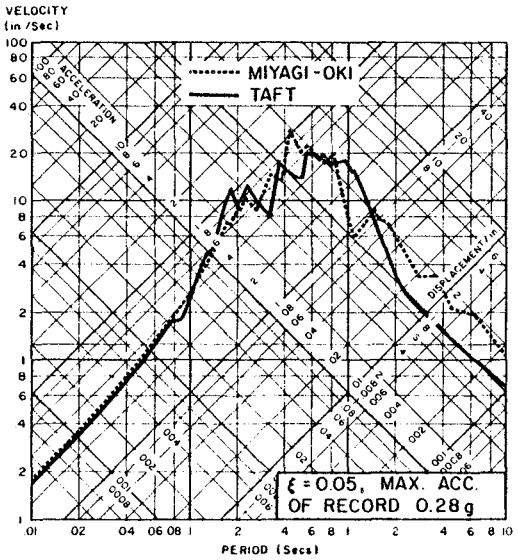

FIG. 5 RESPONSE SPECTRA FOR MODIFIED & FILTERED TAFT & MIYAGI-OKI RECORDS

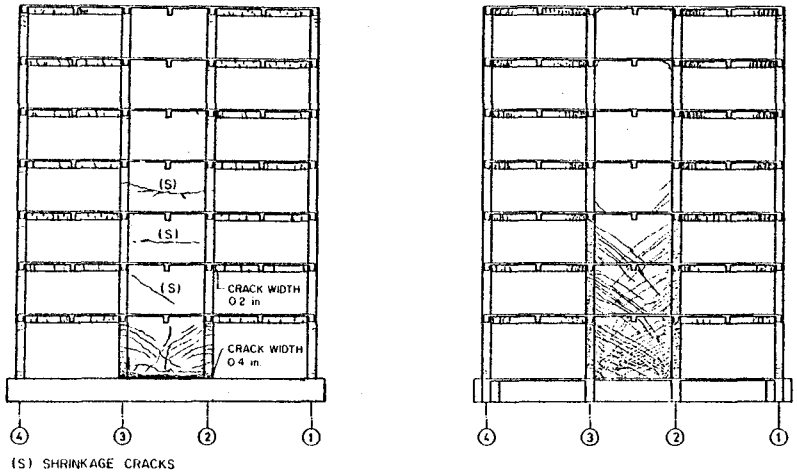

(a) 1/5th SCALE MODEL AFTER T 39.6; 1.47% ROOF DRIFT

(b) FULL-SCALE MODEL AFTER PSD-4; 1.56% ROOF DRIFT

FIG. 7 CRACK PATTERNS OF 1/5th & FULL-SCALE MODELS

OPTIMIZATION-BASED COMPUTER-AIDED DESIGN OF EARTHQUAKE RESISTANT STEEL STRUCTURES

Mark A. Austin(I)
Karl S. Pister(II)
Presenting Author: Mark A. Austin

SUMMARY

This paper describes steps and options available for casting a practical design problem into a mathematical format for the optimization-based, computer-aided design of earthquake resistant steel structures. A critical review of the present DELIGHT.STRUCT system is made, and identification of its favorable attributes and shortcomings is given. Finally, a summary of current and anticipated development at the University of California, Berkeley is presented.

INTRODUCTION

Optimization-based computer-aided structural design may be viewed as a two-stage process. First, a designer has to deal with the conceptual task of recasting a structural design problem into a mathematical formulation that captures its practical nature. A suitable solution procedure is then employed to solve the optimization problem.

While wide attention has been given to the latter stage, less effort has been expended in the area of problem formulation. Thus, the purpose of this paper is to review the mathematical formulation procedure utilized in DELIGHT.STRUCT(Refs. 3,7,8) and its predecessors(Refs. 4,5,6) for the aseismic design of planar steel frames. Experience gained to date has been via investigations of the seismic behavior of moment-resistant (elastic, localized nonlinearities and general nonlinear), base isolated, and friction-braced frames(Refs. 4,5,6,7,8).

BACKGROUND TO DELIGHT AND DELIGHT.STRUCT

DELIGHT is an interactive computer system that was developed to provide engineers from various disciplines with a working environment in which optimization techniques could be applied to engineering design. Its extensive capabilities are outlined in reference 1. DELIGHT.STRUCT is a union of the DELIGHT system and an optimal structural design package called STRUCT. It is capable of dealing with statically and dynamically loaded structures whose response may be linear or nonlinear(Ref. 3).

(I) Graduate Student, University of California, Berkeley, Ca 94720, USA.
(II) Professor of Engineering Science, University of California, Berkeley, Ca 94720, USA.

DESIGN PHILOSOPHY AND METHOD

Currently accepted seismic design philosophy has been well documented(Ref. 2). The limit states design method is particularly amenable to the methodology of an automated design system because it forces the designer to start by identifying all the ways in which a structure may fail to fulfill its intended purpose. Determination of acceptable levels of safety against violation of each limit state is then estimated before a designer proceeds to work through a design in a step-by-step manner until all the aforementioned requirements have been satisfied.

Optimization-based design requires the extra step of recasting the limit states and design objectives into a mathematical statement. By allowing the computer to take care of the subsequent calculations, the designer should be freed to concentrate on the more creative aspects of the design problem. Hence, for example, during convergence to a satisfactory solution, the designer may either interactively complement these calculations with his/her intuitive knowledge or allow automatic information feedback via the optimization algorithm. A balance in use of these two options will in practice be most efficient in leading to a good design.

FORMULATION OF THE OPTIMIZATION PROBLEM

Once a designer has a clear understanding of the design problem he or she can proceed to list mathematical statements for the design objectives and constraints. An optimization algorithm is then specified to solve the mathematical design problem. During the optimization process, the algorithm will call on a simulator to evaluate the cost function and constraint performances. The following sections briefly describe these stages when the process is applied to the aseismic design of steel frames.

Limit States.

Constraints are divided into three general classes of limit states: serviceability, damageability and ultimate strength. Recommendations from the Uniform Building Code(Ref. 10) have been used to set the constraint boundaries so that final designs contain an acceptable level of safety.

Serviceability.

This limit state corresponds to the frame's response to dead and live service loading. In summary:

| column end moments | < 0.6 * column yield moments.
| column axial force | < 0.5 * axial yield or buckling force.
| girder end moments | < 0.6 * girder yield moments.
| girder midspan deflection under live load | < [1/240] * span.
| brace force | < 0.5 * brace yield or buckling force.

Damageability.

This limit state is associated with the frame's response to combined dead plus live gravity loads in addition to a scaled earthquake ground motion of

intensity equivalent to that expected to occur several times during the structure's lifetime. Damage is defined as element yielding. The functional constraints on element response are:

max over time ¦ column end moments ¦ < column yield moments.
max over time ¦ girder end moments ¦ < girder yield moments.
max over time ¦ shear element force ¦ < shear yield force.
max over time ¦ dissipator force ¦ < dissipator yield force.
max over time ¦ brace force ¦ < brace yield or buckling force.

Moreover, non-structural damage should be limited. As this will be related to interstory drifts and floor accelerations, the following two functional constraints are also enforced.

max over time ¦ absolute floor accel ¦ < 0.5 * gravity accel.
max over time ¦ story drift ¦ < 1/200.

Ultimate Strength.

The design philosophy adopted accepts major structural damage possibly beyond repair in the event of a severe earthquake. Collapse is nevertheless prohibited. Large displacements at the top of the frame are used as a measure of the possibility of collapse. Thus, "Sway", defined as the maximum relative horizontal displacement at the top of the frame divided by the frame height, is limited as follows:

max over time ¦ frame sway ¦ < Sway.

This parameter has been set to 0.01. Structural damage will also be closely related to the amount of inelastic deformation. A single cycle at a high ductility range may cause damage equivalent to that of many cycles at a lower ductility range. The following constraint on inelastic energy dissipation under monotonic loading has been adopted(Ref. 7):

$$Ed < Ey * [mu - 1] * [1-S] * [2 + S*[mu - 1]]$$

where Ed = inelastic dissipated energy, Ey = elastic strain energy at yield, mu = allowable ductility factor and S = strain hardening ratio. The beam and column ductility factors have been set to 6 and 3, respectively, and the strain hardening ratio has been assumed to be 0.05.

Objective Functions.

The objective function has been considered to be the weighted sum of the following terms reflecting performance and cost:

1 Volume of structural elements.
2 Moderate earthquake : Sum of squares of minimum story drifts.
3 Severe earthquake : Input energy at frame base.
4 Severe earthquake : Inelastically dissipated energy.
5 Severe earthquake : Energy dissipated by the columns.

Algorithms.

The DELIGHT environment supports optimization algorithms capable of solving linear and nonlinear constrained and unconstrained problems. The main objections in using unconstrained methods for engineering and related problems are well outlined in Nye(Ref. 1). Consequently, the combined Phase I - Phase II method of feasible directions due to Polak et al.(Ref. 11) has recently been used. Although this algorithm may only be expected to converge linearly to a local minimum, it does guarantee an improved design with each iteration. A further strength lies in its ability to accommodate conventional (time independent) functional (time dependent) and box (restrictions on the maximum and minimum allowable section sizes) constraints.

Constraint Evaluation.

The ANSR(Ref. 12) structural simulator has been used to supply response values to software routines for constraint evaluation. Frames are modelled as 2-dimensional and the basic ANSR element types available include beam, column, and truss member behavior. Empirical relations(Ref. 7) may be utilized to extend this range to model shear-beams, natural rubber support bearings and special energy absorbing devices.

Modelling features.

The capabilities of DELIGHT.STRUCT allow elements to be subjectively grouped so that they possess equal properties. Repetition of elements is related to economical construction. Furthermore, the calculation required at each iteration in the feasible directions algorithm will be approximately proportional to the total number of design variables, because partial derivatives of active nonlinear constraints are presently calculated with a forward finite difference scheme. However, section sizes chosen within each group will be bounded by the most critical constraint within the group. Hence, grouping should retain flexibility in the optimal design while simultaneously keeping the problem practical in terms of element repetition and required calculation. The optimization problem is further simplified by reducing the number of unknowns in each element to a single variable. For example, the section moment of inertia is chosen as the primary unknown for beam and column elements. Parameters of secondary importance such as cross sectional area and radius of gyration are obtained from Walker's empirical relationships for wide flange steel sections(Ref. 9).

IDENTIFICATION OF PROBLEM AREAS

The following list summarizes the authors' opinions of attributes and shortcomings of the present system.

a) Although the method of feasible directions assures an improved design with each iteration, the algorithm cannot guarantee convergence to a global minimum. It is therefore essential that the designer be prepared to find a starting design that is close to the anticipated optimal design. Nevertheless, interactive repositioning of the design vector may still be necessary to get the required convergence. Furthermore, the designer should not always expect a substantial improvement in the cost function. Rather, with a good initial design a small improvement may be obtained with, for example, a redistribution of element sizes.

b) Coefficients in the weighted-sum objective function have to be chosen so the final combination reflects a balance in tradeoffs among competing structural performance attributes. Their optimal choice is a major task in itself and is still a subjective decision. Moreover, this approach retains the limitation of hiding the changing importance of each term's contribution to the overall cost as one proceeds through the design process. Consequently, only single term objective functions have been considered to date.

c) When the optimization problem has been formulated, the earthquake loading input and structural modelling parameters are the components of the problem subject to the most uncertainty. The present environment uses a single scaled earthquake record for both the damageability and ultimate strength limit states. Guidelines suggest that the frequency content of the single record should be representative of an ensemble of such records expected to occur at a site. The record should neither contain localized frequency bands of low amplitude motion or envelope all peak response values in the ensemble(Ref. 14).

d) The ANSR simulator uses Rayleigh damping to model a phenomenon that still isn't well understood. Viscous damping is assumed in the elastic range. The nonlinear analyses employ a combination of viscous plus hysteretic damping. Calculations so far indicate that constraint performance is sensitive to the choice of specified damping ratio.

e) In reality, the effect of a single constraint's failure on the overall integrity of a structure will be related to both the constraint's type and coupling to other constraint performances. Even for small frames, this relationship may be extremely complex and probably will never be completely understood. Mahin and Bertero(Ref. 13) also indicate that while peak story drift and floor acceleration frame response parameters are commonly used as an approximate measure of non-structural damage in frames for which non-structural components are not expected to significantly contribute to the response, there is in fact very little reliable data available to make such interpretations more than qualitative. In specifying the boundary between satisfactory and unsatisfactory constraint performance, the designer will be guided by code clauses and technical references for some constraints, and his or her intuition for others. Moreover, designers commonly assert that they cannot express everything they know about a good design in a mathematical formulation. On the basis of these comments and observations of missing information, modelling deficiences, and uncontrollable variations, it is reasonable to contend that a mathematical formulation will often fall short of describing the real design problem. Therefore, the presently used design

a) Although the method of feasible directions assures an improved design with each iteration, the algorithm cannot guarantee convergence to a global minimum. It is therefore essential that the designer be prepared to find a starting design that is close to the anticipated optimal design. Nevertheless, interactive repositioning of the design vector may still be necessary to get the required convergence. Furthermore, the designer should not always expect a substantial improvement in the cost function. Rather, with a good initial design a small improvement may be obtained with, for example, a redistribution of element sizes.

b) Coefficients in the weighted-sum objective function have to be chosen so the final combination reflects a balance in tradeoffs among competing structural performance attributes. Their optimal choice is a major task in itself and is still a subjective decision. Moreover, this approach retains the limitation of hiding the changing importance of each term's contribution to the overall cost as one proceeds through the design process. Consequently, only single term objective functions have been considered to date.

c) When the optimization problem has been formulated, the earthquake loading input and structural modelling parameters are the components of the problem subject to the most uncertainty. The present environment uses a single scaled earthquake record for both the damageability and ultimate strength limit states. Guidelines suggest that the frequency content of the single record should be representative of an ensemble of such records expected to occur at a site. The record should neither contain localized frequency bands of low amplitude motion or envelope all peak response values in the ensemble(Ref. 14).

d) The ANSR simulator uses Rayleigh damping to model a phenomenon that still isn't well understood. Viscous damping is assumed in the elastic range. The nonlinear analyses employ a combination of viscous plus hysteretic damping. Calculations so far indicate that constraint performance is sensitive to the choice of specified damping ratio.

e) In reality, the effect of a single constraint's failure on the overall integrity of a structure will be related to both the constraint's type and coupling to other constraint performances. Even for small frames, this relationship may be extremely complex and probably will never be completely understood. Mahin and Bertero(Ref. 13) also indicate that while peak story drift and floor acceleration frame response parameters are commonly used as an approximate measure of non-structural damage in frames for which non-structural components are not expected to significantly contribute to the response, there is in fact very little reliable data available to make such interpretations more than qualitative. In specifying the boundary between satisfactory and unsatisfactory constraint performance, the designer will be guided by code clauses and technical references for some constraints, and his or her intuition for others. Moreover, designers commonly assert that they cannot express everything they know about a good design in a mathematical formulation. On the basis of these comments and observations of missing information, modelling deficiences, and uncontrollable variations, it is reasonable to contend that a mathematical formulation will often fall short of describing the real design problem. Therefore, the presently used design

approach of forcing all constraints to have less than some preset probability of failure or response performance would seem unjustifiably rigid. A more rational method would only require the designer to specify "Ballpark" estimates of acceptable bounds on response quantities or failure probabilities for constraint performances. He or she could then proceed to find a balanced optimal design by trading off various active constraints and terms in the objective function.

CURRENT AND ANTICIPATED WORK

The software of DELIGHT.STRUCT has recently been extended to permit optimal design under multiple ground motions. This should alleviate the problem of the frequency content of a single ground motion misguiding the final design. It also enables constraints to be described in a probabalistic form. Moreover, since various objective function terms are coupled to the frame response, they can also be considered to be probabalistic. However, the design procedure is still based on the conditional situation of all three limit states having occurred during the structure's lifetime. Work should be initiated to develop a method capable of taking into account the temporal nature of ground motions that correspond to each of the limit states.

It is anticipated that the presently used feasible directions algorithm may be replaced by the recently developed 3 phase multi-objective feasible directions algorithm due to Nye(Ref. 1). In this algorithm, constraints are categorized as being either hard or soft. Hard constraints are those that the designer gives priority to the algorithm satisfying. They might represent a physical boundary such as volume not being permitted to exceed an upper bound. Soft constraints are those in which a moderate violation is tolerable if these violations can be simultaneously traded off against one another or against performance objectives during an optimization run. The importance of a constraint violation is a subjective matter in which the designer assigns good and bad values of constraint performance. These might typically be related to an exceedance probability over the lifetime of the structure or perhaps a code clause whose purpose is to provide a general guide for good design. Good and bad values are also specified for all terms in the objective function. Finally, it is essential that extensive computer graphics be developed to support the user interaction demanded by the design algorithm.

CONCLUDING REMARKS

This paper has reviewed a design procedure that is amenable to an automated design environment. It is philosophically attractive because it demands that a designer start the process by writing down all the information he or she knows about the structure and its desired seismic response. This conceptual task will be constrained by both the flexibility of the optimization algorithm and the ability of the designer.

The authors contend that this approach to design is a step in the right direction and note that the DELIGHT.STRUCT system should be closer to becoming a practical engineering tool after the anticipated program of development has been implemented.

REFERENCES

1. W.T. Nye, " DELIGHT : An Interactive System for Optimization-Based Engineering Design." UCB/ERL M83/33 Univ of Cal, Berkeley, Ca, May, 1983.

2. Recommended Lateral Force Requirements and Commentary, Seismology Committee, Structural Engineers Association of California, San Fransisco, Calif, 1975.

3. R.J. Balling, K.S. Pister, E. Polak," DELIGHT.STRUCT: A Computer Aided Design Environment for Structural Engineering." Report No UCB/EERC 81/79, Earthquake Engineering Research Center, Univ of Cal, Berkeley, 1981.

4. D. Ray, K.S. Pister, E. Polak, " Sensitivity Analysis for Hysteretic Damping Systems : Theory and Applications.", Computer Methods in Applied Mech. and Eng., No 14, 1978, pp. 179-206.

5. M.A. Bhatti, V. Ciampi, J.M. Kelly, K.S. Pister,"An Earthquake Isolation System for Steam Generators in Nuclear Power Plants.", Nuclear Eng. and Design., No 73, 1982, pp 229-252.

6. M.A. Bhatti, "Optimal Design of Localized Nonlinear Systems with Dual Performance Criteria under Earthquake Excitations." Report No EERC 79/15,Earthquake Eng. Research Center, Univ of Cal, Berkeley, Ca, July 1979.

7. R.J. Balling,V. Ciampi,K.S. Pister, and E. Polak." Optimal Design of Seismic-Resistant Planar Steel Frames.", Report No EERC 81-20, Earthquake Eng. Research Center, Univ of Cal, Berkeley, Ca, December 1981.

8. M.A. Austin, K.S. Pister, "Optimal Design of Friction-braced Frames under Seismic Loading." Report no UCB/EERC-83/10, Earthquake Engineering Research Center, Univ of Cal, Berkeley, June 1983.

9. N.D. Walker, "Automated Design of Earthquake Resistant Multistory Steel Building Frames", Report No 77-12,Earthquake Engineering Research Center, Univ of Cal, Berkeley, Ca, May 1977.

10. Uniform Building Code, International Conference of Building Officials, Whittier, Ca, 1979 Edition.

11. E. Polak,R. Trahan,D.Q. Mayne, " Combined Phase I - Phase II Methods of Feasible Directions. " Mathematical Programming, Vol 17, No 1, pp 32-61, 1979.

12. D.P. Mondkar, G.H. Powell, " ANSR-I General Purpose program for Analysis of Nonlinear Structural Response." Report No EERC 75-37, Earthquake Engineering Research Center, Univ of Cal, Berkeley, Ca, December 1975.

13. S.A. Mahin, V.V. Bertero, " Prediction of Nonlinear Seismic Building Behavior. " Journal of Technical Councils of ASCE, TC1, November,1978.

14. H. Seed,C. Ugas,J. Lysmer,"Site-Dependent Spectra for Earthquake-Resistant Design.", No EERC 74-12, Univ of Cal, Berkeley, Ca, 1974.

SOLUTION OF THE THREE DIMENSIONAL SOIL-STRUCTURE INTERACTION PROBLEM IN THE TIME DOMAIN

E. Bayo (I)
E. L. Wilson (II)
Presenting Author: E. L. Wilson

SUMMARY

A general time domain finite element formulation and several efficient numerical techniques are combined to form a new method of analysis for the solution of three-dimensional soil-structure interaction problems. Factors such as structural embedment, arbitrary soil-profile, flexibility of the foundation, spatial variations of free field motions and interaction between two or more structures are all incorporated in the new formulation. For elastic systems the method becomes extremely efficient however its major advantage is its ability to be extended to account for nonlinear effects in the soil and structure.

INTRODUCTION

Solutions to soil-structure interaction problems are commonly carried out in the frequency domain. This is so, among other reasons, firstly because this domain permits, through the use of frequency dependent impedance coefficients, the splitting of the problem into substructures that can be analyzed independently; and secondly, because most of the transmitting boundaries developed to account for the radiation of the energy through the limits of the finite element model, are frequency dependent.

So far these reasons have been powerful enough to inhibit the time domain as the effective environment for the solution of the soil-structure problem. However, frequency domain techniques can not solve true nonlinear soil and structural problems, and are computationally inefficient for three dimensional problems. The purpose of this paper is to present a time domain formulation and efficient numerical techniques that can solve the soil-structure interaction problem in three dimensions, and at the same time allow for the solution of true nonlinear problems, feasible only in the time domain.

The discussion begins with the formulation of the soil-structure interaction problem in the time domain, it continues with the numerical techniques that make the solution of the problem efficient, and ends with a numerical example that shows the accuracy achieved by the new method compared to a frequency domain solution.

FORMULATION IN THE TIME DOMAIN

A given soil-structure interaction problem may be divided as shown in Figure 1 into a free field, and an interaction problem in which the input motion is defined at the nodes corresponding to the buried part of the structure (Ref 1). This partition of the complete problem has a main advantage in eliminating the scattering problem, and only requires that the structural

---

(I) Fellow of the 'Fundacion del Instituto Nacional de Industria'. Spain Assistant Research Engineer. University of California. Berkeley.

(II) Professor of Civil Engineering. University of California. Berkeley.

properties, stiffness, mass and damping, at its embedded level be reduced by those of the soil at the same level. The total displacements may be divided into the interaction and the free field displacements as follows:

$$\mathbf{v}_c^t = \begin{Bmatrix} v^t \\ v_f^t \\ v_g^t \\ v_a^t \end{Bmatrix} \quad \text{and} \quad \tilde{\mathbf{v}}_c = \begin{Bmatrix} 0 \\ \tilde{v}_f \\ \tilde{v}_g \\ \tilde{v}_a \end{Bmatrix} \tag{1}$$

where v represent the motions at the structure, v_f at the buried part, v_a at the soil and v_g at the soil-structure interface. The notation used for the property matrices are:

$$\mathbf{m}_c = \begin{bmatrix} m & m_f & 0 & 0 \\ m_f^T & m_{ff}-\tilde{m}_{ff} & m_{fg}-\tilde{m}_{fg} & 0 \\ 0 & m_{gf}-\tilde{m}_{gf} & m_{gg} & 0 \\ 0 & 0 & 0 & 0 \end{bmatrix} \qquad \tilde{\mathbf{m}}_c = \begin{bmatrix} 0 & 0 & 0 & 0 \\ 0 & \tilde{m}_{ff} & \tilde{m}_{fg} & 0 \\ 0 & \tilde{m}_{gf} & \tilde{m}_{gg} & \tilde{m}_{ga} \\ 0 & 0 & \tilde{m}_{ag} & \tilde{m}_{aa} \end{bmatrix} \tag{2}$$

and in the same manner for the stiffness and damping matrices. The free field equations (Figure 1b) are:

$$\begin{bmatrix} \tilde{\mathbf{m}}_c & \tilde{\mathbf{m}}_b \\ \tilde{\mathbf{m}}_b^T & \tilde{\mathbf{m}}_{bb} \end{bmatrix} \begin{Bmatrix} \ddot{\tilde{\mathbf{v}}}_c \\ \ddot{\tilde{\mathbf{v}}}_b \end{Bmatrix} + \begin{bmatrix} \tilde{\mathbf{c}}_c & \tilde{\mathbf{c}}_b \\ \tilde{\mathbf{c}}_b^T & \tilde{\mathbf{c}}_{bb} \end{bmatrix} \begin{Bmatrix} \dot{\tilde{\mathbf{v}}}_c \\ \dot{\tilde{\mathbf{v}}}_b \end{Bmatrix} + \begin{bmatrix} \tilde{\mathbf{k}}_c & \tilde{\mathbf{k}}_b \\ \tilde{\mathbf{k}}_b^T & \tilde{\mathbf{k}}_{bb} \end{bmatrix} \begin{Bmatrix} \tilde{\mathbf{v}}_c \\ \tilde{\mathbf{v}}_b \end{Bmatrix} = \begin{Bmatrix} 0 \\ 0 \end{Bmatrix} \tag{3}$$

The equations for the interaction problem (Figure 1c) are (Ref 1):

$$\left[\tilde{\mathbf{m}}_c + \mathbf{m}_c \right] \ddot{\mathbf{v}}_c^t + \left[\tilde{\mathbf{c}}_c + \mathbf{c}_c \right] \dot{\mathbf{v}}_c^t + \left[\tilde{\mathbf{k}}_c + \mathbf{k}_c \right] \mathbf{v}_c^t = -\mathbf{m}_c \ddot{\tilde{\mathbf{v}}}_c - \mathbf{c}_c \dot{\tilde{\mathbf{v}}}_c - \mathbf{k}_c \tilde{\mathbf{v}}_c \tag{4}$$

The substitution of Equations (1) and (2) in Equation (4) yields:

$$\left[\tilde{\mathbf{m}}_c + \mathbf{m}_c \right] \ddot{\mathbf{v}}_c^t + \left[\tilde{\mathbf{c}}_c + \mathbf{c}_c \right] \dot{\mathbf{v}}_c^t + \left[\tilde{\mathbf{k}}_c + \mathbf{k}_c \right] \mathbf{v}_c^t = \tag{5}$$

$$-\begin{bmatrix} m_f & 0 \\ m_{ff}-\tilde{m}_{ff} & m_{fg}-\tilde{m}_{fg} \\ m_{gf}-\tilde{m}_{gf} & m_{gg} \\ 0 & 0 \end{bmatrix} \begin{Bmatrix} \ddot{\tilde{v}}_f \\ \ddot{\tilde{v}}_g \end{Bmatrix} - \begin{bmatrix} c_f & 0 \\ c_{ff}-\tilde{c}_{ff} & c_{gf}-\tilde{c}_{gf} \\ c_{gf}-\tilde{c}_{gf} & c_{gg} \\ 0 & 0 \end{bmatrix} \begin{Bmatrix} \dot{\tilde{v}}_f \\ \dot{\tilde{v}}_g \end{Bmatrix} - \begin{bmatrix} k_f & 0 \\ k_{ff}-\tilde{k}_{ff} & k_{fg}-\tilde{k}_{fg} \\ k_{gf}-\tilde{k}_{gf} & k_{gg} \\ 0 & 0 \end{bmatrix} \begin{Bmatrix} \tilde{v}_f \\ \tilde{v}_g \end{Bmatrix}$$

To simplify the notation let the matrices on the R.H.S. be called, $\mathbf{X}_m$, $\mathbf{X}_c$, and $\mathbf{X}_k$ respectively. The free field motions at the embedded nodes (Figure 1b) may be obtained by solving Equation (3) by assuming a desired wave propagation pattern. The simplest pattern is to assume vertical propagation of P and S waves. Equation (5) may be further simplified by dividing the added displacements in two parts: a dynamic component, $\mathbf{v}_c$, plus a pseudostatic component, $\mathbf{v}_c^s$, (Ref 2). The pseudostatic displacements may be derived from Equation (5) by eliminating the dynamic terms. The displacement decomposition is given by the following expression:

$$\mathbf{v}_c^t = \mathbf{v}_c + \mathbf{v}_c^s = \mathbf{v}_c + \mathbf{r}_c \begin{Bmatrix} \tilde{v}_f \\ \tilde{v}_g \end{Bmatrix} \tag{6}$$

where:

$$\mathbf{r}_c = -\left[\tilde{\mathbf{k}}_c + \mathbf{k}_c\right]^{-1} \begin{Bmatrix} k_f & 0 \\ k_{ff} - \tilde{k}_{ff} & k_{fg} - \tilde{k}_{fg} \\ k_{gf} - \tilde{k}_{gf} & k_{gg} \\ 0 & 0 \end{Bmatrix} \tag{7}$$

substituting Equations (6) and (7) into Equation (5):

$$\left[\tilde{\mathbf{m}}_c + \mathbf{m}_c\right]\ddot{\mathbf{v}}_c + \left[\tilde{\mathbf{c}}_c + \mathbf{c}_c\right]\dot{\mathbf{v}}_c + \left[\tilde{\mathbf{k}}_c + \mathbf{k}_c\right]\mathbf{v}_c = \left\{\left[\tilde{\mathbf{m}}_c + \mathbf{m}_c\right]\mathbf{r}_c + \mathbf{X}_m\right\}\begin{Bmatrix} \ddot{v}_f \\ \ddot{v}_g \end{Bmatrix} \tag{8}$$

Equation (8) defines the motion of the system in terms of the dynamic displacements, and as a fuction of the free field ground motions at the buried part of the structure. It is easily seen that the forces in the nonburied part of the structure will depend only on the dynamic displacements, whereas, those in the buried part will now depend on the dynamic as well as on the free field displacements. The nonlinear problem can be solved by dividing the system, as shown in Figure 2, into a scattering and an interaction problem. The interaction motions contain the total displacements of the structure and the nonlinear part of the soil, therefore Equation (4) is suitable for nonlinear analysis in those regions.

REDUCTION OF THE SYSTEM OF EQUATIONS

The authors have demonstrated (Ref 3) that the use of sets of a special class of Ritz vectors (Ref 4) lead to very good solutions for wave propagation and structure-soil interaction problems. Several ways of using them as part of dynamic substructuring techniques have also been shown (Ref 1,3). The reduction in the size of the given problem can be done using those substructuring techniques, however, for simplicity in this discussion we will use the Ritz vectors globally, without making use of any substructuring procedure. Let the following displacement transformation be defined:

$$\begin{Bmatrix} v \\ v_f \\ v_g \\ v_a \end{Bmatrix} = \Phi\, \mathbf{Y} \tag{9}$$

where Φ are the global Ritz vectors and Y are the generalized coordinates. The substitution of the above transformation into Equation (8), and the premultiplication by Φ^T, leads to:

$$\mathbf{M}^*\ddot{\mathbf{Y}} + \mathbf{C}^*\dot{\mathbf{Y}} + \mathbf{K}^*\mathbf{Y} = -\Phi^T\left[\left\{\tilde{\mathbf{m}}_c + \mathbf{m}_c\right\}\mathbf{r}_c + \mathbf{X}_m\right]\begin{Bmatrix} \ddot{v}_f \\ \ddot{v}_g \end{Bmatrix} \tag{10}$$

where

$$\mathbf{M}^* = \Phi^T\left[\mathbf{m}_c + \tilde{\mathbf{m}}_c\right]\Phi \qquad \mathbf{C}^* = \Phi^T\left[\mathbf{c}_c + \tilde{\mathbf{c}}_c\right]\Phi \qquad \mathbf{K}^* = \Phi^T\left[\mathbf{k}_c + \tilde{\mathbf{k}}_c\right]\Phi \tag{11}$$

The numerical integration of the reduced coupled set of equations can be carried out by step-by-step procedures or by decoupling the system with complex eigenvectors, and solving each of the uncoupled equations by the linear force method. The second approach becomes exact for piece-wise linear type of excitation, while the first always introduces errors in the amplitude and periods of the response. For reduced systems of equations (up to 100 mode shapes) the complex eigenvector method is as computationally efficient as the step-by-step methods, and therefore it becomes a better candidate for numerical integration (Ref 1).

MODELING THE SOIL-STRUCTURE SYSTEM

The size of a typical three dimensional soil-structure interaction problem will in general be very large. The use of approximate frequency independent boundaries (Ref 5) still requires moderate sizes of finite element models. In order to further reduce the size of the problem a technique for geometrically modeling the soil-structure system is described bellow. This technique is based on the combined use of solid and axisymmetric elements to model the near and far field respectively. The reason behind this approach is that the behaviour of the soil system in the far field, away from the structure, will tend to be that of an axisymmetric system subjected to non-axisymmetric loads.

Figure 3 shows a method of modeling a soil-structure system. A given structure will be represented with standard finite elements. The foundation will be attached to the near field part of the soil, that is modeled with solid elements. At a certain distance from the structure the solid mesh is attached to the far field that is modeled by means of several harmonic expansions of axisymmetric finite elements. In order to couple both the near and the far fields, the displacements corresponding to the solid elements at the boundary between both regions are expanded in terms of Fourier series. The corresponding displacement transformation matrices (Ref 1), are used to transform the solid mass, stiffness, and damping matrices of the solid elements in contact with the axisymmetric mesh.

Another aspect to consider in modeling the soil-structure system is the internal damping. The damping characteristics of each of the components, soil and structure, can be independently represented by the Rayleigh damping model defined from damping ratios at two different frequencies. Damping ratios for soils are usually kept constant over all the frequency range. A good selection of the frequencies necessary to define the Rayleigh damping model will keep the variation of the damping ratio quite constant over a wide frequency interval, as will be seen in the numerical case given below. For cases where the frequency range of interest is too large several terms of the Caughey series can be considered to maintain a constant damping ratio (Ref 1). Since different damping ratios are considered for the soil and the structure, the resulting global damping matrix will be nonproportional. The consideration of a transmitting boundary will further contribute to the nonproportionality of the damping matrix.

NUMERICAL EXAMPLE

The procedures explained above have been implemented in a special version of the computer program SAP80 (Ref 6) for the solution of soil-structure interaction problems. To evaluate their effectiveness, a three dimensional soil structure system, whose characteristics are shown in Figure 4, is analyzed. The superstructure consists of a 2 degree of freedom system attached to a rigid massless circular foundation. The lumped masses are connected by frame

elements. The foundation is attached to a semi-infinite half-space with the characteristics depicted in Figure 4. The half-space is discretized with axisymmetric finite elements. The length and depth of the model are 5.5 and 5.8 times the radius respectively, with a total number of degrees of freedom equal to 714. The material damping is assigned a constant value for all the frequency range equal to 7 %. In order to represent this behaviour in the time domain the Rayleigh damping model is used. The frequencies taken to match the given damping ratio are 23 and 70 rd/sec. This will insure a variation of the damping ratio of less than 0.9% (ie. 6.1 to 7.9 %) over the frequency range of $21<\omega<87$ rd/sec. This corroborates the fact that Rayleigh damping models can provide a quite constant damping ratio over a wide range of frequencies. Attached to the edges of the model there is a frequency independent transmitting boundary defined at the fundamental frequency of the system (Ref 5) which has been previously computed to be 25.8 rd/sec.

The frequencies of the 2 degree of freedom model on a fixed base are 34.24 and 85.38 rd/sec. The significance of the soil-structure interaction effects in the dynamic response of the system is apparent from the fact that the first resonant frequency for the structural response has been reduced from 34.24 to 25.80 rd/sec. The second resonant frequency varies to a lesser degree from 85.38 to 80.42 rd/sec. The total system of equations is reduced globally, as explained above, with 2 different sets of Ritz vectors, the first one has 15 Ritz functions and the second 40 (2.1 and 5.6 % of the total number of degrees of freedom respectively). By running these two cases the convergence of the Ritz vector approach can be checked. The system is to be subjected to the vertical component of an earthquake excitation represented by the first 8 seconds of a given accelerogram, discretized at time intervals of 0.01 seconds and with peak acceleration equal to 0.26 g. The results obtained with SAP80 are to be compared with those obtained by the computer program SASSI (Ref 7). SASSI solves the problem using a frequency domain formulation. It uses frequency dependent radiation boundaries, and complex stiffness coefficients to account for the constant damping ratio.

The structure-soil model is solved first by SAP80, with 15 Ritz functions and with numerical integration by the complex eigenvectors, and second by SASSI. The total maximum accelerations in "g" obtained by both programs are given in Table 1. The maximum discrepancy is 3.6%. Figure 5 shows the response spectrum at degree of freedom 1 for 5% damping. As can be seen both solutions are very close. The discrepancy between the two solutions at the peak of the spectrum is 9%.

The total maximum accelerations at both degrees of freedom obtained by SAP80 with 40 Ritz functions, and SASSI are given in Table 2. The maximum discrepancy is now 2.5%. The response spectrum at degree of freedom 1 for 5% damping is shown in Figure 6, and indicates how close both solutions are. The differences in the interval of periods between 0.2 and 0.3 seconds are due to the different ways in which both methods represent the material damping. The maximum discrepancy at the peak is now 2.5%.

PROGRAM	DOF1	DOF2
SASSI	-0.440	-0.393
SAP80	-0.456	-0.402

Table 1.

PROGRAM	DOF1	DOF2
SASSI	-0.440	-0.393
SAP80	-0.452	-0.400

Table 2.

In order to see how important the interaction effects are in this case,

the two degree of freedom model is analyzed for the given input considering its base fixed. The maximum accelerations obtained in this way are 0.647 g and 0.424 g, which indicates that the reduction achieved by considering the interaction between soil and structure is of the order of 30%. This difference increases substantially when comparing the response spectrum of the model with and without interaction effects, as illustrated in Figure 7. It shows the drastic reduction of the response and the shifting of the resonant periods due to the interaction. A third resonant period appears at 0.29 seconds due to the participation of the soil.

Another aspect worth of analysis is the importance that the transmitting boundaries have in the response of the system. For this purpose the same example is solved again using 15 Ritz functions, with the bottom boundary fixed and allowing horizontal displacements at the lateral boundaries. Figure 8 illustrates the response spectrum obtained under these conditions compared with those obtained previously, which included the transmitting boundaries. As can be seen the errors introduced by not including transmitting boundaries in the finite element model are considerable, even for an input of short duration as in this case (only 8 seconds).

REFERENCES

1 Bayo, E. and Wilson, E. L. "Numerical Techniques for the Evaluation of Soil-Structure Interaction Effects in the Time Domain". EERC report 83/04. University of California. Berkeley. California. Feb 1983.

2 Clough, R.W., and Penzien, J. "Dynamic of Structures." McGraw-Hill, (1975).

3 Bayo, E. and Wilson, E. L. "Use of Ritz Vectors in Wave Propagation and Dynamic Substructuring Analysis". Earth. Eng. Struct. Dynam. Submitted for Publication.

4 Wilson, E.L., Yuan, M-W, Dickens J.M. "Dynamic Analysis by Direct Superposition of Ritz Vectors". Earth. Eng. Struc. Dynam. Vol 10. pp 813-823 (1982).

5 Bayo, E. and Wilson, E. L. "Transmitting Boundaries for Transient Dynamic Analysis". Earth. Eng. Struct. Dynam. Submitted for Publication.

6 Wilson, E. L. "SAP80 Structural Analysis Programs for Small or Large Computer Systems". CEPA 1980 Fall Conference and Annual Meeting. Newport Beach. California.

7 Lysmer J., Raissi, M., Tajirian, F., Vahdani, S., Ostandan, F. "SASSI- A System For Analysis of Soil-Structure Interaction". University of California Berkeley. Geotechnical report # 81-02. April (1981).

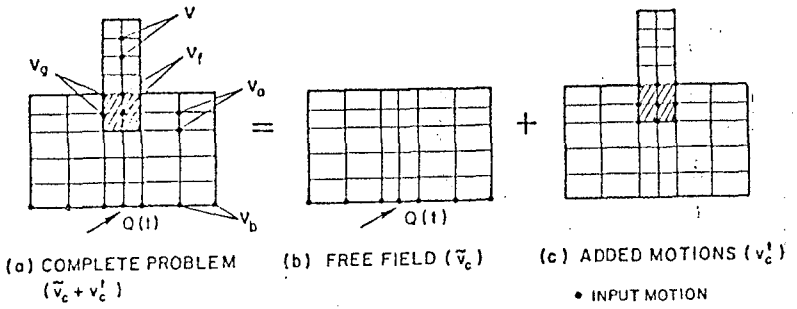

Fig 1.- Division of the complete problem into a free field and an interaction problem.

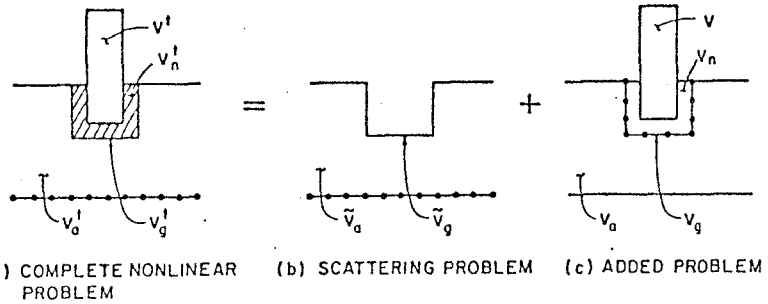

Fig 2.- Two step solution for the nonlinear problem.

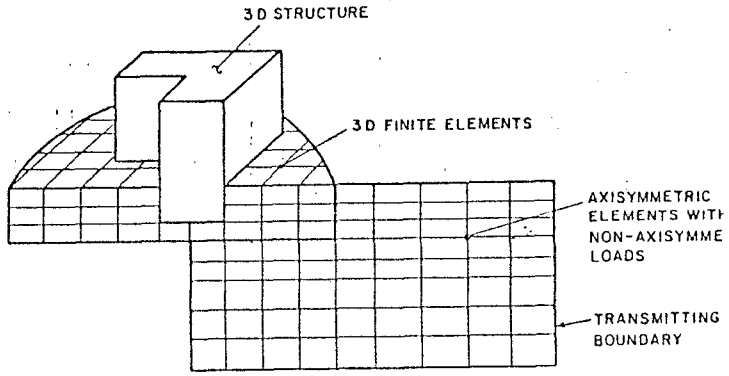

Fig 3.- Modeling soil-structure problems.

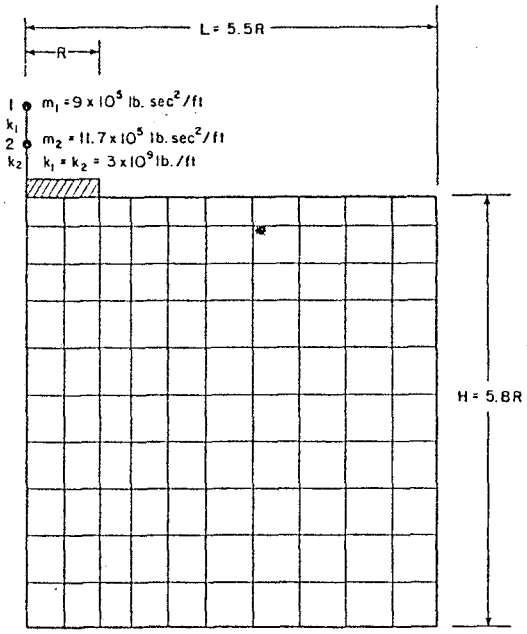

V_p = 4000 ft/sec
V_s = 2000 ft/sec
ρ = 3.11 lb. sec^2/ft^4
R = 42 ft
ν = 1/3
G = 1.244×10^7 lb/ft^2
E = 3.317×10^7 lb/ft^2

Fig 4.- Characteristics of the numerical example.

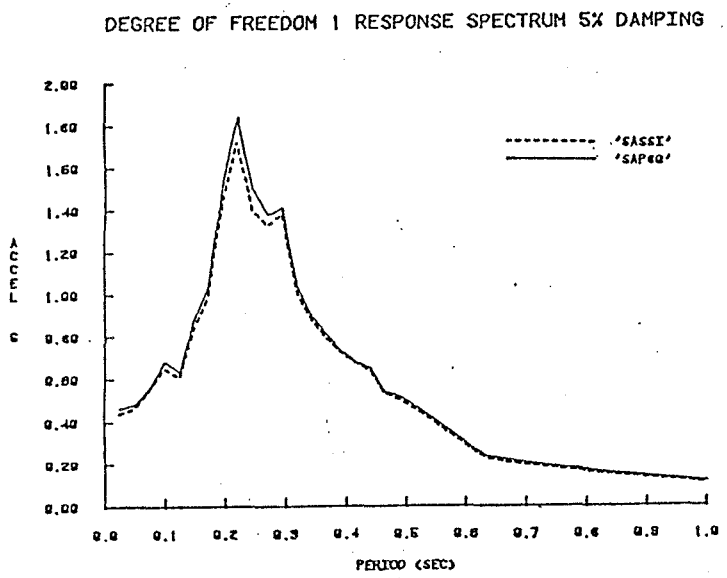

Fig 5.- Response spectrum at DOF1 obtained with SAP80 using 15 Ritz functions, and SASSI.

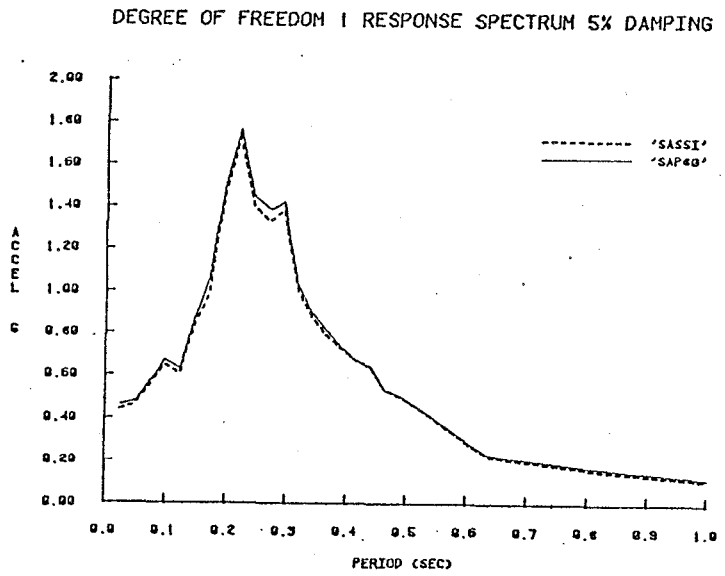

Fig 6.- Response spectrum at DOF1 obtained with SAP80 using 40 Ritz functions, and SASSI.

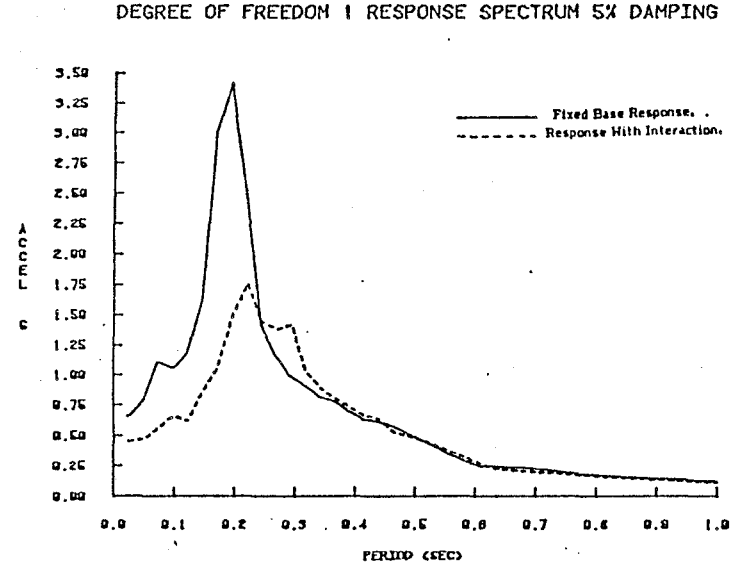

Fig 7.- Response spectrum at DOF1 obtained with and without interaction effects.

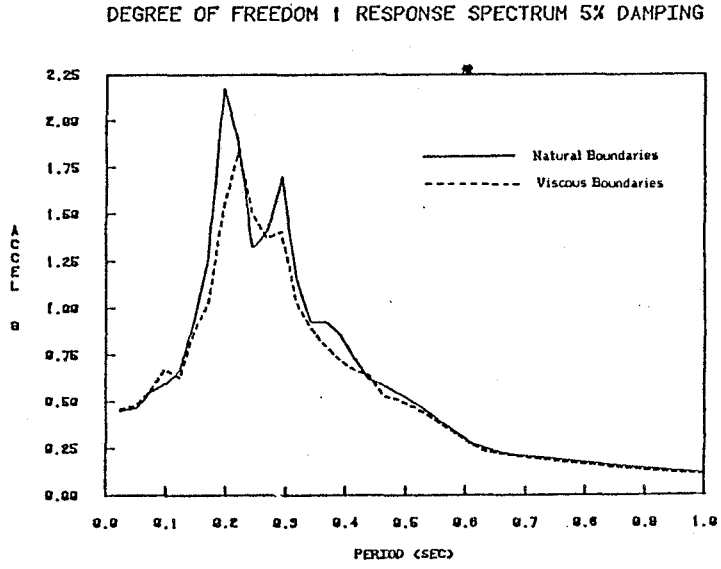

Fig 8.- Response spectrum at DOF1 obtained with and without transmitting boundaries.

STATE OF THE ART AND PRACTICE IN SEISMIC RESISTANT DESIGN OF R/C FRAME-WALL STRUCTURAL SYSTEMS

Vitelmo V. Bertero (I)
Presenting Author: Vitelmo V. Bertero

SUMMARY

The state of the practice in the seismic resistant design of R/C frame-wall structural systems is reviewed by analyzing the performance of buildings designed according to current seismic codes. The state of the art in the seismic resistant design of such structural systems is judged by comparing analytically predicted response to experimentally measured behavior. It is concluded that present U.S. seismic codes can lead to poor design and that the present state of the art in modeling R/C frame-wall structures is inadequate. Changes most urgently needed to improve both states are indicated.

INTRODUCTION

Although the last two decades have witnessed marked improvement in the analysis and seismic resistant design of moment-resisting space frames (DMRSF), the ability to analyze and particularly to design frame-wall structural systems has not been comparably improved. For buildings that exceed ten stories, the use of a dual DMRSF-wall system seems to have great potential in seismic resistant design (Ref. 1).

As with any design, the aim of seismic resistant design should be to optimize the resulting building. Several years ago, the author and his associates developed an automated optimal seismic resistant design for DMRSF (Ref. 2). Despite considerable research on the seismic behavior of R/C wall structures (Refs. 1 & 3), the state of the art in quantifying the design (performance) criteria for the seismic resistant design of frame-wall structures remains limited, and a high degree of uncertainty persists in the establishment of design earthquakes and of demands, and in the provision of the supplies of the components of this type of structural system.

The author believes that these limitations and uncertainties remain of such significance as to deter research on the development of a realistic mathematical formulation for the optimum design of such structures. Efforts should be directed towards improving the understanding of the seismic behavior of this type of structural system and the application of this understanding to what the author has defined as *conceptual design*. The basic ideas on which conceptual design is based are: (1) to control and/or decrease seismic demands and (2) to increase the supplies (particularly the energy dissipation) as much as economically feasible. In this sense, the research recently conducted has been significant in improving the understanding of seismic behavior and therefore in identifying the inadequacies and shortcomings in the seismic resistant design provisions of current building codes and in improving application of conceptual design. These advances have motivated this paper, which has the following objectives: (1) to review the states of the practice and of the art of the seismic resistant design of R/C frame-wall structural systems in the U.S. in light of recent research results; and (2) to formulate recommendations for improving the state of the practice as well as that of the art.

STATE OF THE PRACTICE

The design and construction of most seismic resistant buildings in practice generally follow code design provisions. In Refs. 4 and 5, the author has examined in detail present U.S. seismic code provisions, particularly those specified in the *Uniform Building Code* (UBC) (Ref. 6). Here, the soundness of this code will be judged by analyzing the overall performance of UBC-designed structures, rather than by analyzing in detail individual code provisions.

(I) Professor of Civil Engineering, University of California, Berkeley, U.S.A.

Soundness of UBC Seismic Resistant Design Procedure for R/C Frame-Wall Structures

The performance of code-designed buildings in recent earthquakes has been studied and described in detail in several publications (Refs. 4 & 7), and the following observations have been made: (1) The maximum lateral resistance (strength) of code-designed structures, especially R/C wall structures, is typically higher (usually by more than a factor of 2) than that required by code; (2) Despite this observed greater strength, many code-designed buildings collapse or suffer serious nonstructural or structural damage that constitutes failure. It can be concluded that building design following present seismic code regulations does not guarantee safety against collapse or failure (unacceptable damage); (3) While buildings based on moment-resisting frames usually collapse through pancaking of one or more stories, this type of collapse is not usually observed in buildings with shear walls that continue to the foundation.

Summary of Results of Research Conducted on UBC-Designed Reinforced Concrete Frame-Wall Structures. The overstrength of wall structures has long been observed (Ref. 5). The two specific examples of UBC-designed structural wall systems discussed below confirm this overstrength and permit the soundness of present UBC design procedures to be assessed by comparing overall responses as expected from the code (state of the practice) with analytically predicted behavior using available computer programs for linear and nonlinear dynamic analyses (state of the art) and with experimentally determined responses.

U.S.-Japan Seven-Story R/C Frame-Wall Structure. A full-scale model of the building structure shown in Fig. 1 was tested in Tsukuba, Japan. This building was designed according to the 1979 UBC and Japanese codes.

UBC Expected Response. The relationship between total lateral force, V, and roof displacement, δ_r, according to UBC minimum requirements is shown as curve *OABC* in Fig. 2(a).

Analytically Predicted Response. Before testing the full-scale model, analyses were conducted using available computer programs. Chavez (Ref. 8) predicted a maximum base shear of 661 kips, when the structure was subjected to the N-S component of the Miyagi-Oki (MO) earthquake record normalized to a peak acceleration of 0.36g. This result is indicated in Fig. 2(a). Charney and Bertero (Ref. 9) estimated the responses shown in Fig. 2(a). When a triangular distribution of lateral force was assumed, the static maximum base shear was 664 kips (Fig. 2(a)). Where a rectangular distribution of lateral force was assumed, the static maximum base shear was 819 kips. From the nonlinear dynamic analysis conducted using the computer program DRAIN-2D, it was computed that under the MO record the maximum base shear would be 767 kips, i.e. 16% greater than that predicted by Chavez and between the two statically predicted maximum base shear values (664 and 819 kips), but closer to that predicted assuming a rectangular distribution of lateral force.

Experimentally Measured Response. (1) The full-scale model of the building was subjected to two series of pseudo-dynamic tests in Japan (Ref. 10). In the first series of tests, the model was considered a single-degree-of-freedom system and tested under an inverted triangular distribution of load. The envelope of hysteretic behavior is shown in Fig. 2. The maximum base shear was 954 kips, i.e. three-and-one-half times greater that the UBC-expected lateral resistance as controlled by flexural yielding. This value was 44% and 25% larger than the value predicted analytically by Chavez and Charney and Bertero, respectively, which clearly indicates that the state of the art in predicting mechanical behavior should be improved.

The full-scale model did not fail during the pseudo-dynamic test in which the inverted triangular lateral load distribution was used, although the displacement ductility considering initial yielding of the wall was more than 6 and the effective displacement ductility of the structure as a whole was close to 4. This high observed ductility arises primarily because under the inverted triangular load distribution, the wall and the beams and columns of the frame were subjected to small shear stress. The wall was designed for a unit nominal shear stress, v_u, smaller than $5\sqrt{f_c'(psi)}$ and at the maximum measured $V = 954$ *kips*, v_u was smaller than $12\sqrt{f_c'(psi)}$. The experimental results confirmed the author's previous conclusions: If by proper (conceptual) design, it is possible to keep shear stresses low, R/C shear wall structures can offer sufficient

dissipation of energy (ductility and stable hysteretic behavior) through flexural yielding to resist even the effects of extreme ground shaking.

From comparison of the analytically predicted curves and the experimental envelopes, it can be seen that the structure was considerably stiffer than expected from the UBC and analytically predicted stiffnesses. The full-scale model, after being subjected to the first series of tests with the inverted triangular distribution of lateral load, was repaired. 'Nonstructural' spandrel walls and partitions were also added in all stories except the first. The model was then subjected to a series of tests similar to the first series. Finally, the model was loaded statically using a rectangular distribution of lateral load. As illustrated in Fig. 2(b), the structure under this load was able to resist a maximum base shear of 1315 kips, or 4.8 times the UBC-required design ultimate lateral strength. However, when a base shear of 1315 kips was reached at a lateral displacement of 11.3 in., the wall failed in shear at the first story with a sudden drop in resistance. Note that this displacement was about 16% smaller than that obtained in the first series of tests without failure. Comparison of results from the two test series indicates the importance of the type of loading and the added 'nonstructural' elements to the behavior of frame-wall structures. While resistance may be considerably increased, ductility may be jeopardized.

A 1/5th scale model of the building, shown in Fig. 1, was subjected to several series of tests at the Earthquake Simulator facility at Berkeley, and in Fig. 2 the force-deformation envelope obtained from these tests is compared with those obtained pseudo-dynamically on the full-scale model. As can be seen, the envelope obtained from the 1/5th scale model shows a significant increase in strength when compared with results obtained for the full-scale model using a triangular distribution of lateral force.

Frame-Coupled Wall Structural System. To assess whether R/C frame-coupled wall structural systems designed according to the UBC possess desirable characteristics at all primary limit states and, particularly, at ultimate limit states (damageability and safety against collapse) under the maximum expected earthquake ground motion, Aktan and Bertero (Ref. 3) conducted analytical and experimental studies on the fifteen-story building system illustrated in Fig. 3. This building was designed according to 1973 UBC, 1979 UBC, and ATC-3 provisions.

The 1973 UBC-designed structure was thoroughly analyzed using linear and nonlinear static and dynamic computer programs (Ref. 3). A four-and-one-half story, one-third scale model subassemblage of one coupled wall of the structural system was constructed and tested. In Fig. 4, the code-expected total lateral load-maximum interstory drift values for the coupled wall are compared to those obtained experimentally. The contrast in these values is striking. The stiffness and strength of the coupled wall are observed to exceed significantly the minimum values required by the code. The capacity to dissipate energy is, however, not as large as would be expected according to the strength and the code-assumed displacement ductility. Therefore, the following questions arise: (1) Why is the experimentally observed strength greater (3.4 times) than the strength expected from the code? (2) Why is the measured displacement ductility smaller than expected? (3) What are the possible consequences of this overstrength and relatively small ductility?

The observed overstrength was primarily due to the higher axial-flexural strengths of the coupling girders and of the wall subjected to higher compression. A detailed discussion of the reasons for these observed higher axial-flexural strengths is contained in Ref. 3. A summary of these reasons follows.

The overstrength of the coupling girder axial-flexural strength was caused by: the larger yielding strength and ultimate capacity of reinforcing steel; the compressive axial force in these girders which arose from the shear redistribution in walls; the hypothetical underestimated slab contribution (effective flange width and contribution of the slab steel) as opposed to the actual contribution; and the relatively low nominal shear stress for which these girders were designed ($v_u = 6.4\sqrt{f_c'(psi)}$ versus $10.0\sqrt{f_c'(psi)}$ allowed by the UBC).

The coupling girders developed higher shear due to their higher axial-flexural capacity.

The walls were consequently subjected to axial forces significantly higher than those anticipated by the code. Higher compression resulted in higher axial-flexural resistance. Lower compression or even tension resulted in lower wall flexural capacity. The flexural resistance of the walls under compression and tension contributed 34% and 6%, respectively, to the total moment-overturning capacity.

The total contribution of the axial-flexural strength of the walls to the total overturning moment and, therefore, to the total shear resistance of the structural system was higher than expected due to: larger yield and maximum strength of the actual reinforcing steel bars as opposed to code-specified values; increase in compressive strength of the concrete used; and the enhancement of this strength in the edge members by the high degree of confinement. The axial-flexural strength attained in the compression wall was approximately 6.0 times greater than the code design demand and 1.4 times greater than the analytically predicted supply. Furthermore, the walls were able to develop these higher axial-flexural strengths without failing prematurely in shear because their wall panels were designed for a maximum $v_u = 6.1\sqrt{f_c'(psi)}$ (this value includes the $2.8E$, where E represents earthquake load capacity, and the capacity reduction factor $\Phi = 0.85$) which is less than the UBC-allowed factor of $10.0\sqrt{f_c'(psi)}$.

The significant increase in total shear force that had to be resisted by the coupled walls as a consequence of the actual provided axial-flexural strength was one of the main reasons for the observed relatively small ductility. An even more important reason, perhaps, was the relative distribution of this total shear between the two walls of the coupled system. The typical measured redistribution of shear force at the base of the coupled wall model during a half-cycle of loading is illustrated in Fig. 5 (Refs. 3 & 5). The wall under compression attracted 85% of the total base shear even at the service load level as defined by the 1973 UBC. At the ultimate limit states, the compression wall resisted 90% of the total shear. The nominal shear stresses, v_{max}, in the two walls at the failure of the panel of the wall under compression, amounted to $1.6\sqrt{f_c'(psi)}$ and $16.2\sqrt{f_c'(psi)}$ for the walls in tension and compression, respectively.

Because of the high nominal shear stress developed in the compression wall, $16.2\sqrt{f_c'(psi)}$, it is not surprising that once the maximum lateral resistance capacity was reached (Fig. 4), this wall was not able to undergo large inelastic deformation. The somewhat sharp drop in strength after a relatively short plastic plateau is attributable to panel crushing as a consequence of the high axial compression and shear that developed at the critical region of the compression wall when it began to yield in flexure. Tests conducted on similar walls but under smaller axial and shear force have shown higher ductility and larger energy dissipation capacity, although yielding occurred at a slightly lower total lateral force (Ref. 1).

Concluding Remarks Regarding State of the Practice

The results presented in Figs. 2, 4, and 5 and the above discussion indicate that although UBC-designed structures have a supplied axial-flexural strength significantly higher than the UBC-required strength, the shear forces developed at the critical regions of structures when the yielding axial-flexural capacity is reached may exceed the available shear strength. A semibrittle failure may consequently occur before the wall will be capable of supplying the required energy dissipation capacity. It can therefore be concluded that the UBC seismic provisions and design procedures do not guarantee a sound seismic resistant design of frame-walled structures. The seismic design forces are specified at a fictitious level and the recommended linear elastic analysis procedure cannot predict the actual response under the probable extreme earthquake ground motion. The designer is not properly guided in detailing structures for actual behavior (depicted in Figs. 2 and 4 by the experimental curves), because he/she is required to make computations only and therefore to think and/or visualize seismic behavior according to the code-conceived linear elastic response represented in Figs. 2 and 4 by the line OA.

The large axial-flexural overstrength results from a series of code requirements: in the case of dual bracing systems, walls alone must resist the total shear; the edge (vertical boundary) members along the shear walls must be designed not only to carry all vertical stresses resulting from all gravity loads and the total horizontal forces acting on the wall, but also to account for a capacity reduction factor, Φ, equal to 0.70 or 0.75; neglect or underestimation of

the contribution of floor systems (R/C slabs) to the lateral stiffness and strength, particularly the contribution of the slab reinforcement to the girders' negative end moments; neglect of increases in strength due to the strain hardening of reinforcing bars, which becomes increasingly significant as the required ductility of the structural system increases. For the cases presented in Figs. 2 and 4, another main reason for the observed axial-flexural overstrength was that the strengths of the materials (the f_c' and f_y of the concrete and steel, respectively) were considerably higher than the specified values.

Changes in the UBC seismic provisions are urgently needed. Design against shear failure should be based on the maximum shear that can be developed in structural members according to the actual strength supplied to a building and the actual distribution of total shear among structural members. Numerous suggestions for change needed in the UBC to improve the state of practice have been proposed in Ref. 5.

STATE OF THE ART

Detailed discussion of the state of the art in the seismic resistant design of buildings with particular emphasis on frame-wall structures is provided in Refs. 3-5. In Ref. 4, the author concludes that "despite advances there are many uncertainties involved in: (1) predicting the dynamic characteristics of future earthquakes; (2) modeling the dynamic characteristics of the building-soil foundation system; (3) estimating the actual supplied strength and deformation capacity of buildings; and (4) conducting reliable numerical analyses of the response of mathematical models and therefore in estimating the demands on structures. There is an urgent need to increase our present knowledge through integrated educational, research, and development efforts."

To illustrate deficiencies in the present state of the art, correlations between analytically predicted and experimentally measured behavior of the frame-wall structure shown in Figs. 1 and 3 are briefly discussed below.

U.S.-Japan Seven-Story Reinforced Concrete Wall Structure.

The analytical responses for the full-scale reinforced concrete wall structure did not correlate well with the experimental results (Fig. 2). A primary reason for this discrepancy is the way in which frame-wall structures are modeled. The current modeling technique for a frame-wall system such as that illustrated in Fig. 1 is to consider only in-plane action, using an analytical model similar to that shown in Fig. 6(a) which can be considered a pseudo-three-dimensional model. It is assumed that at the ultimate limit state of collapse, the structure dissipates energy by deforming according to the mechanism illustrated in Fig. 6(b). Note that in this model the shear wall is modeled as a column located at the axis of symmetry of the wall and therefore rotating about the wall centroidal axis at the base. Furthermore, the transverse coupling between the interior frame-wall B and the exterior frames A and C (see Fig. 1) is ignored.

The experiments described here have shown that after yielding of the main shear wall, the behavior of the structure was as illustrated in Fig. 7, i.e. the wall rotated (rocked) practically around the center of its edge member and the three-dimensional frame surrounding the wall outriggered it, restraining its rocking and therefore increasing the axial compressive force acting on it and consequently increasing its flexural resistance. The migration of the longitudinal neutral axis of the wall, the rocking of the wall, and the restraint of this rocking by the outriggering action of the frame surrounding the wall significantly increased the lateral resistance capacity of the three-dimensional structure. For a detailed evaluation of the contribution of the rocking and the outriggering interaction, see Ref. 11. After the experiments on the full-scale model, Kabeyasawa *et al.* (Ref. 12) developed a mathematical model which incorporated these new features. The predicted response correlated very well with the observed response. The importance of integrated experimental and analytical research is thus underscored.

Frame-Coupled Wall Structural System

Code design procedures and most computer programs for linear analyses of structural systems with identical coupled walls assume that the lateral stiffness of these walls is the same and

remains constant during "linear elastic response." For two similar walls that are coupled, each wall is assumed to resist, and is therefore designed for, half of the total shear resisted by the coupled walls. The lateral stiffness (flexural and shear) of R/C structural elements (particularly walls), is sensitive to the amount of axial force. Therefore, the stiffness of the two coupled walls and consequently the amount of shear resisted by each cannot be the same since as a result of the coupling girders, the axial force acting in each coupled wall will start to differ as soon as a lateral force is induced. The difference must increase as the lateral force increases. This has been clearly proved experimentally (see Fig. 5). The effects of variations of axial force on lateral stiffness (flexural and shear) have been studied experimentally in connection with studies conducted on the 1/5th scale model shown in Fig. 1(c) (Ref. 11) and in recent experiments on walls similar to those shown in Fig. 3 which clearly show the tremendous influence of axial force on the lateral flexural and shear stiffness of the wall.

Concluding Remarks Regarding the State of the Art

Sophisticated computational methodologies have been developed for the analysis of three-dimensional mathematical models. *However, the present state of the art of modeling R/C frame-wall building structures does not allow for adequate and/or realistic assessments of force and distortion demands.* The problem is due primarily to the difficulty and uncertainty inherent in assessing axial, shear-flexural, and torsional stiffnesses, strengths, and force-distortion hysteretic capacities of R/C structures. These difficulties and uncertainties are especially acute when the behavior of structural members and/or critical regions is affected by three-dimensional interaction between internal forces and induced distortions. To use computational capabilities efficiently, the state of the art of predicting realistic supplies must first be improved. This improvement can be achieved through *integrated analytical and experimental research on the behavior of buildings or that of realistic three-dimensional physical models* subjected to actual earthquake ground motions or realistic representations thereof.

ACKNOWLEDGMENTS

A large portion of the results described in this paper were obtained in research sponsored by the National Science Foundation. Thanks are also due to Dr. A. E. Aktan and the many graduate students whose work has contributed to the research reported here, and to R. Steele for his work in illustrating the text.

REFERENCES

(1) V. V. Bertero, "Seismic Behavior of R/C Wall Structural System," *Proceedings*, 7th WCEE, Istanbul, Turkey, Vol. 6 (1980).

(2) V. V. Bertero and S. W. Zagajeski, "Optimal Inelastic Design of Seismic-Resistant R/C Framed Structures," *Study No. 14*, Int'l Symposium on 'Nonlinear Design of Concrete Structures,' University of Waterloo, Ontario, Canada (1980).

(3) A. E. Aktan and V. V. Bertero, "States of the Art and Practice in the Optimum Seismic Design and Analytical Response Prediction of R/C Frame-Wall Structures," *Report No. UCB/EERC-82/06*, EERC, Univ. of Calif., Berkeley (1982).

(4) V. V. Bertero, "State of the Art in the Seismic Resistant Construction of Structures," *Proceedings*, 3rd Int'l Earthq. Microzonation Conf., Vol. II, Univ. of Washington (1982).

(5) V. V. Bertero, "Implications of Recent Research Results on Present Methods for Seismic Resistant Design of R/C Frame-Wall Building Structures," *Proceedings*, SEAOC, 51st Annual Convention, San Francisco, Calif. (1982).

(6) *Uniform Building Code*, Int'l Conf. of Building Officials, Whittier, Calif. (1982).

(7) V. V. Bertero, S. Mahin, and J. Axley, "Lessons from Structural Damages Observed in Recent Earthquakes," *Proceedings*, 7th WCEE, Vol. 4, Istanbul, Turkey (1980).

(8) J. W. Chavez, "Study of the Seismic Behavior of Two-Dimensional Frame Buildings: A Computer Program for the Dynamic Analysis—INDRA," *Bulletin of the Int'l Inst. of Seismology & Earthq. Engrg*, Vol. 18, BRI, Tsukuba, Japan (1980).

(9) F. A. Charney and V. V. Bertero, "An Evaluation of the Design and Analytical Seismic Response of a Seven-Story Reinforced Concrete Frame-Wall Structure," *Report No. UCB/EERC-82/08*, EERC, Univ. of Calif., Berkeley (1982).

(10) S. Okamoto *et al.*, "A Progress Report on the Full Scale Seismic Experiment of a Seven-Story R/C Building," *Proceedings*, 3rd Joint Coordinating Comm. Mtg of the U.S.-Japan Cooperative Research Prog., BRI, Tsukuba, Japan (1982).

(11) V. V. Bertero, *et al.*, "Earthquake Simulator Tests and Associated Experimental, Analytical, and Correlation Studies of 1/5 Scale Model," paper to be published in *ACI-SP*.

(12) T. Kabeyasawa, *et al.*, "Analysis of the Full Scale Seven-Story Reinforced Concrete Test Structure: Test PSD3," *Proceedings*, 3rd Joint Coordinating Comm. Mtg of the U.S.-Japan Cooperative Research Prog., BRI, Tsukuba, Japan (1982).

FIGURES

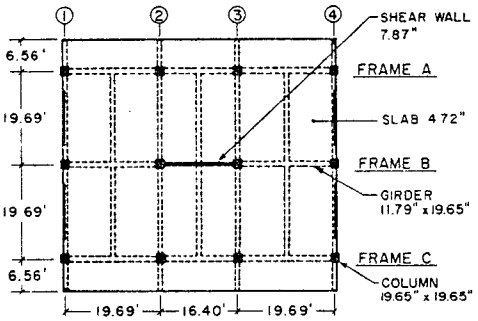

(a) PLAN OF PROTOTYPE

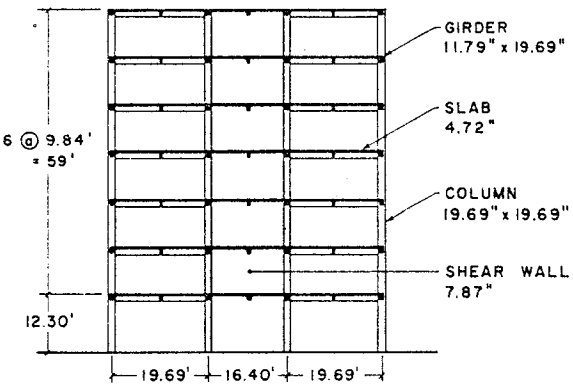

(b) FRAME B OF PROTOTYPE

FIG. 1 SEVEN-STORY REINFORCED CONCRETE FRAME-WALL TEST BUILDING

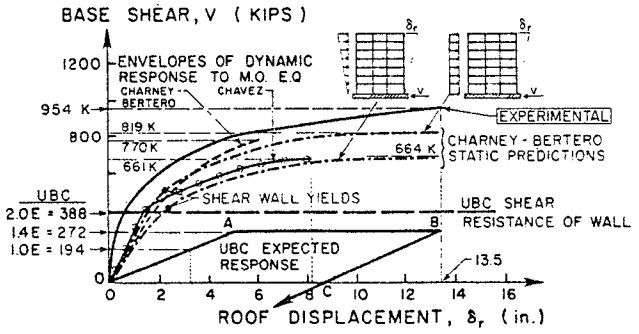

(a) UBC, EXPERIMENTAL, STATIC & DYNAMICALLY PREDICTED RESPONSES

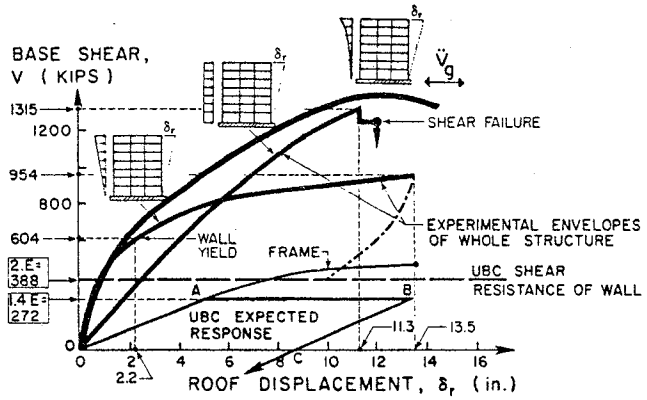

(b) UBC & EXPERIMENTAL ENVELOPES

FIG. 2 COMPARISON OF UBC, STATICALLY & DYNAMICALLY PREDICTED & EXPERIMENTAL TOTAL LATERAL LOAD-ROOF DISPLACEMENT RELATIONS FOR BUILDING IN FIG. 1

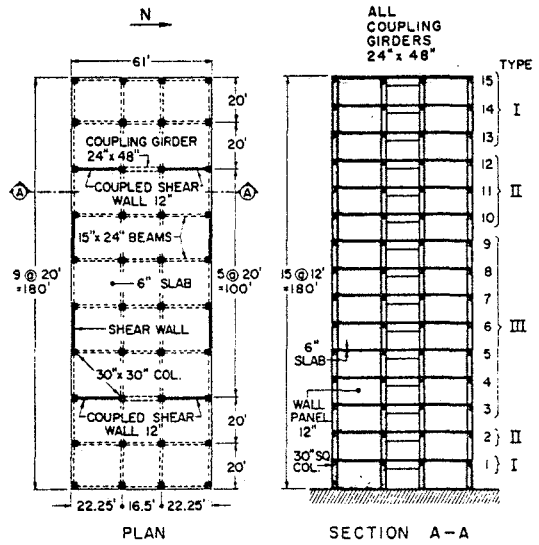

FIG. 3 STRUCTURAL LAYOUT OF 15-STORY R/C FRAME-COUPLED WALL BUILDING

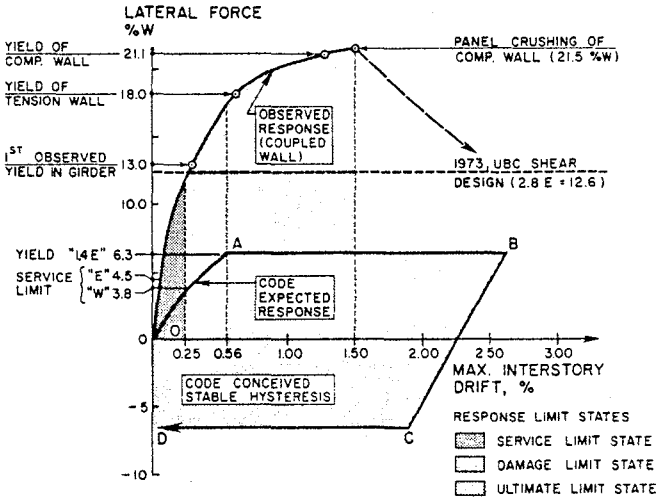

FIG. 4 COMPARISON OF EXPERIMENTAL RESPONSE WITH UBC-EXPECTED RESPONSE OF COUPLED WALL OF BUILDING IN FIG. 3

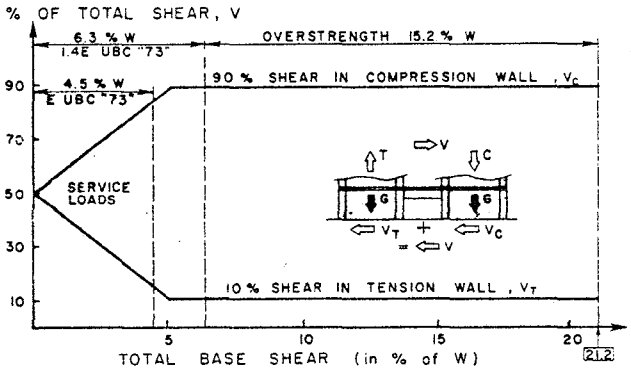

FIG. 5 MEASURED REDISTRIBUTION OF TOTAL BASE SHEAR OF COUPLED WALLS IN BUILDING OF FIG. 3

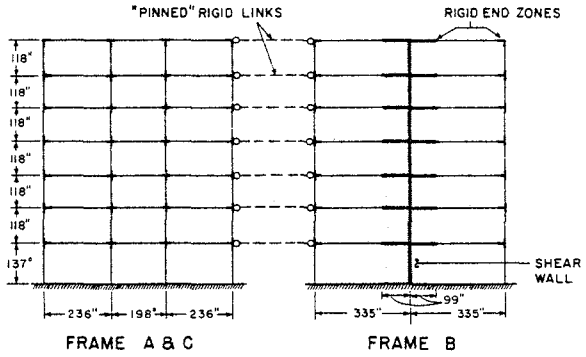

(a) PSEUDO-THREE-DIMENSIONAL MODEL CONSIDERING ONLY PLANAR ACTION

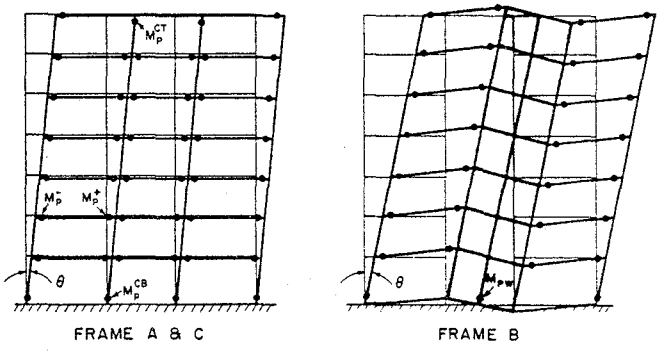

(b) PLANAR MECHANISM OF MOTION

FIG. 6 ANALYTICAL MODEL FOR FRAME-WALL SYSTEM OF FIG. 1

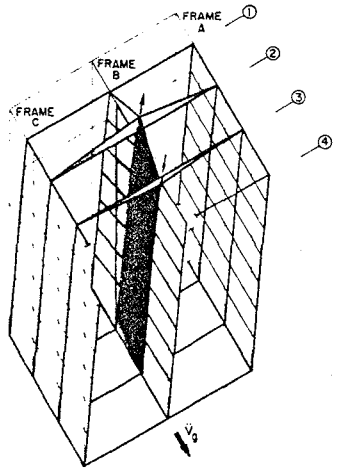

Fig. 7 THREE-DIMENSIONAL INTERACTION OF WALL & FRAMES OF BUILDING IN FIG. 1

THE VARIATION OF STRONG GROUND MOTION OVER SHORT DISTANCES

B. A. Bolt (I)
N. Abrahamson (II)
Y. T. Yeh (III)
Presenting Author: B. A. Bolt

SUMMARY

This study, based on digitally recorded ground motions across the strong-motion array in Taiwan (SMART 1), addresses two problems related to input motions for structural design. First, the average coherence of high amplitude wave motions over distances of a few hundred meters is measured as a function of frequency. High resolution wave-number spectra, computed for sub-sets of the array in the range of 0.5 to 10 Hz, indicate significant dependence of coherence on frequency. Above about 5 Hz, spacially incoherent ground accelerations dominate, probably from scattering. Secondly, changes in direction of approach of body and surface waves in the accelerograms across the array are measured using wave number spectra and ground particle motions. The structurally important ratio of coherent vertical to horizontal wave energy is determined as a function of frequency. Spacial averages of response acceleration (N. Newmark's "tau effect") are computed suggesting tau between 0.6 to unity.

INTRODUCTION

The results presented here are based on recordings of strong ground acceleration obtained with the large-aperture array of digital accelerometers (SMART 1) in northeast Taiwan (Ref. 1). The array consists of 37 three-component force balanced accelerometers arranged in three concentric circles of radii 200 m, 1 km, and 2 km with one station at the center. Each station is triggered independently and the accelerations are recorded digitally on cassette tape. Absolute time is kept accurate to 1 msec.

During the first three years of operation (1980-1983), the array has recorded 25 earthquakes with local magnitudes between 3.8 and 6.9 (Ref. 2). The largest accelerations were recorded during the January 29, 1981, M_L = 6.9 earthquake. During this earthquake, all twenty-seven installed instruments triggered and the maximum horizontal acceleration recorded was 0.24g. The epicenter was located 30 km from the center of the array at an azimuth of 154°. The depth of the focus was 11 km. In order to simplify the presentation all calculations for the present paper use SMART 1 recordings from the January 29, 1981 earthquake.

(I) and (II) Seismographic Station, University of California, Berkeley

(III) Institute of Earth Sciences, Taipei

SPACIAL COHERENCE OF GROUND MOTION

The variability of wave energy across the whole array can be conveniently measured by using a frequency-wave number decomposition (Ref. 3). Such azimuthal spectral plots have been calculated using all 27 recording elements of the array, and for the four sub-arrays defined by the principal quadrants. Comparison between the five power spectra then provides a measure of changes in total wave power, wave scattering and direction and speed of approach of the coherent waves.

Example plots for the radial component of ground motion are given in Figure 1 for a 5 sec time window including the main S waves for the north-east (top) and south-east (bottom) quadrants at a frequency of 2.0 Hz. It is clear that the average coherent power in this earthquake is significantly different in the two quadrants. The peak power (peaks labelled A) has changed by a ratio of 1.75 over a distance of 1.5 km. In the north-east quadrant the coherent wave has an apparent velocity of 6 km/sec and azimuth 19° E of S; in the south-east quadrant the values are 2.6 km/sec at 23° E of S. The peripheral power-peaks in Fig. 1 arise from scattered strong wave motion and differ by quadrant. For the whole array (not shown) these outlying peaks diminish significantly.

Similar calculations of wave number plots at other frequencies and components show coherent wave motion with similar variabilities between sub-sections of the array for frequencies up to 3 Hz on the horizontal components and for frequencies up to 5 Hz on the vertical component. Above these frequencies, there is little coherent motion.

GROUND PARTICLE MOTIONS

One way to identify seismic waves is to plot the orbits of particles of the ground during the passage of the waves. These particle motions have loci of different geometries (straight lines, ellipses, etc.) depending on the wave type (P, SV, SH, Rayleigh, etc.). The orbits, which can be computed from the three orthogonal ground displacement components recorded by SMART 1 accelerometers, also can be compared across the array to measure the spacial variability in the ground motion. Fig. 2 shows the ground displacement orbits for a time interval of 3 sec from the January 29, 1981 earthquake recorded at 3 collinear stations of SMART 1. Although double integration of the accelerograms has greatly smoothed the ground motions, significant differences in the orbits are distinguishable.

First, consider the RT orbits. The arrival of the initial S wave pulse corresponds to the loop in the upper right hand corner. The shape and orientation of the loop is fairly constant for all three stations. There are some small differences in the sharpness of the cusps, but the overall orientation is the same. However, the second swing of the S waves (loop in the lower left hand corner) rotates 15° in a counter-clockwise manner from I-06 to I-12, indicating a sharply bending wave-front over a distance of 400 m. Secondly, the particle motion in the

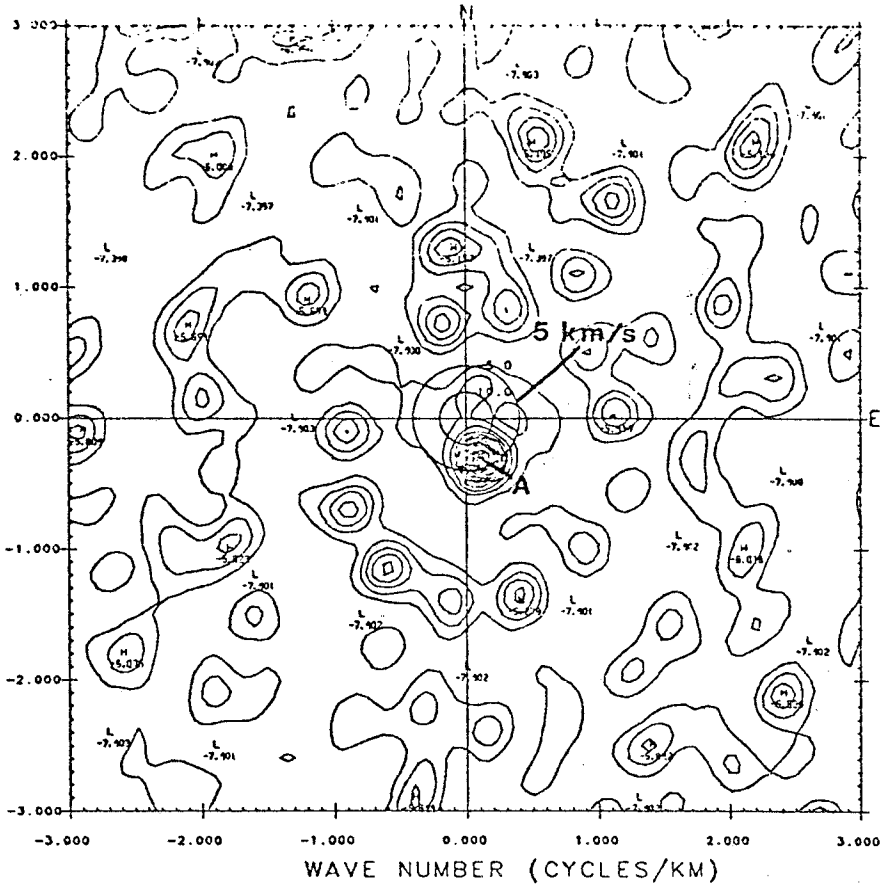

Figure 1. Azimuthal plot of coherent seismic wave power of the radial component at frequency 2 Hz. Power is contoured as a function of db down from the maximum. The vertical and horizontal axes are wave number in the north (N) and east (E) directions. Wave velocity (km/s) is marked on the central circles.

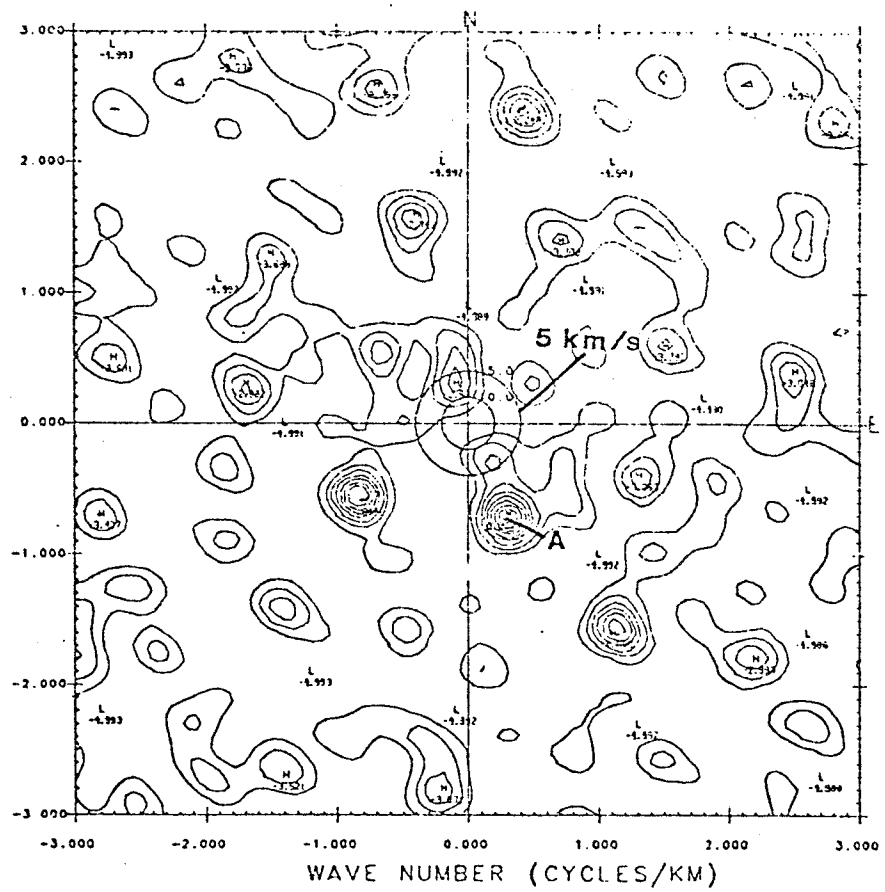

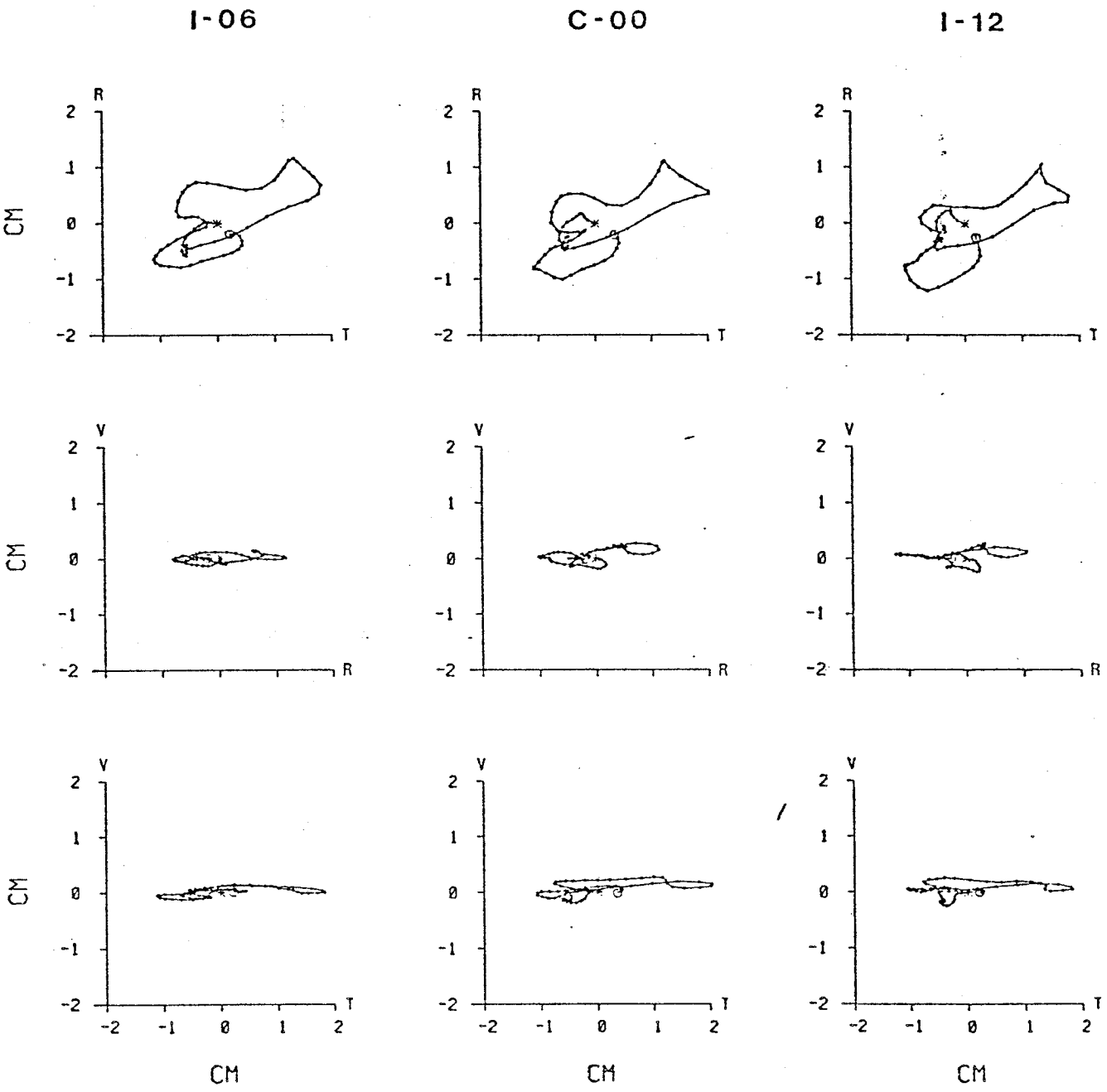

Figure 2. Particle motions of ground displacement (starting at the asterisk and ending at the circle) recorded at 3 array stations (I-06, C-00, I-12) spaced 200 m apart. The selected 3 secs of time history include the main S waves. R, T, and V denote radial, transverse and vertical directions.

VR plane is almost linear at all three stations. Because Rayleigh wave motion is generally retrograde elliptical this motion is probably mainly scattered P and direct SV waves. Variability of over 20 per cent is present in both principal axes.

Finally, the VT diagrams confirm that vertical displacements are relatively small and the ground particles are moving predominantly in a horizontal plane with the largest amplitudes in the transverse direction (SH or Love waves).

RATIO OF VERTICAL TO HORIZONTAL POWER

Wave number spectra for the whole array were analyzed from 1.0 to 8 Hz for a 4 sec time window about the P waves and a 5 sec time window about the S waves. The ratio of the peak power of the vertical to horizontal wave number spectra at various frequencies is shown in Table I. For the P wave window, the vertical power dominates above 4 Hz and for the S wave window the horizontal power dominates up to 5 Hz. Above 5 Hz in this window, the ratio of vertical to horizontal coherent power increases but, as mentioned earlier, there is very little coherent energy at these frequencies.

TABLE I

	Ratio of coherent power V/H	
Frequency	P waves	S waves
1.0	0.78	0.02
2.0	0.85	0.13
4.0	1.37	0.17
5.0	10.60	0.31
6.0	13.60	0.59
8.0	9.60	1.20

SPACIAL AVERAGES OF RESPONSE SPECTRA

A crucial proposal of N. Newmark was that when ground motions are spacially averaged over a structure with a large foundation, there is a decrease in peak (high frequency) acceleration. The reduction results essentially from interference dependent upon the phase lags of the Fourier components of the (horizontally) propagating waves. Array analysis allows a field measurement of this effect.

Consider the transverse ground motion at the adjacent stations C-00 and I-12 with separation comparable to large structural dimensions. Simple addition of the time histories shows a reduction of wave amplitudes for some (but not all) peaks and small phase shifts, particularly for the later (surface) waves. A more meaningful measure of Newmark's average (the "tau effect") is to compute the response of a single degree

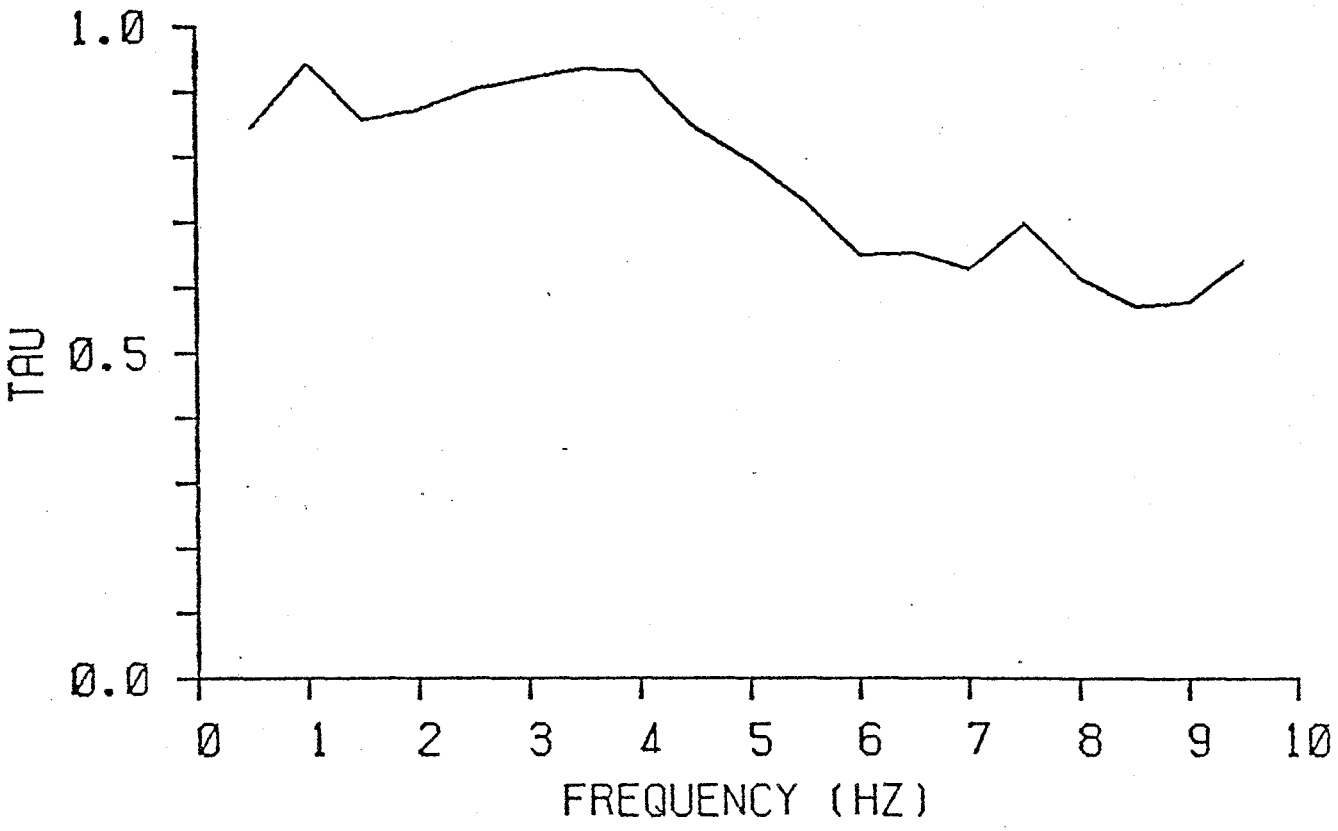

Figure 3. Response spectral ratio (tau) for the averaged response from stations C-00 and I-12 (separated by 200 m). The transverse component was used with a damping of 5 per cent.

of freedom damped oscillator at each station and average the resulting time histories at each oscillator frequency.

The reduction of the response spectrum due to such spacial averaging was computed and is shown in Fig. 3. For each oscillator frequency, the ratio of the averaged response spectrum to the maximum of either input response spectrum is plotted. Below 5 Hz the reduction is about 10 per cent. Above 5 Hz, the response spectrum is reduced by 30-40 per cent.

CONCLUDING REMARKS

The case examined indicates that coherent strong motions are present only up to 3 Hz for S waves and 5 Hz for P waves. An important conclusion is that subsurface structures can produce large changes in the apparent velocity (i.e. changes in angle of emergence) of waves over short distances. This can make prediction of the ratio of vertical to horizontally propagating waves difficult. Significant differences in wave propagation directions occur over short distances with significant rotational motion present. Further detailed results on ground rotation, wave scattering and spacial averages will be presented elsewhere.

REFERENCES

1. Bolt, B. A., C. H. Loh, J. Penzien, Y. B. Tsai, and Y. T. Yeh (1982). Preliminary report on the SMART 1 strong motion array on Taiwan, Report No. UCB/EERC-82/13.

2. Yeh, Y. T., C. B. Ou and C. C. Lin (1982). Determination of a local magnitude scale for Taiwan, Bull. Inst. Earth Sci. Academia Sinica, 2, 37-48.

3. Capon, J. (1969). High-resolution frequency-wave number spectrum analysis, Proc. IEEE, 57, 1408-1418.

PERFORMANCE OF SCHOOL CANOPIES DURING THE 10TH OCTOBER 1980 EL-ASNAM, ALGERIA EARTHQUAKE

J. F. Cartin (I)
Presenting Author: J. F. Cartin

SUMMARY

The performance of canopies in a school near El-Asnam, Algeria, during the earthquake of October 10, 1980, is studied primarily to determine the peak effective acceleration, *EPA*, of the earthquake capable of inducing the observed damage in the city of El-Asnam (Ref. 1). Although a small range of values for *EPA* (i.e., 0.28g to 0.35g) is determined for the two ground motions considered, many uncertainties exist in the determination and use of *EPA*. As the sole parameter by which the damaging potential of an earthquake is judged, the factor *EPA* can be extremely misleading.

INTRODUCTION

On October 10, 1980, a destructive earthquake of Richter magnitude (M) 7.2 occurred near El-Asnam, Algeria. The epicenter was about 10 km (6 mi) east of El-Asnam, with a focal depth of 10 km. The duration of the earthquake was between 35 and 40 seconds. No strong motion records of the main shock were obtained. Field estimates, however, place the peak ground acceleration at more than 0.40g (Ref. 2).

Although the effective peak acceleration, *EPA*, is a quantity theoretically associated with the damaging potential of a ground motion, the parameter has yet to be systematically defined. Blume (Ref. 3) defines *EPA* as "the acceleration which is fully effective in causing structures to respond, whereas any acceleration with a greater value is not effective at all." A detailed analysis of several canopies in a school located 5 km east of El-Asnam was performed in an attempt to ascertain first whether the value *EPA* could be determined and second whether that value represented the damaging potential of a ground motion.

In the series of nonlinear dynamic analyses conducted on these canopies, certain parameters for which no reliable information was available were varied. Due to a lack of data on the mechanical characteristics of the materials used and the sensitivity of the dynamic response of the building to the dynamic characteristics of the ground motion, the results described here should be viewed as crude estimates of *EPA*.

ANALYTICAL MODELING OF THE STRUCTURAL SYSTEM

The structural system of the school consisted of a row of four cylindrical columns supporting a very massive slab (3.50 x 19.45 meters in plan) at the top (Fig. 1). The canopies covered the corridors along and between the classrooms and were completely free of nonstructural components. The seismic response of the canopies thus depended solely on the bare simple structural system.

The structural failure of the canopies was triggered by the failure of the columns at their base in the transverse direction. This failure was, in turn, triggered by flexural yielding of the main reinforcement followed by crushing of the concrete and buckling of the longitudinal compressive steel bars. Some minor damage occurred throughout the columns, especially at the top. The roof of the canopy sustained no damage and the foundation apparently did not move during the shaking, i.e. the foundation behaved as a rigid system. The structural system is illustrated in Fig. 1 and is mechanically idealized as shown in Fig. 2, where: L equals 2.67 m; M (concentrated mass at the roof) equals 1.17 ton-sec^2/m; $\bar{m}$ (distributed mass of the columns) equals 0.0023 (ton-sec^2/m)/m; I_0 (mass moment of inertia of roof) equals 1.23 ton-sec^2-m; EI_{uc} (flexural stiffness of uncracked, transformed cross section of column) equals 1843 ton-m^2; and EI_{cr} (cracked transformed cross section of the column) equals 769 ton-m^2.

(I) Graduate Student/Research Assistant, University of California, Berkeley.

Preceding page blank

While the degrees of freedom of this idealized system are infinite, it can, due to the relatively small value of the mass distributed throughout the column ($\overline{m}$) compared with the mass concentrated at the top of the canopy (M), be adequately represented by an equivalent two-degree-of-freedom system (2D0F), v_1 and v_2, in which the translational and rotational masses are considered to be concentrated at the top of the column of the canopy (Fig. 2). Studies were also conducted in which a single degree of freedom (SDOF) was considered, i.e. v_1 alone.

ESTIMATION OF MECHANICAL (DYNAMIC) CHARACTERISTICS

Mechanical Characteristics of Structural Materials

The canopies were constructed of reinforced concrete. No testing data or design values used for the concrete or the reinforcing steel strengths were available. Based on visual observations of these materials and on conversations with those involved in the construction, the following probable mechanical characteristics were assumed.

1) **Concrete Stress-Strain Relationships.** The following upper and lower bound values for 28-day cylinder strength of the concrete, f_c', were assumed. Case 1: $f_c' = 2100\ t/m^2$; Case 2: $f_c' = 1750\ t/m^2$. The Park-Kent concrete stress-strain curves were used to derive the confined and unconfined curves for both types of concrete (Refs. 4 & 5).

2) **Reinforcing Steel Stress-Strain Relationships.** The following upper and lower bounds for the stress at yield, f_y, were assumed: Case 1: $f_y = 35000\ t/m^2$; Case 2: $f_y = 28000\ t/m^2$.

Although analyses were performed for all combinations of the values given above, the predicted values reported here are those for Case 2, considered to be the more realistic.

Computed and Idealized Moment-Curvature (M-Φ) Relationships of Column Cross Sections

Numerical computations of the M-Φ relationships were conducted using the RCCOLA computer program (Ref. 6), in which the variations of mechanical characteristics stated above and the effect of the following parameters were considered:

1) **Axial Load P.** Since the weight tributary to each of the columns of the canopy was approximately 12 tons, and since the vertical component of the ground motion was estimated to be as high as 1.0g (Ref. 2), the M-Φ curves were calculated for axial loads of 0, 12, and 24 tons. From these curves it was concluded that the effect of axial force on the M-Φ relation could be neglected. A value for P of 12 tons was assumed in subsequent analyses.

2) **Cover Thickness.** The effect of two cover thicknesses, $d' = 0.043$ and 0.056m (where d' is the distance from the center of the longitudinal steel reinforcement to the outside edge of the concrete on the same side of the section), on the behavior of the column was investigated. The main effect of an increase in cover is a decrease in moment yielding and maximum flexural strength of less than 10% (Fig. 3). A value of 0.056m was subsequently used for d'.

The moment rotation capacity rather than the moment-curvature relation of critical regions of reinforced concrete structures is important in determining seismic response. Because the spacing of the circular hoops (0.18m) was larger than the maximum 0.10m permitted by the 1982 UBC [Ref. 7] for seismic zones 3 and 4, and even larger than the eight-bar diameter allowed for buckling (0.15m), the possibility of premature buckling after the confined concrete of the cover shell had spalled had to be considered. In the few canopy columns that remained standing, there was evidence that the bars may just have begun to buckle. The moment-rotation relation, M-Θ, along a region of length l along which the bar could buckle was determined assuming that the moment and curvature along the critical region were constant: $\Theta = \Phi l$. The M-Φ at which buckling would be initiated is illustrated in Fig. 3. The curvature at which buckling would begin was not uniquely determined. Instead, a range of values was obtained which bounded the uncertainty: somewhere between the start of spalling of the concrete shell and the initiation of strain hardening of the steel. However, it was believed that buckling would initially occur at a point closer to the first value: spalling of the concrete shell.

The M-Φ relation was idealized in order that it might be used as input data for the DRAIN-2D computer program (Ref. 8). The elastic/perfectly plastic idealization seemed

reasonable for the range of curvatures investigated. No increase in moment due to strain hardening was considered since buckling of the longitudinal compressive steel bars occurred before then. For the idealized M-Φ curve, the linear elastic stiffness, EI, was estimated to be 769 $t-m^2$ and the maximum moment was 9.24 $t-m$.

Shear Strength of Column

The resistance to shear, V, depends on the shear strength provided by the concrete, V_c, and by the shear reinforcement, V_s. When these two quantities were considered, the available shear strength was found to be considerably higher than the shear demand from the lateral force required to induce flexural failure. However, the 1982 UBC specification, 2626(f)5, requires that the contribution of concrete be neglected when $P_e/A_g < 0.12f_c'$. The columns considered here should thus fail in shear even before yielding begins. Damage in the standing canopies and the type of failure observed in the collapsed canopies revealed that the failure was due to flexural yielding and not to shear. Therefore, although according to present UBC recommendations the shear strength should have controlled the failure, shear was not considered to be a problem.

Damping Ratios and Periods of the Canopy

A damping ratio, ξ, of 2% for the first mode of vibration was chosen since only a simple bare R/C structural system was vibrated. Studies in which ξ was set equal to 5% were also conducted.

When a SDOF system was assumed, the period of the structure was computed using Rayleigh's Method (Ref. 9), and assuming a first mode shape. When the 2DOF system (Fig. 2) was considered, the analyses yielded values for the first mode similar to that computed for the equivalent SDOF system. For the 2DOF system, the following values of T were estimated: 1) $T_1 = 0.46$ sec. and $T_2 = 0.11$ sec. when the column stiffness was computed on the basis of the uncracked, transformed section, EI_{uc}; and 2) $T_1 = 0.72$ sec. and $T_2 = 0.18$ sec. when the column stiffness was computed on the basis of the cracked, transformed section, EI_{cr}. Since the canopy was assumed not to have been cracked significantly prior to the earthquake, a value of T equal to 0.50 sec. was used to estimate the peak ground acceleration (PGA).

ANALYSES TO ESTIMATE THE EFFECTIVE PEAK ACCELERATION (EPA)

Introductory Remarks

Generally, EPA is less than the peak recorded acceleration, PGA, because acceleration pulses of high value but short duration have little effect on the response of most structures, and also because for structures strained into the inelastic range, the number and order of the acceleration peaks, as well as the duration of these pulses and the ground motion, rather than the peak itself, greatly influence damage (Ref. 10).

Besides the estimation of period, damping, and structural mass, as discussed above, the following problems were encountered in estimating EPA:

1) **Type of Ground Motion.** This is probably the main uncertainty in determining EPA. In this study, two types of earthquake were considered to represent the demands of inelastic deformation: the El Centro 1940 S00E and Derived Pacoima Dam 1971 S16E earthquake records. For the demands of inelastic deformation and for structures with $T > 0.4$sec., the El Centro record may be considered a lower bound. Its major effect is thus to amplify the response of these structures by a resonance phenomenon. The Derived Pacoima Dam record is of the impulsive type (intense and long-duration acceleration pulses) and is considered an upper bound on inelastic deformation.

2) **Idealization of Lateral Resistance Function**: R vs. v_1. Estimated M-Φ diagrams (Fig. 3) were used to predict the idealized linear elastic/perfectly plastic lateral resistance functions, R versus v_1, of the canopies (Fig. 4). The range of values of maximum displacement v_u used for these estimates was controlled by the buckling of the longitudinal compressive steel (0.088m - 0.160m). Buckling was assumed to occur approximately at $v_u = 0.10$m.

3) **Displacement Ductility (μ_δ) Determination.** a) *Modified Park and Paulay Approach* (Ref. 5). These authors offer an approximate solution for the relationship between curvature ductility and displacement ductility ratio for a cantilever column with a lateral load at the end. The solution involves an assumed curvature distribution and an estimated length of plastic region, L_P. This approach was modified to include the influence of the top moment on the displacement ductility. Considering the initiation of buckling to be when spalling of the concrete cover occurred, Φ_u = 0.0898 rad/m and a value of μ_δ = 5.0 was determined. B) *Alternative Approach.* The canopies underwent a lateral displacement of at least 0.15m, the distance that separated the canopies and the adjacent classrooms, without failure. With this displacement assumed as an upper bound on v_u and using v_y = 0.029m (Fig. 4), μ_δ = 5 was estimated.

Estimation of EPA

Although different approaches can be used to estimate *EPA*, the approach presented in this paper involves three stages:

First Stage: Procedure Proposed by V. V. Bertero, S. A. Mahin, and R. A. Herrera. The maximum *PGA* is estimated from the charts developed by Bertero *et al.* (Ref. 11). For a given or selected ground motion, it is necessary to determine first the coefficient η which depends on the known or estimated values of period, damping, and displacement ductility (Fig. 5). The value of *PGA* is then computed directly from the following equation:

$$\eta = \frac{C_y}{|PGA|/g} = \frac{R_y}{m|PGA|}$$

For calculated values of m = 1.20 tons-sec^2/m, R_y = 3.46 tons, C_y = 0.29, and T = 0.50 sec, values of *PGA* equal to 0.55g and 0.35g for the El Centro and Derived Pacoima Dam records, respectively, were obtained.

Second Stage: Verification of PGA by DRAIN-2D. In the second stage, an inelastic dynamic computer program, such as DRAIN-2D (Ref. 8), is used to perform a series of time-history analyses for the earthquake motions normalized to values of *PGA* close to those values found in the first stage of the study. Both SDOF and 2DOF models were used.

For the SDOF model and *EI* approximately equal to that for a cracked section, a maximum displacement of approximately 0.10m was obtained for both the El Centro motion normalized to 0.55g and the Derived Pacoima Dam motion normalized to 0.35g (see Table 1). For the 2DOF model, the Derived Pacoima Dam motion of 0.35g also yields this value, but the El Centro 0.55g motion yields only 0.07m. These results indicate that the Bertero *et al.* charts yield good results for SDOF models, but that they do not work well for 2DOF systems, particularly for earthquake motions such as the El Centro motion. They also indicate that a 2DOF model is needed for further inelastic dynamic analyses.

TABLE 1 MAXIMUM LATERAL DISPLACEMENT, v_u

TYPE OF EARTHQUAKE	MODEL	EI (t–m^2) (cracked)	v_u (m)
El Centro 1940 (normalized to 0.55g)	SDOF	769	0.106
	2 DOF	769	0.070
Derived Pacoima Dam (normalized to 0.35g)	SDOF	769	0.105
	2 DOF	769	0.100

The results of the analyses show that to attain a v_u of 0.10m, the *PGA* should be close to 0.35g for the normalized Derived Pacoima Dam record and 0.65g for the normalized El Centro 1940 record.

Third Stage: Estimation of EPA by the "Clipping" Method. In the third stage, DRAIN-2D was used to carry out analyses assuming the two earthquake ground motions discussed above, but clipping the peak accelerations of these motions in order to study the influence that such "clipping" has on the response of the canopies.

By analyzing variations in the time-histories of the ground motions and the displacement response, the time at which the maximum displacement occurred can be determined and the peak of ground motion at which this displacement was produced can be identified. It is then possible to estimate how much the ground acceleration record can be clipped in order not to decrease the maximum response of the canopy.

The maximum top displacement of the canopy does not necessarily occur when the unclipped ground motion is used as input. When the peak ground accelerations that are clipped occur before the pulses inducing the maximum v_u, the clipping operation might modify the response of the structure in such a way that the particular values of the response at the time that the critical pulses begin favor the increase of the displacement due to these pulses. The acceleration clipping should be continued until the maximum displacement begins to decrease. The clipped (or unclipped) acceleration at which the maximum displacement occurred is considered the *EPA* for the case under consideration and for the specified earthquake. The effects of clipping are illustrated in Fig. 6 and in Table 2 the effect of clipping on the maximum lateral displacement response is summarized.

TABLE 2 EFFECT OF CLIPPING EL CENTRO NORMALIZED TO 0.55g & DERIVED PACOIMA DAM NORMALIZED TO 0.35g ON DISPLACEMENT RESPONSE OF THE CANOPY

DESCRIPTION OF EARTHQUAKE	PEAK CLIPPED ACCELERATION	MAXIMUM v_u TIME (sec)	v_u (m)
EL Centro 1940	0.55g	2.01	0.070
normalized	0.32g	5.38	0.098
to 0.55g	0.28g	5.38	0.104
	0.22g	5.37	0.101
Derived Pacoima Dam	0.35g	3.65	0.100
normalized to 0.35g	0.30g	3.65	0.089

For the Derived Pacoima Dam record normalized to 0.35g, any clipping of the ground acceleration decreases the lateral displacement response. Therefore, the *EPA* is 0.35g. The lateral displacement response increases, however, when the El Centro record is clipped, in this case from 0.070m (for the unclipped record normalized to 0.55g) to 0.104m when the record normalized to 0.55g is clipped to 0.28g. Since this value of v_u is close to 0.10m, the value sought, it was not necessary to increase the normalization of the El Centro record to, say, 0.65g as had been predicted in the second stage of the analysis.

In summary, for the El Centro record normalized to 0.55g, a value of 0.28g was estimated for the *EPA*. For the Derived Pacoima Dam record normalized to 0.35g, the predicted *EPA* equaled 0.35g.

SUMMARY AND CONCLUSIONS

1) A 2DOF model, rather than a SDOF system, must be considered.

2) Among the parameters that affect *EPA* are: a) the idealization of the lateral resistance function (which in turn depends on assumed material properties, concrete cover, axial load, buckling of longitudinal compressive steel bars, and fixed-end rotation, among other factors); b) model idealization (SDOF or 2DOF); c) period and damping, and d) ground motion characteristics.

3) Because the assumed recorded ground motions did not produce the observed response, these ground motions must be normalized to values of *PGA* as determined in the first two stages of the investigation. The values of *EPA* determined in the present investigation (i.e., 0.28g and 0.35g for the El Centro and Derived Pacoima Dam earthquake motions) were therefore derived from clipping distorted records, due to the normalization of *PGA* to 0.55g and 0.35g. In other words, the originally recorded El Centro record unnormalized with *PGA* equal to 0.35g produces low values of canopy displacement and therefore would not have resulted in

the observed damage, i.e. collapse of the canopy. Also, depending on the stiffness *EI* used in the analysis (and thus on the period), the *EPA* was or was not equal to the *PGA*. The amount of clipping therefore depends on the normalization of an earthquake.

4) The results obtained indicate that for the two assumed types of ground motion, the *EPA* needed to induce the observed damage is in the range 0.28g to 0.35g. This small range is apparently fortuitous given the wide range of the parameters that affect the result. Generally, *EPA* depends both on the type of earthquake considered and on the interaction of the dynamic ground motion characteristics and the soil-foundation-structure system. Furthermore, *EPA* will depend on the limit state under consideration. Although the use of *EPA* can provide an idea of the relative damaging potential of a given ground motion, its use as the sole parameter to define this damaging potential can be very misleading.

ACKNOWLEDGMENTS

The research on which this report is based was supported by the National Science Foundation under Grant No. CEE-81-10050 and has been carried out under the supervision of Prof. V. V. Bertero of the University of California at Berkeley. The assistance of Mary Edmunds and Richard Steele in producing the illustrations is greatly appreciated.

REFERENCES

(1) J. F. Cartin and V. V. Bertero, "Performance of School Canopies During the 10th October 1980 El-Asnam Earthquake, Algeria," *Master of Engineering Thesis*, Dept. of Civil Engrg, Univ. of California, Berkeley (in preparation).

(2) V. V. Bertero and H. Shah (coordinators) *et al.*, "El-Asnam, Algeria Earthquake October 10, 1980: A Reconnaissance and Engineering Report," Nat'l Research Council, Committee on Nat'l Disasters, Engineering Research Institute with support from the National Science Foundation, Berkeley, California (1983).

(3) J. A. Blume, "On Instrumental Versus Effective Acceleration and Design Coefficients," *Proceedings*, The 2nd Nat'l Conference on Earthquake Engineering, Stanford University, Stanford, California, pp. 868-882 (1979).

(4) D. C. Kent and R. Park, "Flexural Members with Confined Concrete," *Journal of the Structural Div.*, Am. Soc. of Civil Engineers, Vol. 97, ST7, July 1971.

(5) R. Park and T. Paulay, *Reinforced Concrete Structures*, John Wiley & Sons, Inc., New York (1975).

(6) S. A. Mahin and V. V. Bertero, "RCCOLA—A Computer Program for Reinforced Concrete Column Analysis—User's Manual and Documentation," Dept. of Civil Engrg, NISEE, Univ. of California, Berkeley (1977).

(7) *Uniform Building Code*, Internat'l Conference of Bldg Officials, Whittier, California (1982).

(8) A. E. Kannan and G. H. Powell, "DRAIN-2D—A General Purpose Computer Program for Dynamic Analysis of Inelastic Plane Structures with User's Guide," *Reports No. EERC 73-6 & EERC 73-22*, Earthquake Engrg Research Ctr, Univ. of California, Berkeley (1973 & 1975).

(9) R. W. Clough and J. Penzien, *Dynamics of Structures*, McGraw-Hill, Inc., 1975.

(10) V. V. Bertero, "Implications of Recent Research Results on Present Methods for Seismic Resistant Design of R/C Frame-Wall Building Structures," *Proceedings*, 51st Annual Convention, SEAOC, California (1982).

(11) V. V. Bertero, S. A. Mahin, and R. A. Herrera, "Aseismic Design Implications of Near-Fault San Fernando Earthquake Records," *Earthquake Engrg and Structural Dynamics*, Vol. 6, 31-42 (1978).

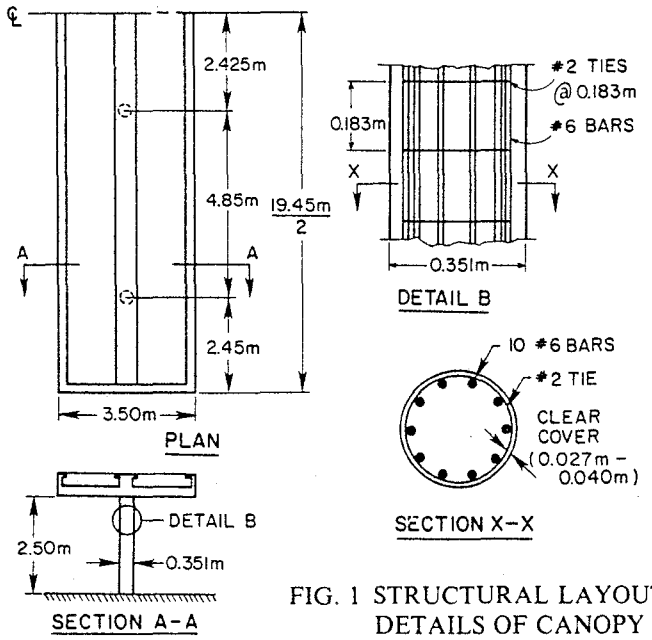

FIG. 1 STRUCTURAL LAYOUT & DETAILS OF CANOPY

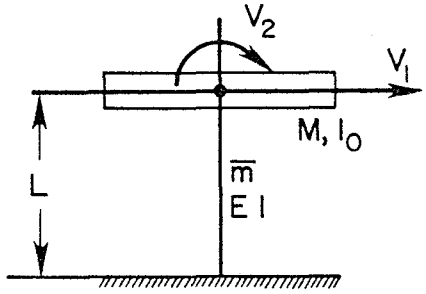

FIG. 2 ANALYTICAL MODEL OF CANOPY

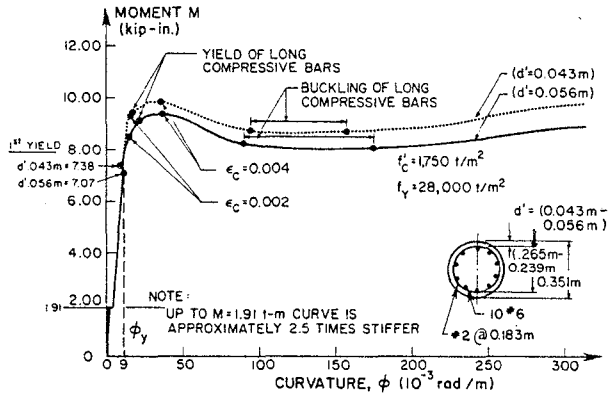

FIG. 3 EFFECT OF COVER THICKNESS ON M-Φ RELATION OF COLUMN CROSS SECTION UNDER $P = 12t$

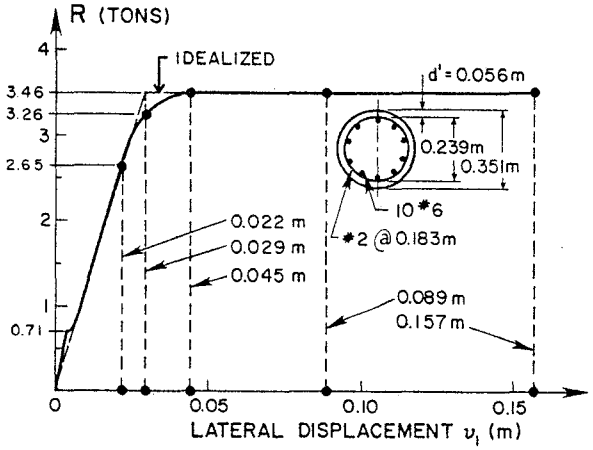

FIG. 4 LATERAL RESISTANCE FUNCTION, R vs. V_I

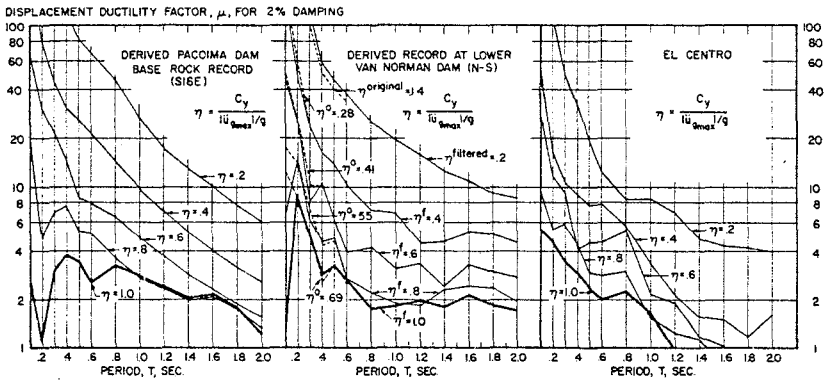

FIG. 5 INELASTIC RESPONSE SPECTRA FOR 2% DAMPING

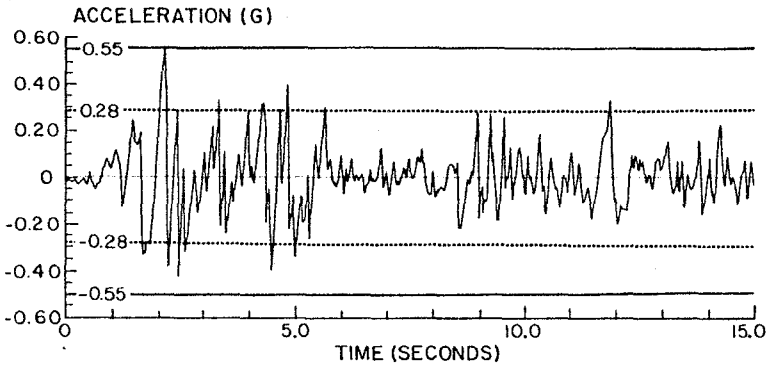

(a) EL CENTRO 1940 NORMALIZED TO 0.55g

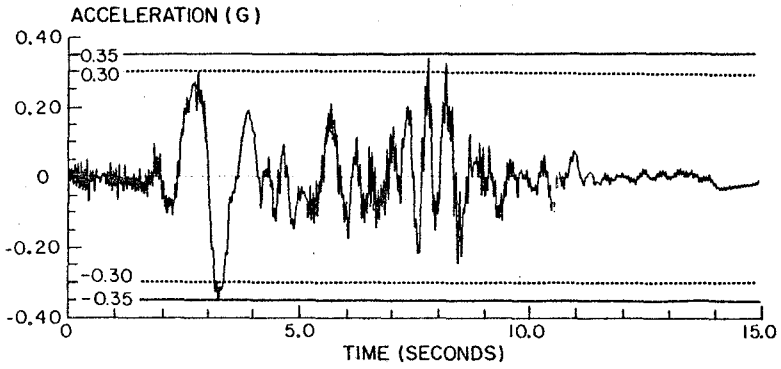

(c) DERIVED PACOIMA DAM NORMALIZED TO 0.35g

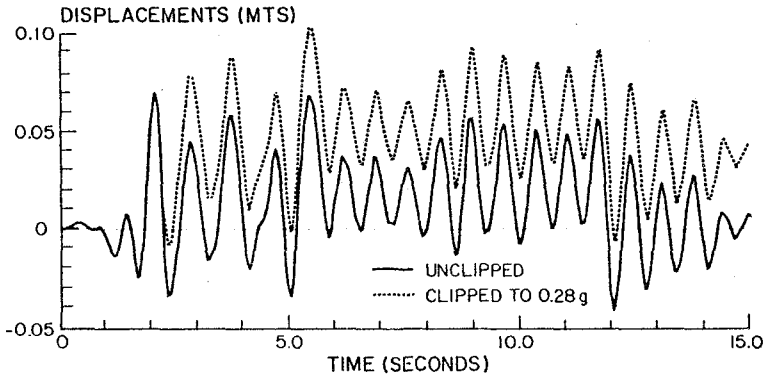

(b) DISPLACEMENT RESPONSE OF CANOPY TO EL CENTRO NORMALIZED TO 0.55g: UNCLIPPED & CLIPPED TO 0.28g

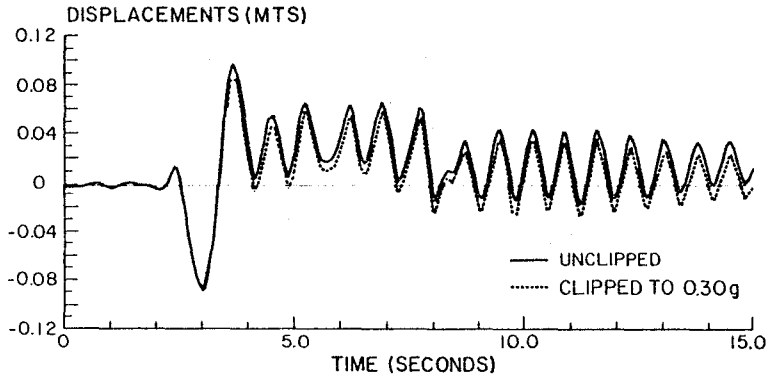

(d) DISPLACEMENT RESPONSE OF CANOPY TO DERIVED PACOIMA DAM NORMALIZED TO 0.35g: UNCLIPPED & CLIPPED TO 0.30g

FIG. 6 EFFECT OF CLIPPING EL CENTRO NORMALIZED TO 0.55g & DERIVED PACOIMA DAM NORMALIZED TO 0.35g ON DISPLACEMENT RESPONSE OF CANOPY

EVALUATION OF SIMPLIFIED EARTHQUAKE ANALYSIS PROCEDURES FOR INTAKE-OUTLET TOWERS

Anil K. Chopra (I)
Ka-Lun Fok (II)
Presenting Author: Ka-Lun Fok

SUMMARY

The internal forces in uniform and tapered intake-outlet towers induced by earthquake ground motion, characterized by a smooth design spectrum, are computed for a range of fundamental vibration period by modal analysis and by the Montes-Rosenblueth procedure. Based on these results it is shown that the latter procedure is excessively conservative in many cases. The limitations of other available simplified analysis procedures, and the requirements for a reliable but simple analysis procedure for preliminary design of towers are identified.

INTRODUCTION

Intake-outlet towers should be designed to elastically resist the relatively frequent moderate intensity earthquakes; and may be permitted to yield significantly, but without collapse, in the event that very intense ground shaking occurs. An approximate analysis procedure that considers only the most important effects in the earthquake response of towers, and yet is simple to apply, is required in the preliminary stages of elastic design. The available simplified analysis procedures (Refs. 1-3) are evaluated in this paper.

VIRTUAL MASS OF TOWER

It has been established that the effects of surrounding water (Fig. 1) on dynamics of towers may be approximately represented by the added mass shown in Fig. 2 (Ref. 4). The virtual (or total) mass of the tower is

$$m(z) = m_o(z) + m_i(z) + m_a(z) \qquad (1)$$

in which $m_o(z)$ = the mass of the tower by itself, $m_i(z)$ = the mass of water inside the tower, and $m_a(z)$ = the added mass due to interaction with surrounding water.

The added mass $m_a(z)$ presented in Fig. 2 is for cylindrical towers with a circular cross-section for a range of values of the ratio r_o/H, in which r_o = the outside radius; and H = the depth of surrounding water. Strictly speaking these results are valid only for towers with radius r_o constant over height; however they are even useful for towers with a variable radius. It is recommended that the added mass at any location, z, above the base be computed from the curve for $r_o/H = r_o(z)/H$ pertaining to that location. This simply obtained approximate value checks well with accurate solutions based on a finite element analysis of the fluid domains surrounding variable-radius towers (Ref. 5).

(I),(II) Prof.& Grad.Student, Dept.of Civil Engrg., Univ.Calif,Berkeley,CA.USA

The inside water is treated as moving rigidly with the tower, an appropriate idealization for slender towers.

MODAL ANALYSIS

The earthquake analysis of a free-standing tower partially submerged in water proceeds in the standard manner, with its mass defined by the virtual mass m(z) instead of just its own mass $m_o(z)$. Thus, the maximum response of a tower to earthquake ground motion can be estimated from the design (response) spectrum corresponding to the ground motion by the following procedure:

1. Define structural properties: compute virtual mass m(z) and flexural stiffness EI(z); and estimate modal damping ratios ξ_n.
2. Compute the frequencies ω_n, periods $T_n = 2\pi/\omega_n$, and mode shapes $\phi_n(z)$, n = 1, 2,..., of several natural modes of vibration of the tower.
3. Compute the maximum response in individual modes of vibration by repeating the following steps for the lower modes of vibration:
   (a) Corresponding to period T_n and damping ratio ξ_n, read the ordinate S_{an} of the pseudo-acceleration from the design spectrum.
   (b) Compute equivalent lateral forces from

$$f_n(z) = (L_n/M_n)\, S_{an}\, m(z)\phi_n(z) \tag{2}$$

   where $L_n = \int m(z)\phi_n(z)dz$ and $M_n = \int m(z)\phi_n^2(z)dz$.

   (c) Compute the shear V_n and moment M_n at any section by static analysis of the tower subjected to the equivalent lateral forces:

$$V_n(z) = \int_z^{H_s} f_n(\zeta)d\zeta \; ; \quad M_n(z) = \int_z^{H_s} f_n(\zeta)(\zeta - z)d\zeta \tag{3}$$

4. Determine an estimate of the maximum shear V(z) and moment M(z) at any section by combining the modal maxima $V_n(z)$ and $M_n(z)$ in accordance with the following equation:

$$V(z) \doteq \sqrt{\sum_n V_n^2(z)} \quad ; \quad M(z) \doteq \sqrt{\sum_n M_n^2(z)} \tag{4}$$

MONTES-ROSENBLUETH PROCEDURE

This is a simplified analysis procedure developed by Montes and Rosenblueth for estimating earthquake forces in chimneys (Ref. 3). By using the virtual mass m(z) to define the mass, the procedure can be applied to free-standing intake-outlet towers in the following steps:

1. Construct two envelopes of the design spectrum: (a) flat spectrum and (b) hyperbolic spectrum with cut-off, as shown in Fig. 3. The ordinate of the flat spectrum, which represents a constant pseudo-acceleration, is equal to the maximum value over all periods less than the fundamental period T_1. The hyperbolic spectrum, which represents pseudo-acceleration varying with period as a hyperbola or a constant pseudo-velocity, passes through the ordinate of the design spectrum at T_1; the spectrum is cut-off to a flat branch for all periods less than $T_1/10$.

2. Compute shears and moments in the tower associated with the flat spectrum from the following equations:

$$V(z) = 0.647(\tilde{S}_{a1}/g)W[1 - (z/H_s)^3] \tag{5a}$$

$$M(z) = 0.461(\tilde{S}_{a1}/g)WH_s[1 - (z/H_s)]^{3/2} \tag{5b}$$

where $\tilde{S}_{a1}$ is the maximum value of $S_a(T)$ over periods less than T_1 and W is the total, virtual weight of the tower.

3. Compute shears and moments in the tower corresponding to the hyperbolic spectrum with cut-off from the following equations:

$$V(z) = 1.553(S_{a1}/g)W\{[1 - (z/H_s)^2]^{1/2} - 6.25(z/H_s)^2[1 - (z/H_s)]^2\} \tag{6a}$$

$$M(z) = 0.519(S_{a1}/g)WH_s[1-(z/H_s)] \tag{6b}$$

4. The M-R (Montes-Rosenblueth) estimate of the shear (and moment) at any section is provided by the smaller of the two values for the shear (and moment) obtained in steps 2 and 3 (Fig. 4).

The approximate expressions for shear and moment in steps 2 and 3 were obtained in Ref. 3 from results of analysis of uniform towers for the two idealized spectra mentioned above. The M-R estimates are equal for two towers with the same total weight, independent of the weight and stiffness distribution.

PRESENTATION AND DISCUSSION OF RESULTS

The two types of towers analyzed are: (a) Uniform towers with mass per unit height $m(z) = m$ and flexural stiffness $EI(z) = EI$, both constant over height; and (b) tapered towers with mass and stiffness decreasing linearly from the base (z=0) to the top (z=H) with $m(H) = m(0)/9$ and $EI(H) = EI(0)/10$. The latter represents an extreme taper, more than usually encountered in real towers, chosen to cover all practical cases and, in part, to indirectly and roughly consider the variation in virtual mass that would be introduced by the added mass (Fig. 2). For the limited objectives of this paper, it is not necessary to explicitly include the added mass $m_a(z)$ and the virtual, total mass m(z) is defined directly as described above.

The parameters selected for the ground motion are: maximum acceleration $\bar{a}_g$, velocity $\bar{v}_g$, and displacement $\bar{d}_g$ = 1g, 48in/sec, and 36in., respectively. Starting with these parameter values, the design spectrum is constructed by the procedures of Ref. 6 for 5% damping ratio and 84.1 percentile level of response (Fig. 5). The response results are presented in dimensionless form so that they are valid for ground motions of any intensity, provided $\bar{a}_g$, $\bar{v}_g$, and $\bar{d}_g$ are in the ratio 1g:48in/sec:36in.

The internal forces (shears and moments) in two types of towers induced by earthquake ground motion characterized by the design spectrum of Fig. 5 were computed for a range of fundamental vibration periods by modal analysis and by the Montes-Rosenblueth Procedure. The natural frequencies and mode shapes of vibration required in modal analysis are available in text books as standard results for a uniform cantilever. For the tapered tower they were obtained by the Rayleigh Ritz method with the shape functions selected as the

mode shapes of a uniform tower. The variation of shears and moments with height in uniform towers with different fundamental vibration periods are presented in Fig.6; similar results for tapered towers are presented in Fig. 7. For three selected values of fundamental period T_1, the heightwise variation of shears and moments obtained by modal analysis and by Montes-Rosenblueth (M-R) procedure are presented in Figs.8-10 for uniform towers and in Figs.11-13 for tapered towers. The variation of base shear and moment with fundamental vibration period, obtained by the two analysis procedures, is presented in Figs. 14 and 15.

These response results demonstrate that the M-R estimates for shears and moments are reasonably good only for uniform towers with fundamental vibration period which is either rather long, near the long-period end of the constant pseudo-velocity branch of the spectrum; or short enough to fall on the constant pseudo-acceleration branch of the spectrum. In the first case, the M-R estimate is controlled by eq.6 associated with the hyperbolic spectrum; and in the latter case by eq.5 associated with the flat spectrum. At intermediate-periods the M-R estimate is excessively large, because the response is affected by both types of spectra, a situation illustrated in Fig. 4. The mass and stiffness distribution over height does not enter into the M-R estimate for shears and moments; only the total weight enters into eqs.5 and 6. When presented in dimensionless form the M-R estimate is thus identical for uniform and tapered towers. However, the results of modal analysis demonstrate that the dimensionless responses of a tapered tower are much smaller than those of a uniform tower. Thus the M-R estimate for the response of tapered towers is excessively conservative over the entire period range.

The presented response results demonstrate that, over a wide range of fundamental periods, excellent results for shears and moments in towers are obtained by considering only the first two vibration modes in modal analysis. For short period towers, with fundamental period shorter than the value at the corner of constant pseudo-acceleration and constant pseudo-velocity branches of the spectrum, only the first mode contributes significantly to the forces, and even the second mode need not be included. For towers with longer vibration periods, the one-mode analysis recommended in Ref.1 is inadequate because the second mode has significant contributions. The second mode response should be explicitly considered because, contrary to what was suggested in Ref.2, it can not be satisfactorily approximated by simply increasing the first mode response.

REFERENCES

1. Chopra & Liaw, J. Struct. Div, ASCE, 101, ST7, 1975, 1349-1366.
2. Chopra & Liaw, Proc. U.S. Japan Seminar...Lifeline Systems, Tokyo, 1976, 381-397.
3. Montes & Rosenblueth, "Cortantes y Momentos Sismicas en Chimeneas,"Segundo Congreso Nacional de Ingenieria Sismica, Veracruz, Mexico, 1968.
4. Liaw & Chopra, Int. J. Earthq. Engng. Struct. Dyn., 3, 1974, 33-49.
5. Liaw & Chopra, Int. J. Earthq. Engng. Struct. Dyn., 3, 1975, 233-248.
6. Newmark & Hall, Chapter 29-Part I in Shock and Vibration Handbook (Ed: Harris & Crede), McGraw-Hill, 1976.

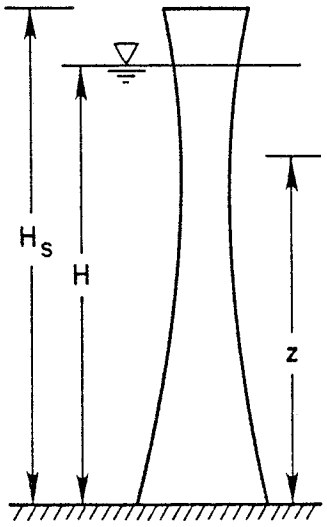

Fig. 1 Tower Submerged in Water.

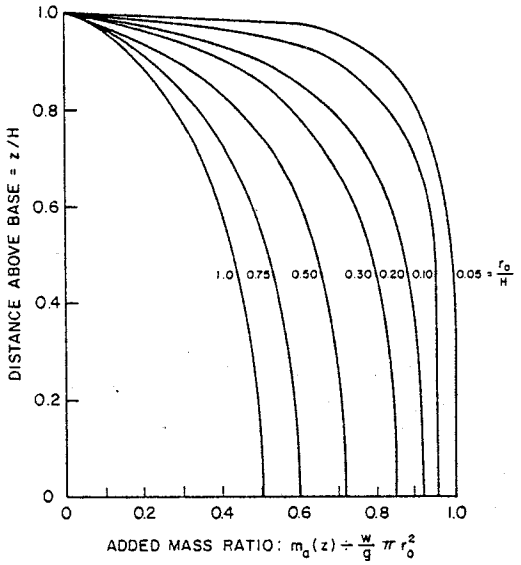

Fig. 2 Added-mass Representing Hydrodynamic Effects.

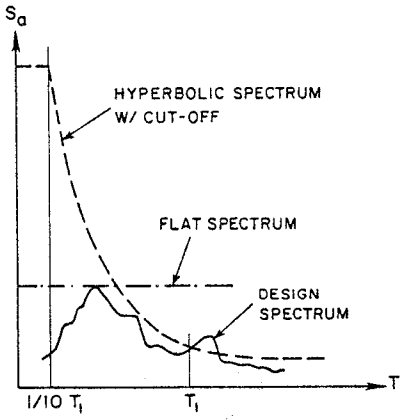

Fig. 3 Envelopes of Design Spectrum.

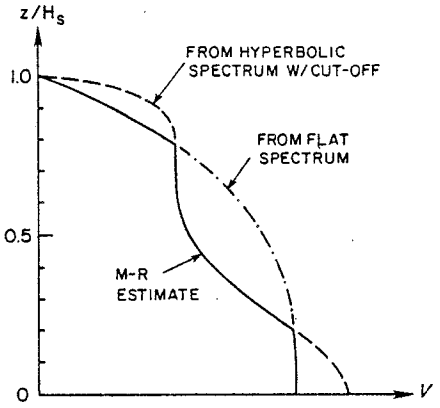

Fig. 4 Explanatory Sketch to Obtain M-R Estimate of Shears.

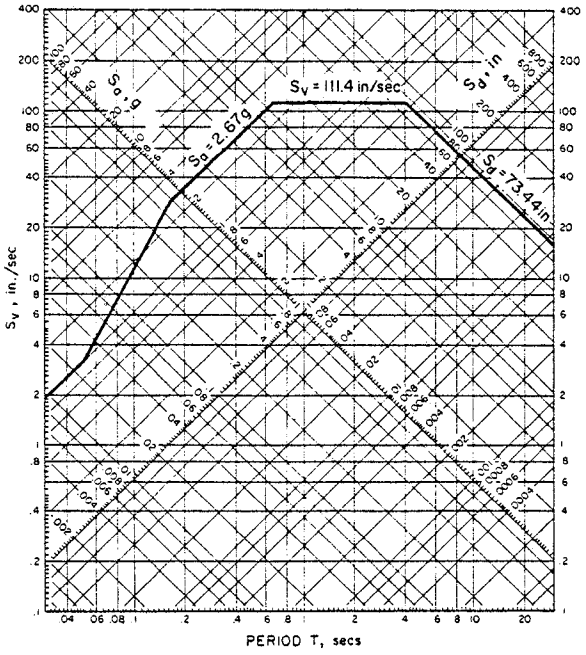

Fig. 5 Earthquake Design Spectrum.

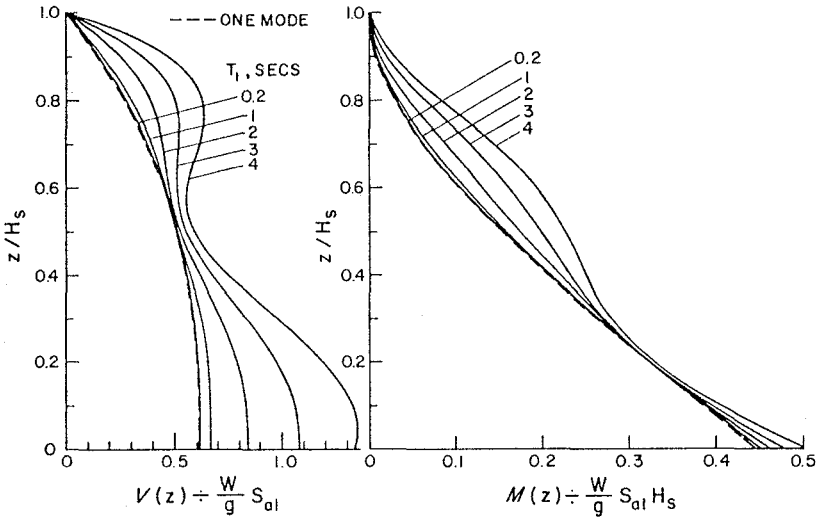

Fig. 6 Heightwise Variation of Shears and Moments in Uniform Towers.

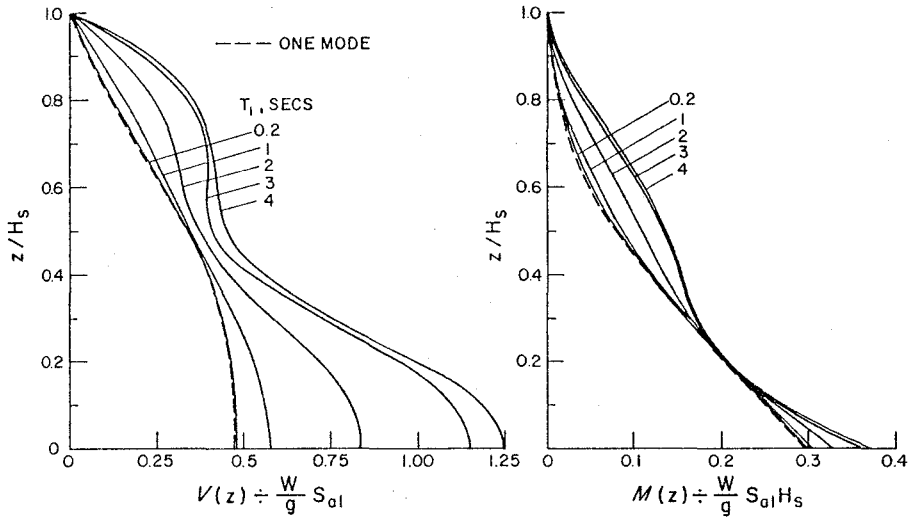

Fig. 7 Heightwise Variation of Shears and Moments in Tapered Towers.

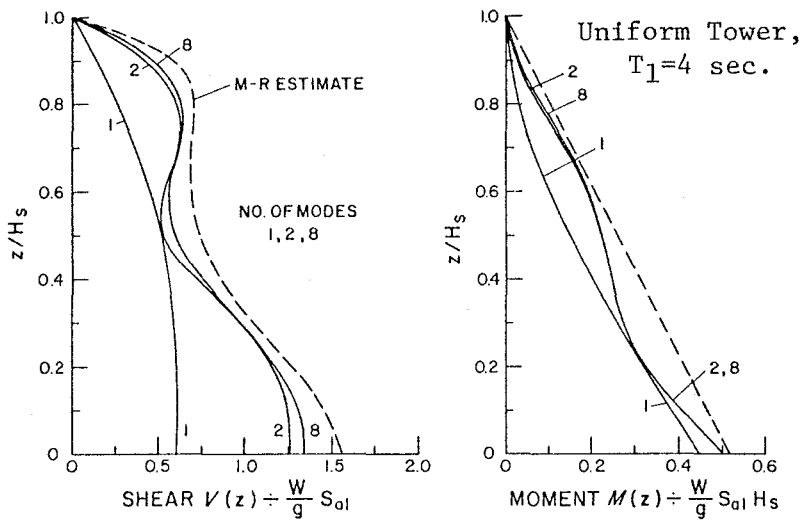

Fig. 8 Comparison of Shears and Moments from Modal Analysis and M-R procedure.

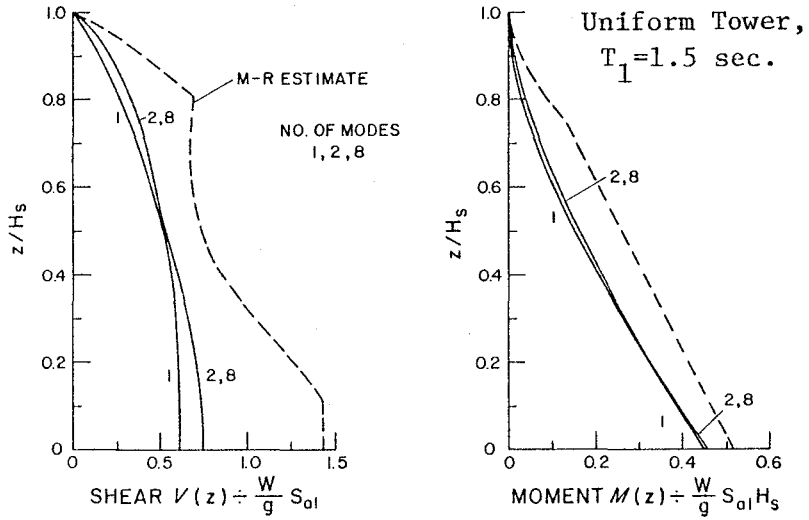

Fig. 9 Comparison of Shears and Moments from Modal Analysis and M-R Procedure.

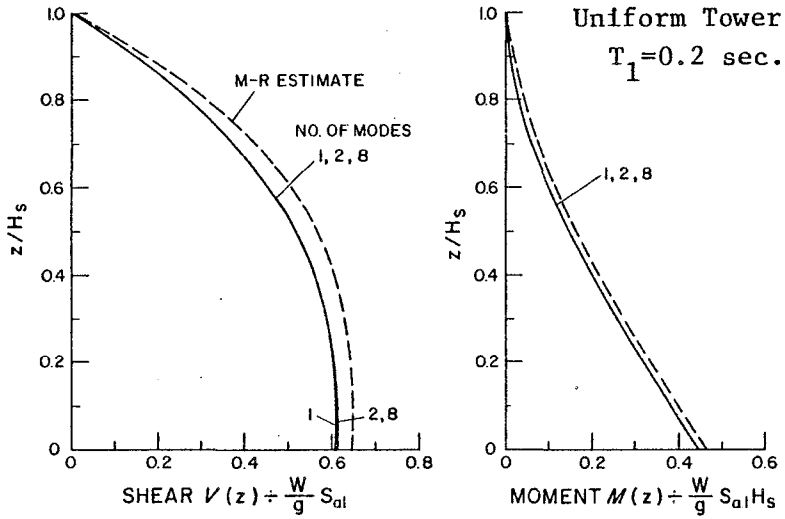

Fig. 10 Comparison of Shears and Moments from Modal Analysis and M-R Procedure.

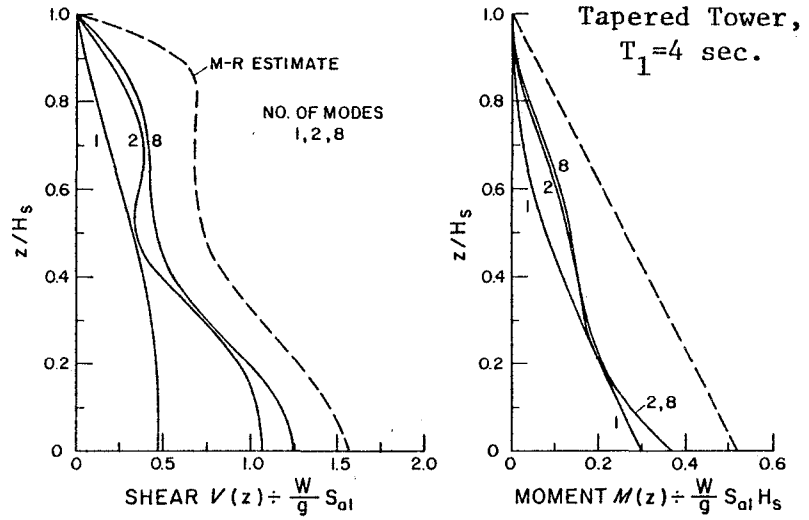

Fig. 11 Comparison of Shears and Moments from Modal Analysis and M-R Procedure.

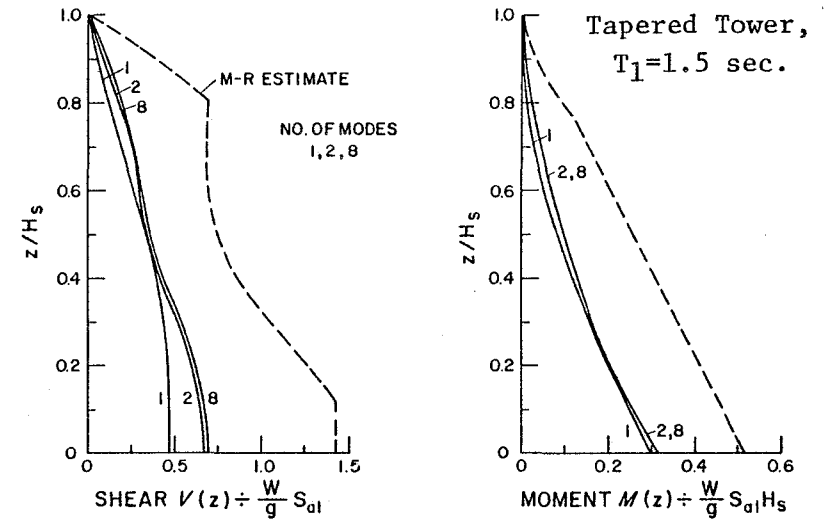

Fig. 12 Comparison of Shears and Moments from Modal Analysis and M-R Procedure.

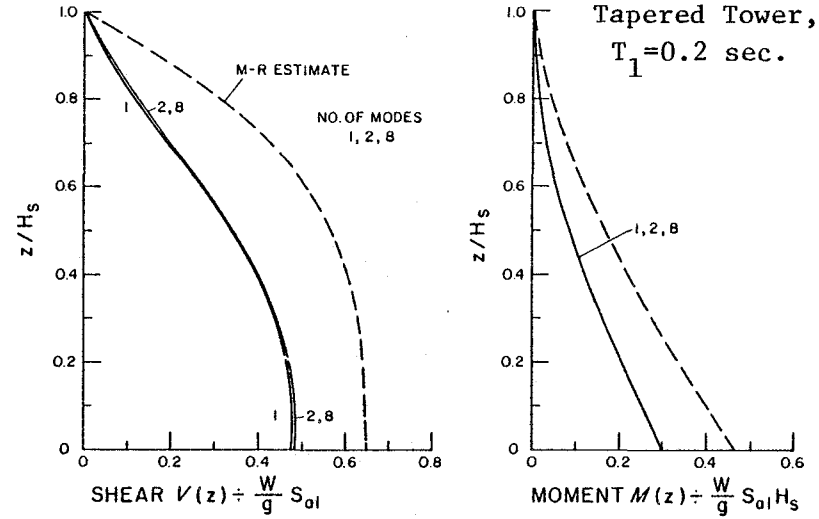

Fig. 13 Comparison of Shears and Moments from Modal Analysis and M-R Procedure.

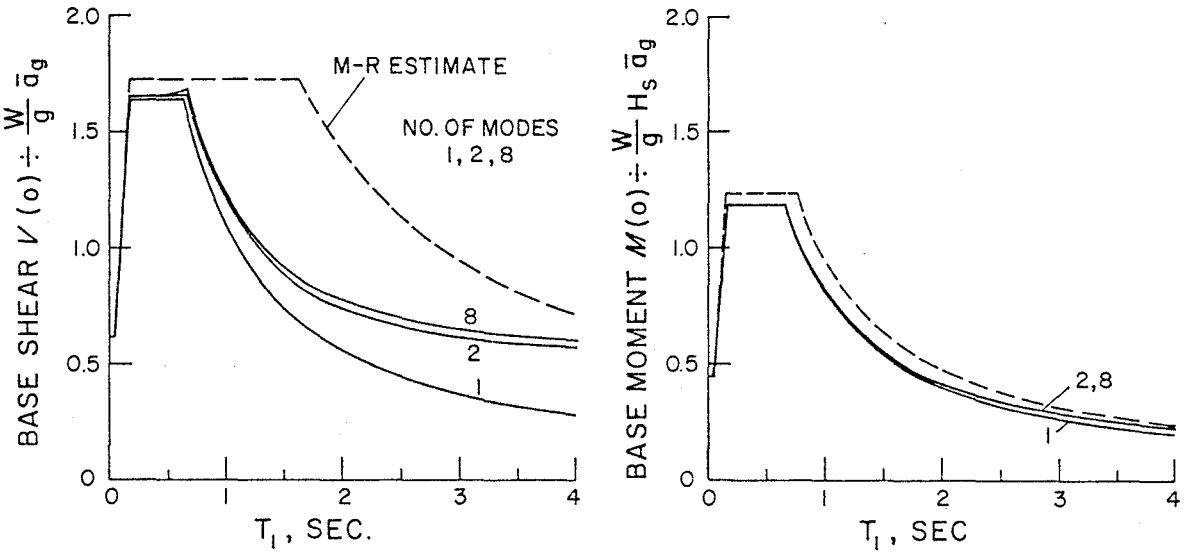

Fig. 14 Comparison of Base Shears and Moments in Uniform Towers from Modal Analysis and M-R Procedure.

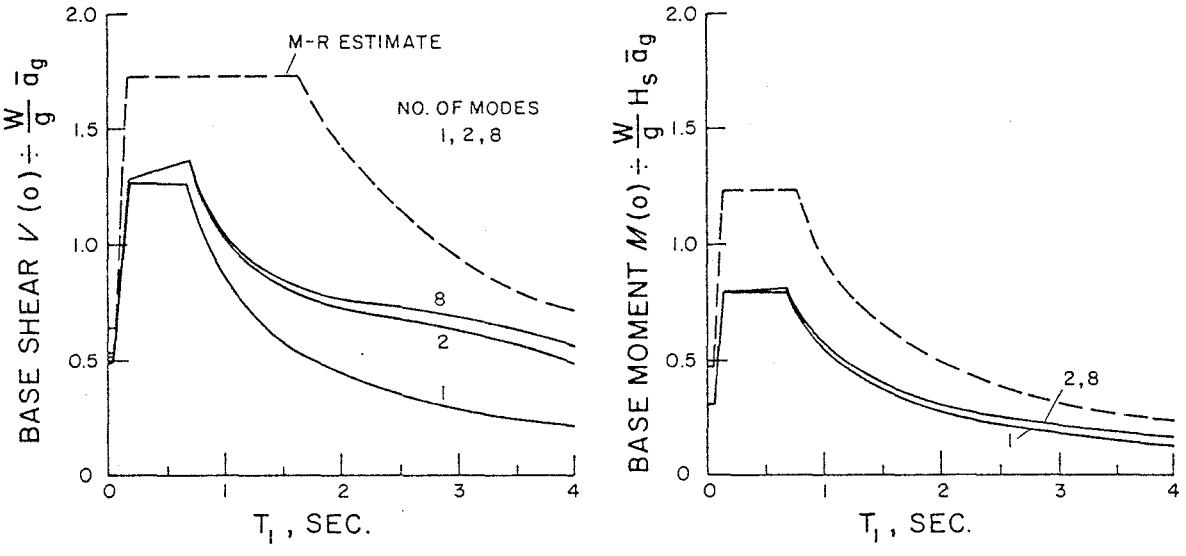

Fig. 15 Comparison of Base Shears and Moments in Tapered Towers from Modal Analysis and M-R Procedure.

VIBRATION BEHAVIOR OF XIANG HONG DIAN DAM

R. W. Clough(I), K. T. Chang(II), R. M. Stephen(III)
H.-Q. Chen(IV), G. P. Lu(V)
Presenting Author: R. W. Clough

SUMMARY

Results of a field measurement program on Xiang Hong Dian Dam in Anhui Province, PRC, are presented and correlated with finite element model analytical predictions. Forced vibration tests were carried out using 4 coupled rotating mass shakers newly developed in China, having an upper frequency limit of 25 Hz and force capacity of 4000 Kg per unit. Good correlation is indicated between calculated and measured mode shapes, frequencies, and hydrodynamic pressures, demonstrating the validity of the modeling of the dam and of its interaction with the reservoir, and the foundation.

INTRODUCTION

The effects of reservoir and foundation interaction on the dynamic behavior of arch dams is the subject of a three year research program presently being carried out under the U.S.-China Protocol for Scientific and Technical Cooperation in Earthquake Studies. The cooperating organizations are the Scientific Research Institute of Water Conservancy and Hydroelectric Power (SRIWCHP) Beijing, together with Tsinghua University and the Scientific Research Institute of Water Conservancy of Anhui Province (SRIWCAP) acting for China, and the Earthquake Engineering Research Center (EERC) of the University of California, Berkeley, acting for the United States. The investigation is being carried out under the supervision of Professor K. T. Chang (Tsinghua University) and Professor R. W. Clough (EERC). The complete investigation will include making detailed measurements of the vibration properties of two arch dams in China (single curvature and double curvature) and comparing the results with predictions calculated using state of the art mathematical models. During later stages of the work, improved models will be formulated, based on indications from the test data.

Xiang Hong Dian (XHD) Dam in Anhui Province was selected as the subject of the first field measurement program. In August 1982 vibration tests were made and recorded mainly by teams of workers from SRIWCHP and SRIWCAP; supplementary

(I) Nishkian Professor of Structural Engineering, University of California, Berkeley, U.S.A.

(II) Vice President, Tsinghua University, Peking, People's Republic of China.

(III) Principal Development Engineer, University of California, Berkeley, U.S.A.

(IV) Vice-Head of Earthquake Engineering, Scientific Research Institute of Water Conservancy and Hydroelectric Power, Peking, PRC.

(V) Deputy Director, Anhui Province Water Conservancy Research Institute, Hefei, PRC.

measurements of hydrodynamic pressures and of foundation rock motions during the tests were obtained by the two co-authors from EERC. This paper reports partial results of the test on Xiang Hong Dian Dam; full details of the work will be published as a joint EERC-SRIWCHP report.

TEST PROGRAM

Description of the Dam

XHD Dam is located in the middle reach of the Pi river in Jinshai county of Anhui Province, China. It is a non-overflow gravity arch structure completed in 1958, 87.5 m high with a crest length of 361 m. The upstream face is a vertical cylindrical surface with 180 m radius; the thickness is 5 m at the crest and 39 m at the base. It is divided into 25 blocks of 14 m length between vertical contraction joints. Four horizontal walkways are located on the downstream face, as may be seen in Fig. 1.

Test Equipment

A system of four synchronized eccentric mass shakers, newly designed at SRIWCHP, was used to vibrate the dam. Principal features of the system are as follows: (1) the maximum force produced by each shaker is 4000 Kg; eccentric mass is provided by weights in rotating "baskets"; (2) frequency limits are 0.5 to 25 Hz in three ranges (0.5-5, 1-10, 2.5-25) with a maximum error in each range of 0.5%; (3) units can be set arbitrarily to act in phase or 180° out of phase with the master unit; control of phase is accurate to $\pm$ 5 degrees. Phase and frequency of each unit is indicated digitally. In this test the four exciters were deployed at the dam crest, located symmetrically at distances of approximately 47 m and 93 m from the centerline and oriented to apply forces in the radial direction.

The vibrations of the dam were sensed by two sets of velocity transducers provided by SRIWCHP and SRIWCAP, respectively; these generally were set in the integrating mode so as to indicate displacements directly. A total of 57 stations on the dam were established for these instruments: at the crest and along the four walkways, including some stations on the adjacent abutment rock. In addition, EERC established 14 stations for Ranger seismometers. These very sensitive instruments were used to measure motions of the foundation and abutment rock in order to study the foundation interaction mechanism; accordingly all but one of these stations were on rock, the other being at the dam crest to provide correlation with one of the SRIWCHP velocity meters. Because there were more recording stations for each type of instrument than there were instruments, it was necessary to repeat the tests with the transducers moved to new locations. Four repetitions were required to obtain all of the Ranger readings. Figure 2 shows the locations of the exciters and of the two types of instruments.

Experimental Procedure

Vibration properties were evaluated both from ambient vibration measurements as well as from the response to the coupled shear units, but only forced vibration results are discussed here. For the forced vibration tests, the frequency was varied gradually over the range from about 4 to 18 Hz, and the radial displacement amplitude was observed at several stations along the crest. In the frequency ranges near modal resonance, where the response varied rapidly with

frequency, the frequency increments were made very small (<0.05Hz) in order to identify the peak frequencies accurately. When all resonant frequencies had been identified, the exciters were operated successively at each frequency, and both radial and tangential response amplitudes were recorded for all transducer stations on the dam and foundation rock. In addition, readings of hydrodynamic pressure against the face of the dam were obtained at depths of 5, 15, and 25 m at three stations to the right of the centerline. Relative values of all readings were determined for each transducer to establish the vibration mode shapes.

ANALYTICAL STUDIES

Computer Program

Analyses of the dam vibration properties were made using the finite element computer program ADAP (1). This program models the arch dam body by special "thick shell" or "3D shell" elements, and the foundation rock by 8 node "brick" elements. In addition, the program has been extended from its original form to model the reservoir by 16-node incompressible liquid elements (2), the "added mass" of the reservoir being added to the mass of the concrete in establishing the mathematical model. The program solves the undamped eigen-problem of the finite element model to obtain the vibration mode shapes and frequencies, and then uses mode superposition to calculate earthquake response. For the purposes of this investigation, the program also was modified to give the mode superposition response to a set of harmonic forces applied at the dam crest. Thus, it is possible to duplicate analytically the forced vibration tests.

Mathematical Model

In this study, the dam was modeled using 30 thickshell or 3D shell elements. The foundation rock was assumed to extend to a distance equal to the dam height in the upstream and downstream directions, as well as beneath the dam base; the total rock volume was represented by 80 massless brick elements. In initial calculations the elastic modulus of the concrete was taken to be 4×10^6 T/M^2, and parametric studies of foundation interaction were made using ratios of rock to concrete moduli equal to 1.3, 0.65, and 0.325. Then by comparison of the calculated vibration shapes at the rock-concrete interface with the measured shapes, it was determined that the ratio of 1.3 gave the best correlation. Thus, this ratio was adopted in subsequent analyses.

The reservoir was modeled by incompressible liquid 16-node elements having nodes matching the nodes at the concrete interface. In addition, liquid elements followed the topography of the reservoir bottom, and extended upstream to a rigid vertical plane at a distance of 300 meters from the dam face (4.2 times the reservoir depth); by numerical experiment it was demonstrated that the rigid boundary had no significant effect at this distance.

Types of Analyses

In addition to eigenvalue analyses of the reservoir-foundation-dam finite element model, the response of the model was evaluated when subjected to harmonic excitation simulating the input of the four shaking machines. The displacements of selected gage points on the dam and hydrodynamic pressures at

the pressure gage locations were determined at various modal frequencies; in addition frequency response curves were obtained by calculating the displacement amplitudes of selected gage points as the frequency was varied below and above resonance.

CORRELATION OF RESULTS

Vibration Frequencies

Because only a rough approximation of the dynamic modulus of the concrete could be obtained from test specimens, the first step in the correlation of analytical and experimental results was adjustment of the concrete modulus to obtain a least squares best fit of the frequencies. Only the first four modes were used in this adjustment because they are considered to be most reliable; the resulting concrete modulus was found to be 3.532×10^6 T/M^2 (4.945×10^6 psi). Values of the frequencies obtained analytically using this modulus are listed in Table 1, together with the corresponding experimental values. The designation S or AS associated with the measured frequencies indicates whether the shakers were operated in a symmetric or antisymmetric pattern during the test. The discrepancy between experimental and analytical values for the first four modes averages only 1.3 percent, which is well within the precision of the individual experimental results; even for the higher modes the agreement generally is remarkably good.

Mode Shapes

The first three vibration mode shapes, calculated and measured at the dam crest and at the upper two walkway levels, are plotted in Figs. 3-5. The analytical values have been normalized to the amplitude of displacement measured at one location in each mode. The apparent quality of correlation could have been improved in some modes by normalizing to a different location, but these figures clearly show that the mathematical model reproduces the essential behavior in the four modes. Although not shown for lack of space, the fourth and fifth mode shapes correlate equally well at these three levels, but the analytical results for Mode 5 show a phase reversal at the lower levels which is not evident in the measured results. However, it is believed that the sign change was overlooked in the experimental data because the readings were so small.

Frequency Response Curves

The experimental modal frequencies were determined by operating the shaker system at a sequence of closely spaced frequencies and plotting the resulting response amplitude measured at an appropriate point on the dam crest; similar analytical results were obtained by duplicating the procedure mathematically. The resulting frequency response curves for the first two modes obtained with symmetric excitation are shown in Fig. 6, and for the first two antisymmetrically excited modes in Fig. 7; experimental and analytical results are shown respectively by dashed and solid lines. The additional peak in the experimental response curve of Fig. 7 corresponds to the second peak in Fig. 6; this mode was excited by both symmetric and antisymmetric input patterns, but less strongly in the antisymmetric case.

As expected, the peaks of the analytical and experimental curves indicate the same frequency discrepancies shown in Table 1. The amplitudes of the

analytical curves were matched to the experimental data by iterative adjustment of the modal damping ratio. The "experimental" damping ratio was obtained from the experimental frequency response curves by the half-power method. The damping ratios listed on the two figures show excellent agreement between analysis and experiment.

Missing Mode

It will be noted in Table 1 that no experimental frequency is indicated for Mode 6. In order to determine why this mode was not observed experimentally,the frequency response curve in the vicinity of the 6th mode frequency was calculated by combining the responses to symmetric excitation of Modes 5, 6, and 7. The result (solid curve in Figure 8) clearly demonstrates that the contribution of mode 6 (which does have a peak at 7.62 Hz) is completely overwhelmed by that of mode 5; thus, the test data did not suggest the existence of mode 6. To study the problem further, the frequency response was calculated by combining Modes 4, 5, and 6. This standard analysis for Mode 5, shown by the dash-dot curve in Fig.8, may be compared with the experimentally determined (dashed line) response curve for mode 5. The reason for the obvious frequency discrepancy is not known, but the mode 5 damping value correlates well. The possible missing of a mode, as noted here for mode 6, is a basic difficulty of the forced vibration test procedure when frequencies are closely spaced. In this case, the analytical shape of mode 6 (not shown for lack of space) is nearly the same as mode 5 at the crest; the shapes differ in the vertical sections, but the crest measurements made in this test procedure offer no clue to the missing mode.

Correlation of Hydrodynamic Pressures

Hydrodynamic pressures measured at various points on the face of the dam during excitation at the first and second mode frequencies are plotted in Fig. 9; also shown are the analytically predicted pressure variations across the dam at these same levels. The agreement between the analysis and these few experimental values is remarkable. So far as is known, this is the first correlation that has been reported between measured modal hydrodynamic pressures and corresponding analytical results, and it certainly suggests that the incompressible reservoir model is valid, at least for the combinations of dimensions and frequency involved in these two modes.

CONCLUSIONS

The excellent agreement between analysis and experiment obtained in this study demonstrates the high quality of results that can be obtained using modern experimental equipment and refined mathematical models; however, the fact that several modes were not identified experimentally among the first twelve demonstrates a basic limitation of the forced vibration test procedure. On the other hand,the measurements of foundation rock motions and of hydrodynamic reservoir pressures indicate the potential of this experimental technique for studying reservoir and foundation interaction with concrete dams. A complete report on the results of such interaction studies will be presented in the final phase of the investigation after reduction of the data recorded on both dams.

REFERENCES

1. Clough R. W., Raphael, J. M., and Mojtahedi, Soheil, "ADAP-A Computer Program for Static and Dynamic Analysis of Arch Dams", University of California, Earthquake Engineering Research Center, Report No. UCB/EERC-73/14, 1973.

2. Kuo,J.S.-H.,"Fluid-Structure Interaction-Added Mass Computations for Incompressible Fluids",University of California, Earthquake Engineering Research Center, Report No. UCB/EERC-82/09, 1982.

TABLE 1: MODAL VIBRATION FREQUENCIES (Hz)
(Water Level = 126.9 m)

Mode No.	Measured	Calculated
1	4.1 S	3.977
2	4.3 AS	4.347
3	5.1 S	5.156
4	6.0 AS	5.996
5	7.0 S	7.501*
6	--	7.623*
7	8.2 AS	8.381*
8	--	9.100*
9	9.5 S	10.509
10	--	10.656
11	10.8 AS	10.967*
12	12.5 S	12.665*

*Analysis showed 2nd mode shape in cantilever direction; experiment did not show this shape.

System Properties

Rock: $E_f = 4.592 \times 10^6$ T/m^2 (6.531×10^6 psi), $\gamma = 0$

Concrete: $E_f = 3.532 \times 10^6$ T/m^2 (5.024×10^6 psi), $\gamma = 150$ pcf.

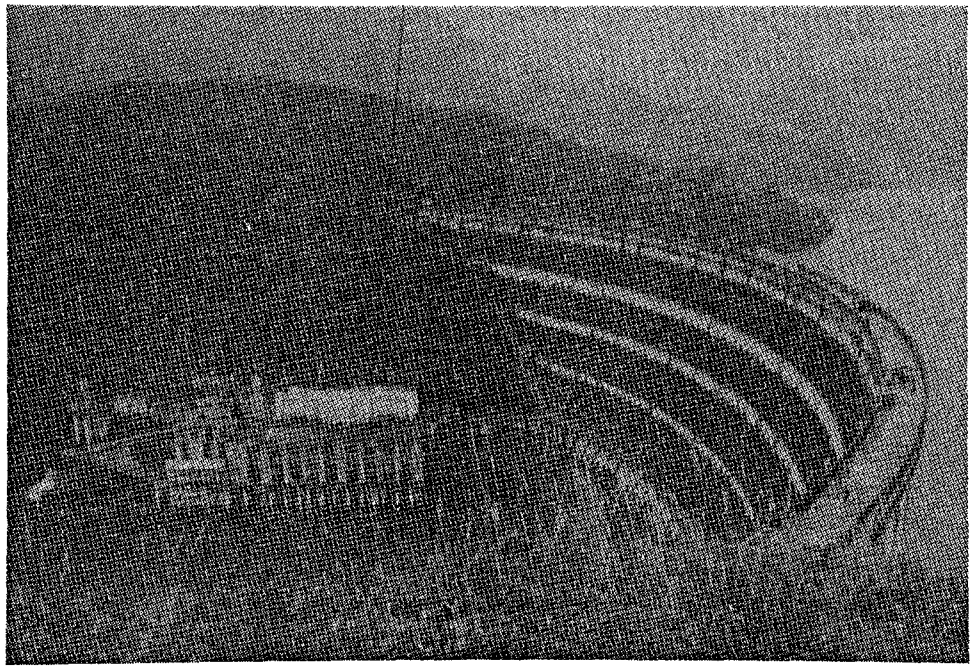

FIG. 1 XIANG HONG DIAN DAM

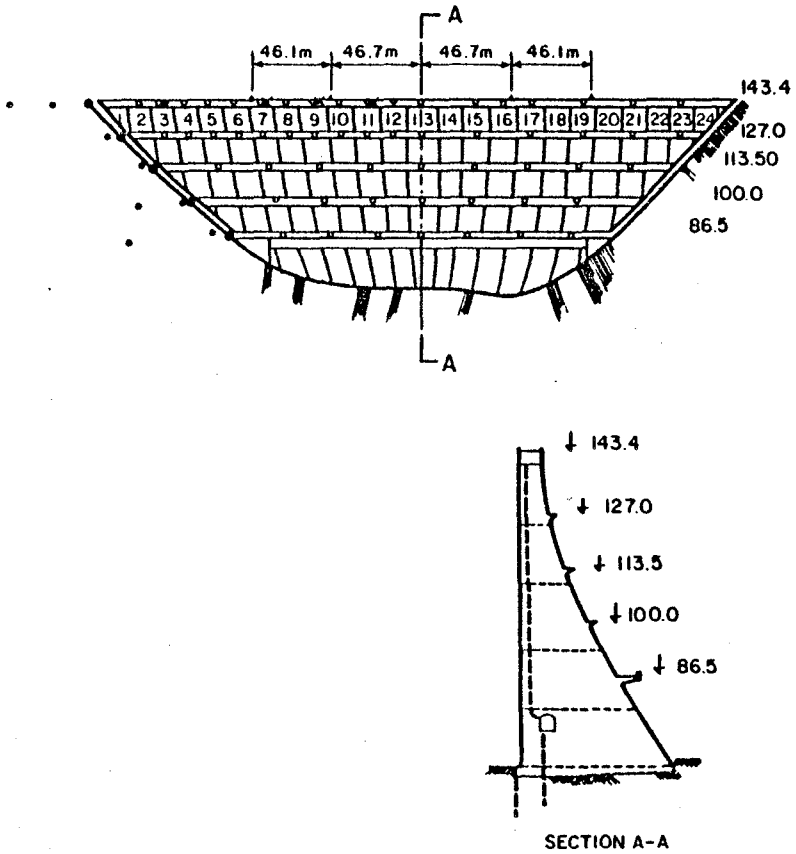

△ ROTATING MASS SHAKER

○ SRIWCHP AND SRIWCAP STATION

● EERC STATION FOR DISPLACEMENT

⊠ EERC STATION FOR HYDRODYNAMIC PRESSURE

FIG. 2 DAM GEOMETRY AND INSTRUMENT LOCATIONS

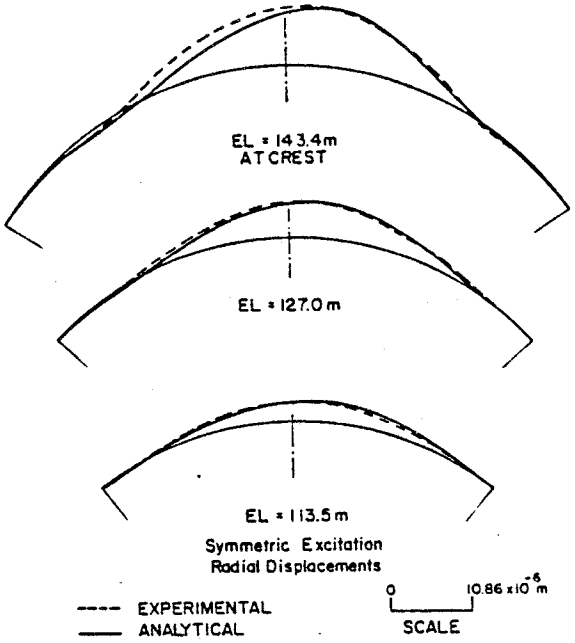

FIG. 3 FIRST MODE SHAPE,
f = 4.14 Hz

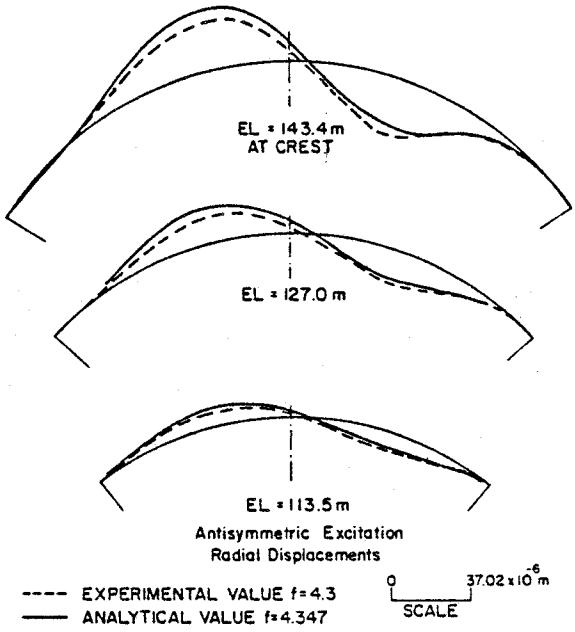

FIG. 4 SECOND MODE SHAPE,
f = 4.3 Hz

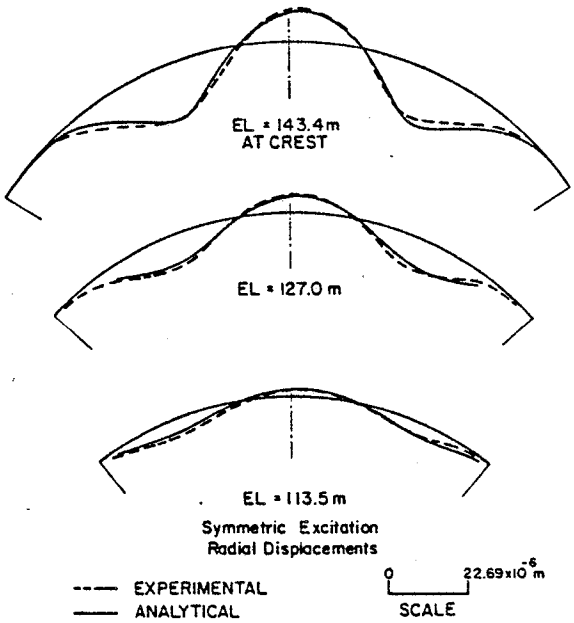

FIG. 5 THIRD MODE SHAPE,
f = 5.1 Hz

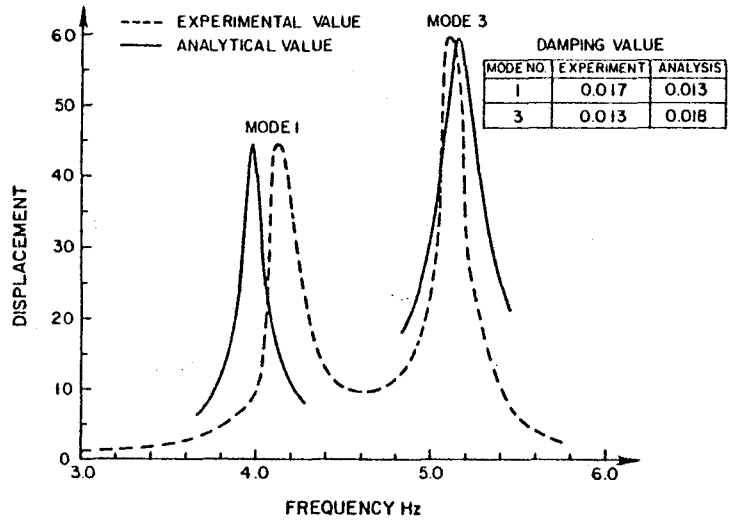

FIG. 6 FREQUENCY RESPONSE CURVES FROM SYMMETRIC EXCITATION

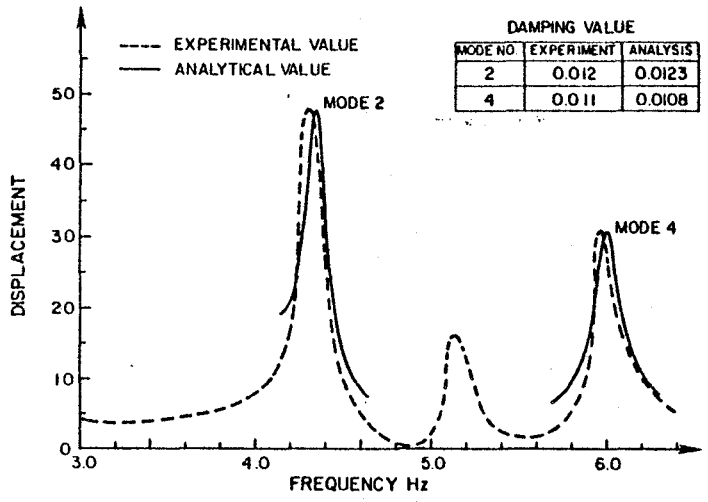

FIG. 7 FREQUENCY RESPONSE CURVES FROM ANTISYMMETRIC EXCITATION

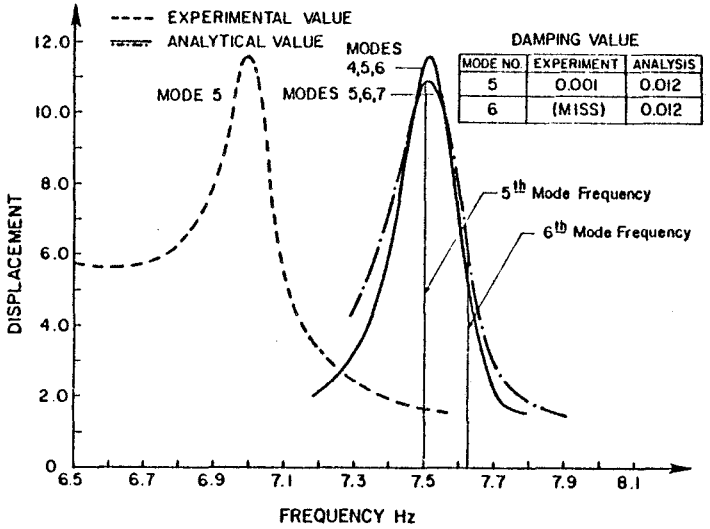

FIG. 8 SYMMETRIC EXCITATION RESPONSE NEAR 6th MODE

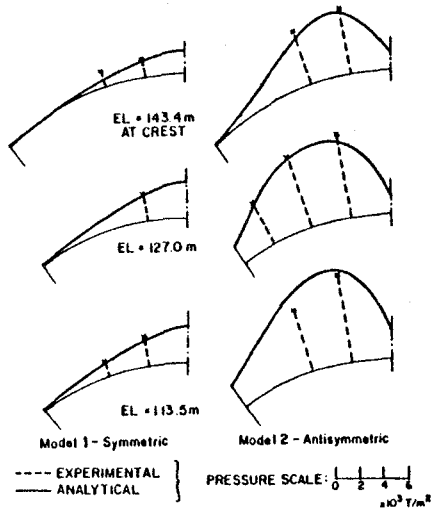

FIG. 9 HYDRODYNAMIC PRESSURES AT DAM FACE

AN EVALUATION OF THE RESPONSE SPECTRUM METHOD FOR LATERAL ANALYSIS OF BUILDINGS

Ernesto Cruz (I)
Anil K. Chopra (II)
Presenting Author: Ernesto Cruz

SUMMARY

The ensemble average of the maximum response of a class of multistory buildings to simulated ground motions, computed by time history analysis (THA) and response spectrum analysis (RSA) procedures, is plotted against the fundamental vibration period of the building in the form of response spectra. The dependence of the contributions of the higher vibration modes, and of the errors in the RSA results, on the fundamental vibration period and on the joint rotation index ρ, a measure of the relative beam to column stiffness of the building, is discussed.

INTRODUCTION

In most practical analyses of multistory buildings, the maximum earthquake response of a structure is determined directly from the response or the design spectrum. Furthermore, most building code specifications for earthquake forces are based on simplifications of the response spectrum method of analysis. In order to develop better simplified analysis procedures suitable for building codes, it is necessary to evaluate the accuracy of the response spectrum estimates of maximum response and to better understand the contributions of the various vibration modes in the response. This paper reports on a small part of a National Science Foundation sponsored research project designed to fill this need; it is an extension of Ref. 1.

SYSTEMS, GROUND MOTIONS, AND ANALYSIS PROCEDURES

Systems

The systems analyzed are idealized as single-bay, five-story moment-resisting plane frames with constant story height = h, and bay width = 2h. All the beams have the same stiffness I_b and the column stiffness I_c does not vary with height. The structure is idealized as a lumped mass system with the same mass m at all the floor levels. The damping ratio for all the natural modes of vibration is assumed to be five percent. Only two additional parameters are needed to completely define the system: the first mode period T_1 and the joint rotation index ρ (Ref. 2). For the selected class of building frames $\rho = I_b/4I_c$. By varying ρ the complete range of behavior of the frame can be covered, from the bending beam ($\rho = 0$) to the shear beam ($\rho = \infty$). Intermediate values of ρ represent frames with both beams and columns undergoing flexural deformations.

(I) Graduate student, Civil Engineering Dept., U. of Calif., Berkeley USA

(II) Professor of Civil Engineering, U. of California, Berkeley, USA

Ground Motions

Eight simulated ground motions were generated as samples of a filtered stationary Gaussian white noise amplified by a time dependent intensity function. The average of the response spectra of these eight ground motions for five percent damping is presented on Fig. 1 together with the ensemble averages of the maximum ground acceleration, velocity, and displacement.

Analysis Procedures

Standard procedures were employed for both the time-history analysis (THA) and the response spectrum analysis (RSA) of the dynamic response of the idealized frame to the simulated ground motions. The THA was carried out by the mode superposition method. The maximum of each of the response quantities of interest during each simulated motion was determined. The ensemble average of the maximum response was obtained by averaging the maximum value corresponding to each of the eight simulated ground motions. In the RSA the maximum value of each of the response quantities of interest was estimated as the square-root-of-the-sum-of-the-squares (SRSS) combination of the individual modal maxima, computed directly from the average response spectrum of Fig. 1. The SRSS combination rule is adequate because the idealized frame has well spaced vibration frequencies.

PRESENTATION AND DISCUSSION OF RESULTS

The ensemble average of the maximum response, computed by including the contribution of all five vibration modes in the time-history analysis (THA) and in the response spectrum analysis (RSA) procedures, is plotted against the fundamental vibration period of the building in the form of response spectra; also included in these plots is the maximum response due only to the fundamental vibration mode, which is obviously identical whether computed by THA or RSA procedures. Such plots are presented in Figs. 2-7 for three values of $\rho = 0$, 0.125, and ∞ and six response quantities: top floor displacement u_5, base shear V_o, base overturning moment M_o, the largest moment M_b among all the beams, the largest moment M_c among all the columns, and the largest axial force P_c among all the columns. The response quantities are presented in dimensionless form as defined in Figs. 2-7, where $\bar{u}_g$ and $\bar{a}_g$ are the ensemble averages of the maximum ground displacement and ground acceleration respectively; W_1 and h_1 are the effective weight and effective height for the first vibration mode of the building. The normalization factors for V_o and M_o are the base shear and moment for a rigid single-degree-of-freedom system with lumped weight W_1 and height h_1.

The response contributions of the vibration modes higher than the fundamental mode increase, and apparently as a result the differences in THA and RSA results increase, with increasing fundamental vibration period T_1. Because, for a fixed ρ, the modes shapes and ratios of vibration frequencies do not change with T_1, the increased contribution of the higher modes is due only to the relative values of the response spectrum ordinates, which in turn depend on the spacing of the vibration periods and on the shape of the response spectrum. For the selected spectrum, as the fundamental vibration period increases the ordinate for a higher vibration mode generally increases relative to that for the fundamental mode, resulting in increased response contributions of the higher vibration modes and increased errors in the RSA

results.

The response contributions of the higher vibration modes increase, and consequently the differences in THA and RSA results increase, with decreasing value of the joint rotation index ρ. A change in ρ affects the vibration modes shapes as well as the ratios of vibration frequencies. These two effects can be interpreted as separate, because the change in mode shapes affects the distribution of forces and displacements while the change in frequency ratios affects the relative importance of the dynamic amplification factor for the different modes. As ρ decreases the effective weight for the first mode tends to decrease and correspondingly the effective weights for the higher modes, especially for the second mode, tend to increase. At the same time the frequency ratios increase, spreading the frequencies over a wider portion of the spectrum, thus increasing the effects of the spectrum shape discussed above. Both of these factors contribute to increased response due to the higher vibration modes.

While the errors in the RSA results depend on the response quantity they are all below five percent for structures with fundamental vibration period less than four seconds. Among the overall response quantities the largest errors occur in the base shear values, with much smaller errors in the base overturning moment, and almost no errors in the top displacement. Among the local response quantities the largest errors occur in the column moments, while the errors in the beam moments and column axial forces are very similar; but these errors are all smaller than those in the base shear.

In addition to the already discussed trends in the results, the base shear, and to a lesser degree the base overturning moment, show some discrepancies between the RSA and the THA results for very short periods (Figs. 3 and 4), with the errors increasing as T_1 decreases in this range. The individual modal responses of a short period structure are essentially all in phase, resulting in the combined response being close to the sum of absolute values of modal responses and larger than the SRSS estimate which is close to the first mode response.

Although the results presented are for a one-bay five-story frame with uniform distribution of mass and stiffness over height subjected to a small set of simulated ground motions, the trends observed can be explained in terms of both basic principles of static and dynamic analysis and the characteristics of the model and the average spectrum of the ground motions. Therefore, the same trends are expected to be found in the responses of a much wider range of structures, with different number of stories and with distributions of mass and stiffness that change gradually over the height, under the action of excitations with spectra similar to the one used here.

In order to provide a complete evaluation of the RSA the results presented here need to be extended. The areas in which further research is planned include: effects of the heightwise distribution of mass and stiffness, and effects of the model frame characteristics (number of stories, number of bays, and bay-width to story-height ratio).

REFERENCES

1) Roehl, J. L., "Dynamic Response of Ground-excited Building Frames," Ph.D. Thesis, Rice University, Houston, Texas, Oct. 1971.

2) Blume, J. A., "Dynamic Characteristics of Multi-story Buildings," Journal of the Structural Division, ASCE, Vol 94, No ST2, Feb. 1968, pp. 337-402

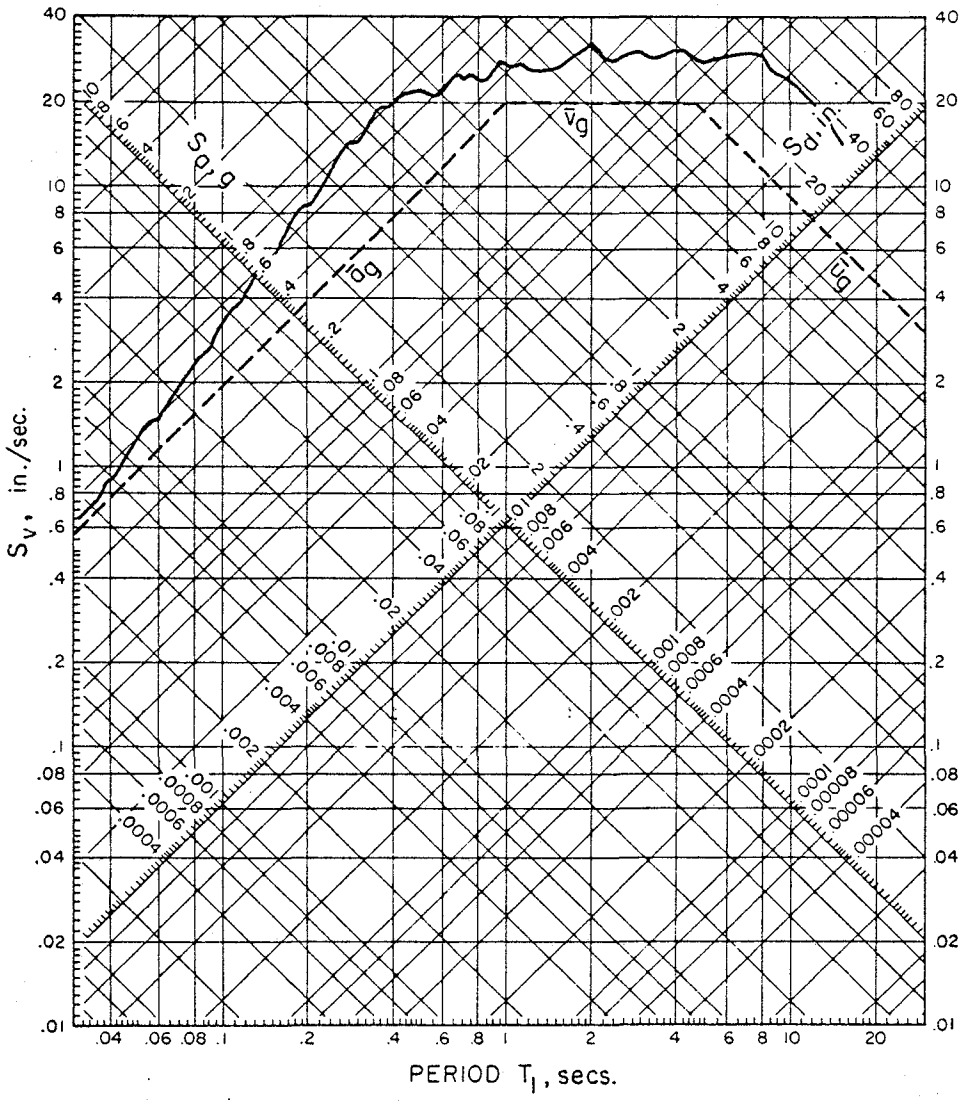

Fig. 1 Average Response Spectrum (5% damping) for Eight Simulated Motions.

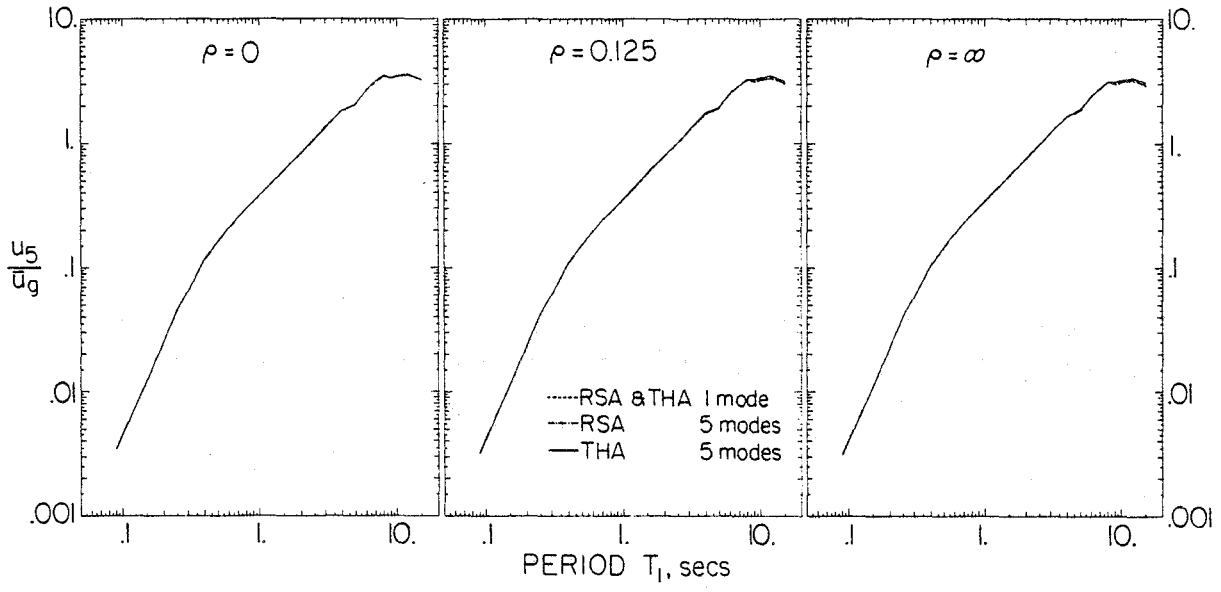

Fig. 2 Maximum Top Story Displacement.

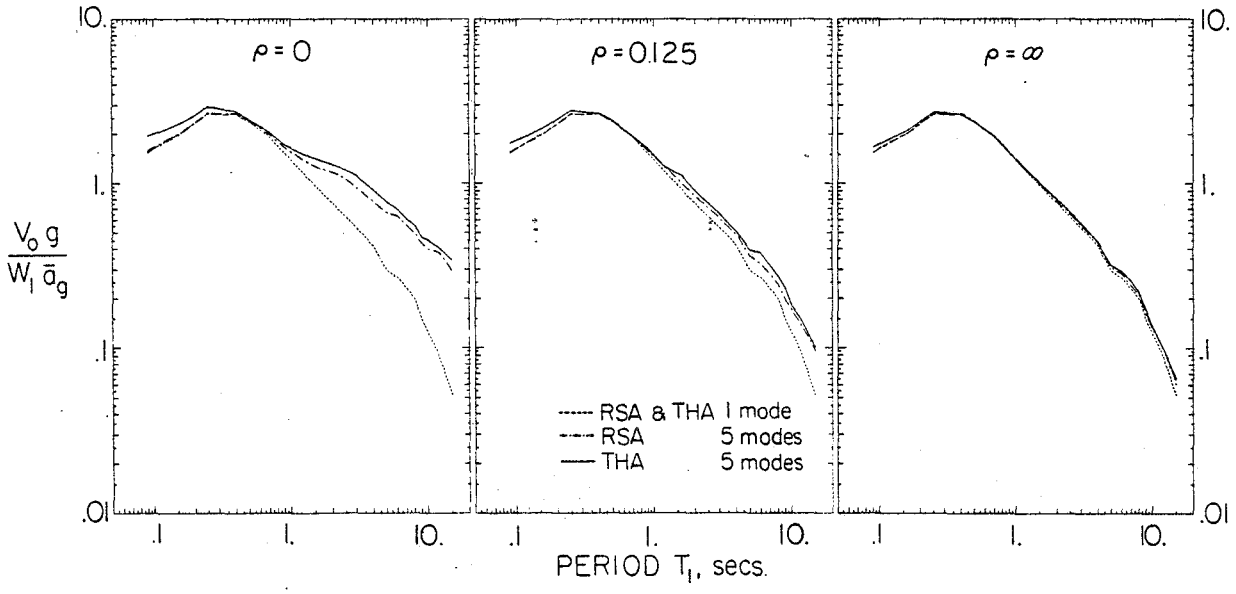

Fig. 3. Maximum Base Shear.

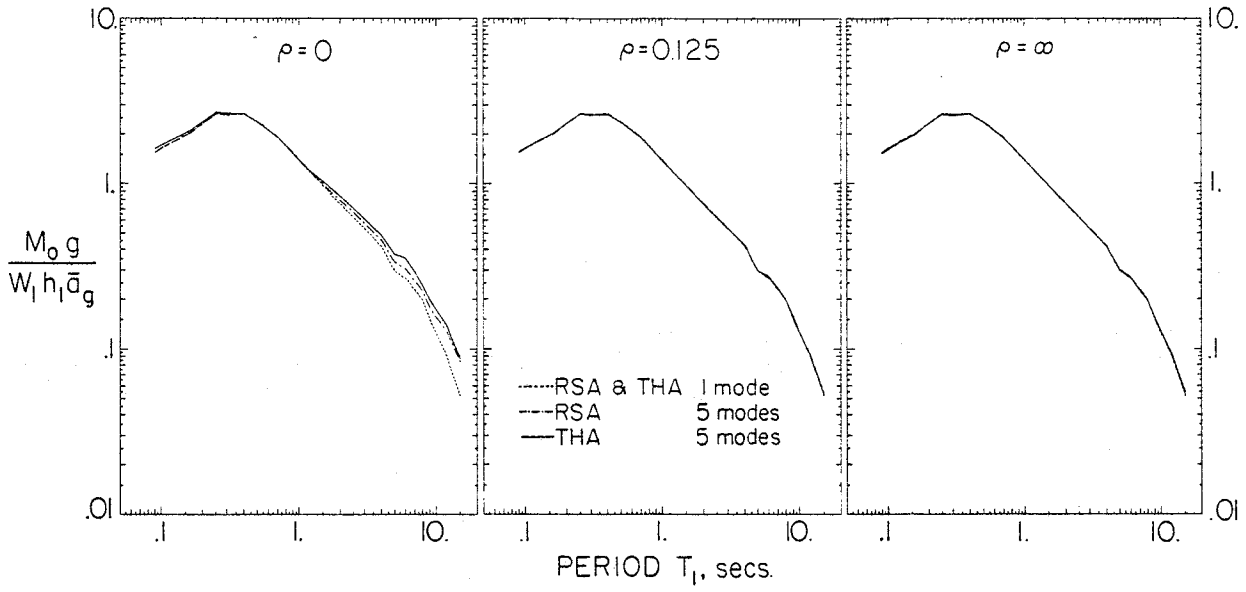

Fig. 4 Maximum Base Overturning Moment.

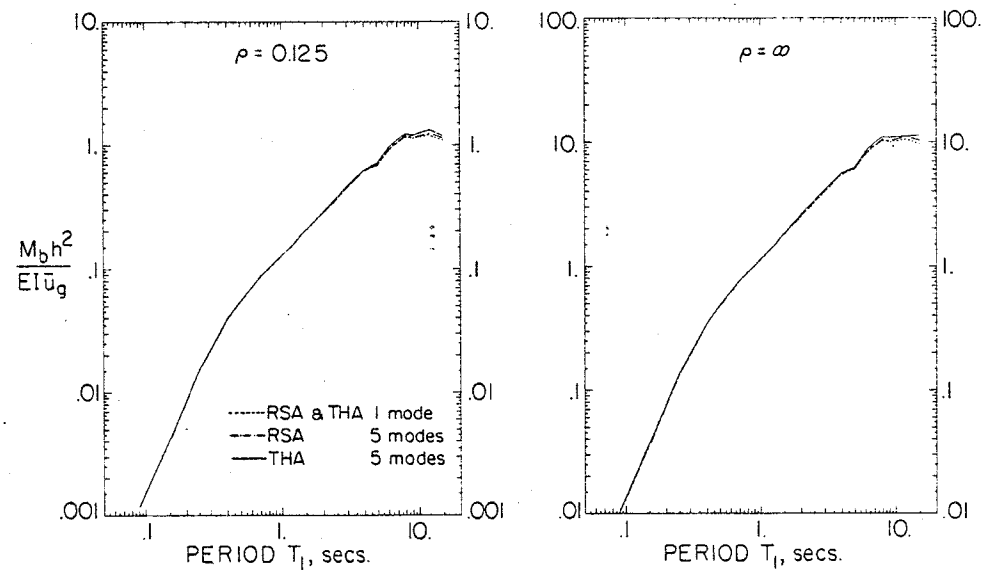

Fig. 5 Maximum Beam Moment.

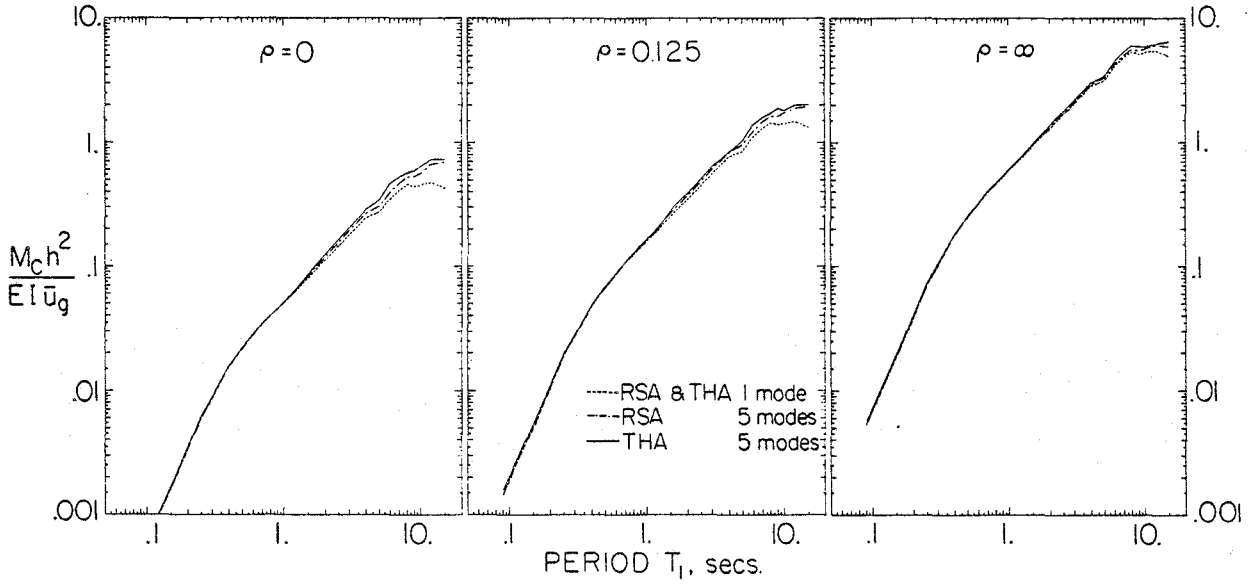

Fig. 6 Maximum Column Moment.

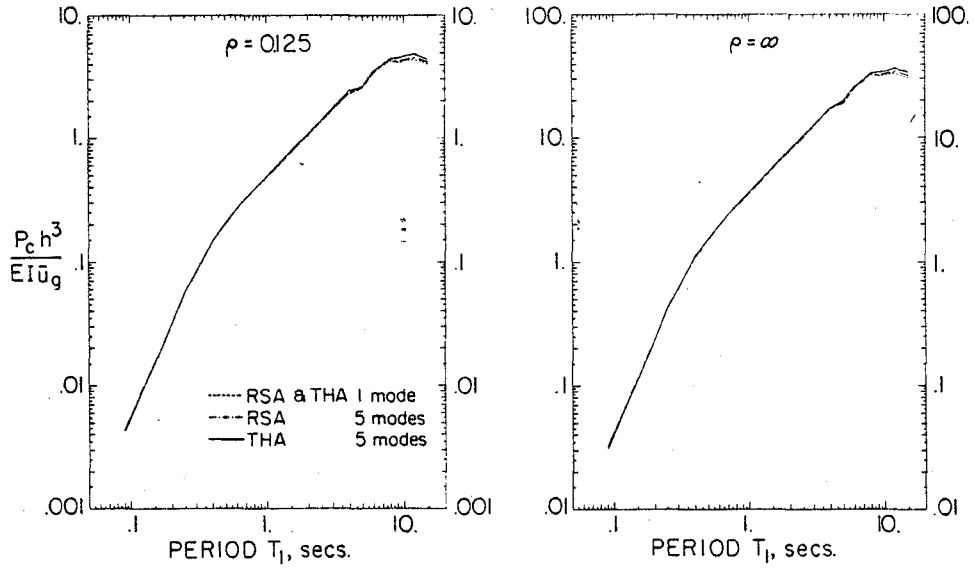

Fig. 7 Maximum Column Axial Force.

MATHEMATICAL MODELING OF A FRAME WITH JOINT ROTATION

by

Jerry S. Dimsdale (I)
Hugh D. McNiven (II)

Presenting Author: Hugh D. McNiven

SUMMARY

This paper shows the considerable influence that joint behavior in a frame plays in the response of the frame to a dynamic forcing function. The behavior is demonstrated by means of experimental results obtained when a three-story steel frame is subjected to seismic motions on a shaking table and the results are used to formulate a mathematical model of the frame using system identification.

INTRODUCTION

To date most mathematical models of moment-resisting frames are formulated using the geometric and material properties of the members and assuming that the joints are continuous. This assumption implies that the joints are rigid and that at a joint all members rotate the same amount. As many frames are constructed so that the stiffnesses of the columns and girders are relatively the same, the deformation that occurs when the frames are subjected to earthquake motions will involve joint rotations as well as floor translations; thus, the behavior of a joint during rotation is significant in many frames. When a mathematical model of such a frame is constructed using this traditional method, the model predicts quite poorly the responses recorded when the frame is subjected to an earthquake input on the shaking table at the Earthquake Engineering Research Center, University of California, Berkeley. To our knowledge the first detailed study that associate the shortcomings of the traditional mathematical model with the assumption of continuity of the joints was conducted by Kaya and McNiven[1]. They gained physical insight into the problem by using system identification to construct a number of mathematical models of a frame. They accounted for joint deformation in a somewhat oblique way. They constructed their best mathematical model by introducing a set of parameters; one parameter was associated with the geometric length of each column and girder and an additional parameter accounted for viscous damping. When the cost function was minimized using a Gauss-Newton optimization algorithm and the resulting "best set" of values for the parameters was inserted into the model, it predicted response of the frame extremely accurately. The length of a member times the parameter associated with it was considered to be the "effective" member length. As the effective length differed from the geometric length, Kaya and McNiven concluded that the joints did in fact change shape during the deformation of the frame and that when this change of shape is accounted for, the model is significantly improved.

In this paper we take what we think is the next logical step in improving the formulation of the mathematical model of a moment-resisting frame. The

(I) Senior Development Engineer, Earthquake Engineering Research Center, University of California, Berkeley, California, U.S.A.
(II) Professor of Engineering Science and Director, Earthquake Engineering Research Center, University of California, Berkeley, California, U.S.A.

Preceding page blank

step is to isolate each joint to be considered as a separate element in the frame behavior. The formulation described in what follows has a number of advantages over the previous formulation by Kaya and McNiven. First, we have not resorted to static condensation of the stiffness matrix which results in a relationship between translation and joint rotation that depends on the continuity of the joint behavior we know is violated. We are able to reduce from eight to four the number of free parameters to be identified by optimization, thus reducing considerably the computer costs of this operation. We take advantage of symmetry, as did Kaya and McNiven, but further find that the same parameter suffices for all three columns and that no adjustment is needed for the girder lengths. We consider that when a joint deforms it can do so both due to shear and to the moments imposed upon it. An in-depth study, shows that when we associate a parameter with each of these deformations, the parameters, during optimization, do not behave independently, so that one parameter is sufficient to account for joint deformation. We arbitrarily choose to associate the parameter with the shear deformation. The third parameter reveals the viscous damping and the fourth accounts, as in the previous study, for the rocking of the shaking table during excitation.

System identification requires experimental results and we are fortunate to have the results of experiments conducted by Clough and Tang [2]. The experiments were conducted on a three-story steel frame with welded connections between girders and columns. The stiffnesses of the girders and columns were of the same order of magnitude. We are particularly fortunate for this study in that Clough and Tang conducted two series of tests, designated Phase I and Phase II, wherein the only difference in the frames for the two phases was in the joints. For Phase II the joints of Phase I were stiffened significantly. In our mathematical modeling of the frames for the two phases we are able to show that the parameters associated with the columns and the rotation of the table are essentially the same. The damping of the Phase II frame is somewhat higher than that for Phase I, as one would expect. The parameters for the joints, however, differ significantly, the parameter for the stiffened joint being more than twice that for the joint of Phase I.

THE THREE-STORY FRAME

The test structure consisted of two parallel, single-bay, three-story, moment-resistant steel frames. The frames were fabricated from standard rolled shapes of ASTM A-36 grade steel. Two frames, designated A and B, were separated by 6'. They were connected at floor levels by removable cross beams and bracing angles, producing the effect of a floor diaphragm rigid in its own plane. The Total height of the structure was 17'14". The story heights were 6'8", 5'4", and 5'4". The bay width was 12'0". Sections W5-16 and W6-12 were used for columns and girders, respectively.

Fully penetrated welded girder to column connections were used. The panel zone thickness was 1/4" (i.e., the column web thickness) for Phase I of the experiments, and 1" (column web reinforced by 3/8" doubler plates on both sides) for Phase II.

The frames were instrumented with linear potentiometers at each floor to measure floor translation. The frames had strain gauges attached to both flanges at the top and bottom of each column. Assuming a linear variation of bending strain along the length of a column, the relative rotation of the ends will be

given by:

$$\theta = \frac{L}{h} \frac{\varepsilon_a + \varepsilon_b}{2}$$

where ε_a and ε_b are the bending strains at either end, L is the length of the column, and h is its depth.

The table excitation used was the El Centro earthquake.

CONSTRUCTION OF THE MATHEMATICAL MODEL

The mathematical model associated with the dynamic behavior of an n degree of freedom linear elastic structure subjected to rigid base motion is:

$$\underline{m}\frac{d^2\underline{u}}{dt^2} + \underline{c}\frac{d\underline{u}}{dt} + \underline{k}\underline{u} = -\underline{m}\underline{r}\frac{d^2\underline{u}_g}{dt^2} \tag{1}$$

$$\frac{du(0)}{du} = \underline{u}(0) = 0 \tag{2}$$

where $\underline{m}$ is the mass matrix, $\underline{c}$ is the damping matrix, and $\underline{k}$ is the stiffness matrix. $\frac{d^2\underline{u}}{dt^2}$, $\frac{d\underline{u}}{dt}$, and $\underline{u}$ are vectors for relative acceleration, velocity, and displacement. $\frac{d^2\underline{u}_g}{dt^2}$ is the base acceleration and $\underline{r}$ is a column vector whose elements are static displacements due to a unit displacement of the structure.

It is possible to find a matrix, $\underline{P}$, so that $\underline{M}=\underline{P}^t\underline{m}\underline{P}$ and $\underline{K}=\underline{P}^t\underline{k}\underline{P}$ are both diagonal matrices; i.e., $M_{ij}=0$ if $i \neq j$. If we make the change in variables:

$$\underline{u} = \underline{P}\underline{Y} \tag{3}$$

then the differential equation of motion can be rewritten:

$$\underline{M}\frac{d^2\underline{Y}}{dt^2} + \underline{C}\frac{d\underline{Y}}{dt} + \underline{k}\underline{Y} = \underline{F}(t) \tag{4}$$

where

$$\underline{C} = \underline{P}^t\underline{c}\underline{P} \quad \text{and} \quad \underline{P}(t) = -\underline{P}^t\underline{m}\underline{r}\frac{d^2\underline{u}_g}{dt^2} \tag{5}$$

Developed here is a finite element model in which joint panel zones are assumed to be rigid in reacting to flexural and axial forces, but shear distortions are allowed. The column element stiffnesses will be given by:

$$\underline{k} = k' \begin{Bmatrix} 2+\beta & 1-\beta & 0 \\ 1-\beta & 2+\beta & 0 \\ 0 & 0 & \frac{A}{2I}(1+2\beta) \end{Bmatrix} \tag{6}$$

The girder stiffnesses will be given by:

$$k = \frac{3EI}{L(1+2\beta)} \tag{7}$$

The joint stiffnesses will be given by:

$$k = Gbht \tag{8}$$

where:

$$k' = \frac{2EI}{L(1+2\beta)} \qquad \beta = \frac{6EI}{L^2 A'G} \tag{9}$$

and E, I, A, and A' denote Young's modulus, moment of inertia, section area, and effective shear area, respectively. The displacement transformation matrices, A_i, for each element are given by:

Girders:

a)	0	0	0	1	0	0	-1/1	0	0	1	0	0	0	0
b)	0	0	0	0	1	0	0	-1/1	0	0	1	0	0	0
c)	0	0	0	0	0	1	0	0	-1/1	0	0	1	0	0

Columns:

a)	-1/1	1/1	0	1	0	0	0	0	0	0	0	0	0	0
	-1/1	1/1	0	0	1	0	0	0	0	0	0	0	0	0
	0	0	0	0	0	0	1	-1	0	0	0	0	0	0
b)	0	-1/1	1/1	0	1	0	0	0	0	0	0	0	0	0
	0	-1/1	1/1	0	0	1	0	0	0	0	0	0	0	0
	0	0	0	0	0	0	0	1	-1	0	0	0	0	0
c)	0	0	-1/1	0	0	1	0	0	0	0	0	0	0	0
	0	0	-1/1	0	0	0	0	0	0	0	0	0	1	1
	0	0	0	0	0	0	0	0	1	0	0	0	0	-72

Joints:

a)	0	0	0	0	0	0	0	0	0	1	0	0	0	0
b)	0	0	0	0	0	0	0	0	0	0	1	0	0	0
c)	0	0	0	0	0	0	0	0	0	0	0	1	0	0
d)	0	0	0	0	0	0	0	0	0	0	0	0	1	0

Table Spring:

0	0	0	0	0	0	0	0	0	0	0	0	0	72

The global stiffness matrix will be:

$$\underline{K} = \Sigma \underline{A}_i^t \underline{k}_i \underline{A}_i \tag{10}$$

The formulation at this stage accommodates a large family of models. Five models are constructed as groundwork for preparation of the final model, the one in which the joints are considered as separate elements. This preliminary work has two purposes. The first is to confirm the major findings of Kaya and McNiven: (a) if rotation is to be accommodated in the model, the response quantities for the cost function must include joint rotation as well as floor translation time histories and (b) consideration of the pitching of the shaking table has a significant effect on the parameters associated with the girders. The second purpose is to investigate whether the number of parameters introduced by Kaya and McNiven can be reduced without appreciably affecting the ability of the model to predict the experimental frame response.

Identification Using Only Floor Displacements

For the first three models, only the floor translation (displacement) time histories are used and only the first six seconds of response. These time histories are constructed primarily to explore the number of separate parameters needed for association with the columns. In model one, three parameters are used, along with mass proportional damping and optimization resulted in the parameters for the top two floors being almost identical but different from the lowest floor column. Model two uses only three parameters, one for the top two columns, one for the lowest column, and one for damping. The error for the optimized parameters remains unchanged. The third model then uses only one parameter for all three columns but associates three additional parameters with the girders. With damping there are five parameters. The major finding here confirms what was pointed out by Kaya and McNiven: that is, if only the floor translation time histories are used, the parameters associated with the girders are not unique and there could be a family of models that would predict the time histories of the floor translations.

Identification Using Both Displacements and Rotations

It appears that the girder and column length factors do not form an independent set of parameters with respect to displacement response data. However, the rotation data, inferred from strain measurements, are not of the same magnitude as the displacement data. If the rotation data are used directly in identifying the parameters they could be expected to have little or no effect. The rotation data, therefore, are scaled by the modulus of elasticity of the steel, $E=29.6\times10^6$ psi. While somewhat arbitrary, this causes the two sets of data to be of the same order of magnitude.

In the fourth model twelve seconds of response data are used with the same set of parameters as model three but using both floor translation and joint rotation responses. The findings of Kaya and McNiven are confirmed. The column parameter and the three girder parameters are of the same order of magnitude, the parameter for the column being greater than one and the three for the girders less than one. However, in this latter case they are unique.

Finally, in model five an additional parameter is introduced to account for the pitching of the table. The initial value of this parameter is the one suggested by Tang [3]. An examination of the parameter resulting from optimization shows that the algorithm tends to "soften" the system by increasing the base stiffness and, to compensate, decreases the effective girder lengths. Thus, it appears that the girder and base parameters do not form an independent set.

Model 6: The Final Model

In the previous models, the parameter adjustment primarily took place in the effective girder lengths. In contrast, model six is an attempt to permit the joints to accommodate the response. Thus, a four-parameter model is formulated, with one parameter associated with the columns, one parameter with the base stiffness, one parameter with the effective joint panel thickness, and one for damping. After identification, parameter values are as follows:

Parameter	Phase I Value	Phase II Value
column	1.09	1.07
base	.96	.97
joint	2.16	5.27
damping	1.35	1.53

Note that the column and base parameters are close to their estimated values and are unaffected by the stiffening of the joints. The Phase II frame has a higher damping factor than the frame for Phase I, which we would anticipate. The most significant observation is that the joint parameter for the Phase II frame is significantly higher than the comparable parameter for the Phase I frame, indicating that joint stiffness plays a major role in the model.

The influence of the joint behavior is exhibited in the figures. The responses predicted by the "traditional" model, neglecting joint deformation, and by model six are each compared to the recorded experimental responses for both floor translations and joint rotations. Examination shows that model six predicts the seismic response of the frame significantly better than the model neglecting joint deformation.

REFERENCES

1. Kaya, I. and McNiven, H. D., "Investigation of the Elastic Characteristics of a Three Story Steel Frame Using System Identification", Report No. EERC-78-24, Earthquake Engineering Research Center, University of California, Berkeley, November 1978.

2. Clough, R. W. and Tang, D. T., "Earthquake Simulator Study of a Steel Frame Structure, Vol. I: Experimental Results", Report No. EERC-75-6, Earthquake Engineering Research Center, University of California, Berkeley, April 1975.

3. Tang, D. T., "Earthquake Simulator Study of a Steel Frame Structure, Vol. II: Analytical Results", Report No. EERC-75-36, Earthquake Engineering Research Center, University of California, Berkeley, October 1975.

DISPLACEMENTS AT THIRD FLOOR
(inches vs. seconds)

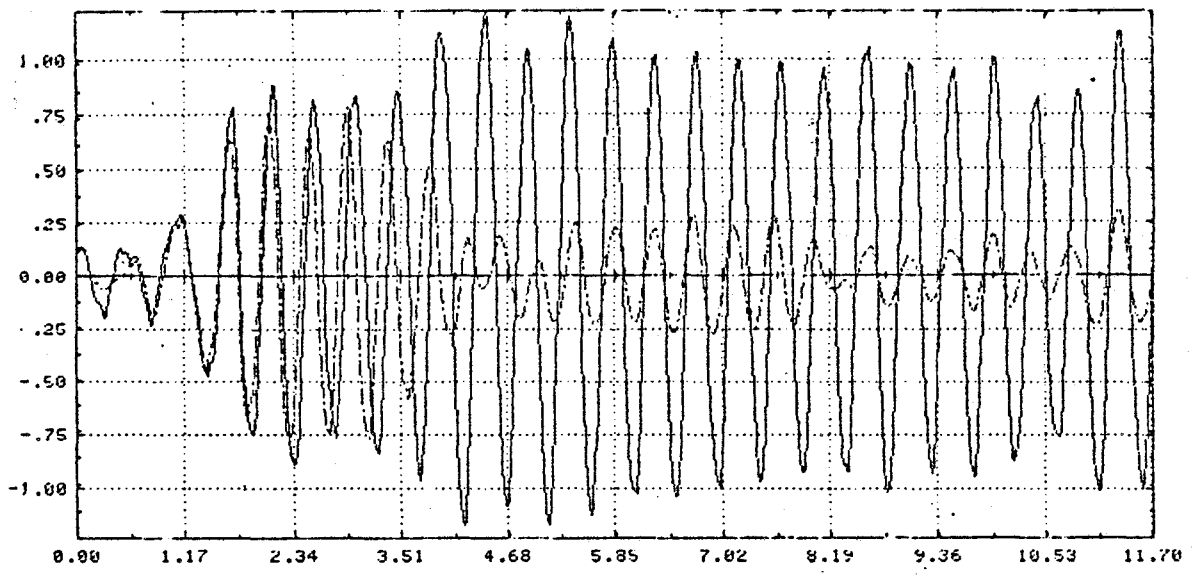

FIGURE 1
Comparison with Response from Traditional Model

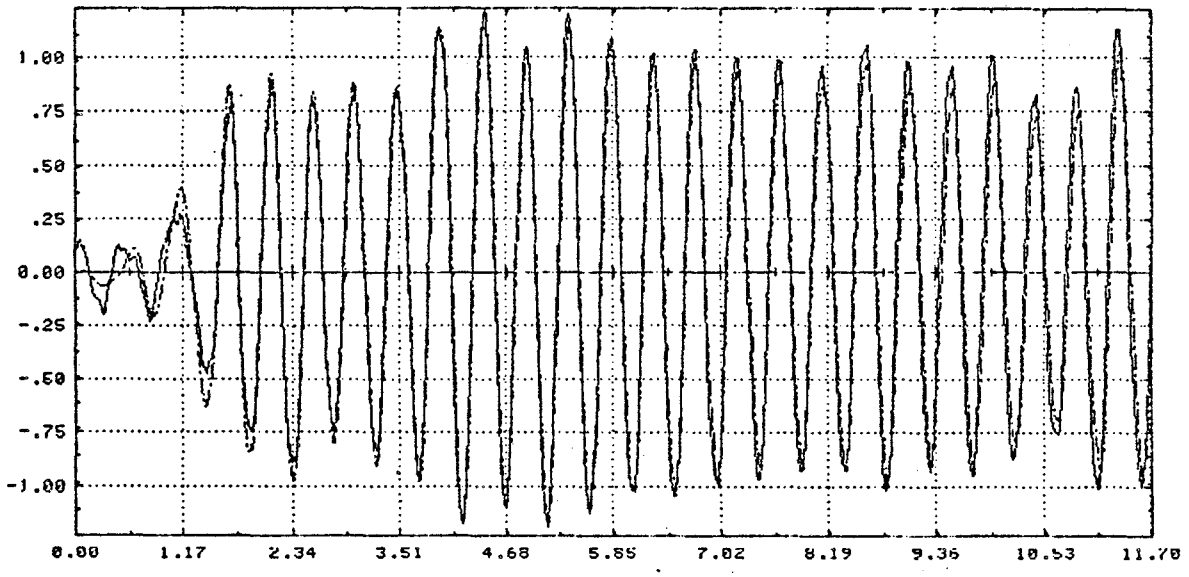

FIGURE 2
Comparison with Response from Model Six

ROTATIONS AT FIRST FLOOR
(milliradians vs. seconds)

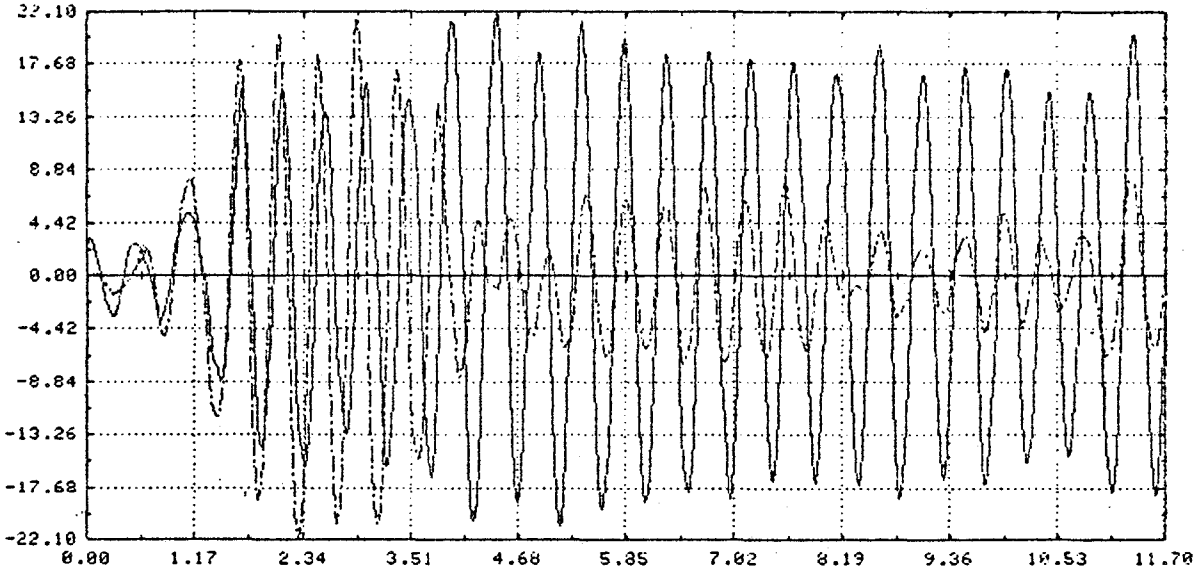

FIGURE 3
Comparison with Response from Traditional Model

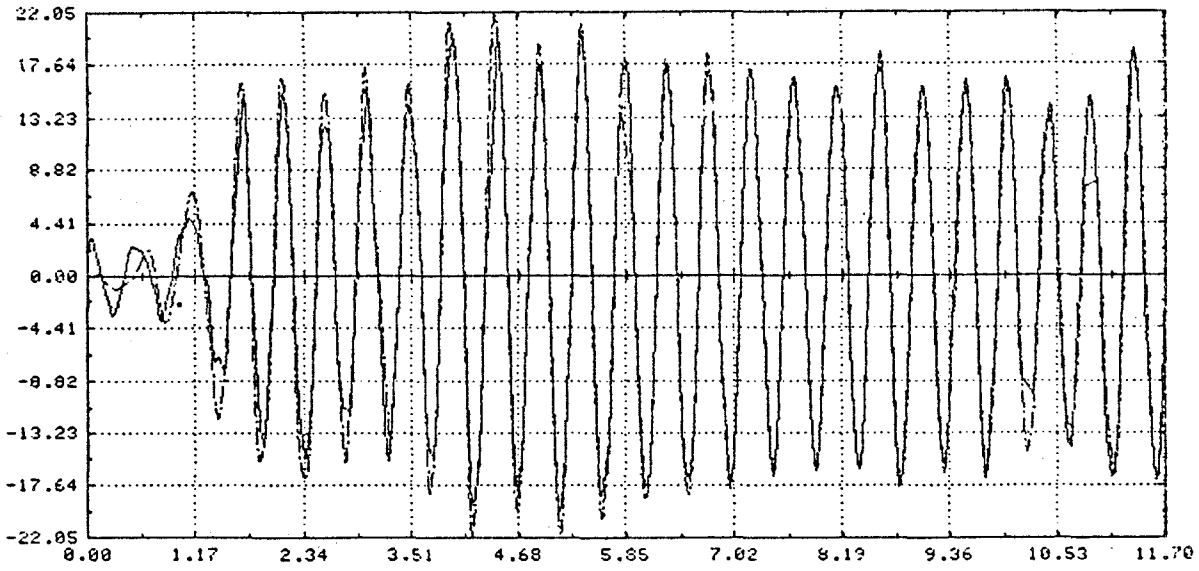

FIGURE 4
Comparison with Response from Model Six

A MIXED FINITE ELEMENT METHOD FOR DYNAMIC ANALYSIS OF SEISMICALLY-LOADED STRUCTURES - APPLICATION TO COUPLED SHEAR WALLS

F. M. El-Kamshoshy (I)
K. S. Pister (II)
Presenting Author: F. M. El-Kamshoshy

SUMMARY

A mixed finite element method is presented for the dynamic analysis of seismically-loaded structures. For time-history dynamic analysis of coupled shear walls, the principal internal forces are introduced in the problem formulation and they are computed in the process of backsubstitution. Thus, the computation of a large number of secondary time-histories and element stresses is avoided. Since explicit relations can easily be established between various internal forces, the method lends itself to the normal force-moment and shear-torsion strength interaction relations, plastic design, and collapse analysis.

INTRODUCTION

Design assessment of large structures which are subjected to earthquake excitations usually seeks relatively few principal internal forces and kinematic measures. (By "principal internal forces" we mean forces that are critical to the design process.) On the other hand, finite element analysis of these structures typically involves a large number of nodal variables. Regardless of how small the number of principal internal forces is, computation of the entire system of response variables is generally inevitable; this is a definite shortcoming of the usual finite element analysis. As an alternative, principal internal forces can be introduced in the analysis process via a mixed finite element technique. This technique is particularly advantageous for the time-history analysis of seismically-loaded structures, where the computation of a large number of secondary time-histories is thereby avoided. The technique is applied here to the analysis of coupled shear walls and selected results are obtained utilizing the "ANSYS" computer program (Ref. 2).

Finally, several applications are briefly discussed: imposing interaction strength relations between internal forces, plastic design, and collapse analysis.

DESIGN AND ANALYSIS

The process of structural design requires a series of analyses of alternative trial structures to ensure acceptable performance. Principal internal forces play a key role in member and joint design and in the assessment of structural safety. Design criteria, a basic knowledge of structural behavior, and practical experience are essential elements in

(I) Independent consultant.

(II) Professor, University of California, Berkeley, California, USA

choosing appropriate principal internal forces. However, natural locations of these forces are found at the structural joints and points of concentrated loads.

To illustrate the approach, design of coupled shear walls in a seismic zone is considered, Fig. 1(a). Under strong horizontal ground motion, the structure is normally allowed to undergo plastic deformation. Since wall collapse is to be avoided, failure should be confined, wherever possible, to the beams. Thus, natural candidates for the principal internal forces are the beam coupling moments. Moreover, the determination of internal forces at several wall sections, especially the base, is needed to insure an adequate design. To incorporate these internal forces in the analysis, a mixed finite element is used. Such elements are introduced to directly bring into the formulation the coupling moments and other internal forces, as explained in the following section.

COUPLED SHEAR WALLS BY MIXED FINITE ELEMENTS

The theoretical background for the method employed here is in Ref. 1; the walls are divided into conventional stiffness elements, and mixed finite elements are used for the coupling beams and at principal joints of wall elements. A typical finite element layout is shown in Fig. 1(b).

For the coupling beam element,* Fig. 1(c), $\underset{\sim}{x}_b$ is the vector $[v_1, \theta_1, v_2, \theta_2, m]^T$; $\underline{A}_b$ is a mixed matrix given below; $\underset{\sim}{b}$ is the vector $[0,0,0,0,\bar{\theta}_b]$ comprising the beam fixed end loads (zero) and the total plastic rotational deformation of the beam ($\bar{\theta}_b$); m is the coupling moment

$$\underline{A}_b = \left[\begin{array}{cccc|c} 0 & 0 & 0 & 0 & 2/S \\ & 0 & 0 & 0 & 1 + 2\ell_1/S \\ & & 0 & 0 & -2/S \\ & & & 0 & 1 + 2\ell_2/S \\ \multicolumn{4}{c|}{\text{Symmetrical}} & -f \end{array}\right] \qquad (1)$$

where $$f = \frac{S}{3EI} + \frac{4}{SGA'} \qquad (2)$$

A moment-originating element is introduced to bring into the formulation the internal moment at the principal joints of the walls. For this element,* Fig. 1(d) : $\underset{\sim}{Y} = [\theta_i, \theta_j, M_w]^T$; $\underline{B}$ is the matrix given below; and $\underset{\sim}{c} = [0, 0, \bar{\theta}_w]^T$

---

*See nomenclature.

$$\underline{B} = \begin{bmatrix} 0 & 0 & 1 \\ & 0 & -1 \\ \text{Symmetrical} & & 0 \end{bmatrix} \qquad (3)$$

M_w is the internal moment at the wall joint and $\bar{\theta}_w$ is the corresponding plastic rotational deformation.

The shear-originating element is found, from the preceding element, by replacing θ_i, θ_j, M_w, and $\bar{\theta}_w$ by u_i, u_j, V_w, and $\bar{u}$, respectively. V_w is the shearing force at the joint and $\bar{u}$ is the corresponding plastic displacement. Similarly, a normal force-originating element is obtained from the shear element by changing the horizontal displacement and shearing force to vertical displacement and normal force, respectively.

The major steps in the time-history dynamic analysis are shown in Fig. 2:

(i) Formulation of element

(ii) Assembly of elements

(iii) Coordinate condensation (A) into dynamic degrees of freedom and principal internal forces

(iv) Coordinate condensation (B) into dynamic degrees of freedom

(v) Solution

(vi) Utilizing the process of back-substitution, determining the time-histories of the principal internal forces, which were condensed in step (iv)

(vii) For nonlinear analysis, steps (iv) and (vi) are eliminated.

Numerical Application

To examine the method presented in the linear range, an 18-story coupled shear wall structure (taken with minor modification from Ref. 3 was analyzed. For this structure;* h = 105, S = 38, ℓ_1 = 63.2, ℓ_2 = 67.5 in; A_1 = 5550, A_2 = 5650, A = 672 sq. in.; $I_1 = 66 \times 10^5$, $I_2 = 90 \times 10^5$, $I = 1.52 \times 10^4$ in^4; E = 5000 k/in^2; and lumped mass/story = 0.5 k - sec^2 - in^{-1}.

The principal internal forces included coupling moments and forces at the wall bases. This structure was subjected to the first four seconds of the El-Centro Earthquake record, N-S component, May 18, 1940, scaled by 1/3. Considering Rayleigh damping, a damping ratio of 5% is assumed for the first and second modes. Numerical integration was carried out using a time step of .01 second.

*See nomenclature.

After performing the solution, using the "ANSYS" computer program (Ref. 2), the backsubstitution process resulted in the time-histories of the principal internal forces, shown in Fig. 3. The maximum values of coupling moment at the 2nd, 10th, and 18th stories are 3972, 33831 and 957 kip-in, respectively. The maximum forces at wall bases are: M_1 = .789 x 10^5 and M_2 = 1.027 x 10^5 kip-in; v_1 = 269 and v_2 = 304 kip; and N_1 = 2836 kips.

To evaluate the computational saving of the mixed method, a block diagram is provided in Fig. 4 for the stiffness formulation of the coupled shear walls. The dynamic relations are first established in terms of the entire coordinate system (114 coordinate). By condensation, these relations are reduced to 19 dynamic degrees of freedom. Solving these relations yield their time-histories. By backsubstitution, the time-histories of the remaining 95 degrees of freedom are computed. Finally, the time-histories of the element internal forces are found using the time-histories of the element nodal variables and element relations. The first two steps are referred to as the "Displacement Pass," while the last two steps are termed the "Stress Pass." However, by using the mixed finite element technique, the "stress pass" is reduced to the backsubstitution in 24 relations: 18 coupling moments and 6 forces acting at the bases. Although the exact saving in the computational time is not available, taking the above discussion into consideration, it is estimated that the computational time is reduced by over 50%. This saving generally increases for taller shear walls and other large structures.

DISCUSSION

In the mixed finite element analysis, unlike the typical stiffness formulation, internal forces are included in the model coordinate system. Naturally, explicit relations can easily be established between various internal forces. Consequently, for an indeterminate structure, the method lends itself to imposing the normal force-moment and shear-torsion strength interaction relations. Moreover, if the principal internal forces are chosen among design variables, the method will be a useful tool for plastic design and collapse analysis.

CONCLUSION

A mixed finite element method is presented for the dynamic analysis of seismically-loaded structures. The method utilizes a mixed finite element model whose coordinate system includes principal internal forces. The method is applied to time-history dynamic analysis of coupled shear walls, where the computation of secondary time-histories is avoided. Numerical results are obtained for linear analysis. Since explicit relations can easily be established between various internal forces, the method lends itself to the normal force-moment and shear-torsion strength interaction linearized relations, plastic design and collapse analysis.

REFERENCES

1. El-Kamshoshy, F. M., "Mixed Finite Element Method for Optimal Seismic Design of Earthquake Resistant Structures," Ph.D. Dissertation, University of California, Berkeley, June 1981.

2. "ANSYS" Engineering Analysis System Users Manual, Revision 4, Swanson Analysis Systems, Inc., Houston, TX, U.S.A., 1982.

3. Nayar, K. K., and Coull, A., "Elasto-Plastic Analysis of Coupled Shear Walls," J. of Structural Division, ASCE, Proc. Paper, Vol. 102, No. ST9, Sept. 1979, pp. 1845-1860.

NOMENCLATURE

A_i Cross section area of wall (i), (i = 1,2)

A Beam cross section area

A' Beam shear area

E Young's modulus

G Shear modulus

h Story height

I Beam moment of inertia

I_i Moment of inertia of wall (i), (i = 1,2)

ℓ_1 Distance from centroidal axis of wall (1) to connected beam end

ℓ_2 Distance from centroidal axis of wall (2) to connected beam end

m_j Coupling moment at story (j), (j = 1,18)

M_i Moment at base of wall (i), (i = 1,2)

N_i Normal force at base of wall (i), (i = 1,2)

r_j Lateral displacement of story (j), (j = 1,18)

S Beam clear span

u Horizontal displacement

v_i Vertical displacement of wall (i), (i = 1,2)

V_i Shearing force at base of wall (i), (i = 1,2)

θ Rotation

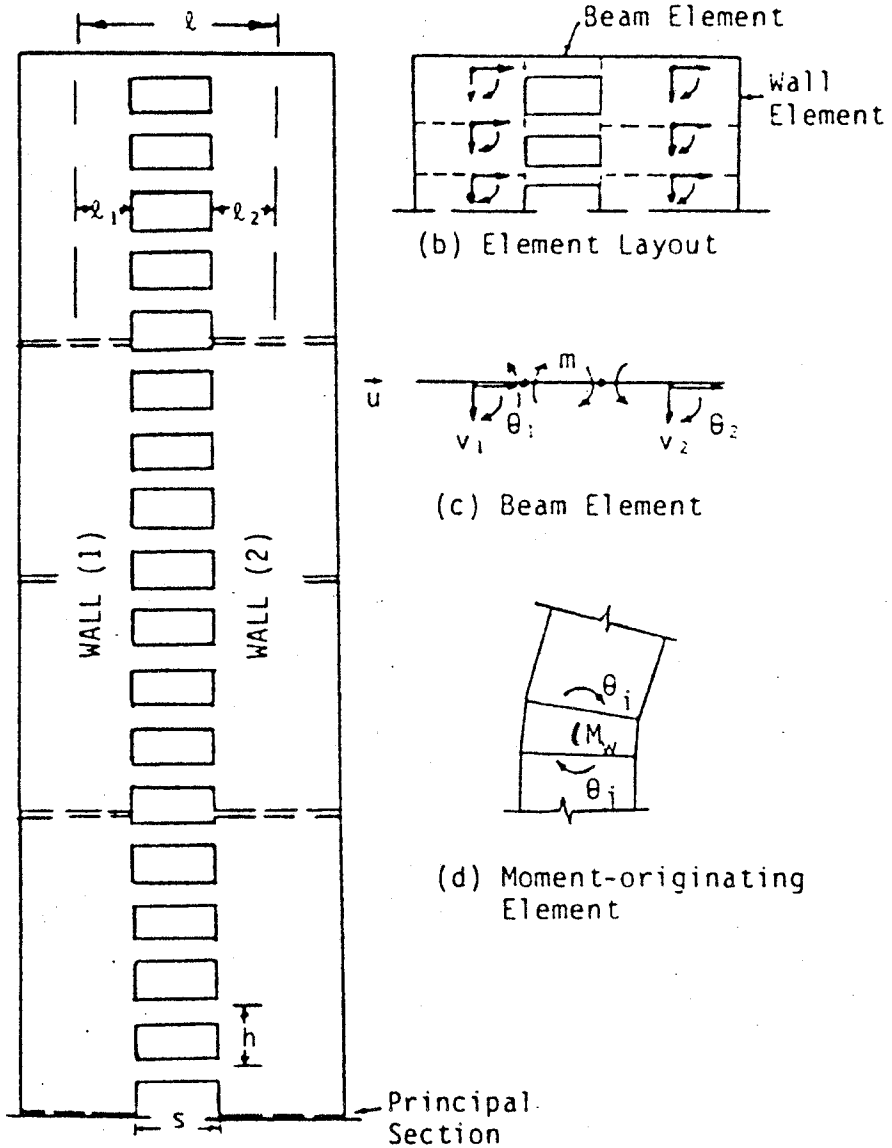

Fig. 1. Coupled Shear Walls

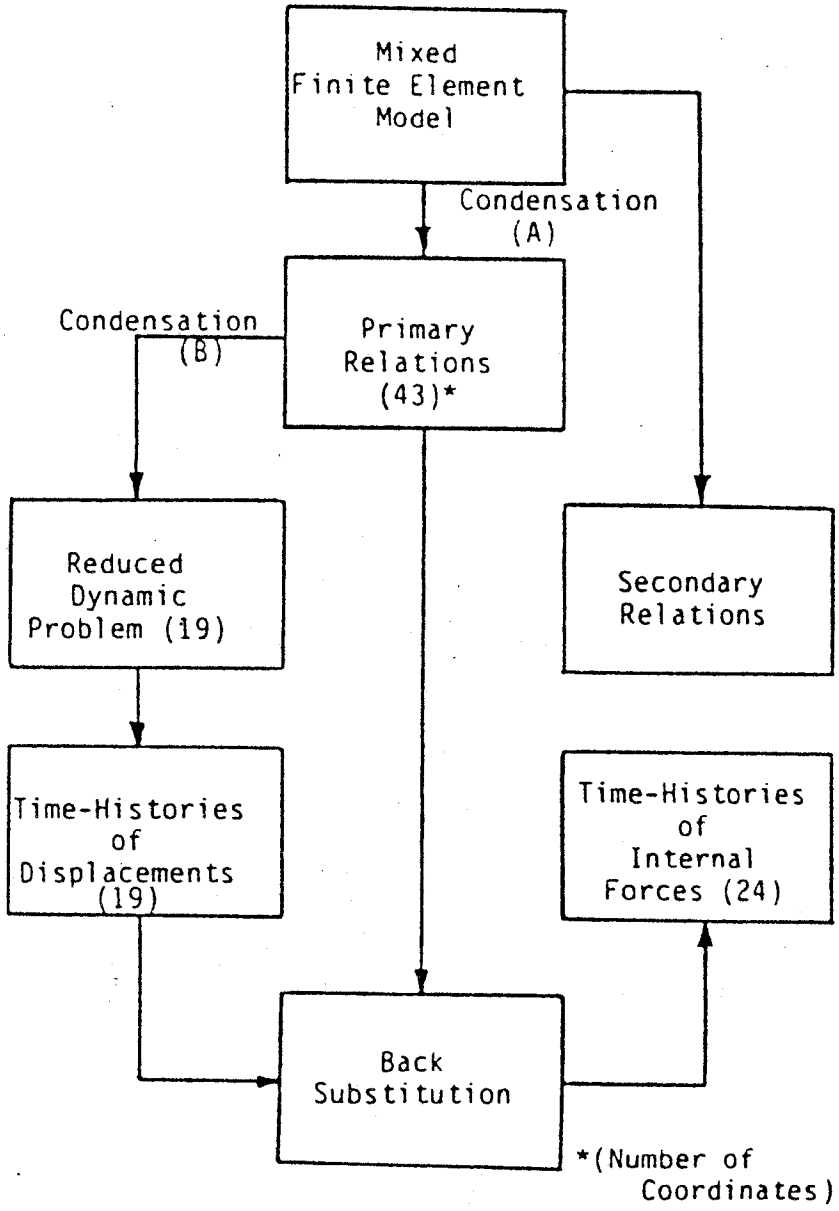

Fig. 2. Time-History of Primary Variables

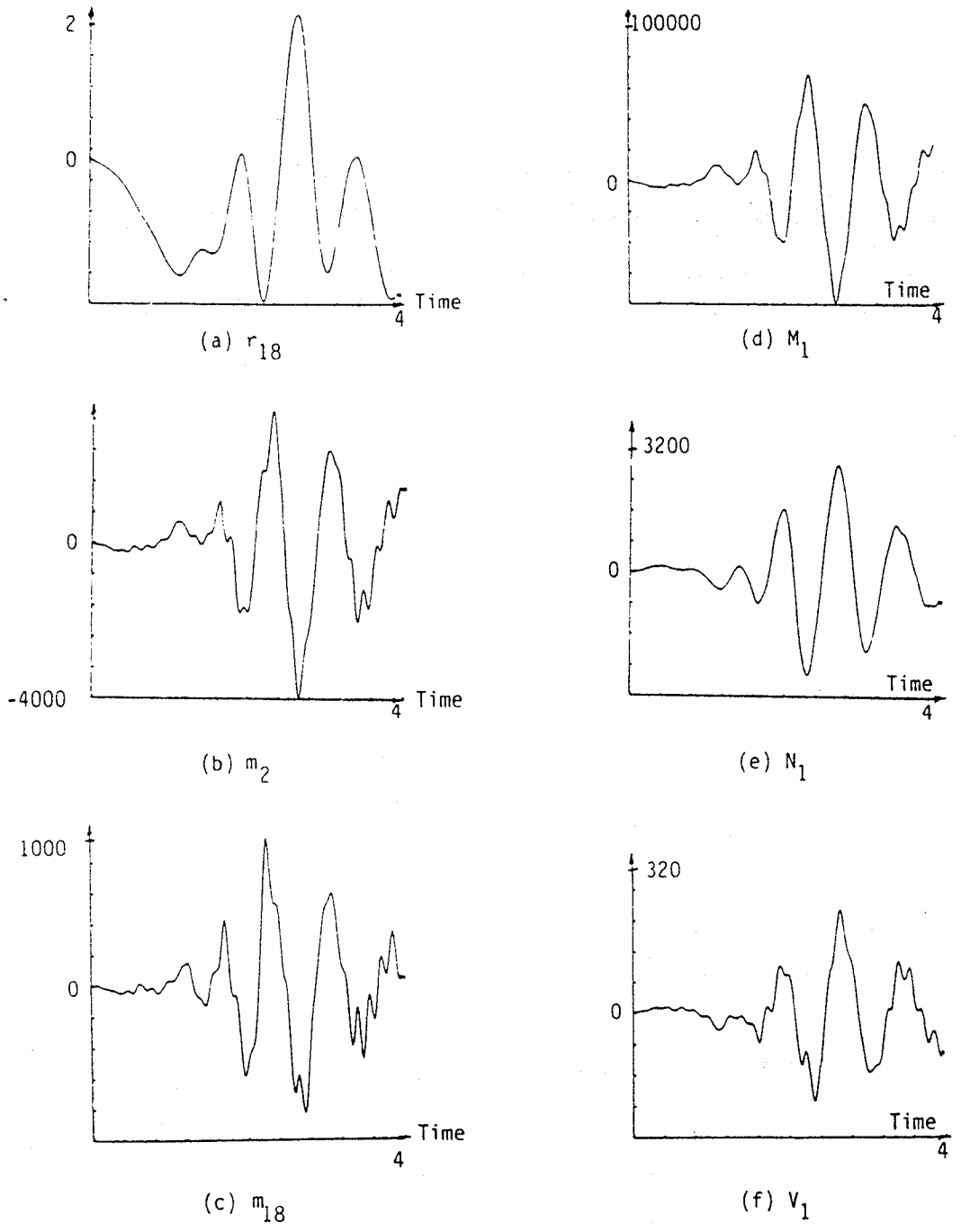

Fig. 3. Numerical Results (kip-in-sec.)

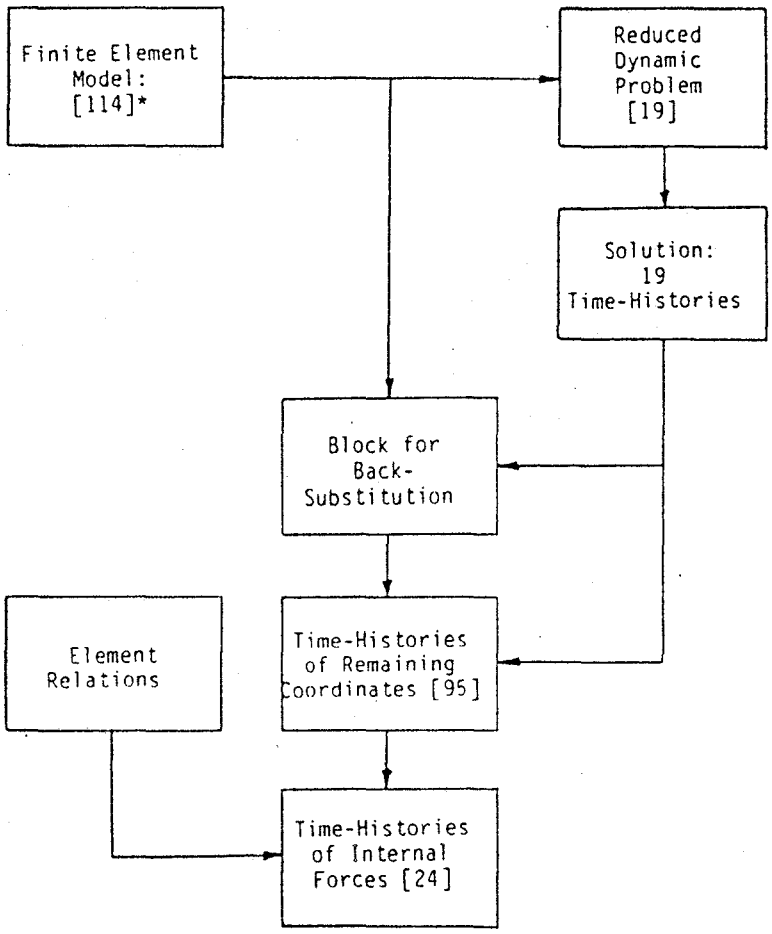

Fig. 4. Typical Finite Element Time-History Dynamic Analysis (Stiffness Formulation)

*[Number of coordinates]

HYSTERETIC BEHAVIOR OF REINFORCED CONCRETE BEAMS AND JOINTS

Filip C. Filippou (I)
Egor P. Popov (II)
Presenting Author: Filip C. Filippou

SUMMARY

This paper presents a general analytical model which describes the hysteretic behavior of reinforced concrete joints and gir er inelastic regions under large deformation reversals. The interaction of reinforcing steel and surrounding concrete through bond and the deterioration of such interaction under cyclic load reversals is taken into account. In order to satisfy the equilibrium of horizontal forces and bending moments at cracked R/C sections a new layer model is presented which accounts for the deterioration of bond in the vicinity of the crack. The model is applied to an interior beam-column joint and analytical predictions are compared with experimental evidence on the hysteretic behavior of interior beam-column subassemblages. A series of parametric studies on the hysteretic response of interior joints is also presented.

INTRODUCTION

Reinforced concrete structures designed according to present building codes are expected to deform well into the inelastic range and dissipate the energy input by an extreme base motion through stable hysteretic behavior of structural components. Since inelastic deformations are typically concentrated at certain critical regions within the structure (Ref. 1), the accurate prediction of the mechanical behavior of a structure during earthquake excitations depends on the development of reliable analytical models which describe the hysteretic behavior of these regions. Following present earthquake resistant design philosophy the energy input by the base motion should be dissipated in the largest possible number of inelastic regions within the structure. Ductile moment resisting frames as well as coupled wall systems are designed so that yielding starts to develop at the girder ends. Columns of a ductile moment resisting frame should remain elastic during the earthquake response, except at the base of the building, to avoid the formation of a partial sidesway collapse mechanism. Attention is thus focused on understanding and predicting the hysteretic behavior of critical regions in girders as well as that of beam-column or girder-wall joints.

In modeling the hysteretic behavior of reinforced concrete members under large deformation reversals the interaction of reinforcing steel and surrounding concrete through bond and the deterioration of such interaction under cyclic load reversals appears to be an important factor. Cyclic bond deterioration has however received only limited attention in previous analytical studies (Refs. 2, 3 and 4) mostly due to lack of reliable experimental data on the bond behavior of deformed bars embedded in R/C members and subjected to cyclic load reversals.

(I) Asst. Professor of Civil Engineering, Univ. of California, Berkeley, USA
(II) Professor of Civil Engineering, Univ. of California, Berkeley, USA

PROPOSED ANALYTICAL MODEL

In order to formulate an analytical model describing the hysteretic behavior of R/C members with due account of cyclic bond deterioration between reinforcing steel and concrete, the region of the member undergoing inelastic action is divided into a number of subregions at locations where cracks form (Fig.1). In members subjected to severe moment reversals with low shear stresses, cracks run almost vertically to the axis of the member through the depth of the cross-section. The positions where cracks are expected to form are not known a priori and can be established in the course of an analysis by determining the sections where the concrete tensile strength is first exceeded. In the present model for reasons of simplicity the cracks have been assumed to run vertically across the section and form at predetermined locations. This is, strictly speaking, true only at beam-column interfaces of interior and exterior joints and at the ends of coupling girders (Fig.2).

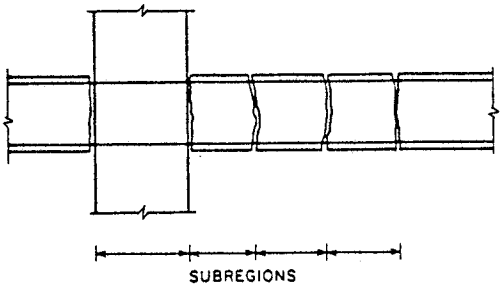

FIGURE 1 SUBDIVISION OF R/C MEMBER INTO SEVERAL SUBREGIONS

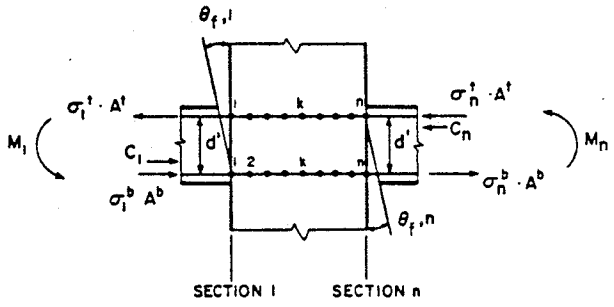

FIGURE 2 ANALYTICAL MODEL FOR INTERIOR BEAM-COLUMN JOINT

The hysteretic response of each subregion is determined by satisfying the equilibrium of horizontal forces and bending moments at both end sections and by establishing the stress transfer between steel and concrete within the region. The effect of shear stresses is neglected. The analytical model thus consists of two main parts:

(1) a model describing the transfer of stresses between reinforcing steel and surrounding concrete within the subregion. This model is based on a solution of the differential equations of bond using a mixed finite element method. It results in a nonlinear transfer matrix which relates steel stress and relative slip increments at section 1 to those at section n of the subregion (Figs.1 and 2). In order to describe the reinforcing steel stress-strain relation under arbitrary strain reversals the model proposed by Menegotto and Pinto in Ref. 5 has been modified to include isotropic strain hardening as a function of plastic strain history. In modeling the bond stress-slip behavior between reinforcing steel and surrounding concrete the model proposed by Eligehausen et. al in Ref. 6 has been modified to include a gradually increasing slope during reloading as shown in Fig. 3 (curve (d)).

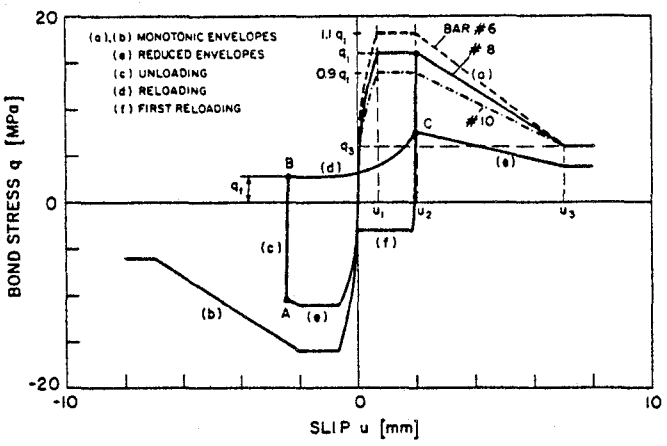

FIGURE 3 PROPOSED BOND STRESS-SLIP RELATION

(2) a section layer model for cracked reinforced concrete sections which determines the relative contribution of reinforcing steel and concrete to the equilibrium of horizontal forces and bending moments at a cracked section. Since the relative slip of reinforcing bars with respect to the surrounding concrete can be computed with the aid of the model under (1) it is possible to compute and trace the time history of crack width at the level of the top and bottom reinforcing layer (Fig.4(a)). Using a simple extrapolation formula the crack width at the top and bottom of the cracked R/C section can be estimated (Fig.4(b)). Once the crack width at the top and bottom of a cracked R/C section can be estimated at each load step, a crack closure criterion determines whether the crack is open or closed. If the crack is open, the concrete contribution to the equilibrium of horizontal forces and bending moments at the cracked section is equal to zero. If the crack is closed, a rule derived from experimental evidence relates the strain increments in the reinforcing bars to concrete strain increments in the section layer containing the bars. Once the distribution of concrete strain increments over the depth of the cross-section is established the concrete contribution to the equilibrium of section forces can be readily determined. More details on this new layer model for cracked R/C sections are presented in Ref. 7.

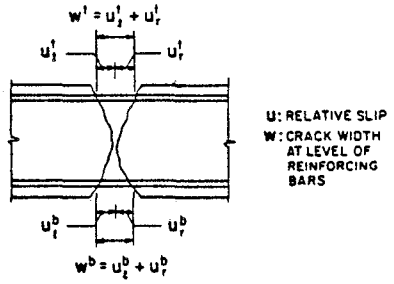

FIGURE 4a DEFINITION OF RELATIVE SLIP AND CRACK WIDTH AT A CRACKED REINFORCED CONCRETE SECTION

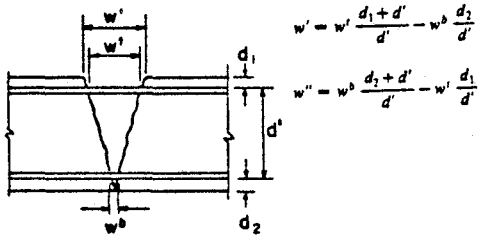

FIGURE 4b COMPUTATION OF CRACK WIDTH AT THE TOP AND BOTTOM OF A CRACKED R/C SECTION

RESULTS ON INTERIOR BEAM-COLUMN JOINTS

The validity of the analytical model was tested by comparing its predictions with experimental results from interior beam-column subassemblages subjected to cyclic loading simulating the effects of severe seismic excitations; two specimens from Ref. 8 were used as sample cases. The two specimens were subjected to entirely different load histories: specimen BC4 was subjected to a single large displacement reversal simulating a very severe seismic pulse; specimen BC3 was subjected to a large number of deformation reversals of gradually increasing magnitude. Only the results pertaining to specimen BC3 will be presented here. A more complete discussion along with results from specimen BC4 is presented in Refs. 7 and 9.

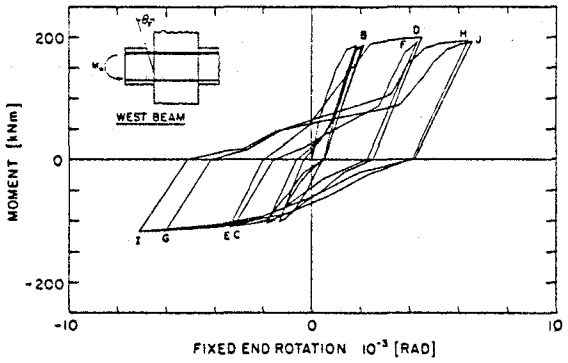

FIGURE 5a END MOMENT VERSUS FIXED-END ROTATION. SPECIMEN BC3

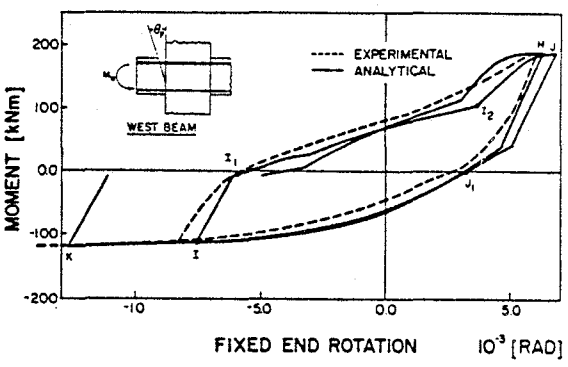

FIGURE 5b END MOMENT VERSUS FIXED-END ROTATION. SPECIMEN BC3

Fig. 5a depicts the analytically predicted moment-fixed end rotation relation at the west beam-column interface of specimen BC3. Selected loops are compared with experimental evidence in Fig. 5b indicating very satisfactory agreement. It should be noted that fixed-end rotations are computed by considering the relative slip of top and bottom reinforcing bars at the interface and dividing by the distance between the top and bottom reinforcing layer. In calculating the relative slip of reinforcing bars at the beam-column interface only the influence of bond deterioration along the column anchorage length was accounted for in order to facilitate comparison with experimental results. The effect of bond deterioration in the girder inelastic regions adjacent to the column is thus not included in the fixed-end rotations depicted in Figs. 5a and 5b, since it is accounted for when computing the rotation of the girder inelastic region.

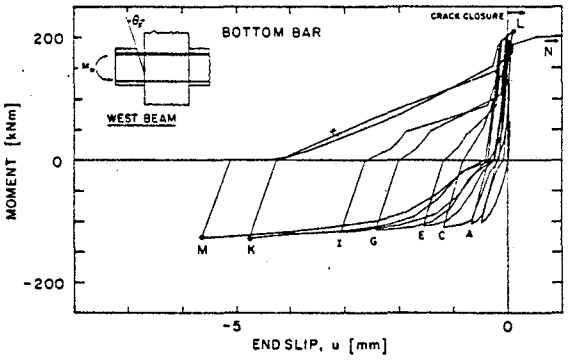

FIGURE 6a END MOMENT VERSUS RELATIVE BAR SLIPPAGE AT BEAM-COLUMN INTERFACE. SPECIMEN BC3

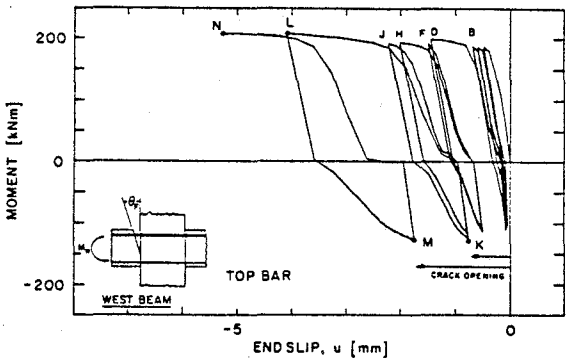

FIGURE 6b END MOMENT VERSUS RELATIVE BAR SLIPPAGE AT BEAM-COLUMN INTERFACE. SPECIMEN BC3

Figs. 6a and 6b depict the relative slip of the bottom and top reinforcing bars, respectively, at the west beam-column interface. Capital roman letters correspond to points of load reversal in Fig. 5a. It is observed that at load point K both the crack at the bottom and that at the top of the cross-section are open indicating that the crack is open through the depth of the beam-column interface. This is due to unequal amounts of top and bottom reinforcement which prevents the crack at the top from closing when the bottom reinforcing bars are subjected to tensile stresses.

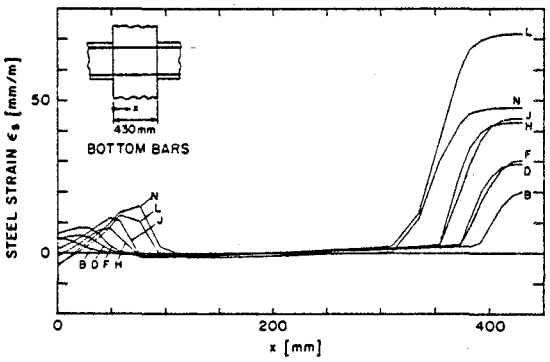

FIGURE 7a DISTRIBUTION OF STEEL STRAIN ALONG THE BOTTOM REINFORCING BARS WITH INCREASING MAGNITUDE OF END SLIP

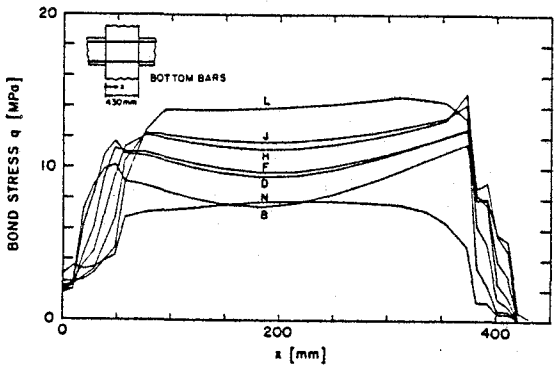

FIGURE 7b DISTRIBUTION OF BOND STRESS ALONG THE BOTTOM REINFORCING BARS WITH INCREASING MAGNITUDE OF END SLIP

Figs. 7a and 7b depict the distribution of steel strains and bond stresses along the column anchorage length of the bottom reinforcing bars with increasing magnitude of end slip. It is observed that up until the moment when bond is completely destroyed within the column (load point N) a portion of the reinforcing bars remains elastic.

ANALYTICAL PARAMETRIC STUDIES

Using the developed analytical model studies regarding the influence of various parameters such as yield strength of reinforcing bars, ratio of top to bottom reinforcement, reinforcing bar diameter and bond strength can be conducted. Such studies are presented in some detail in Ref. 7. A small selection of the findings is presented below.

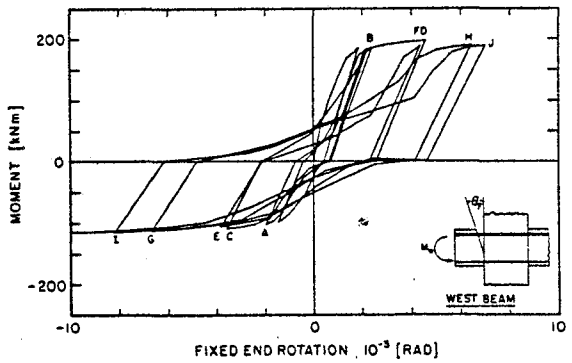

FIGURE 8a END MOMENT VERSUS FIXED-END ROTATION. BOND STRENGTH REDUCED BY 15% ALONG TOP AND BOTTOM REINFORCING BARS

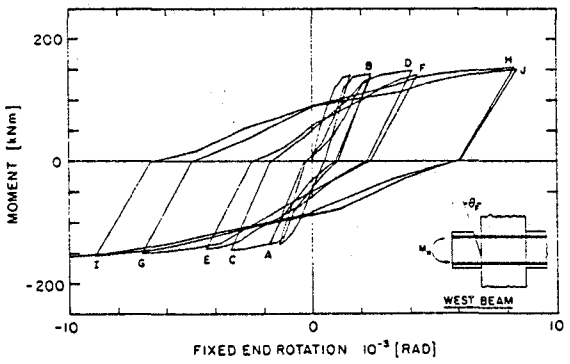

FIGURE 8b END MOMENT VERSUS FIXED-END ROTATION. EQUAL RATIO OF TOP TO BOTTOM REINFORCEMENT

In Fig. 8a the analytical moment-fixed end rotation relation resulting when the bond strength along the top and bottom reinforcing layer is reduced

by 15% is presented. All other parameters are kept the same as those in specimen BC3. When comparing Fig. 8a to Fig. 5a it is concluded that a small reduction in bond strength considerably influences the hysteretic behavior of interior joints resulting in more pronounced pinching of hysteresis loops and less energy dissipation capacity. This fact has important consequences in practice. Poor construction quality and workmanship can lead to a substantial decrease in the energy dissipation capacity of R/C joints.

Fig. 8b depicts the analytical moment-fixed end rotation relation when the total area of bottom reinforcing bars is set equal to the area of reinforcement at the top of the girder. Considerable improvement in hysteretic behavior results in this case as a consequence of the reduction in the pinching of hysteretic loops leading to an increase in energy dissipation capacity of the joint.

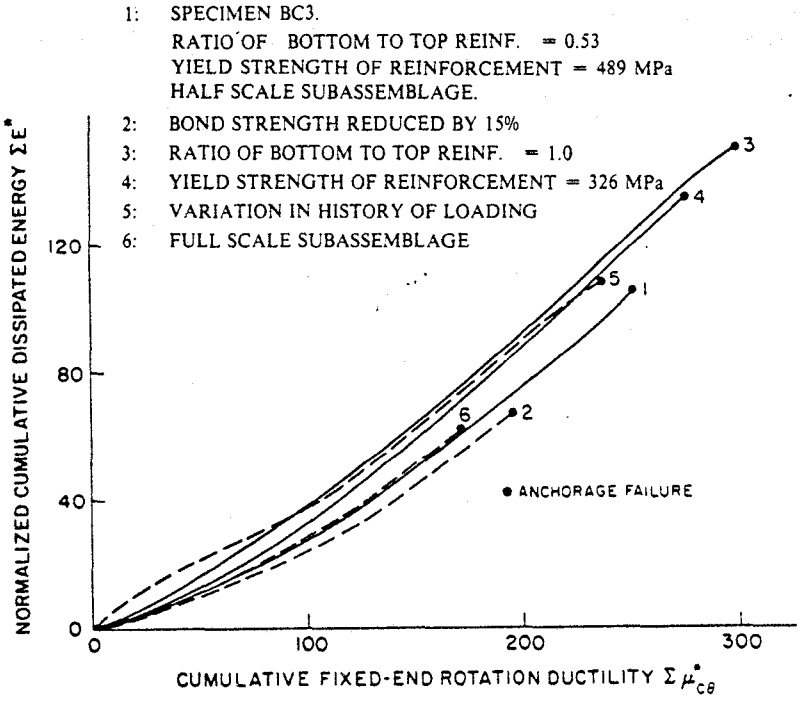

FIGURE 9 NORMALIZED TOTAL ENERGY DISSIPATION VERSUS CUMULATIVE FIXED-END ROTATION DUCTILITY FOR INTERIOR BEAM-COLUMN JOINT UNDER VARIATION OF PARAMETERS

In order to compare the behavior of interior beam-column joints under variation of different parameters, the normalized cumulative dissipated energy of the joint is plotted versus the cumulative fixed-end rotation ductility for a number of parametric studies in Fig. 9. The following parameters have been studied in addition to the bond strength and the ratio of top to bottom reinforcement: yield strength of reinforcing bars, history of loading, and influence of scale of the subassemblage. The following conclusions can be drawn from Fig. 9:

(a) Increasing the ratio of bottom to top reinforcement or decreasing the yield strength of reinforcing bars (which results in an increase in the number of bars if the yield moment remains the same) leads to considerable improvement in the total energy dissipation capacity of R/C joints.

(b) The history of loading affects the hysteretic behavior of R/C beam-column joints.

(c) The total energy dissipation capacity of a full-scale joint is considerably smaller than that of a half-scale beam-column joint.

RECOMMENDATIONS FOR FUTURE RESEARCH

The proposed model can be used in conducting additional investigations which go beyond the studies presented in this paper. In this sense it is recommended:

(i) to extend the model for predicting the hysteretic behavior of critical regions of reinforced concrete columns, shear-walls and coupling beams in coupled shear-walls. The hysteretic behavior of critical regions in girders should also be investigated. These studies can help in developing analytical models which improve upon existing ones which are based on point plastic hinges or on distribution of curvatures along the empirically estimated length of the plastic hinges,

(ii) to derive simple analytical models which account for the effects of bond deterioration in the seismic response of moment resisting frames,

(iii) to use the proposed model in connection with cyclic shear models at a cracked reinforced concrete section, since it allows computation and tracing of crack width in time. As it is well established, the crack width is the main parameter which affects the contribution of aggregate interlock and of the dowel action of reinforcing bars to the shear resistance at crack interfaces,

(iv) to include the effect of joint shear and diagonal cracking in the hysteretic behavior of interior and exterior joints. In many cases the transfer of shear stresses in the joint can significantly affect the overall behavior of the member.

ACKNOWLEDGEMENTS

The authors express their deep appreciation to Professor V. V. Bertero who co-supervised the research reported in this paper. The study reported herein was supported by the National Science Foundation under Grant No. CEE 81-07217. This support is gratefully acknowledged. The help of Gail Feazell in preparing the figures is greatly appreciated.

REFERENCES

[1] Bertero, V.V., "Seismic Behavior of Structural Concrete Linear Elements (Beams, Columns) and Their Connections", Introductory Report to Theme II, AICAP-CEB Symposium, Structural Concrete Under Seismic Actions, Rome 1979; Comité Euro-International Du Béton, Bulletin D' Information No. 131, Vol. 1, pp. 125-212.

[2] Emori, K. and Schnobrich, W.C., "Inelastic Behavior of Concrete Frame-Wall Structures", Journal of the Structural Division, ASCE, Vol. 107, No. ST1, Jan., 1981.

[3] Otani, S., "Inelastic Analysis of R/C Frame Structures", Journal of the Structural Division, ASCE, Vol. 100, No. ST7, July, 1974.

[4] Tassios, T.P., and Yannopoulos, P.J., "Analytical Studies on Reinforced Concrete Members Under Cyclic Loading Based on Bond Stress-Slip Relationships", ACI Journal, Vol.78, May-June 1981.

[5] Menegotto, M. and Pinto, P., "Method of Analysis for Cyclically Loaded Reinforced Concrete Plane Frames Including Changes in Geometry and Nonelastic Behavior of Elements under Combined Normal Force and Bending", presented at the 1973, IABSE Symposium on the Resistance and Ultimate Deformability of Structures Acted on by Well-Defined Repeated Loads, held at Lisbon, Portugal.

[6] Eligehausen, R., Popov, E.P., and Bertero, V.V., "Local Bond Stress-Slip Relationships of Deformed Bars under Generalized Excitations", Report No. UCB/EERC 83-23, Earthquake Engineering Research Center, University of California, Berkeley, Oct., 1983.

[7] Filippou, F.C., Popov, E.P. and Bertero, V.V., "Effects of Bond Deterioration on Hysteretic Behavior of Reinforced Concrete Joints", Report No. UCB/EERC 83-19, Earthquake Engineering Research Center, University of California, Berkeley, Aug., 1983.

[8] Viwathanatepa, S., Popov, E.P. and Bertero, V.V., "Seismic Behavior of Reinforced Concrete Interior Beam-Column Subassemblages", Report No. UCB/EERC 79-14, Earthquake Engineering Research Center, University of California, Berkeley, Aug., 1979.

[9] Filippou, F.C., Popov, E.P. and Bertero, V.V., "Modeling of Reinforced Concrete Joints under Cyclic Excitations", Journal of Structural Engineering, ASCE, Vol. 109, No. 11, Nov. 1983.

ON SEISMIC DESIGN OF ECCENTRICALLY BRACED STEEL FRAMES

Kazuhiko Kasai (I)
Egor P. Popov (II)
Presenting Author: Kazuhiko Kasai

SUMMARY

This paper describes the basic characteristics and the available design methods for eccentrically braced frames (EBFs). It is shown that the selected bracing scheme and the ratios of brace eccentricity lengths to beam span lengths play dominant roles on the elastic and plastic behavior of EBFs. A new general method for a rapid preliminary plastic design of EBFs is described and its accuracy is demonstrated by comparisons with elasto-plastic solutions. A summary of the current research being conducted at the University of California at Berkeley is also given.

INTRODUCTION

Since publication of a research paper on EBFs for seismic bracing in 1978 (Ref. 1), this concept has been rapidly adopted in practice. Several major buildings in California have already been constructed using this approach, and others are under construction or are being designed employing this system of bracing. Fig. 1 illustrates several possible types of EBFs: the D-brace, K-brace, and V-brace frames. In all such frames the axial forces in the braces are transmitted to the columns through bending and shear action by a portion of the beam called an "active link." If designed correctly, EBFs possess greater ductility and are more versatile than the concentrically braced frames (CBFs). Moreover, for drift control they offer significant advantages of economy in comparison with moment-resisting frames (MRFs).

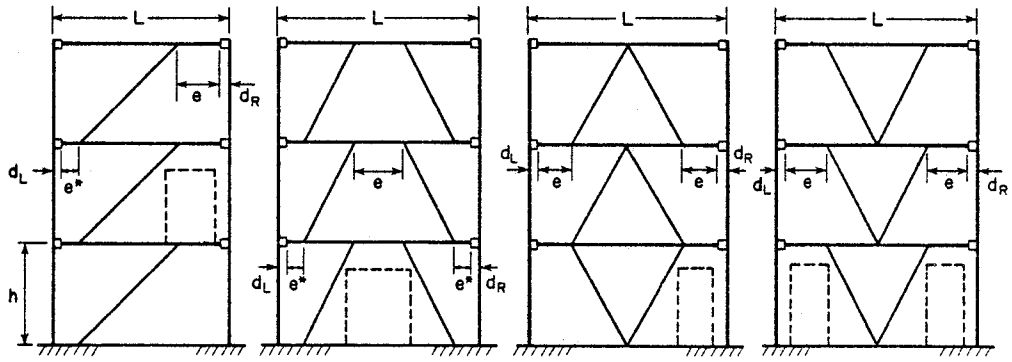

FIG. 1 Various Types of EBFs

(I) Research Assistant, Department of Civil Engineering, University of California, Berkeley, California 94720, USA.

(II) Professor Emeritus of Civil Engineering, University of California, Berkeley, California 94720, USA.

INELASTIC CHARACTERISTICS OF EBFs

Inelastic Behavior of Shear Links. The performance of an EBF depends largely on the active links. As shown in Fig. 2, for a well-designed structure the inelastic activity is widely distributed so that a large portion of the energy generated by an earthquake can be dissipated. Based on recent analytical and experimental studies at Berkeley, the classification of links given earlier in Ref. 2 is somewhat modified. It is convenient to identify three types of hinges shown in Fig. 2:

1. Plastic hinges of moment M_p [Hinges (1)].
2. Plastic hinges of moment larger than M_p^* and less than M_p which are also subjected to relatively high shear [Hinges (2)].
3. Plastic hinges with moments equal to or less than M_p^* accompanied by web yielding in shear of V_p^* [Hinges (3)].

The basic quantities M_p, M_p^*, and V_p^* associated with the above hinges are defined as follows:

$$M_p = \sigma_y Z \; ; \quad M_p^* = \sigma_y (d - t_f)(b_f - t_w)t_f \; ; \quad V_p^* = (\sigma_y/\sqrt{3})(d - t_f)t_w \quad , \tag{1}$$

where σ_y, Z, d, t_f, b_f, and t_w are the yield stress, plastic modulus, height, flange thickness, flange width, and web thickness of the beam section, respectively. Figure 3 shows a typical M-V interaction curve for the wide flange beam section. The curves can be approximated by Neal's expression as follows (Refs. 3, 4):

$$\frac{(M - M_p^*)^2}{(M_p - M_p^*)^2} + \frac{V^2}{V_p^{*2}} = 1 \quad (M \geq M_p^*) \; ; \qquad V \simeq V_p^* \quad (M < M_p^*) \quad . \tag{2}$$

The maximum shear hinge length b* can be expressed as:

$$b^* = 2M_p^*/V_p^* \quad . \tag{3}$$

The length e for an active link should be less than or equal to b* to ensure that the web yields in shear. Such a link will be called a "shear link." This type of link appears to offer excellent ductility under cyclic loadings if appropriately sized and spaced web stiffeners are provided to prevent web buckling (Refs. 4,5). A link longer than b* is called a "moment link."

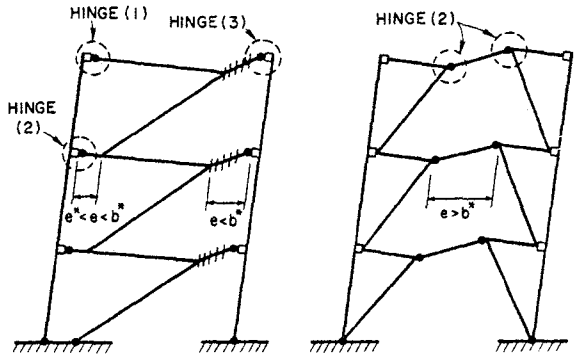

FIG. 2 Collapse Mechanisms of EBFs

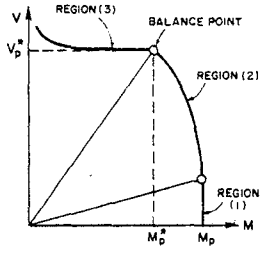

FIG. 3 M-V Interaction Curve for Wide Flange Beams

Collapse Mechanism and Ductility Demand. Fig. 4 shows an appropriate collapse mechanism of a D-brace frame. Subject to kinematic constraints, some latitude in selecting the collapse mechanism is possible. For this selected mechanism to occur, the columns should remain elastic, except for plastic hinges at the base; accordingly, the following recurrence formulas for rigid-plastic displacement fields may be obtained for the ith floor level:

$$\begin{aligned}
\theta_{D(i)} &= [(e^*)^{i-1}/(L - e - e^* - d_L - d_R)^i]\,(e^* + d_L)\theta \simeq 0 \\
\theta_{A(i)} &= L\theta/e - e^*\theta_{D(i-1)}/e \simeq L\theta/e \quad (\theta_{D(0)}: \text{use above eq.}) \\
\theta_{B(i)} &= \theta_{A(i)} - \theta_{D(i)} \simeq L\theta/e \\
\Delta_{B(i)} &= (L - e - d_R)\theta + e^*\theta_{D(i)} \simeq (L - e - d_R)\theta
\end{aligned} \tag{4}$$

The approximate equations are in good agreement with exact solutions for multistory frames; therefore, for purposes of design, Eqs. (4) can be used to estimate the relationships between local member ductility and lateral structure plastic displacement, which can be defined as a displacement after yielding by applying the bilinear approximation on the global structure displacement field. The ductility demand to the active link can be reduced by making the value of e as large as possible.

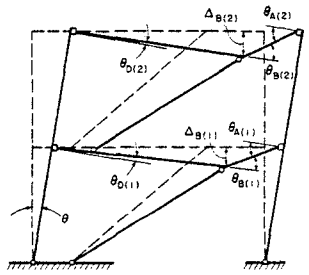

FIG. 4 Rigid Displacement Field of an EBF

The same equations can be used for the K-brace or V-brace frames, making use of geometrical similarity, since they basically have geometry similar to the D-brace. It is then to be noted that, in V-brace frames, if two links of length e equal to that in a D-brace frame are used, the link ductility demand is one-half that for a D-brace frame, provided that the span length L is the same for both frames. The link ductility demand for the K-brace frames is the same as that for the D-brace frames.

Plastic Capacity of EBFs. The discussion above forms a basis for predicting plastic capacity of EBFs. Based on the study in Ref. 6, the upper bound estimate of a collapse load for a frame with shear links can be easily made. For a given virtual displacement θ, the internal work W_I and the external work W_E for the frame of the type shown in Fig. 4 can be expressed as:

$$W_I = \sum_{i=1}^{N} [V^*_{p(i)} e_{(i)} (\theta_{A(i)} + \theta_{B(i)})/2 + M_{D(i)}\theta_{D(i)}] \simeq \sum_{i=1}^{N} V^*_{p(i)} L\theta \tag{5a}$$

$$W_E = \mu \sum_{i=1}^{N} [P_{(i)} h_{(i)} \theta] , \tag{5b}$$

where $P_{(i)}$ and $h_{(i)}$ are, respectively, the generalized lateral load and distance from the ground in the corresponding floor level i in an N-story EBF. The first set of expressions in W_I can be approximated using Eqs. (4), result-

ing in the simplified second expression. In obtaining the latter useful expression, it should be noted that the neglected second term is very small compared to the first, implying that the active hinges absorb most of the energy in an EBF system. By the same token, if columns are fixed at the ground, the energy absorbed by the hinge at the base can usually be neglected, still yielding a good approximation of W_I.

On equating W_I and W_E, one obtains a collapse load factor μ. If vertical loadings are applied to the beams, different collapse mechanism may occur, especially when e* is not zero. (The authors are grateful to Professor H. Gesund for suggesting to emphasize this possibility.) Fig. 5(a) shows the mechanisms of the frame subjected to both lateral and vertical loading equivalent to 0.06 k/in; these mechanisms were obtained with the aid of elasto-plastic large displacement analysis using a newly developed shear beam element (Ref. 7). The beam section used was W14 × 53 and σ_y was assumed to be 36 ksi. The columns and braces were selected such that they remained elastic. The proportions of the frames are the same as the D-brace frame shown in Fig. 8, except that e* = 0 for the frame in Fig. 5(b).

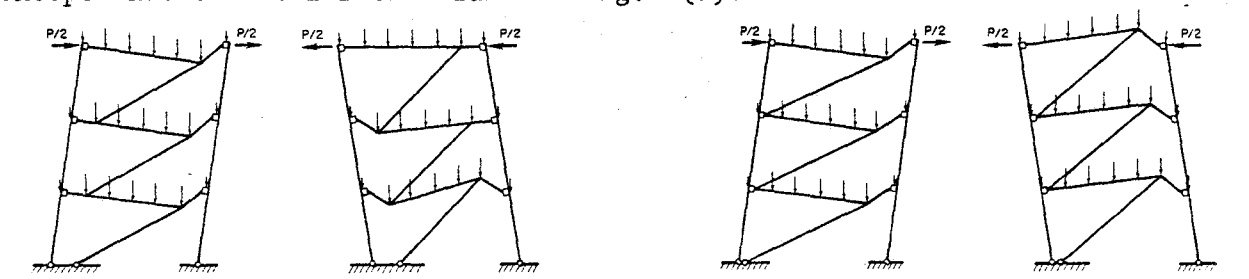

FIG. 5 Mechanism of EBFs due to Lateral and Vertical Loads

In these figures, P_{ult} indicates the magnitude of P obtained at 2% average structure drift in elasto-plastic analysis. It should be noted that for the frame in Fig. 5(a), the location of the active hinges varies depending on the direction of the lateral load when vertical loadings are present, which requires reconsideration of ductility demand on the links. Sometimes this may not be economical, since one has to place web stiffeners on the links of length e*. On the other hand, the frame in Fig. 5(b) shows the fully cyclic inelastic action of the active link can be expected. The same results were obtained for K-brace frames, whereas the V-brace frames showed only one kind of mechanism. Further analyses were done increasing the magnitude of the vertical load by three, and the same mechanisms were found.

Another important aspect of plastic capacity of EBFs can be explained with the aid of Fig. 6. For an assumed typical ratio of Mp* to Mp, the plastic capacity of an EBF can be obtained for the given e/L ratio using Eqs.(2) and (5). The plateau in the figure indicates the range of e/L where shear yielding of the link occurs. It can be seen that the shear link gives a much larger capacity than does the moment link. In extreme case, depending on the span length, the shear link in an EBF can provide 4.5 to 9 times the lateral load resisting capacity of an MRF

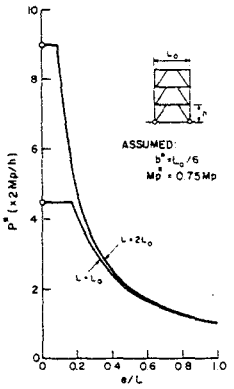

FIG. 6 Capacity of two EBFs vs. e/L

, for which P* = 2Mp/h. Further, the capacity of an EBF with a shear link is proportional to the span length, which follows from Eq. (5), whereas the capacities of EBFs with moment links are almost the same regardless of the span length, when the ductility demand on the links is the same.

PLASTIC DESIGN OF EBFs

Background. The design methods for EBFs were previously presented by Roeder (Ref. 8), Manheim (Ref. 9), and Teal (Ref.10). The first two methods are plastic design methods based on the lower and upper bound theorems for inelastic structures, whereas the latter method is an allowable stress design method utilizing modified safety factors based on code provisions. However, as explained in Ref. 11, these methods seem to present problems of ease of application, accuracy, or consistency; therefore an alternative approach was developed.

Formulation of Solution. Fig. 7 shows a free-body diagram of a D-brace frame at a typical story level, which is subjected to lateral loads P_L and P_R. The magnitudes of the forces transferred from the top of the frame, H_1', H_2', M_1', M_2', P_1', P_2', and B_V', are known from analysis of the floor above. At the top floor level, these quantities are zero. The task is to find both statically and kinematically admissible solutions of the frame. Fortunately, as noted earlier, a unique collapse mechanism can be selected for any given structure, meaning that one can assign plastic hinges deterministically on the frame.

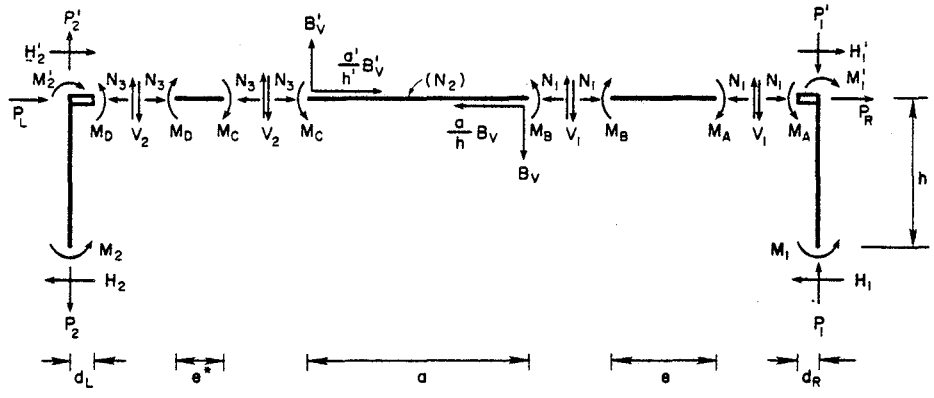

FIG. 7 Free Body Diagram for Design Method

To reduce the static indeterminacy of the system, it is necessary to assume the location of inflection points on the columns, which can be located by a parameter α, the ratio of the bottom to the top column end moments. Further, the following three equations should be considered:

$$M_A = \beta_A(eV_1/2) \quad ; \quad M_B = (2 - \beta_A)(eV_1/2) \quad ; \quad M_D = \beta_D(eV_1/2) \; . \tag{6}$$

By assigning the values α, β_A, and β_D, one could solve for a statically admissible field; therefore, an appropriate selection of these parameters is important. It has been found that the values of α vary between 1 and 1.3 when the lateral loading on the structure varies smoothly from story to story. (For a concentrated load at the top, a different assumption must be made.) Also, it is necessary to take

$$\beta_A = b^*/e \geq 1 \ , \qquad (7)$$

meaning that the moment of M_D^* develops at points such as A in Fig. 7. It should be noted that this assumption implies unequal end moments in the links, i.e., M_B is less than or at most equal to M_A. In general, the inequality indicated in Eq. (7) applies in order to assure shear link behavior.

β_D can be assumed to be the same as β_A in Eq. (7) if e* is the same as e. However, as stated earlier, it is possible to set e* much smaller than e for a more economical and efficient design. In such a case, β_D can be assumed to be a fraction of β_A. Based on some numerical experimentation, the following equation was found to be useful:

$$\beta_D = [0.2 + 0.8(e^*/e)]\beta_A \ . \qquad (8)$$

Assigning the above parameters in the above manner, one can obtain all member forces starting from the top. For a better estimate of β_A given by Eq. (7), an iteration can be performed using the actual b* value of the selected beam, which was found to be very stable. Due to the simplicity of the above procedure, a computer design program based on this method was developed (Ref. 11).

Design Example. The frame types appearing as the first and fourth illustrations in Fig. 1 were used to test the design method. Lateral loads of 200 kips were applied to the top of each frame. The proportions, as well as member sections for the two frames selected by the computer program, are shown in Fig. 8.

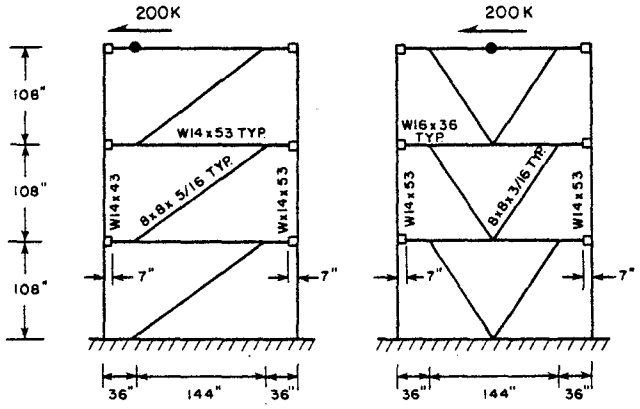

FIG. 8 Proportions and Member Sections for EBFs

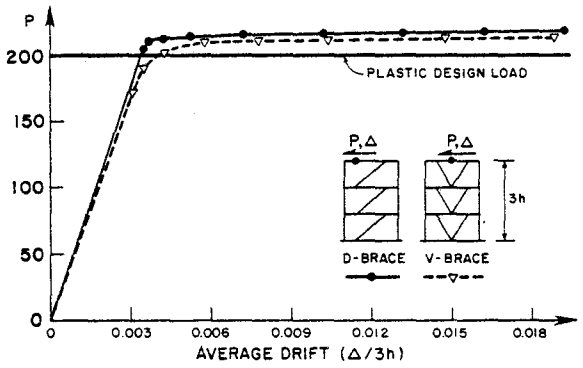

FIG. 9 Load-Deflection Behavior of Designed EBFs

It can be seen from Fig. 9 that the designed frame attained expected capacity. Somewhat earlier yielding of the V-brace links had occurred because lighter sections were selected for the beams than for the D-brace frame. However, the plastic shear deformations of the links at a considerable story drift were about half those in the D-brace frame, as indicated earlier in this paper. The comparison between the moments predicted by the proposed method and elasto-plastic analysis is shown in Figs. 10(a) and 10(b). Some discrepancies, which are not significant from the design viewpoint, occur because the capacities of the selected beams somewhat exceed the design forces. The excess beam capacity was larger in D-brace than in V-brace frames. For the latter frame, the initial design moments in the beams are in excellent agreement with

the results of an elasto-plastic analysis, leading to the conclusion that the proposed design method is exceptionally accurate.

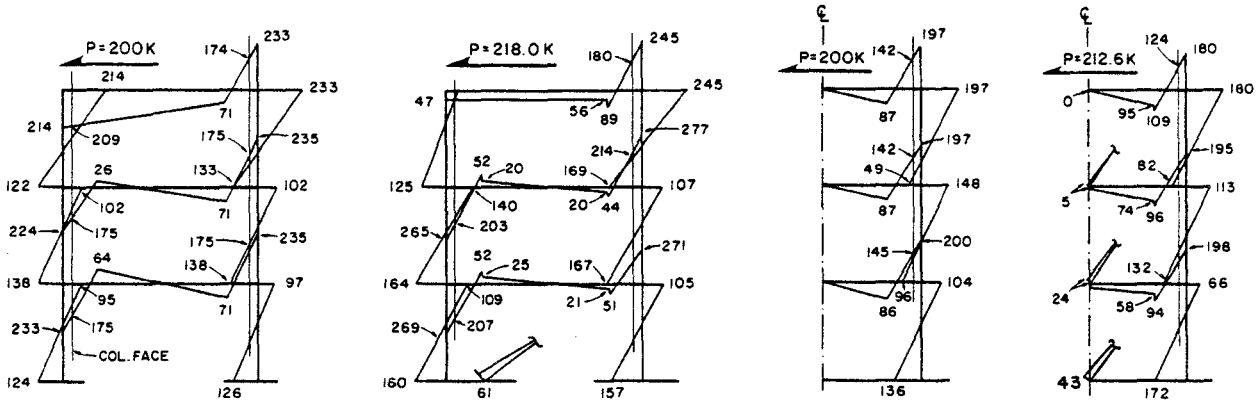

FIG. 10 Comparison of Design and Analysis Moments

ELASTIC CHARACTERISTICS OF EBFs

One of the unique features of an EBF is that the elastic story stiffness can be controlled by varying the e-value at each story while maintaining its capacity. Research was carried out to determine what range of stiffness is available for this purpose. First, as shown in Fig. 11, the 20-story EBFs employing three types of bracing schemes were plastically designed using the computer program developed. The proportion and design lateral force for those EBFs were in the practical range and similar to those used in Ref. 8. Corresponding to the various values of e, four one-story panels with simulated boundary conditions were analyzed at different floor levels.

Fig. 12 exhibits analytical results for elastic story shear drift of the panels located from these analyses at the 3rd and the 19th floor levels subjected to correcponding plastic design loads. The horizontal axis in this figure indicates the eccentricity ratios, which are e/L for the D-brace and K-brace frames, and 2e/L for the V-brace frame, since a comparison under the same ductility demand on the links is intended. For modeling, shear deformation of the beam was considered and a rigid end zone was assumed based on heights of the beam and column sections.

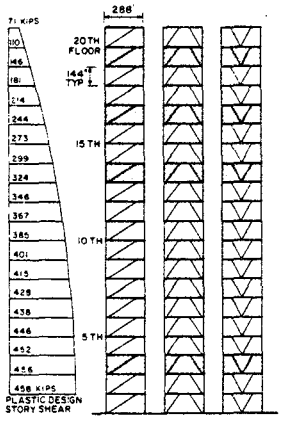

FIG. 11 Plastic Design of 20 story EBFs

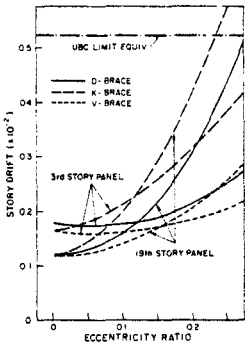

FIG. 12 Dependence of Elastic Shear Drift on Basic Parameters

From this figure, it should be noted that designed EBFs easily satisfy UBC story drift limits (Ref. 12). Also, the maximum stiffness in some case can be attained with no-zero eccentricity. The important point to

observe is that the stiffness of the V-brace frame is much greater than that of the others when the eccentricity ratio is larger than 0.1. The K-brace appears to be the most flexible of all. The decrease of stiffness for increasing the eccentricity ratio is more pronounced for the 19th floor level panels. For further details, see Ref. 11.

CONCLUDING REMARKS

The design and analysis of EBFs discussed above was limited to static loadings. Further work remains to establish rapid methods for dynamic analyses. The development of a computationally efficient shear link element is particularly necessary. Cyclic strain hardening behavior of the link must be included in the algorithm to correspond more accurately with experimental results. The influence of the floor slab and the effect of the axial force on the cyclic behavior of links need further attention. This work currently is being pursued at Berkeley.

ACKNOWLEDGEMENTS

The study reported herein was supported by the National Foundation under Grant No. CEE 81-07217. This support is greatly acknowledged. The help of Gail Feazell in preparing the figures, and of Cindy Polansky in typing the manuscript is greatly appreciated.

REFERENCES

(1) Roeder, C. W. and Popov, E. P., J. Structural Division, ASCE, Vol. 104, No. ST3, March 1978, pp. 391-412.
(2) Popov, E. P. and Malley, J. O., Chapter 11, ASCE Manual on Beam-to-Column Building Connections, in review.
(3) Neal, B. G., J. Mech. and. Engrg. Sci. 3, No. 3, 258 (1961).
(4) Hjelmstad, K. D. and Popov, E. P., J. Structural Engineering, ASCE, Vol. 109, No. ST10, October, pp. 2387-2403.
(5) Malley, J. O. and Popov, E. P., J. Structural Engineering, ASCE, in review.
(6) Manheim, D. N. and Popov, E. P., J. Structural Engineering, ASCE, Vol. 109, No. ST10, October, pp. 2404-2419.
(7) Hjelmstad, K. D. and Popov, E. P., EERC Report 83-15, Earthquake Engineering Research Center, University of California, Berkeley (July 1983).
(8) Roeder, C. W. and Popov, E. P., EERC Report 77-18, Earthquake Engineering Research Center, University of California, Berkeley (Aug. 1977).
(9) Manheim, D. N., D. Eng. thesis, University of California, Berkeley (Feb. 1982).
(10) Teal, E., Structural Steel Educational Council, California Field Ironworkers Administrative Trust.
(11) Kasai, K. and Popov, E. P., EERC Report 83, Earthquake Engineering Research Center, University of California, Berkeley, in preparation.
(12) Uniform Building Code, International Conference of Building Officials, Whittier, California (1982).

URBAN DESIGN VULNERABILITY COMPONENTS

Henry J. Lagorio (I)
Presenting Author: H. J. Lagorio

SUMMARY

As part of regional hazards mitigation programs, it is increasingly necessary to anticipate and predict the performance of the entire urban system in our metropolitan centers prior to, or during, major earthquake events for planning purposes. Despite recent technological advances in the testing and analysis of individual buildings and other physical facilities, it is clearly evident that components of the urban infrastructure in major cities remain vulnerable to major seismic activity.

The urban environment is a complex and closely knit system composed of many interdependent activities, services, functions, building types, lifeline elements, communication lines, and other critical facilities. The failure of any single, major component can severely affect the functioning of others and render the entire metropolitan area inoperable.

In this paper assessment is made of specific components which are essential to the continued operation of urban areas during earthquake events. Interrelationships between specific component parts are identified and assessed on the basis of urban scale considerations and impact on the infrastructure of metropolitan centers. They are examined for greater understanding of vulnerability characteristics of metropolitan areas so that cities can effectively anticipate their seismic performance and recovery after a major earthquake event on an urban scale.

INTRODUCTION

The San Fernando, California, earthquake of 1971 focused attention on the importance of seismic vulnerability on an urban scale when major freeway systems and several emergency service facilities collapsed, or were sufficiently damaged, to obstruct recovery efforts. In a similar manner, damaging earthquakes, with which the author has personal knowledge and which are the basis for this paper, occurred in the following cities after the San Fernando event and confirmed the lessons learned from an urban scale point of view as shown in Table 1 below.

(I) Director, Center for Environmental Design Research, University of California, Berkeley.

TABLE 1

URBAN CENTERS IMPACTED BY DAMAGING EARTHQUAKES SINCE 1971

Urban Center/Region	Location	Year
Managua	Nicaragua	1972
Tangshan	China	1976
Campania-Basilicata	Italy	1980
El-Asnam	Algeria	1980
Coalinga	California	1983

Despite considerable technological advances in the analysis and design of individual building systems after the referenced earthquakes shown in Table 1, it is clear that the total urban infrastructure in major cities remains vulnerable to severe, damaging earthquakes. While the design of individual buildings may be the primary responsibility of the design professional, urban-scale seismic resistant design is a shared responsibility between all parties involved in the planning, design, delivery, administration, and occupancy of cities: the architect, engineer, planner, consultant, seismologist, geologist, geophysicist, social scientist, developer, government official, private sector representative, and public. It is obvious in dealing with such a complexity of interrelationships as exhibited by a metropolitan center that life safety can not be achieved without the contribution of all parties involved. When coping with a major, damaging earthquake, it has been calculated that total damage to the urban infrastructure system can exceed by a margin of three to ten times the damage absorbed by all of the building stock located in the metropolitan area (EERI 1983).

URBAN SCALE VULNERABILITY COMPONENTS

The factors which define the components of urban scale vulnerability have received consideration by the earthquake engineering community on an individual basis, but due to the complexities of the problem, the interrelationships which make up the entire urban fabric are difficult to assess in a wholistic manner and it is only recently that they have received attention. Accordingly, it is appropriate to identify the major components of urban scale vulnerability and to understand how they may be evaluated by the role which they are expected to assume in earthquake hazard reduction programs. As presented in this paper, some of the major components which have a significant role to play in the vulnerability assessment of specific and critical metropolitan areas are indicated in Table 2 below.

TABLE 2

LISTING OF URBAN SCALE VULNERABILITY COMPONENTS

Component	Function/Implication
Existing Building Stock Classes	Urban Pattern
Adjacency of Buildings	Urban Density
Hazardous Contents	Fire/Explosion/Toxic Fumes
Location of Buildings/Systems	Land Use/Site Planning
Emergency/Critical Facilities	Response/Recovery
Lifelines	Life Support/Circulation
Bridges/Overpasses	Transportation
Communication Lines	Mass Media/Public Information
District Zoning	Urban Character
Street Patterns	Access/Egress
Reservoirs/Dams	Water Supply/Downstream Pop.
Open Spaces	Evacuation Areas

Failure of any components listed in Table 2 to perform effectively during an earthquake could lead to serious consequences in the function and operations of an urban system. A poor performance by any one of them can drastically exacerbate immediate post-earthquake recovery efforts.

Existing Building Stock Classification

This is perhaps the most important component in the vulnerability assessment of an urban area. In taking a comprehensive inventory of the existing building stock by building type classification to obtain construction data and characteristics, it is possible to evaluate the performance of buildings and assess potential damage losses by calculating the probable maximum loss on an aggregate basis for the entire urban region. Data rendered from building loss evaluations will produce important information for the computation of life loss, injuries, debris removal, residual capacities of urban functional and operational capabilities, and post-earthquake recovery time estimates.

The inventory will also reveal the amount and location of existing, older, hazardous buildings which are known to be extremely vulnerable to earthquake forces. The City of Coalinga is the most recent example in the United States of this phenomenon in which an entire eight block area in the central business district was demolished due to the collapse, or severely damaged condition, of older, unreinforced, masonry bearing wall type buildings. In this seismic event which occurred in 1983, it remains a miracle no immediate deaths occurred as a direct result of the earthquake and that there were few serious injuries.

Hazardous Contents

Fire following earthquake is a distinct threat to the urban area. This situation is exacerbated in metropolitan areas where the storage of

hazardous materials occurs inside buildings or outside on the open ground. This is particularly true in industrial areas of the city where LPG plants, chemical materials, and other toxic substances are manufactured and kept in storage on inventory for later use.

All such locations of hazardous materials should be identified and mapped for future reference as potentially precarious areas which warrant monitoring during and after a severe earthquake. Unless the risk in these areas is taken into account before the event, consequences can be severe following a damaging earthquake if they are not given appropriate attention and respect.

Adjacency of Buildings

Several recent earthquakes have indicated that the spacing between buildings on adjacent properties is a critical component from the site planning point of view in congested areas of a metropolitan center. Rather than limit the vulnerability to the performance evaluation of a single, individual building, it obviously is necessary to analyze the performance of a cluster, or group of buildings, to fully realize their behavior on an urban scale. Examples have been recorded which clearly illustrate how a tall, slender, flexible building may be severely pounded to the point of collapse by a closely placed short, squat, stiff structure which is its immediate neighbor (Managua 1972 and Campania-Basilicata 1980).

On hill sites it has been documented that the collapse of older, existing, hazardous buildings may cascade down the hillside on top of the neighboring, newer, more earthquake resistant structures below and destroy them in a "domino effect" (Campania-Basilicata 1980). The three dimensional implications here, by their very nature, are peculiar to urban scale vulnerability aspects found in the topography and topology of a hilly metropolitan area not unlike those found in many cities located in the West Coast areas of the United States.

Location of Buildings/Systems

Another aspect of urban scale vulnerability which must be given serious attention is consideration of the location of buildings and systems within the city from a geologic point of view. Geologic mapping of hazardous areas is essential to a comprehensive understanding of critical areas in a metropolitan setting which have the potential of creating problems due to severe ground shaking effects. Poor soils areas known to have a high potential of liquefaction, subsidence, or landslide need to be mapped and designated critical zones. From an urban scale perspective, major damage to all physical facilities including buildings, lifelines, overpasses and bridges, communication lines, and dams, may be expected.

From an urban planning and design point of view, such areas are to be avoided, or identified as special study zones. No new construction, with the exception of single family wood frame houses, should be considered for these areas without a prior study of all geological conditions of the site to insure public safety (California, Alquist-Priolo Act, 1972). Mapping

of such vulnerable areas has become an essential part of microzonation maps used in conjunction with post-earthquake reconstruction activities (Campania-Basilicata 1981, Ech-Chleff 1983).

Emergency/Critical Facilities

Hospitals, police stations, fire stations, communication centers and other emergency facilities are essential structures for the operational and survival functions of an urban area following a disaster. These facilities should be designed to higher performance standards to resist earthquake forces than other less critical facilities. The threat of an urban conflagration following an earthquake depends on the continued functioning of fire stations and other fire fighting equipment. The survival of hospitals is essential for immediate post-earthquake recovery efforts and their construction requires higher standards so that they may remain operational and functional after a damaging earthquake (California Hospital Act 1972). Without the availability of communication centers, it would be impossible to transfer information on the extent of the disaster or to assess total damage in the urban area. These three examples are not meant to be all inclusive, but are used as representative illustrations of the importance of emergency and critical facilities remaining operational and functional during and after major disasters.

Lifelines

It is clear that an urban center can not exist, or continue to operate, without the use of its lifelines. Even though there may not be any structural collapses of buildings or emergency facilities in an area, a city will not survive without electric power, water supply, sewage treatment systems, natural gas lines, freeways, and other types of lifeline facilities if its function depends on the continued operation of any one. Failure of one may cripple a city for a long period of time and render it inoperable during the emergency period. There have been many examples of this situation being confronted by specific cities after a major earthquake. Lifeline systems, therefore, require special attention to be certain that they will continue to function after a major disaster (Coalinga 1983, San Fernando 1971).

Bridges/Overpasses

In contemporary cities, the flow of surface traffic is an important element in its day to day operations. Automobile freeways which allow high speed access to, and egress from, important areas of a city are dependent on overpasses and bridges to keep all vehicles moving in an orderly manner. Damage or collapse of overpasses or bridges due to earthquake forces will serve to cut off and isolate a metropolitan center from the surrounding area, and disrupt vital transportation routes, including railroad lines. Search and rescue teams, and other emergency vehicles, will not be able to reach their target areas. After the San Fernando earthquake in 1971, the State of California concluded a multi-million dollar program which achieved the reinforcement of all its major, existing freeway overpasses and bridges throughout the state as testimony to the

importance of this urban component.

Communication Lines

During the period immediately following a major, damaging earthquake, it is essential that an urban area have the capability fo communicate with areas outside of the impacted area for emergency assistance in many categories. Communication lines must be kept open so that the extent of damage and public needs may be indicated to emergency service units and emergency management agencies. In many cases it is wise to have "back-up" systems available in order to keep communication lines open following an earthquake.

District Zoning

It is important to remember that a city is made up of many districts which are quite distinct from one another in character, topography, and topology. This is part of the urban scale fabric which makes our metropolitan centers distinctive from surrounding rural areas. Accordingly in earthquake hazards mitigation criteria must be established for different zones of the city. For example, a performance criteria for a residential area must be quite different than that required for the central business district, or financial district. Industrial areas require a performance criteria all their own. Each district must be reviewed for its own unique characteristics, and mitigation plans developed accordingly.

Street Patterns

Debris in the street which blocks access and egress from severely impacted areas following an earthquake is a common occurrence in congested urban centers. It is a function of the heights of buildings on each side of the street and the width of the street itself. Many downtown centers of metropolitan areas are represented by older, congested parts of the city with narrow streets and financial districts with dense population. Access and egress from these areas, especially if there is the potential of a fire break-out following the earthquake, is essential. Accordingly, street patterns on an urban scale need close examination and should be made part of any mitigation plan developed for an urban area. Part of the plan should also indicate potentially safe evacuation routes and/or alternate, secondary arterials which would be relatively free from falling debris. Wide streets, the centers of which would not be blocked by falling debris, are a particular asset in hazards mitigation when dealing with urban vulnerability.

Resevoirs/Dams

The catastrophic failure of major dams and resevoirs in an urban area is a distinct threat to public safety, particularly to downstream population. The near failure of the Van Norman Dam during the 1971 San Fernando earthquake led to the evacuation of over 70,000 persons who occupied the downstream flood plain area. Other examples, such as in Italy, have been recorded where the primary cause of life loss and building damage were related to dam failure in hill areas which channeled mud,

flood waters, and debris into the centers of inhabited spaces.

Urban hazards mitigation programs should contain an element dealing with the potential failure of major dams and reservoirs. Part of the element should deal with the calculation of the downstream population at risk and its evacuation. Analysis of the extent and size of the downstream flood plain and the rate of water flow in case of a catastrophic failure should also be completed (California Dam Safety Act 1972).

Open Spaces

Open spaces in metropolitan areas have always been considered an important planning element by contemporary occupants of our cities as population pressures and urban growth place a strain on the urban fabric. Primarily serviceable as parks, and for recreation purposes, they are also useful as evacuation areas, emergency housing and medical treatment spaces, or emergency feeding and food distribution points following a major earthquake disaster (San Francisco 1906, Managua 1972, Campania-Basilicata 1980, Coalinga 1983). In California and other areas, public schools designed under higher seismic standards and their grounds have also been targeted for such uses after a major disaster.

Urban vulnerability mitigation programs should identify all public, serviceable open spaces in the metropolitan area for potential use after a damaging earthquake. These should be earmarked as having the capacity to serve specific post-earthquake recovery functions.

CONCLUSION

This paper has presented a general overview of eleven major components dealing with the urban scale vulnerability of metropolitan areas. It is not intended to be an exhaustive list, but rather singles out the components believed to be the most critical in earthquake hazards reduction. By identifying the interrelationships of these components to the urban environment, it recognizes the fact that some earthquake hazards are more correctly approached on an urban scale rather than from the analysis of an individual building or facility. It is hoped that this paper gives a better understanding of the characteristics, range, and features of earthquake hazards reduction programs as an urban scale problem.

References:

Botsai, Elmer, et al, "US/Japan Joint Seminar: Urban Design and Seismic Safety, University of Hawaii, 1978.

Heikkala, Susan, et al, "Urban Scale Vulnerability, Proceedings of the US-Italy Colloquium on Urban Design and Hazard Mitigation", University of Washington, June 1982.

Lagorio, Henry, "Urban Design and Earthquakes", Technical Paper for the Second Summer Institute on Architects and Earthquakes, American Institute of Architects Research Corporation, Washington, D.C., 1977.

Lagorio, Henry, and Mader, George, "The Campania-Basilicata, Italy, Earthquake 1980: Architectural and Planning Aspects", Earthquake Engineering Research Institute, Berkeley, California, 1981.

Scholl, Roger, "EERI Delegation to the People's Republic of China", Earthquake Engineering Research Institute, Berkeley, January 1982.

Steinbrugge, Karl, and Lagorio, Henry, "Earthquake Vulnerability of Honolulu and Vicinity", Department of Defense, Civil Defense Division, State of Hawaii, 1982.

Stratta, James, et al, "Earthquake in Campania-Basilicata, Italy: November 23, 1980", National Research Council and Earthquake Engineering Research Institute, National Academy Press, Washington, D.C., 1981.

IDENTIFICATION OF WAVE TYPES, DIRECTIONS, AND VELOCITIES USING SMART-1 STRONG MOTION ARRAY DATA

C. H. Loh (I)
J. Penzien (II)
Presenting Author: C. H. Loh

SUMMARY

Presented in this paper is a method for identifying wave types, directions, and velocities contained in strong earthquake ground motions. After transforming the motions into components along their principal axes, use is made of a principal variance ratio R(f), defined as the ratio of the minor principal variance to the major principal variance for those components of motion within frequency band Δf centered on frequency f_o. At those frequencies where R(f) has very low values, single wave types dominate the motions. Using directions of principal axes and phase lag information, wave types, directions, and velocities are identified.

INTRODUCTION

At a meeting in Hawaii during May 1978, the need for strong earthquake ground motion arrays was discussed and plans were developed for promoting such arrays in many locations on a world-wide basis (Ref. 1). One site selected at the workshop as having high potential for frequently experiencing future strong motions was north-eastern Taiwan. Responding to the great need, a strong motion array was installed in this area in the town of Lotung in the fall of 1980 under the joint effort of the Academia Sinica in Taiwan and the University of California, Berkeley, with financial support provided by the National Science Council and the National Science Foundation (Ref. 2).

The strong-motion array in Lotung, called SMART-1, is a two-dimensional surface array consisting of a center station C00 and three concentric circles (inner I, middle M, and outer O) each having 12 stations with radii of 200 meters, 1 km, and 2 km, respectively, as shown in Fig. 1. This arrangement of 37 stations was selected to optimize the expected information to be obtained from both the engineering and seismological points of view. The instruments in this array record digitally with a common time base accurate to 1 millisecond over a duration which includes 2.5 seconds of pre-trigger memory. Fortunately, many earthquakes have triggered the array since the installation providing a wealth of strong ground motion data.

It is the purpose of this paper to present selected results of a single study carried out using SMART-1 data in which a promising method for identifying wave types, directions, and velocities was developed. Due to space limitations, application of the method herein is restricted to a limited number of motions recorded during the earthquake of January 29, 1981 (Event 5);

(I) Associate Professor of Civil Engineering, National Central Universtiy, Taipei, Taiwan, China

(II) Professor of Structural Engineering, University of California, Berkeley, California, U.S.A.

see Ref. 2. This earthquake was centered 30 km S26°E of the center of the array. Its focal depth was 11 km and its Richter magnitude calculated locally by the Institute of Earth Sciences in Taipei was 6.9.

CROSS CORRELATIONS AND PRINCIPAL DIRECTIONS

In an attempt to identify wave types, directions, and velocities produced by the earthquake of January 29, 1981 (Event 5), let us first examine the cross correlation coefficient given by

$$\rho_{ij}(\tau) \equiv \frac{R_{ij}(\tau)}{\sqrt{R_{ii}(0)\ R_{jj}(0)}} \tag{1}$$

where

$$R_{ij}(\tau) \equiv \int_{t_o - \frac{\Delta T}{2}}^{t_o + \frac{\Delta T}{2}} x_i(t)\ x_j(t+\tau)\ dt \tag{2}$$

and where $x_i(t)$ and $x_j(t)$ are the recorded acceleration time-histories in the x-direction (East-West) at stations i and j, respectively; see Fig. 2. In Eq. (2), ΔT is a time window centered on time t_o, and τ is a time lag. If the ground motions at these stations were produced primarily by a single travelling wave, then the above cross correlation coefficient, which can range from +1 to -1, would show high correlation for τ equal to the time required for the wave to travel between the two stations. This value of τ would, of course, depend upon the direction of wave propagation as well as wave velocity.

Using t_o = 50.3 sec and ΔT = 7.0 sec so as to include the significant high intensity portions of the motions recorded at all stations in the time window of Eq. (2), cross correlation coefficients were generated over the range $0<\tau<3$ sec for many station pairs. It is pertinent to point out that the plots of these coefficients against time lag τ are not characteristic of those produced by pairs of motions dominated by a single travelling wave. Their shapes and low values of cross correlation suggest the simultaneous presence of multiple waves travelling in different directions with different velocities. Selecting the maximum cross correlation coefficient on each plot, one can examine the relationship between maximum cross correlation and distance (true distance; not projected distance) as shown in Fig. 3. In this figure, the exponential curve was derived by a least squares fitting of the data points shown. The rapid loss of maximum cross correlation with distance supports the above suggestion that multiple waves having different wave velocities and directions are simultaneously present at all stations. As a consequence of this observation, it was concluded that resolution of the motions into their frequency components and into their principal directions was required before identification of wave types, directions, and velocities could be made possible.

Following along these lines, let us transform the x and y recorded components of horizontal ground motion at a point into their $\tilde{x}$ and $\tilde{y}$ components in accordance with Fig. 2; thus,

$$\begin{aligned} \tilde{x}(t) &= x(t)\ \cos\phi + y(t)\ \sin\phi \\ \tilde{y}(t) &= -x(t)\ \sin\phi + y(t)\ \cos\phi \end{aligned} \tag{3}$$

Next, using time and frequency domain windows, the Fourier transforms of these new components are calculated using relations of the type

$$A_{\tilde{x}}(f) \equiv \int_{t_o - \frac{\Delta T}{2}}^{t_o + \frac{\Delta T}{2}} \tilde{x}(t) \exp(-i2\pi ft)dt \tag{4}$$

$$\tilde{x}(t) = \int_{-f_o - \frac{\Delta f}{2}}^{-f_o + \frac{\Delta f}{2}} A_{\tilde{x}}(f) \exp(i2\pi ft)\, df + \int_{f_o - \frac{\Delta f}{2}}^{f_o + \frac{\Delta f}{2}} A_{\tilde{x}}(f) \exp(i2\pi ft)\, df \tag{5}$$

where window lengths ΔT and Δf are centered on time t_o and frequency f_o, respectively.

The direction of maximum intensity as a function of frequency f_o can be obtained by maximizing the variance function

$$R_{\tilde{x}_i\tilde{x}_i}(\tau=0,\phi) = R_{x_ix_i}(0)\cos^2\phi + R_{y_iy_i}(0)\sin^2\phi + 2R_{x_iy_i}(0)\cos\phi\sin\phi \tag{6}$$

with respect to ϕ giving (Refs. 3,4,5)

$$\phi_o(f_o) = \frac{1}{2}\tan^{-1}\frac{2R_{x_iy_i}(0)}{R_{x_ix_i}(0) - R_{y_iy_i}(0)} \tag{7}$$

Angle $\phi_o(f_o)$ in Eq. (7) denotes two principal directions which are 90° apart; one being the major principal direction, the other the minor principal direction. The corresponding principal variances will be denoted by $R_{\tilde{x}_i\tilde{x}_i}(f_o)$ and $R_{\tilde{y}_i\tilde{y}_i}(f_o)$, respectively.

PRINCIPAL VARIANCE RATIO

Let us now define a principal variance ratio as given by

$$R(f_o) \equiv \frac{R_{\tilde{y}_i\tilde{y}_i}(f_o)}{R_{\tilde{x}_i\tilde{x}_i}(f_o)} \tag{8}$$

which varies over the range $0<R<1$. If we examine the motion at station i for discrete values of f_o, consistent with the discrete frequencies of the Fast Fourier Transform (FFT) method used in evaluating Eqs. (4) and (5), we find the following results: (1) When $R(f_o)=1$, there are no principal directions because the harmonic motion at frequency f_o moves along a circular path at constant angular velocity $2\pi f_o$ as shown in Fig. 4; i.e., the motion is equivalent to two resultant harmonics in orthogonal directions having equal amplitudes but being 90° out-of-phase, (2) When $0<R(f_o)<1$, principal directions do exist with the motion being along an ellipse; i.e., the motion is equivalent to two resultant harmonics in orthogonal directions with different amplitudes and they are 90° out-of-phase, and (3) When $R(f_o)=0$, principal directions exist but the motion is along a straight line; i.e., a pure harmonic exists. For $R(f_o)>0$, the two orthogonal waves could be made up of the superposition of multiple waves moving in different directions. Thus, in the interest of identifying wave types,

directions, and velocities, attention should be concentrated on those discrete frequencies having low values of $R(f_o)$. Fortunately for the SMART-1 data analyzed, these frequencies represent frequencies of high energy transmission as will be shown subsequently.

Figure 5 shows plots of the major principal variance $R_{\tilde{x}_i\tilde{x}_i}(f_o)$, the principal variance ratio $R(f_o)$, and the dominant (or major principal) direction $\phi_o(f_o)$ for the horizontal ground motions recorded at stations C00, I03, and I06. It is significant to note that at frequencies f_1, f_2, f_3, and f_4, representing high intensity motions, i.e., high major principal variances, the corresponding principal variance ratios are low indicating dominant wave transmissions in the neighborhood of these frequencies. Note that the dominant directions are nearly toward the epicenter for frequencies f_1 and f_2 but are much closer to the normal direction for frequencies f_3 and f_4. If the dominant waves are propagating in the general direction away from the epicenter, this observation suggests that Rayleigh waves are the primary source of energy transmission for frequencies less than about 2.5 Hz and that shear waves (SH waves; perhaps in part Love waves) are the primary source of energy transmission for frequencies from 2.5 Hz to about 6 Hz. Above these frequencies, the directions of propagation are quite variable.

Let us now examine in further detail the dominant directions of motions at frequencies f_1 = 1.17 Hz and f_3 = 2.85 Hz for many stations in addition to stations C00, I03, and I06 represented in Fig. 5. As suggested above, the dominant ground motions at these frequencies seem to be caused primarily by Rayleigh and shear (SH) waves, respectively. Figures 6 and 7 show the dominant direction at frequencies 1.17 Hz and 2.85 Hz, respectively, at many stations as given by Eq. (7). The average dominant direction ϕ_o over the array is also shown in these figures. Note that the average dominant direction in Fig. 6 is reasonable close to the epicentral direction while the average dominant direction in Fig. 7 is close to the normal direction.

We may now use these two average dominant directions to generate corresponding functions

$$R_{\tilde{x}_i\tilde{x}_j}(\tau) \equiv \int_{t_o - \frac{\Delta T}{2}}^{t_o + \frac{\Delta T}{2}} \tilde{x}_i(t)\, \tilde{x}_j(t+\tau)\, dt \qquad (9)$$

for ground motions recorded at many station pairs across the array. Noting the maximum cross correlation for each station pair over the entire range of τ and the corresponding relative distance between stations as projected on the average dominant axis, valuable plots can be obtained as shown in Fig. 8. Each data point represents a station pair. The upper plot in Fig. 8 is for f_o equal to 1.17 Hz while the lower plot is for f_o equal to 2.85 Hz. Straight lines fitted by least squares yield wave velocities (inverse values of the line slopes) equal to 2.4 km/sec and 5.3 km/sec for the Rayleigh and shear wave velocities, respectively.

Because a uniform elastic half space transmits Rayleigh waves at a velocity equal to 0.9 times the shear wave velocity, an explanation is needed of the mixture in the same time window of SH waves with local velocity of 5.3 km/sec and Rayleigh waves with velocities of 2.4 km/sec. The usual seismological interpretation of this large difference in local apparent velocities is that

the SH waves are associated with longer travel paths from the earthquake source to the array in the vicinity of which the SH wave fronts move steeply upwards through the soil. Thus, the apparent shear wave velocity is largely controlled by the more rigid, deeper rocks in the crust. On the other hand, the Rayleigh waves develop near the surface between the source and the array so that their wave velocities are largely controlled by the shallower less stiff materials.

According to this explanation the vertical components of ground motion in the time window studied should be significant in the frequency range of the Rayleigh waves but relatively insignificant in the frequency range of the transverse shear waves described above. This prediction was tested by computing the three-dimensional particle motions as a function of frequency f_o. The results show that the particle orbits agree well with the above prediction; i.e., significant vertical displacements are present in the frequency band 0.25 to 1.5 Hz, but relatively small vertical displacements are present in the frequency band 2.5 - 3.1 Hz.

CONCLUDING STATEMENT

Although further verification is needed, the method presented herein for identifying wave types, directions, and velocities making use of major principal variances and directions and a principal variance ratio shows considerable promise. Since generating the above results, the authors have generalized the method to a consistent three-dimensional form which permits further improvement of the results.

ACKNOWLEDGMENTS

The authors express their sincere thanks and appreciation to the National Science Council and the National Science Foundation for their financial support of the SMART-1 array project through grants Nos. CEE-7908982 and 70-0202-M0001-03, respectively.

REFERENCES

1. Iwan, W. D. (Editor), Proc. Int. Workshop Strong Motion Earthquake Instrument Arrays, Hawaii, 103 (1978).

2. Bolt, B. A., Loh, C. H., Penzien, J., Tsai, Y. B., and Yeh, Y. T., "Preliminary Report On The SMART-1 Strong Motion Array In Taiwan," Earthquake Engineering Research Center Report UCB/EERC-82/13, University of California, Berkeley, (1982).

3. Penzien, J. and Watabe, M., "Characteristics of 3-Dimensional Earthquake Ground Motion," Earthquake Eng. Struct. Dynamics, 3, 365-373, (1975).

4. Kubo, T. and Penzien, J., "Analysis of Three-Dimensional Strong Earthquake Ground Motions Along Principal Axes, San Fernando Earthquake," Earthquake Eng. Struct. Dynamics, 7, 265-278, (1979).

5. Kubo, T. and Penzien, J., "Simulation of Three-Dimensional Strong Ground Motions Along Principal Axes, San Fernando Earthquake," Earthquake Eng. Struct. Dynamics, 7, 279-294, (1979).

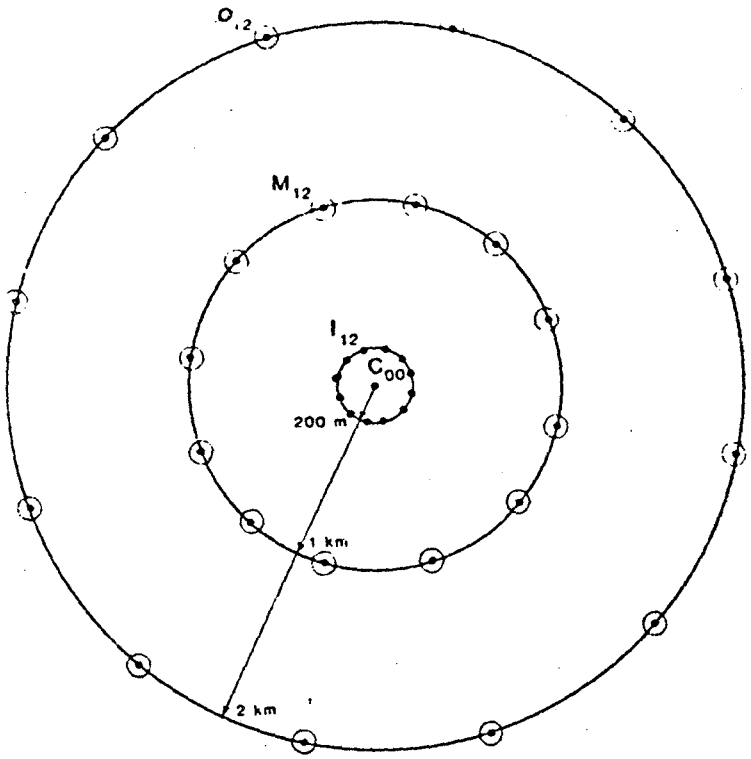

Fig. 1 The SMART 1 array

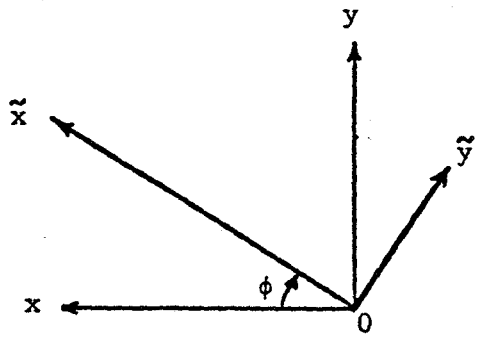

Fig. 2 Coordinate transformation of two horizontal components

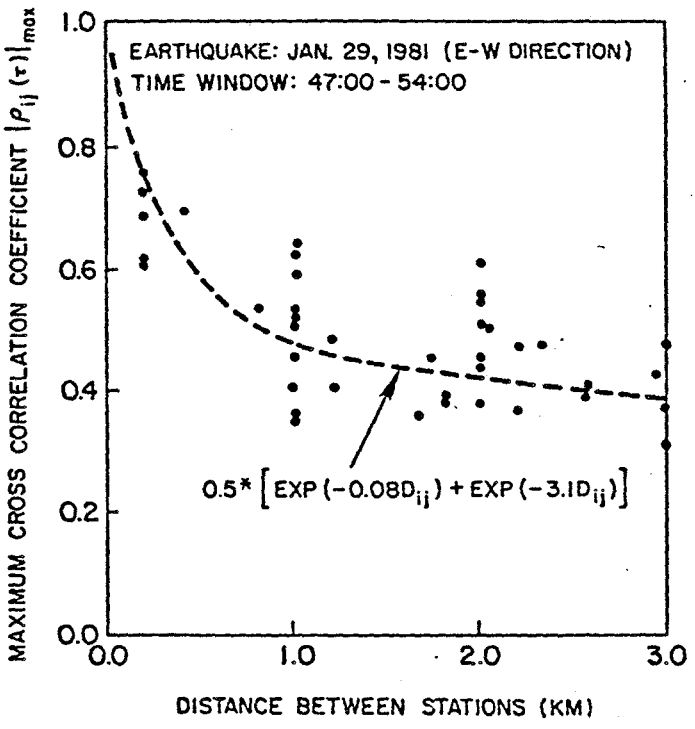

Fig. 3 Attenuation of correlation coefficient ρ

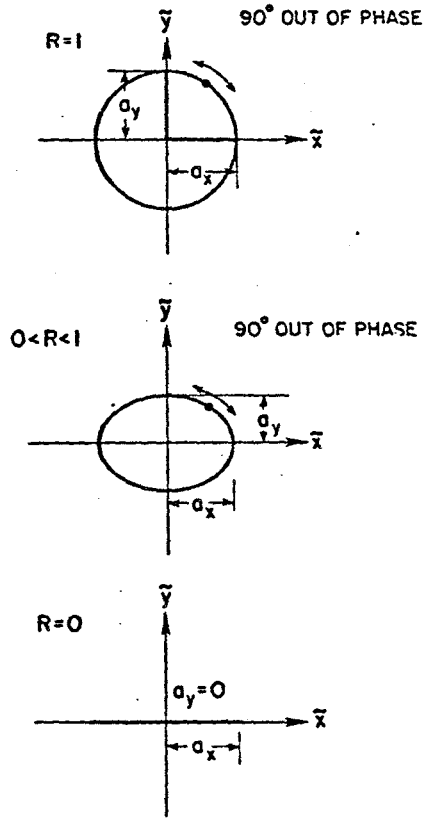

Fig. 4 Physical meaning of principal variance ratio

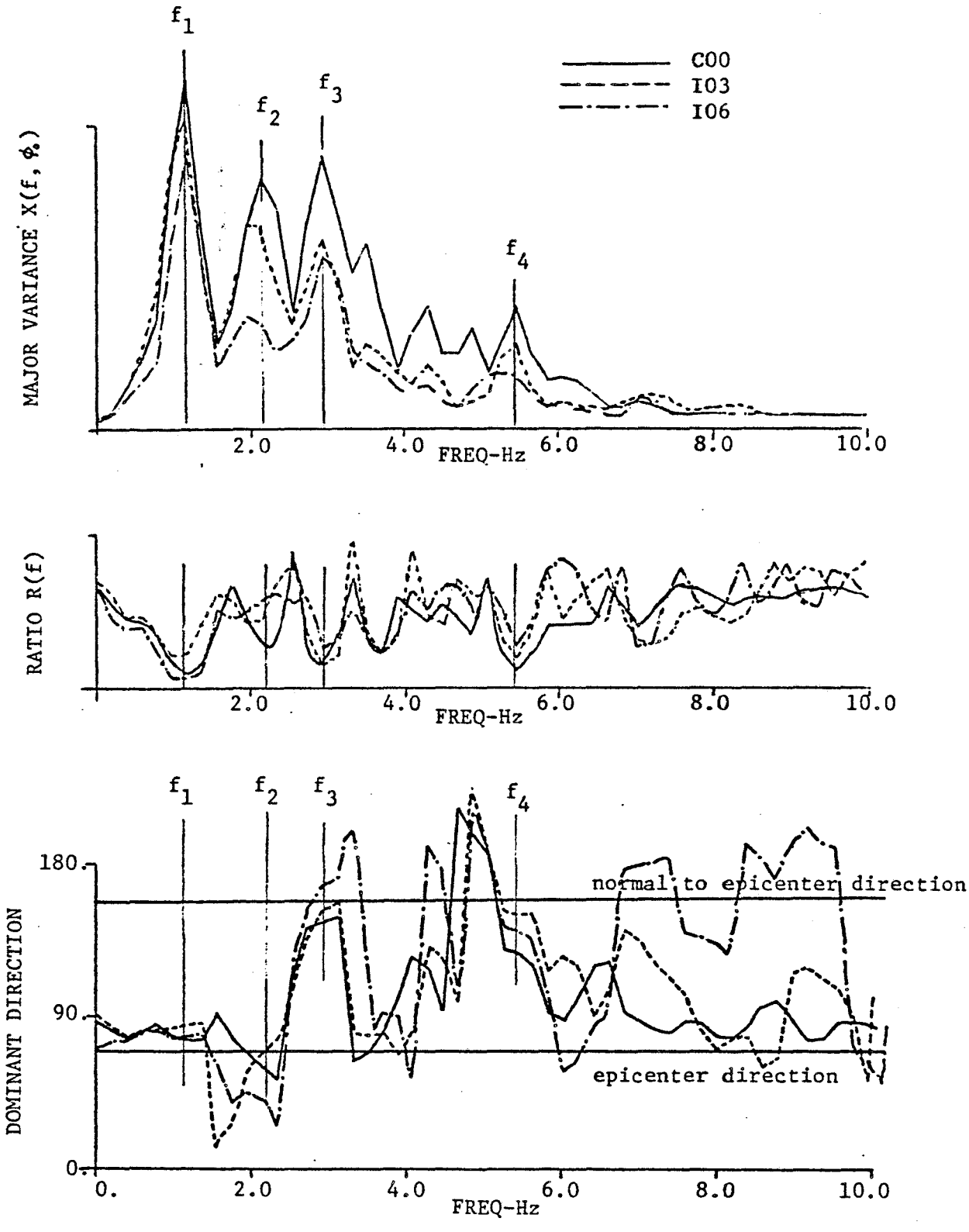

Fig. 5 Major principal variance, variance ratio and dominant direction for Event 5

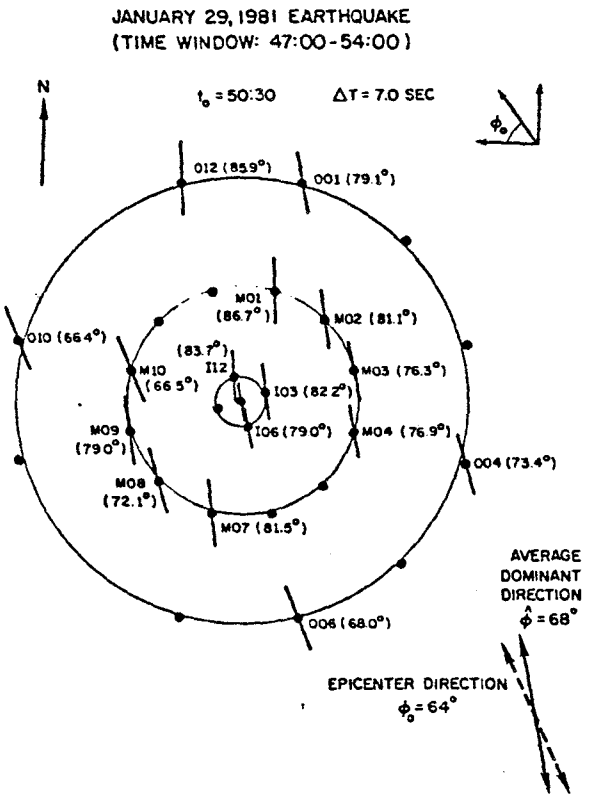

Fig. 6 Dominant directions at 1.17 Hz for Event 5

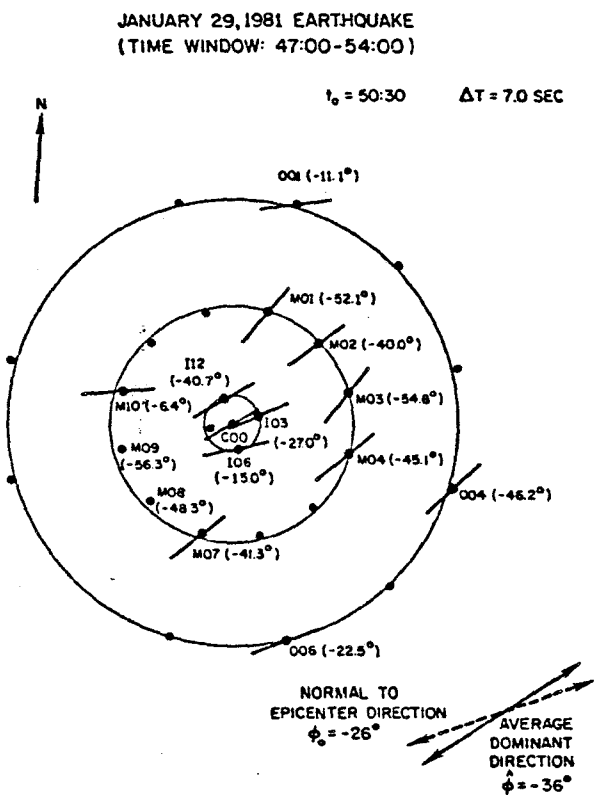

Fig. 7 Dominant directions at 2.85 Hz for Event 5

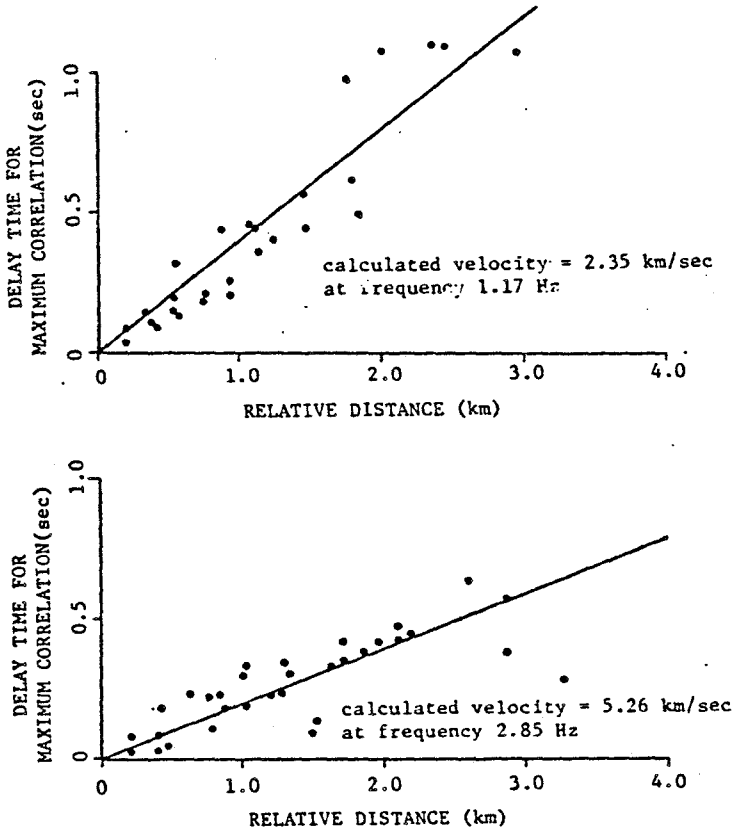

Fig. 8 Identification of wave velocity at frequencies 1.17 Hz and 2.85 Hz

A THREE COMPONENT SHAKING TABLE STUDY OF THE DYNAMIC RESPONSE OF A SINGLE STORY MASONRY HOUSE

G. C. Manos (I)
R. W. Clough (II)
R. L. Mayes (III)

Presenting Author: G. C. Manos

SUMMARY

Earthquake damage to masonry construction during recent years underscores the need for a better understanding of the seismic response of these structures and the establishment of rational reinforcing requirements. An experimental investigation aimed at determining reinforcing requirements for single-story masonry dwellings in Uniform Building Code Seismic Zone 2 areas of the United States has been conducted at the University of California at Berkeley. During the most recent tests the masonry walls of a house model were simultaneously subjected to two horizontal (in-plane and out-of-plane) as well as to vertical input motions. The earthquake performance of the unreinforced as well as the partially reinforced house model is discussed. The unreinforced house model withstood satisfactorily simulated earthquake motions of moderate intensity; the partially reinforced house model withstood satisfactorily simulated motions of very high intensity.

INTRODUCTION

During the past seven years the U.S. Department of Housing and Urban Development has supported a series of shaking table tests at the Earthquake Engineering Research Center (EERC) of the University of California at Berkeley. The investigation was entitled "Laboratory Studies of the Seismic Behavior of Single Story Masonry Houses in Seismic Zone 2 of the U.S.A.".

The objective of this program has been to evaluate the Department of Housing and Urban Development (HUD) requirements for single story masonry dwellings in seismic Zone 2 areas of the Uniform Building Code, by investigating the earthquake performance of single story masonry house models, constructed with full scale components and subjected to simulated earthquake input produced by the EERC earthquake simulator facility.

In what follows some essential details and results obtained in the most recent shaking table tests will be discussed. Complete data on the test procedures, instrumentation and test results are contained in the project report [1].

During earlier tests four house models were studied, namely House 1, 2, 3 and 4 [2], [3]. In all these tests the direction of the horizontal motion was parallel to two of the walls of the model (in-plane) and perpendicular to the other two walls (out-of-plane). During the present study of House 5, a model essentially the same as the previously tested House 4, was oriented on the shaking table with its axes at 30° to the horizontal direction of table motion,

(I) Assist. Research Engineer, University of California, Berkeley, U.S.A. on leave from the Lab. of Struc. Analysis, Univ. of Thessaloniki, Greece.
(II) Professor of Civil Engineering, Earthquake Engineering Research Center, University of California, Berkeley, U.S.A.
(III) Principal, Computech, Berkeley, California, U.S.A.

so that its walls were simultaneously subjected to in-plane and out-of-plane excitation as well as to vertical input motion. In this way the importance of the combined in-plane and out-of-plane action of earthquake input on the masonry walls was investigated.

TEST PROCEDURES

The test structure consisted of four walls with standard size door and window openings (Fig. 1). The walls were not interconnected at the corners but only at the top level by a wooden roof. Like the earlier models, House 5 was square in plan with 16 ft wall length and 8 ft 8 in. wall height. 12,000 lb weight was added at the top of the roof in order to simulate the load per unit length of prototype loadbearing walls, which were assumed to be three times longer and to support a roof load of 20 lb/sq ft. House 5 was built on a continuous concrete foundation and was transported to the shaking table fully assembled. The foundation block was a rigid system representing stiff-soil site conditions for moderate earthquakes without any soil-structure interaction. The masonry was built of standard hollow concrete blocks with nominal dimensions 6 x 4 x 16 in. laid in running bond with mortar across the shell faces and with mortar joints carefully tooled on both masonry faces. The compressive strength of the mortar was 2,229 psi and the compressive and diagonal tensile strength of the masonry was 2,200 psi and 69 psi, respectively. The simulated input was based on accelerograms recorded at the El Centro 1940, Taft 1952 and Greenville 1980 earthquakes. All simulated earthquake records had one horizontal and the vertical component with no time scaling; the simultaneous action of two horizontal input components on the model masonry walls resulted from the orientation of the walls with respect to the axis of horiozntal table motion (Fig. 1).

TEST RESULTS

Table 1 lists the tests applied to the unreinforced House 5. After completion of these eight tests, the model was partially reinforced using the reinforcing arrangement shown in Figure 1.

Observations from the performance of the unreinforced House 5 follow:

a. The first structural crack appeared during test No. 5 (Table 1). This crack was at a horizontal mortar joint near the right bottom corner of loadbearing wall B. The dynamic crack opening during test No. 5 attained the value of 0.060 in. However, the permanent deformations were negligible. The time histories of the base accelerations applied during this test are shown in Figure 2.

b. The dynamic house response after the formation of this first structural crack is dominated by large uplift displacements of wall B at the crack location,inducing large in-plane displacements for wall B and large out-of-plane displacements for wall A1 (Figure 4).

c. Figure 5 depicts the magnified deformed shape of House 5 at the top-of-the-wall level at particular time instants selected to coincide with peak values of the acceleration or displacement response. The arrows depict the measured acceleration values at the top of each wall; the shaking table input acceleration is also plotted with an arrow at the center of the sketch. All plotted accelerations and displacements are horizontal. The displacement and acceleration scales used to plot these measurements also are shown.

Significant out-of-plane displacement response for walls A1 and B1 as well as torsional and distortional response for the house as a whole can be seen in Figure 5.

d. All masonry walls of House 5 have been subjected to a combination of significant in-plane and out-of-plane inertial forces (Table 1) and developed significant in-plane and out-of-plane displacement response (Figures 4 and 5).

e. The first unacceptable damage for unreinforced House 5 occurred during test No. 7 (Table 1) in the form of partial loss of support for the door lintel beam of wall B. The term "unacceptable damage" was defined in this investigation as permanent cracking or sliding displacements in excess of 1/4 in. The performance of unreinforced House 5 during the test program is depicted in Figure 8; the abscissae in this figure represent the sequential test number and the ordinates the test intensity in terms of base accelerations.

Observations on the performance of House 5 after it was partially reinforced were as follows:

a'. The partially reinforced House 5 was subjected to a large number of tests. Table 2 lists a summary of the base motions used for ten of these tests and Figure 3 depicts the time histories of the base accelerations for test No. 5(a). The observed damage of partially reinforced House 5 is well within acceptable levels even for tests of very high intensity (Figure 8).

b'. The large displacement and acceleration response as well as the torsional and distortional response observed during the tests of the unreinforced House 5 after the formation of the first structural crack (Figures 3 and 4) was well controlled by the partial reinforcement (Figures 6 and 7).

c'. A comparison of the earthquake performance of the partially reinforced House 5 and 4, which were essentially the same except that the partial reinforcement of the loadbearing wall A of House 4 was not provided with dowels, shows that House 5 exhibited satisfactory performance, whereas the undowelled partial reinforcement of wall A in House 4 was unable to contain the damage within acceptable levels [3].

CONCLUSIONS

1. The unreinforced House 5 performed satisfactorily with no cracks for simulated earthquake motions with base peak accelerations of 0.25g parallel to walls A,B; 0.15g parallel to walls A1,B1; and 0.22g vertical.

2. After formation of the first structural crack the unreinforced House 5 performed satisfactorily, despite significant in-plane and out-of-plane displacement and acceleration response for the masonry walls and torsional distortional response for the house as a whole; the base peak accelerations were 0.32g, 0.18g and 0.21g, respectively, along the three axes.

3. The first unacceptable damage, in the form of partial loss of support for the door lintel beam, developed in unreinforced House 5 for base peak accelerations of 0.37g, 0.21g and 0.26g, respectively, along the three axes.

4. The simultaneous action of in-plane and out-of-plane inertial forces on all the unreinforced masonry walls of House 5, for moderate to moderately high intensities of simulated earthquake input, did not result in any noticeable increase of the damage of House 5 as compared with the damage of House 4, which was not subjected to this in-plane and out-of-plane coupling. Thus, the assumption made in Reference 4 when interpreting the results of Houses 1 to 4, increasing the expected seismic input by 50 percent for the unreinforced houses in order to account for the coupling effect, is overly conservative.

5. The partially reinforced House 5 earthquake performance was satisfactory throughout a large number of tests, some of them very high intensity simulated earthquake motions; the maximum peak accelerations at the base were 0.87g parallel to walls A,B; 0.50g parallel to walls A1,B1; and 0.56g vertically. The effectiveness in containing damage of partial reinforcement of the shear-resisting elements (when connected to the foundation by dowels) becomes evident by the performance of this model.

6. The importance of the roof-to-walls connections used in this study must be underlined. This type of connection, typical of standard construction practice, withstood a large number of simulated earthquake motions of moderate to very high intensity without signs of any significant distress. Loss of support for the roof from the failure of these connections would have been extremely detrimental to the overall earthquake performance of the test structure.

REFERENCES

1. Manos, G. C., Clough, R. W. and Mayes, R. L., "Shaking Table Study of Single Story Masonry Houses: Dynamic Performance under Three Component Seismic Input and Recommendations", Earthquake Engineering Research Center Report No. UCB/EERC-83/11, July 1983.

2. Gülkan, P., Mayes, R. L. and Clough, R. W., "Shaking Table Study of Single-Story Masonry Houses: Volume 1: Test Structures 1 and 2", Earthquake Engineering Research Center Report No. UCB/EERC-79/23, September 1979.

3. Gülkan, P., Mayes R. L. and Clough, R. W., "Shaking Table Study of Single-Story Masonry Houses - Volume 2: Test Structures 3 and 4", Earthquake Engineering Research Center Report No. UCB/EERC-79/24, September 1979.

4. Clough, R. W., Mayes, R. L. and Gülkan, P., "Shaking Table Study of Single-Story Masonry Houses - Volume 3: Summary, Conclusions and Recommendations", Earthquake Engineering Research Center Report No. UCB/EERC-79/25, Sept. 1979.

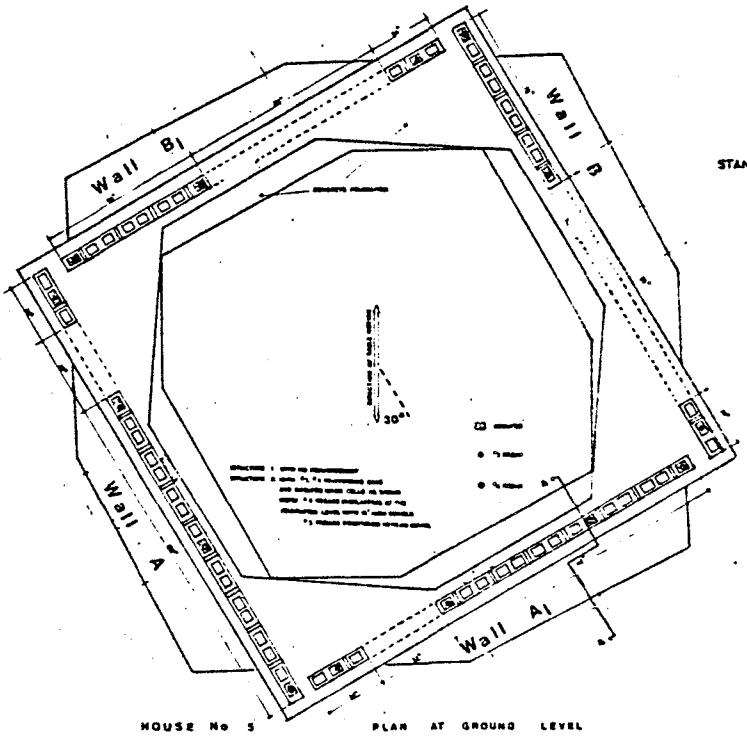

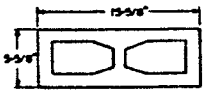

STANDARD CONCRETE BLOCK UNIT FOR HOUSE 5

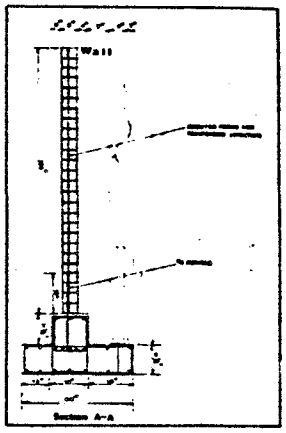

WALL A

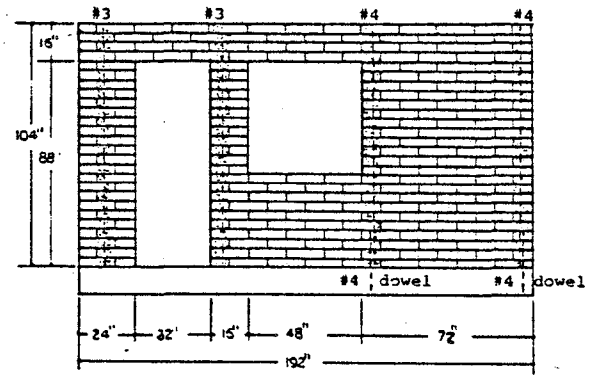

WALL A1

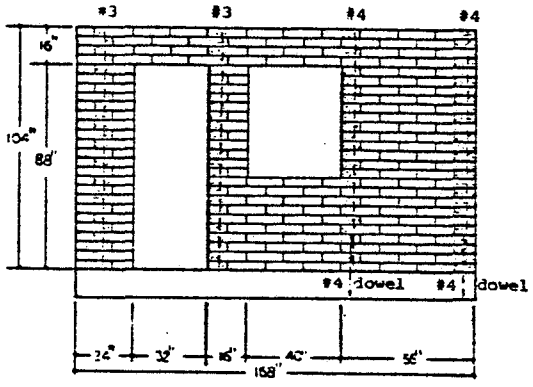

WALL B

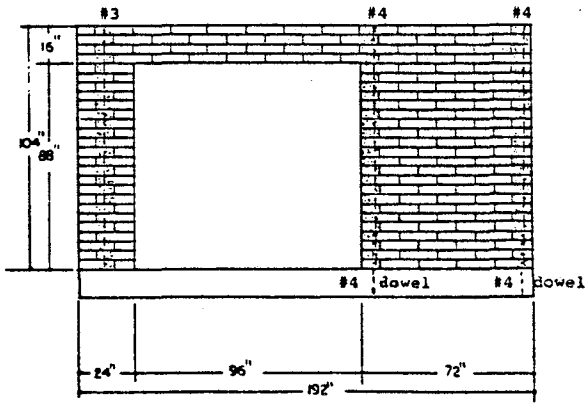

WALL B1

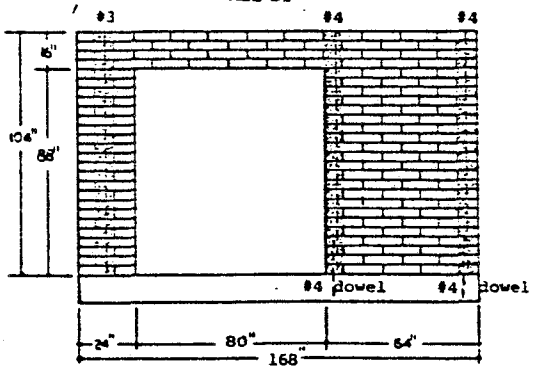

Fig. 1. structure 2 : PARTIALLY REINFORCED HOUSE 5
(structure 1 : unreinforced house 5 as above without reinforcement)

TABLE 1. PEAK VALUES OF TABLE-BASE ACCELERATION FOR UNREINFORCED HUD-HOUSE No. 5

E.Q. Motion Test No.	Peak Hor. Table Acc. (g)	Peak Ver. Table Acc. (g)	Peak Hor. Acc. at base // to walls A and B (g)	Peak Hor. Acc. at base // to walls A1 and B1 (g)
1) EL CENTRO	-.131/.120	-.057/.052	0.113	0.066
2) EL CENTRO	-.215/.191	-.113/.107	0.186	0.108
3) EL CENTRO	-.292/.269	-.217/.164	0.253	0.146
4) TAFT	-.205/.264	-.132/.110	0.229	0.132
5) EL CENTRO*	-.363/.331	-.211/.199	0.314	0.182
6) TAFT	-.295/.366	-.400/.209	0.317	0.183
7) EL CENTRO*	-.427/.340	-.263/.264	0.370	0.214
8) TAFT	-.330/.427	-.439/.232	0.368	0.213

* The intensity of the earthquake motion for these tests is approximately the same as the intensity of the original ground shaking

// denotes parallel

TABLE 2. PEAK VALUES OF THE TABLE ACCELERATION FOR PARTIALLY REINFORCED HUD-HOUSE No. 5

E. Q. Motion Test No. (s)	Peak Hor. Table Accelerat. (g)	Peak Ver. Table Accelerat. (g)	Hor. Acc. at base parallel to walls A and B (g)	Hor. Acc. at base parallel to walls A1 and B1 (g)
1) EL CENTRO	-.519/.408	-.364/.346	0.450	0.260
2) TAFT	-.426/.543	-.319/.258	0.470	.272
3) EL CENTRO	-.662/.486	-.419/.490	0.573	0.331
4) TAFT	-.586/.768	-.414/.356	0.665	0.384
5) EL CENTRO	-.895/.558	-.450/.520	0.775	0.448
6) TAFT	-.766/1.01	-.567/.462	0.872	0.504
7) TAFT	-.766/1.03	-.567/.462	0.890	0.514
8) GREENVILLE	-.656/.322	-.192/.231	0.568	0.328
9) TAFT	-.580/.758	-.420/.360	0.656	0.379
10) EL CENTRO	-.969/.604	-.412/.476	0.839	0.485

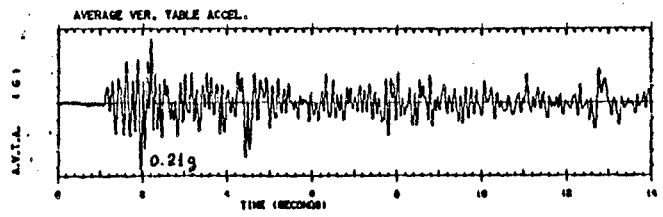

Fig. 2. UNREINFORCED HUD-HOUSE 6 , EL CENTRO H=0.36G V=0.21G
DISPLACEMENTS, ACCELERATIONS AND HOR. FORCE AT BASE LEVEL

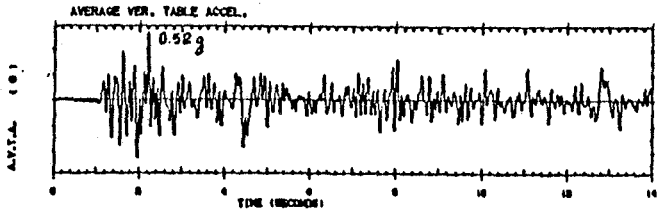

Fig. 3. REINFORCED HUD-HOUSE 5 , EL CENTRO H=0.90G V=0.62G
DISPLACEMENTS, ACCELERATIONS AND HOR. FORCE AT BASE LEVEL

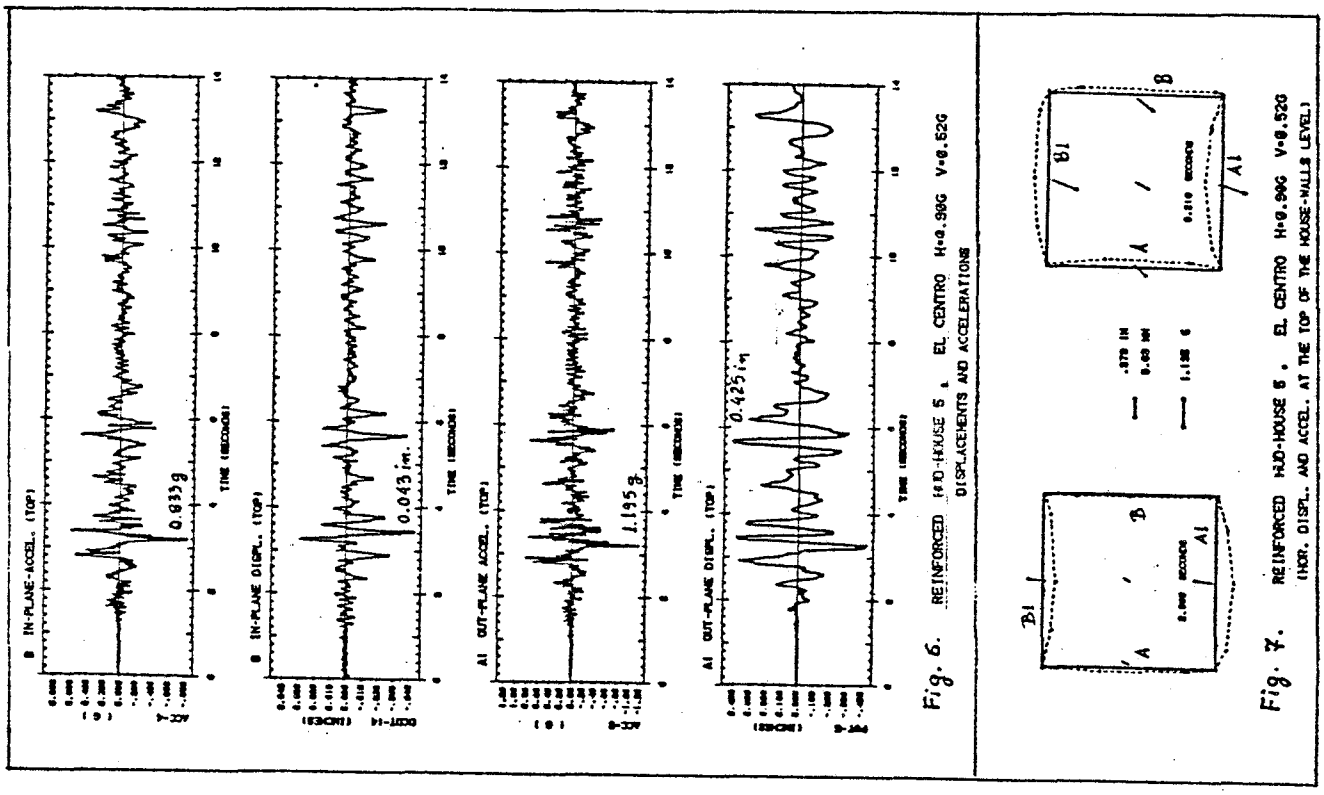

Fig. 6. REINFORCED HUD-HOUSE 5 , EL CENTRO H=0.39G V=0.52G
DISPLACEMENTS AND ACCELERATIONS

Fig. 7. REINFORCED HUD-HOUSE 5 , EL CENTRO H=0.39G V=0.52G
(HOR. DISPL. AND ACCEL. AT THE TOP OF THE HOUSE-WALLS LEVEL)

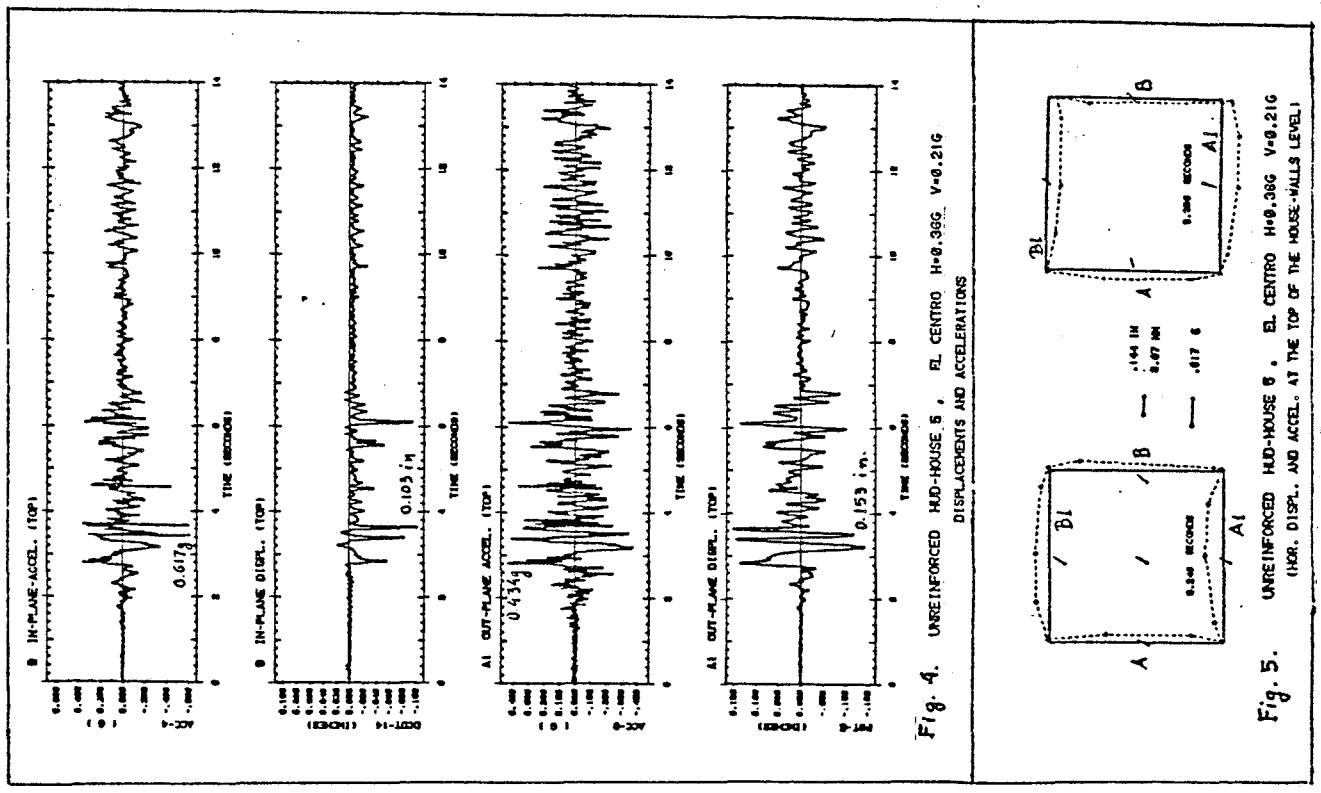

Fig. 4. UNREINFORCED HUD-HOUSE 5 , EL CENTRO H=0.39G V=0.21G
DISPLACEMENTS AND ACCELERATIONS

Fig. 5. UNREINFORCED HUD-HOUSE 5 , EL CENTRO H=0.39G V=0.21G
(HOR. DISPL. AND ACCEL. AT THE TOP OF THE HOUSE-WALLS LEVEL)

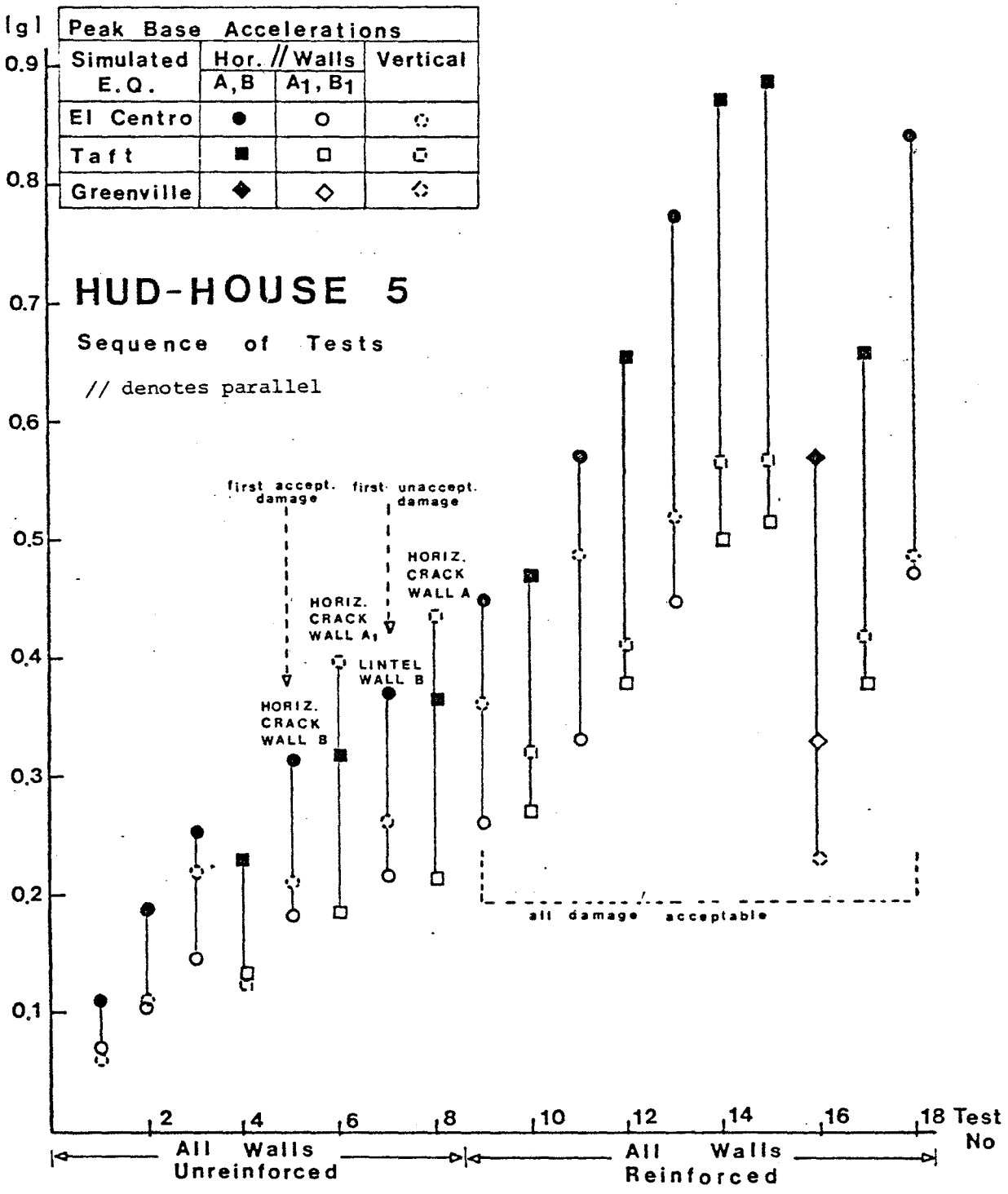

Fig. 8. Sequence of tests for unreinforced and partially reinforced House 5.

EXPERIMENTAL STUDY OF A FLAT-PLATE BUILDING MODEL

J. P. Moehle (I)
J. W. Diebold (II)
H. L. Zee (II)
Presenting Author: J. P. Moehle

SUMMARY

An experimental and analytical study of the seismic behavior of a two-story reinforced concrete flat-plate framed model is described. The model was constructed at approximately one-third scale with details following recommendations in United States for structures in regions of low to moderate seismic risk. Primary tests include low, moderate, and high intensity earthquake simulations on a shaking table. This paper documents the experiments and discusses some of the observed responses.

INTRODUCTION

Occasional failures of reinforced concrete flat-plate framing systems during severe ground shaking have led to widespread rejection of the flat plate as a viable system in regions of high seismicity. Economics and good performance under gravity loads have led to equally widespread acceptance of the system in regions of lower seismic risk. Recently, growing awareness of the potential for strong ground shaking in eastern and midwestern regions of the United States has given rise to concerns about performance of the flat plate during low to moderate-intensity shaking. In response to these concerns, an experimental research program has been undertaken to study behavior of a flat-plate frame under low, moderate, and high-intensity base motions. A one-third scale model of a two-story, three-bay flat plate with edge beams has been constructed and tested on the University of California Earthquake Simulator. Component tests of isolated plate-column connections provide insight into local behavior of the complete structure. This paper describes the test structure and some of the test results.

DESIGN OF PROTOTYPE STRUCTURE

The prototype structure is a two-story flat-plate frame having three bays along one principle axis and multiple bays along the other. Columns are arranged regularly at 6.1 m (20 ft) on centers. An edge beam spans the perimeter of each floor.

The frame is proportioned for gravity loads according to strength design provisions of Ref. 1. Live load is assumed at 2.87 kPa (60 psf).

(I) Assist. Prof. of Civil Engrg., Univ. of California, Berkeley.

(II) Research Assistant, University of California, Berkeley.

Under full dead and live loads (with no load factors), the nominal shear stress on a section half a slab thickness from the column is $0.083\sqrt{f'_c}$ in MPa units ($1.5\sqrt{f'_c}$ in psi units) for interior slab-column connections. Nominal shear stresses attributable to shear and moment transfer at exterior connections are such that edge beams are required. Nominal axial stress at the base of interior columns is $0.1f'_c$.

Seismic design assumes a maximum probable event represented by intensity VII on the Modified Mercalli scale (Zone 2 of the UBC, Ref. 2). The equivalent static lateral force method of the UBC is used for determining seismic effects. For lateral-load analysis, the flat-plate frame is modelled by gross-section properties with equivalent beams having flexural inertia of half the slab width. Using these assumptions and load combinations recommended by either ACI or UBC, it is found that seismic design forces do not govern the proportions.

DIMENSIONS AND DETAILS OF TEST STRUCTURE

The test model was constructed at a scale of 1 to 3.33, and only two bays of the multiple-bay direction were constructed. The scaled test model is depicted in Fig. 1. Base columns were cast monolithically with stiff "footings", which in turn were supported on stiff transducers. Thus, fixity at the column base level was not achieved completely, and might be considered qualitatively similar to the degree of fixity afforded by a real soil foundation. Stiffness of the combined footing-transducer system exceeds the stiffness of an equal length of column.

Care was taken to simulate materials and details of full-scale construction. Concrete was cast in three lifts, one for footings and one each per floor. Mean concrete strengths at time of test were 37 MPa (5300 psi) in compression and 4.8 MPa (700 psi) in modulus of rupture tests. Longitudinal column and edge-beam steel was No. 2 deformed bar having mean yield stress of 470 MPa (68 ksi). Slab reinforcement was 4.52-mm (0.178-in.) diameter deformed bar having mean yield stress of 440 MPa (63 ksi). Transverse column and edge-beam reinforcement was plain 3.0-mm (0.12-in.) diameter wire with mean yield stress of 620 MPa (90 ksi).

All details follow closely recommendations given in Ref. 3 for structures in regions of low-to-moderate seismic risk. Details of slab reinforcement at an interior joint are in Fig. 2. An extra mat of reinforcement is provided near the column region to enhance behavior. Longitudinal steel ratio in columns is 0.013. At column ends, all bars are restrained in the corner of a tie having spacing of 51 mm (2.0 in.). Stirrup spacing in end regions of edge beams is 25 mm (1.0 in).

Supplementary lead weights were supported on tops of slabs. The weights were positioned to simulate moments and shears due to slab dead loads occuring in the prototype structure. Connections ensured that the weights did not slip during testing and did not enhance stiffness or strength of the model. Total weight of the model including lead ballast was 210 kN (47 kips).

TESTS AND INSTRUMENTATION

Base motions simulated the motion recorded in El Centro during the 1940 Imperial Valley Earthquake. In some tests, a single horizontal base motion (modelling the NS component) was imparted parallel to the three-bay direction of the structure (Fig. 1). In other tests, the horizontal component was augmented by the corresponding vertical component. The time scale of base motions was compressed by a factor of 1.71. The horizontal acceleration record obtained during the "design" test is plotted in Fig. 3. Test intensities were increased incrementally, with horizontal peak base accelerations ranging between 0.015 and 0.83 g.

Before the first simulation and subsequent to each, a free vibration test was conducted by initially displacing the model with a constant force and then releasing suddenly.

Instrumentation provided continuous response records of relative floor displacements and absolute floor acceleration. Base shears could be obtained by the product of floor accelerations and masses, and checked by the sum of shears measured by transducers located below footings (Fig. 1). Strain gauges were at selected locations on slab and column reinforcement.

INITIAL DYNAMIC PROPERTIES

Initial dynamic properties are obtained from free-vibration responses before the earthquake simulations. The initial period was 0.21 sec. For the full-scale building this corresponds to a period of 0.38 sec, which is substantially larger than the value given by 0.1N, where N = number of stories, as given by the UBC (2). This is indicative of the flexibility inherent in flat-plate framing. Using half the slab width as an equivalent beam (Ref. 4) the period is computed to be 0.19 sec for gross-section stiffness. The slightly longer measured period can be attributed to initial minor cracking. Initial equivalent viscous damping obtained by the log decrement is approximately 1.5 percent of critical. This value is typical for uncracked or lightly-cracked reinforced concrete structures.

RESPONSES TO SIMULATED EARTHQUAKES

Five earthquake simulations were conducted with peak horizontal accelerations below 0.1g so that responses to low-level events could be observed. Maximum drift levels reached only 0.1 percent of structure height. Vibration periods and damping factors obtained in free-vibration tests were the same as those obtained before testing, indicating that damage was negligible. Only slight cracking was observed.

The design-level test had a peak horizontal acceleration of 0.19g, with no vertical input (Fig. 3). Top-floor relative displacement and base-shear records (Fig. 4) reveal that displacement and base-shear responses were predominantly first mode. Maximum top displacement was only 0.3 percent of structure height, a value well within accepted limits for drift control. The base shear coefficient obtained was 0.29 (ie, 29

percent of structure weight).

Damage induced by the design-level test was light. Cracking was apparent in slabs around the columns and in columns at the footing level. Maximum crack widths did not exceed 0.3 mm, and there was no indication of shear distress. Yield was not detected by any strain gages. During a subsequent free-vibration test, the vibration period was 0.22 sec and the damping factor had increased noticeably to 0.025. The effective period during the peak response, taken as time between three successive zero crossings, was 0.26 sec, indicating an effective stiffness during peak response of approximately 65 percent of the initial stiffness.

Responses to a subsequent test for which peak horizontal base acceleration was 0.61 g are plotted in Fig. 5. For this test, maximum drift level was 3.4 percent of height, and peak base-shear coefficient was 0.8. During the peak response, the period was 0.54 sec, indicating an effective secant stiffness of only 15 percent of the initial gross-section stiffness. Viscous damping obtained during a free-vibration test was 5 percent of critical. Flexural cracking, with widths indicative of yield, was observed on both top and bottom surfaces of slabs and ran the entire width of the slab. Fan-shaped cracks were apparent around all interior columns, and wide torsion cracks were apparent in edge beams. In addition, crushing was observed at the base level of columns.

A final simulation having peak horizontal and vertical accelerations of 0.83 and 0.20 g, respectively, resulted in top drift of 5.5 percent, and base-shear coefficient of 0.84. The pattern of cracking indicated that punching failure was imminent at one of the first-floor interior columns. Severe torsional damage to the edge beams resulted in loss of cover concrete near the columns. Column base crushing was apparent, but bar buckling did not occur.

LOAD-DEFORMATION RESPONSE OF STRUCTURE

The measured envelope relationship between base shear and top displacement is in Fig. 6. The relationship does not indicate a sharp cracking or yielding point. This can be expected because cracking and yielding occur initially in the slab at the columns and spread gradually in the transverse direction.

The initial stiffness can be approximated using the gross section with half the slab width as an equivalent beam, and with lateral loads distributed uniformly over height. By assuming loads are uniform over height, computed stiffness is approximately ten percent higher than if loads vary linearly. The experiments indicate the true variation was typically between these extremes. The initial calculated slope compares reasonably with the measured slope (Fig. 6) It is consistent with observed damage in that it indicates deviation (hence, cracking) beyond displacements of approximately 0.3 to 0.4 percent of structure height.

The maximum base-shear coefficient obtained near collapse was 0.84,

which is significantly in excess of design base shears stipulated by design codes (2). Significant deviations between design base shear and actual base shear are frequently attributable to member overdesigns, material overstrengths, and internal force redistribution which is not considered in the design analysis model. This situation is exacerbated for the test structure because requirements for gravity load design exceed those for seismic design.

Observed damage indicates a collapse mechanism involving plastic hinges in slabs at all columns and in columns at the base. Flexural capacities of slab-column connections have been determined experimentally from reversed-loading tests on slab-column subassemblies. Assuming a uniform lateral-load distribution, computed base shear capacity is 156 kN. Measured capacity exceeds this value by approximately ten percent. The overstrength might be attributable to enhancement of material strengths due to strain-rate effects, or redistribution of internal forces in the continuous model which was not possible in the simpler slab-column subassemblies.

Using measured load-deformation behavior of the isolated slab-column subassemblies, it is possible to reconstruct the load-deflection behavior of the complete structure. As a simple approximation, a model was devised which assumed inflection points at midlengths of slabs and columns, and which assumed lateral displacements of floor levels varied linearly over height (as observed during the tests). Under the uniform lateral-load distribution, the calculated relationship between base shear and top displacement is as depicted in Fig. 6. Agreement with the measured envelope is acceptable.

SUMMARY AND CONCLUSIONS

A two-story, reinforced concrete flat-plate frame with edge beams was designed and detailed according to current building code provisions for regions of low to moderate seismic risk. A one-third scale model of the frame was subjected to simulated earthquakes of various intensities. Based on data and discussions presented in the main body of this paper, the following are concluded:

(1) Gravity load is likely to control proportions of low-rise flat-plate frames. As a consequence, seismic forces may be significantly in excess of those indicated by current code provisions.

(2) Load-deflection behavior of the complete flat-plate frame to failure could be interpreted with reasonable accuracy using measured behavior of isolated plate-column subassemblies.

(3) Under lateral loads, the flat plate is relatively more flexible than a conventional beam-column structure, but sufficiently stiff for low-rise structures during low to moderate seismic excitations.

(4) The test structure possessed sufficient strength and stiffness

to stand alone during moderate-intensity shaking, and sufficient ductility to act in parallel with a more rigid structural system for strong base motions. It must be qualified that this conclusion may not be general, and structures with higher nominal slab shear stresses, less-continuous reinforcement details, less-regular framing system, and multi-directional base excitation may not fare so well. Damage in the edge beams indicated that collapse would have been likely during moderate shaking had the edge beam (or other form of "shear" reinforcement) been eliminated at the edge of the plate.

REFERENCES

(1) "Building Code Requirements for Reinforced Concrete (ACI 318-77)," American Concrete Institute, Detroit, 1977.

(2) "Uniform Building Code," International Conference of Building Officials, Whittier, California, 1982.

(3) ACI Committee 318, "Proposed Revisions to Building Code Requirements for Reinforced Concrete (ACI 318-77) and Commentary on Building Code Requirements for Reinforced Concrete (ACI 318-77)," Concrete International V. 4, No. 12, December 1982, pp. 38-127.

(4) Pecknold, D. A., "Slab Effective Width for Equivalent Frame Analysis," ACI Journal, April, 1975, pp. 135-137.

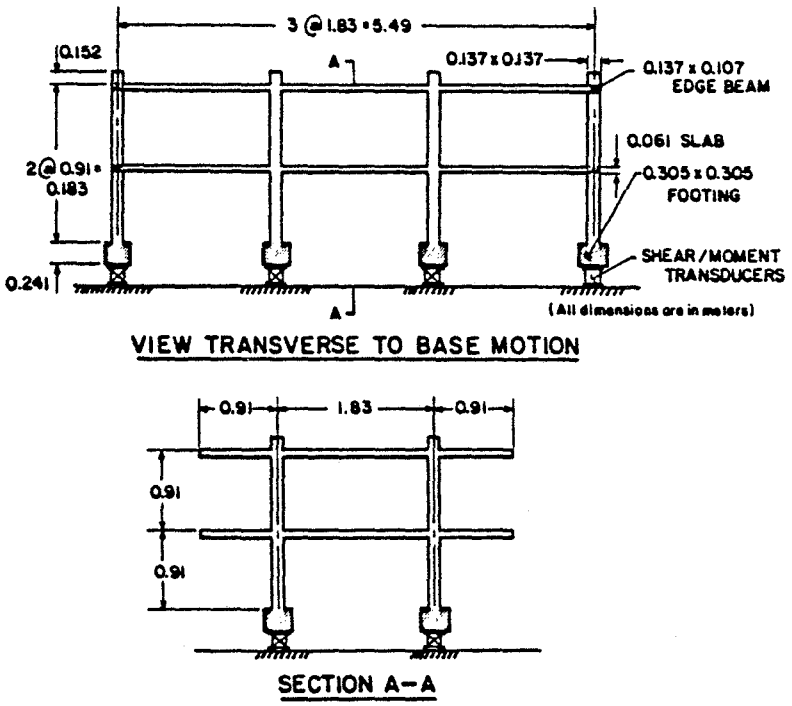

Fig. 1. Test Structure Configuration.

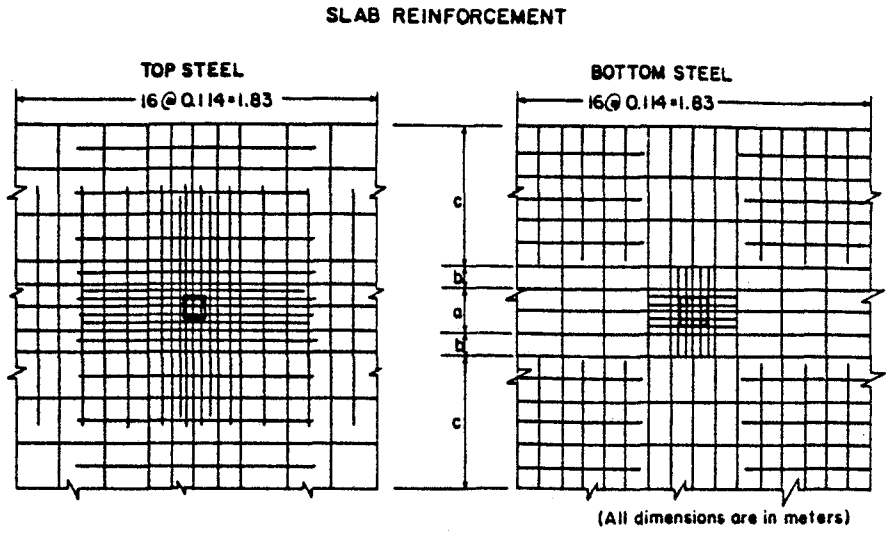

Mark	Width	TOP STEEL REINFORCEMENT Spacing	Bar Lengths	d_b	BOTTOM STEEL REINFORCEMENT Spacing	Bar Lengths	d_b
a	0.229m	0.038	2 @ 1.12 2 @ 1.22 2 @ 3.632	.0045	0.038	4 @ 0.457 3 @ 3.632	.0045
b	0.114m	0.057	1 @ 1.22	.0045	NO BARS IN THIS SPACE		
c	0.686m	0.114	3 @ 1.22 4 @ 3.63	.0045	0.114	3 @ 1.372 4 @ 3.632	.0045

Fig. 2. Interior Slab Reinforcement Details.

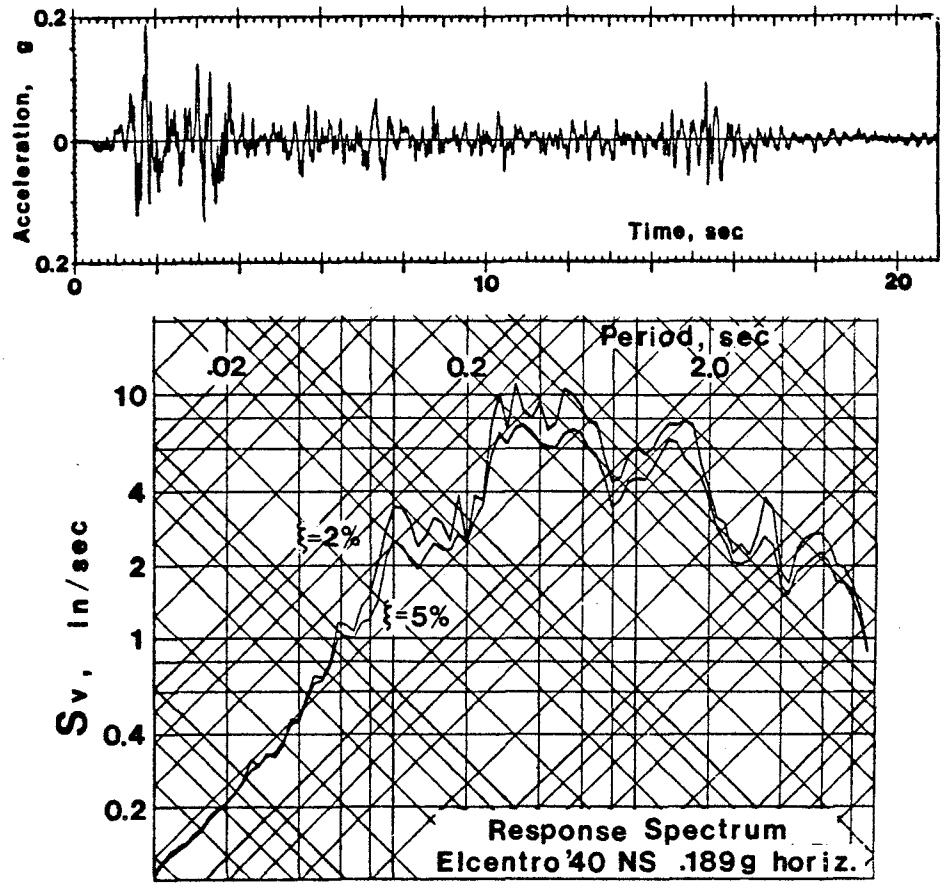

Fig. 3. Base Acceleration and Response Spectrum for "Design" Test.

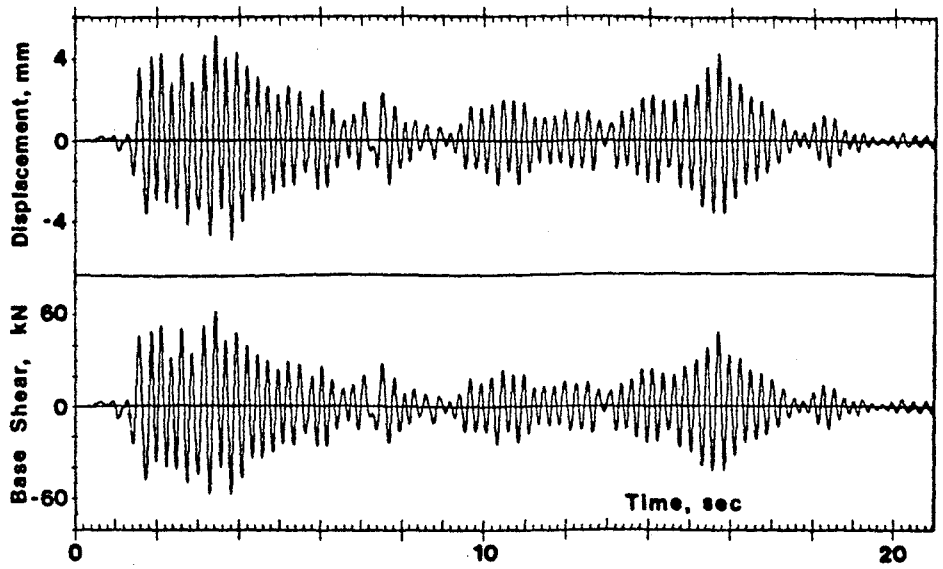

Fig. 4. Top-Floor Displacement and Base-Shear Records for "Design" Test.

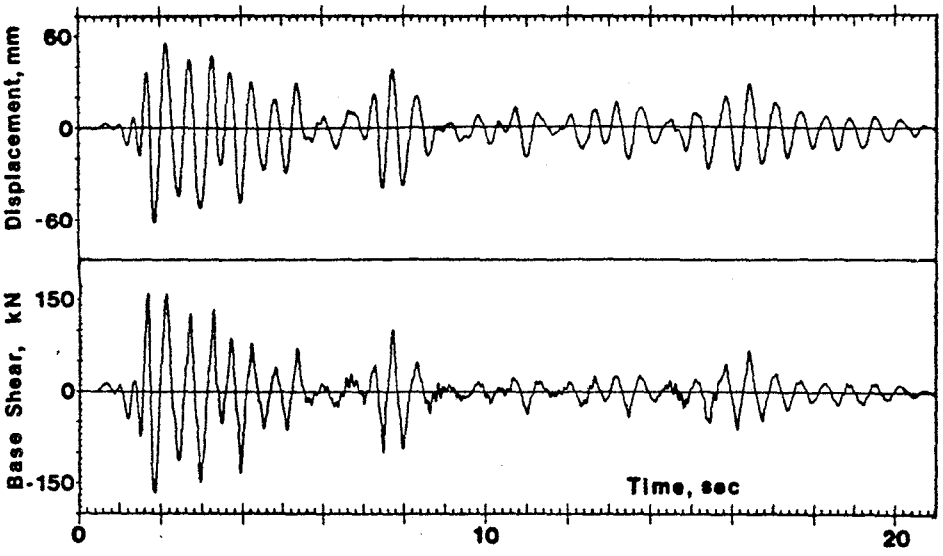

Fig. 5. Top-Floor Displacement and Base-Shear Records for 0.6g Test.

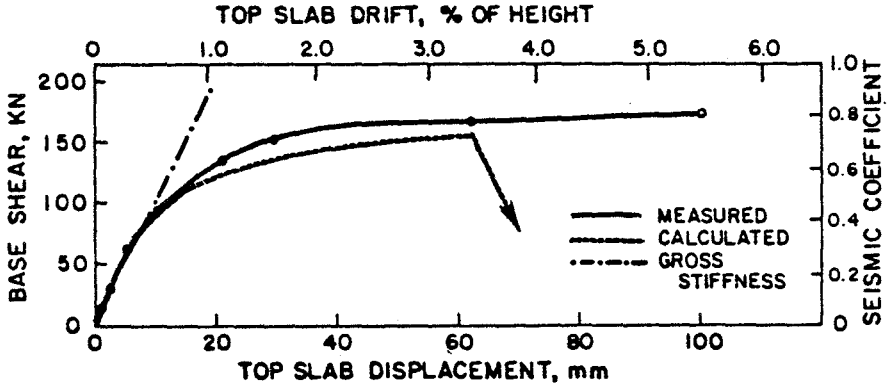

Fig. 6. Envelope of Top-Floor Displacement and Base Shear.

SHAKiNG TABLE TESTS OF WET JOINTED PRECAST PANEL WALLS

Michael G. Oliva [1]
Bahram M. Shahrooz [2]
Presenting Author: M. G. Oliva

SUMMARY

Experimental results from shaking table tests of large scale precast panel wall systems are presented. One-third size true scale models were tested under simulated earthquake motions. Qualitative and quantitative results are preceded by a brief description of the model configurations, testing, and instrumentation. Examination of model behavior and data indicated that rocking motion of the precast panels provided the major contribution to the overall displacement. Shear-slip motion was effectively constrained by shear keys. The rocking motion isolated the wall from ground motion and limited the amplitude of the base shear which could be transferred into the wall system.

INTRODUCTION

Precast large panel concrete structures are being used extensively throughout the world to meet a growing demand for residential housing. Economic limitations within many countries have required that the demand be met with large scale industrially produced units which can be erected with semi-skilled labor. Many such building systems exist with varied design, mateials, and assembly techniques. The research described in this paper concerns one such system using factory produced precast concrete elements with cast-in-place field joints.

Panelized buildings, as considered in this paper, are composed of vertical panels supporting horizontal floor panels to form a complete box like structure. The vertical panels act as load bearing shear walls and the horizontal panels act as roof and floor systems with diaphragm action. These structures present a unique challenge in terms of behavior and design because of the usage of the vertical panels to resist combined vertical and lateral loading (with a failure in either mode likely to result in collapse) and because of the necessary field joints between panels. The lack of secondary mechanisms to carry loads if wall panels fail is particularly important with

---

1. Assistant Professor, Civil Engineering, University of Wisconsin, Madison, Wisconsin, U.S.A.
2. Research Assistant, University of Wisconsin, Madison, Wisconsin, U.S.A.

their increasing use in regions of seismic risk.

The large panel system, composed of strong precast wall elements with relatively weak and often brittle interconnecting joints, tends to exhibit two prime deformation mechanisms when overloaded. The first mechanism is a result of overturning moments induced by the lateral loading. The joint between vertical panels is generally designed with a minimum of continuous reinforcing between upper and lower panels to simplify field assemblage.

The lack of vertical reinforcing across the joint, and hence tensile capacity, results in flexural cracking at the joint and a rocking of the panel above as exhibited in Figure 1. The second mechanism involves a shearing along the joint, a result of shear force induced by lateral load, and subsequent slip between joined panels as seen in Figure 1. The flexural mechanism is difficult to model using beam analogy because of the wall's deep narrow cross section.

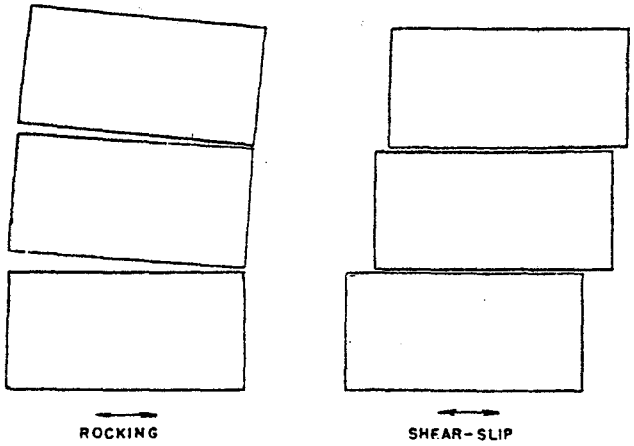

Fig. 1. Wall deformation mechanisms

Shear-slip involves numerous resistance sources including friction, aggregate interlock, dowel action and key strength. The capacity of the mechanisms is difficult to define analytically, requiring experimental verification.

The behavior of the structure with weak joints has been analytically investigated by various studies including Becker [Ref.1], Mueller [Ref.2] and Schricker [Ref.3]. Behavior of individual resisting mechanisms within the wall systems has been experimentally studied at the PCA [Ref.4] and other researchers [Refs. 5, 6, and 7] under statically applied loads either monotonic or cyclic. The present study considered the behavior of a complete wall system, at a reduced scale, under actual dynamic earthquake motion.

MODEL DESCRIPTION

Three large scale models of various precast wall panel configurations were tested under earthquake motions at the University of California Earthquake Simulator Laboratory to establish quantitative data describing the behavior of wall systems in seismic conditions. The one-third scale models were composed of precast components produced by RAD Construction of Belgrade, Yugoslavia with wet joint connections completed at the University of California Laboratory. Each model was a three story wall segment in variations including a plain solid wall, wall panels with door openings, and wall panels with adjoining end flange walls. The specimens were carefully instrumented and tested with earthquake motion of varying amplitude.

The test wall configuration was a derivative of the Balency system developed by RAD, the University of Beograd and IZIIS of Skopje. All connections were of the wet joint type with panels providing forming for the

poured joints. Details of the panels and connections are illustrated in Figures 2 and 3. The three story walls were designed and loaded to simulate conditions near the middle of a 15 story structure. Added mass blocks above the specimens created necessary axial stresses and lateral load. Near the central height of medium rise buildings the gravity axial loads are relatively small, decreasing the friction portion of shear resistance, yet the shear and overturning moments may be high enough to crack the section. Vertical continuity is provided by small cast in place columns with continuous reinforcing in vertical joints between wall panels, and from a single bar extending from the top and bottom at each end of the wall panel welded to the similar bar in adjoining panels (Figure 4). The test specimens were true scale models, at one-third scale, made of prototype material. Stresses in the model would be equal to prototype stresses to correctly simulate the inelastic response.

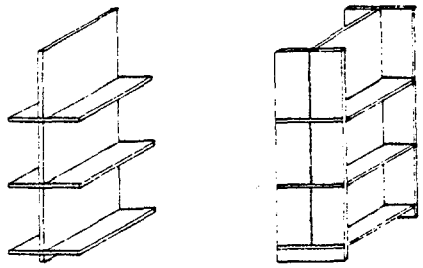

Fig. 2. Precast test walls

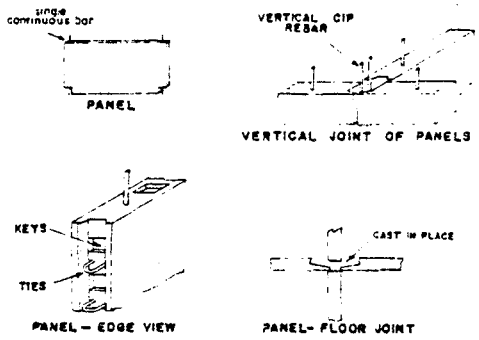

Fig. 3. Joint details

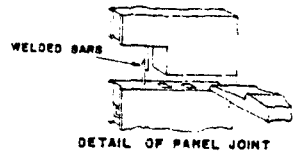

Fig. 4. Detail: cont. panel bar

TEST METHOD

All of the tests took place on the U.C. shaking table. In each model a small amplitude test, during which the model remained essentially elastic, was followed by a high amplitude test and a subsequent medium amplitude test simulating an aftershock.

INSTRUMENTATION

Three categories of test information were recorded using precision instrumentation and a high speed data acquisition system. The instrumentation was designed to monitor: (1) actual table motion, (2) overall global deformation of the models, and (3) local deformations-particularly in joint region. A total of 85 instruments recorded most of the critical quantities occurring during the test. Measured dynamic response included displacements,

accelerations, base shear, slip and uplift of panels at horizontal joints, and strain. The instrumentation was particularly designed to provide response information which might be needed to verify proposed analytic response modelling techniques [Refs. 3, 8].

BEHAVIOR OF SOLID WALL

The solid wall model was subjected to three shaking tests. The first test occurred with a maximum ground acceleration of 0.18g, small enough to induce solely elastic response. The second test was intended to create major damage and used a peak ground acceleration of 0.67g. A final test, to simulate aftershock response of a damaged structure had a 0.50g base acceleration. All of the tests used the same shaped time scaled displacement record, each at a different amplitude. The described step from low amplitude to high amplitude motion was necessary to avoid progressive deterioration which might occur under a gradual program of increasing intensity.

Visual Observations:

There was no visible damage apparent after the initial shake. The structure did experience extensive deformation during the second test. Rocking of the wall system above the lower horizontal joint was predominant during the test. Shear-slip behavior couldn't be detected, however later viewing of slow motion films of the test proved that limited slip had been occurring.

Inspection of post test damage, particularly cracking, showed that rocking motion had opened the first floor joint above the cast in place joint concrete. The concentrated compression induced by the rocking had crushed concrete at the wall ends and in the key elements. Two of the vertical reinforcing bars at the south wall end had buckled and the continuous panel bar ruptured. Figure 5 illustrates the damage.

The "aftershock" test showed continued rocking motion.

Fig. 5. Damage, south end of wall

There was little additional damage other than concrete spalling in regions that had previously been crushed.

Measured Behavior:

The initial stiffness of the wall system, as determined during the low amplitude test from base force and top displacement, was 96kN/cm.(54k/in.). Measured deformations and strains indicated that the behavior had remained essentially linear elastic.

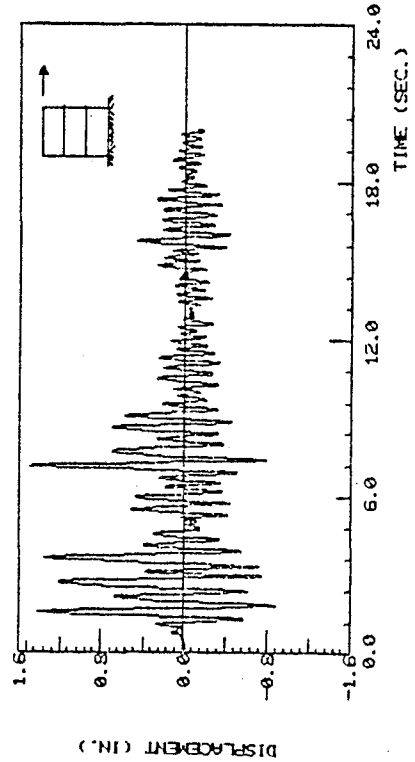

Fig. 7. Wall top displacement history

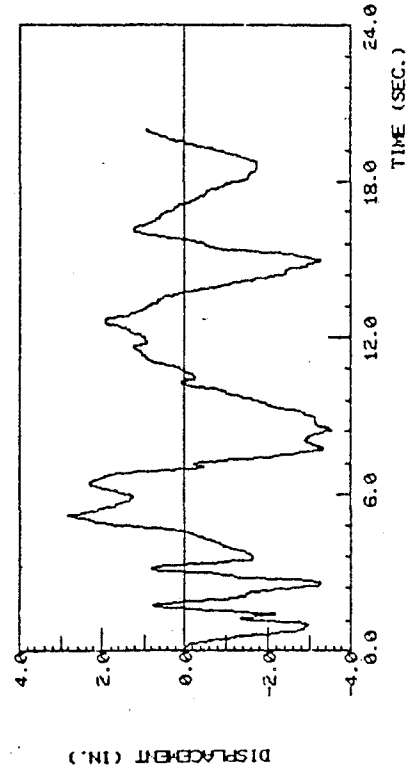

Fig. 6. Displacement history-shaking table

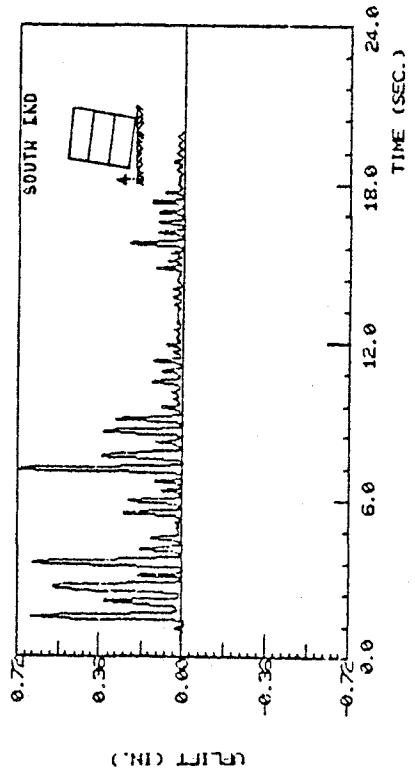

Fig. 9. Uplift at south end of wall

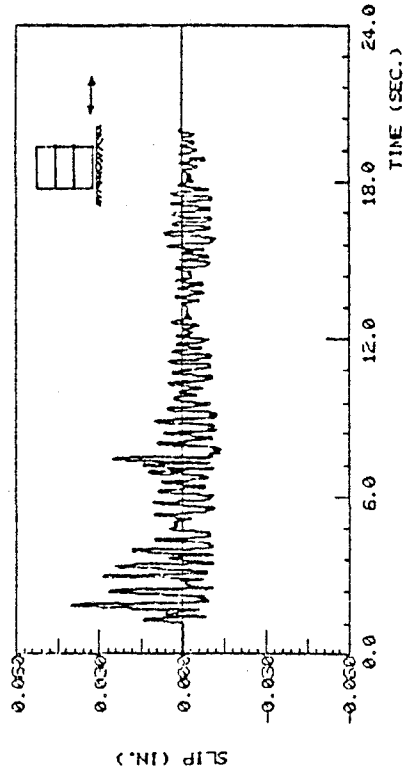

Fig. 8. Slip at bottom of wall

The second test was at a considerably higher amplitude with the wall's base motion as shown in Figure 6. The ground motion reached a peak displacement of 9.0cm (3.6 in.) and acceleration of 0.67g. Response of the wall to that base motion may be seen in the relative top of wall displacement time history in Figure 7. Maximum relative wall displacement was 3.8cm (1.5 in.).

The overall wall displacement was primarily a result of the 2 basic inelastic mechanisms described previously, slip and rocking. Slip along the lower joint was directly measured and is plotted in Figure 8. Comparing the slip and top of wall displacement, it can be concluded that rocking probably caused much of the top of wall motion. The first positive wall displacement peak, Figure 7, above 3.0cm is coincident with rocking to the north and rupture of the vertical panel bar in the base of the wall at the south end. Both of the other south bars exhibited large strains at the same time (Fig. 5). The average natural frequency changed from 5.1Hz to 3.8Hz during that peak. The wall uplift measured at the south end is plotted in Figure 9. The periods of maximum uplift can also be seen to be correlated with periods of maximum north displacement. The maximum south end uplift reached 1.8cm (0.7 in.).

The overall behavior of the system might be characterized by Figure 10 which simultaneously shows the measured base shear, as determined by force transducers, plotted with wall displacement. An initial stiffness of 89kN/cm (50 k/in.) was measured. Yielding is obvious with both north and south displacements but the total displacement is much more severe in the north direction. The first major north displacement excursion occurred while the south end rebar were rupturing and stretching. Explanations for the drops in load and erratic behavior have not been determined yet; Further detailed study is currently underway.

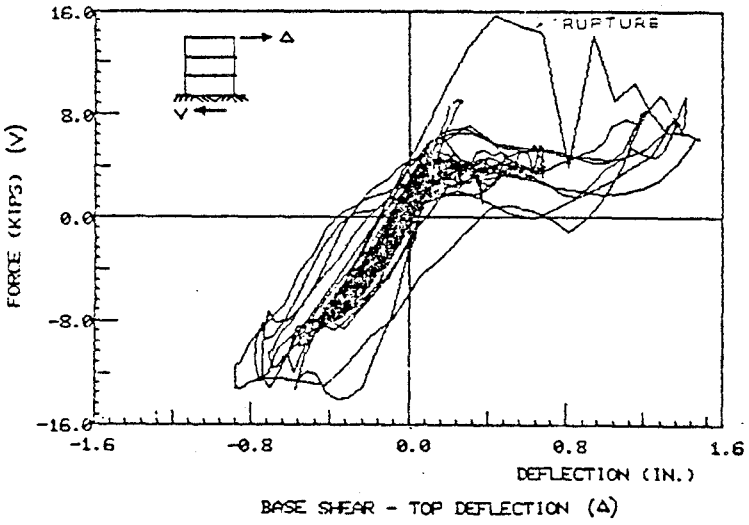

Fig. 10. Base shear and top deflection, + displacement to north, bar rupture occurred at south end

Preliminary Conclusions:

Previous analytic studies [Refs. 1,2,3,8] have shown that the behavior of a panel wall system under earthquake excitation may have dangerous characteristics depending on combination of loading and construction detailing. Llorente [8] concluded that the shear-slip mechanism occurring in horizontal joints between wall panels may be unreliable for force isolation or energy dissipation because of the possibility of reduced normal loading and due to wall instability resulting from unlimited slip associated with friction type resistance. The rocking mechanism might also threaten overall stability yet it was noted as preferred due to its load limiting behavior.

The wall in this test had dominant rocking behavior with limited shear-slip. Slip was controlled by the joint detailing which included a block key at each wall corner used primarily as a space to field connect the single continuous panel bars. The secondary value of the key became obvious during testing when wall slip was seen to be very low until the panel material and the adjacent key began to crush and the wall gradually gained a limited slip distance along the crack between the upper precast wall and the field placed joint concrete (see Figure 11). While rocking behavior dominated the motion there was little indication of instability though the

Fig. 11. Constrained rocking motion

load-displacement behavior contains some peculiar characteristics which will require further study to explain fully. Rocking effectively controlled the level of overturning moment and shear which could be induced in the wall by the ground motion. Once the vertical reinforcing was stretched by rocking, additional damage was small yet important, consisting mainly of concrete crushing at the wall's ends as uplift gaps shut and concentrated concrete compression caused cumulative crushing. During the aftershock test there was no additional visible damage apparent- possibly due to the reduced stiffness and load limiting behavior of the rocking mechanism. Further data analysis is currently being carried out with particular attention focused on the local deformations and the ability of proposed analytical techniques and models to simulate the measured response.

Note:

The testing described in this paper was carried out at the Earthquake Simulator Laboratory of the University of California under the direction of Professor Ray W. Clough as an adjunct to the U.S.-Yugoslav research program sponsored by the National Science Foundation. Data analysis and correlation studies are currently underway at the University of Wisconsin through a grant provided by the U.W. Graduate School.

REFERENCES

1. Becker, J.M., Mueller, P., "The Role of Connections in the Aseismic Design of Large Panel Buildings", Research Conference, U.S.-Yugoslav Joint Board of Scientific and Technological Cooperation, Skopje, July 1980.

2. Mueller, P., Becker, J.M., "Seismic Characteristics of Composite Precast Walls', 3rd Canadian Conf. On Earthquake Engineering, Montreal, Canada, June 1979.

3. Schricker, V., Powell, G., "Inelastic Seismic Analysis of Large Panel Buildings", EERC Report 80/38, University of California, Berkeley, California, Sept. 1980.

4. Hanson, N., Portland Cement Association, "Design and Construction of Large-Panel Structures, Supp. C, Seismic Tests of Horizontal Joints", PCA, Skokie, Illinois, Jan. 1979.

5. Verbic, B., "Test of Panel Joints in Vranica Type Large Panel Building", Institute of Materials and Construction, Sarajevo, Yugoslavia, 1977.

6. Cholewicki, A., "Loadbearing Capacity and Deformability of Vertical Joints in Structural Walls of Large Panel Buildings", Building Science, V6, 1971.

7. Wiss, Janney, Elstner and Assoc., "Cyclic and Monotonic Shear Tests on Connections Between Precast Concrete Panels", report for Massachusetts Institute of Technology, Vol. I & II, July 1981.

8. Liorente, C.A., "Inelastic Behavior of Precast Concrete Shear Walls", MIT Report No. 5, Massachusetts Institute of Technology, Cambridge, Massachusetts, August 1981.

COUPLED LATERAL-TORSIONAL RESPONSE OF BASE-ISOLATED STRUCTURES

Tso-Chien Pan (I)
James M. Kelly (II)
Presenting Author: Tso-Chien Pan

SUMMARY

A typical base-isolated structure on rubber bearings is liable to have a small eccentricity and closely spaced frequencies causing coupled lateral-torsional response. In seismic analysis, the structure is modeled as a rigid deck with lumped masses supported on axially inextensible bearings. The Green's functions for displacement response are derived for undamped and damped cases with small and large eccentricities. An interaction equation for normalized displacements is established for an idealized flat velocity spectrum. Numerical results for a specific building are carried out for comparison.

It is shown that the effect of torsional coupling on the response of base-isolated structures subjected to transient loadings is generally negligible due to the combined effects of the time lag between the maximum translational and torsional responses and the influence of damping in the bearings.

INTRODUCTION

Base isolation is an aseismic structural design strategy in which a building is uncoupled from the damaging horizontal components of an earthquake by a mechanism that attenuates the transmission of horizontal acceleration into the structure. The concept of base isolation has become a practical possibility with the recent development of multilayer elastomeric bearings. An extensive literature survey on the history of base isolation is given in Ref. 1, and the results of a series of experiments on this concept carried out at the Earthquake Engineering Research Center, University of California, Berkeley, have been published (Ref. 2-5). These results have established the effectiveness of this approach to aseismic design. While base isolation has generally been proposed for new construction (Ref. 6,7), the concept can be adapted to the rehabilitation of older buildings of architectural and historical merit. The economic feasibility of rehabilitation by base isolation has been studied for a building in downtown San Francisco (Ref. 8) from which physical parameters are taken for use in later analyses .

For an idealized base-isolated building, where bearings under columns are designed to carry exactly the vertical load and to have precisely the desired lateral stiffness, the center of mass of the superstructure will coincide with the center of rigidity of the bearings. In practice, however, this situation can rarely be achieved and there is generally an eccentricity. The dynamic response of such a structure is more complex when the natural frequencies are closely spaced.

The effects of torsion in buildings appears to have first been studied by Ayre (Ref. 9) for shear beam models. Recent studies of single and multiple story elastic systems through deterministic (Ref. 10) and probabilistic (Ref. 11) approaches have provided valuable insight into the general features of torsional coupling. It has been concluded by many studies that a strong coupling between lateral and torsional motions can occur if the corresponding frequencies are close together, even when the eccentricity between the centers of mass and rigidity is small (Ref. 9-12).

In this analysis, a base-isolated structure is idealized as a rigid deck with tributary masses lumped at column locations, Fig. 1. The rigid deck is supported on massless, axially inextensible bearings. The three degrees of freedom of the system are the horizontal displacements, u_x and u_y, at the center of mass of the system along the principle axes, x and y, of the structure and the rotation, θ, of the deck about the vertical axis. However, the rotational displacement $u_\theta = r\theta$, in which r is the radius of gyration of the deck, will be used in place of θ.

The dynamic response of this system to a horizontal ground motion along the x-axis is investigated. Closed form solutions for the coupled lateral-torsional response of the system are presented

---

(I) Senior Engineer, Nuclear Fuel Operations, Bechtel National Inc., San Francisco, CA. USA

(II) Professor of Civil Engineering, University of California, Berkeley, CA. USA

first. They will be followed by an interaction equation for normalized displacements of the system when an idealized flat velocity spectrum is used to characterize the ground motion.

It is shown in the analysis that coupling can be important, particularly in the estimation of the maximum displacement at the corners of the building. However, it is also shown that the coupling reduces the translational displacement at the center of mass. In addition, damping in the bearings has the effect of absorbing these coupled lateral and torsional motions. Damping in elastomeric isolation systems can be as high as 8% to 10% in the isolated modes and for these values torsional coupling is negligible for transient inputs, such as earthquake motions.

EQUATIONS OF MOTION

Let k_{xi} and k_{yi} be the translational stiffnesses of the ith bearing in the x and y directions and $k_{xi}=k_{yi}=k_i$. The total translational stiffnesses of the bearings, $K_x = K_y = \sum k_i$, are simply the sum of individual bearing stiffness in the x or y direction. The total torsional stiffness of the isolation system defined at the center of mass is given by $K_\theta = \sum k_i(y_i^2+x_i^2)$ where x_i and y_i are the distances of the ith bearing measured from the center of mass.

Three frequency parameters ω_x, ω_y, and ω_θ are defined as follows:

$$\omega_x = \left(\frac{K_x}{m}\right)^{1/2}, \quad \omega_y = \left(\frac{K_y}{m}\right)^{1/2}, \quad \omega_\theta = \left(\frac{K_\theta}{mr^2}\right)^{1/2} \tag{1}$$

in which m is the total mass. These frequencies may be interpreted as the uncoupled frequencies of the system. In general, the individual bearing stiffness k_i will be selected to ensure that $k_i=m_i\omega_0^2$ where m_i is the tributary mass on the ith bearing and ω_0 is the design frequency for all the bearings. If this holds exactly, all the frequencies will be equal and result in $\omega_x=\omega_y=\omega_\theta=\omega_0$.

In this analysis, a Rayleigh damping equal to 2α times the stiffness matrix is assumed and the equations of motion of the system can be written as

$$\{\ddot{u}\} + 2\alpha[K]\{\dot{u}\} + [K]\{u\} = \{\ddot{u}_g\} \tag{2}$$

where $\{u\}=\{u_x,u_\theta,u_y\}^T$, $\{\ddot{u}_g\}=\{\ddot{u}_{gx},0,0\}^T$ with $\ddot{u}_{gx}$ being the ground motion along the x-axis, and

$$[K] = \begin{bmatrix} \omega_x^2 & -\frac{e_y}{r}\omega_x^2 & 0 \\ -\frac{e_y}{r}\omega_x^2 & \omega_\theta^2 & \frac{e_x}{r}\omega_y^2 \\ 0 & \frac{e_x}{r}\omega_y^2 & \omega_y^2 \end{bmatrix} = \begin{bmatrix} \omega_0^2 & -\frac{e_y}{r}\omega_0^2 & 0 \\ -\frac{e_y}{r}\omega_0^2 & \omega_0^2 & \frac{e_x}{r}\omega_0^2 \\ 0 & \frac{e_x}{r}\omega_0^2 & \omega_0^2 \end{bmatrix} \tag{3}$$

in which e_x and e_y are the static eccentricities in the x and y directions, respectively. It should be noted that $[K]$ depends only upon the dimensionless parameters e_x/r and e_y/r.

ANALYSIS PROCEDURE

The frequency equation for the system is given by $[K]\{\phi_n\}=\omega_n^2[I]\{\phi_n\}$, in which ω_n is the eigenvalue of the nth mode; $\{\phi_n\}$ is the corresponding eigenvector; and [I] is the identity matrix. The eigenvalues of the system take the form

$$\omega_1 = \omega_0\left(1-\frac{e}{r}\right)^{1/2}, \quad \omega_2 = \omega_0, \quad \omega_3 = \omega_0\left(1+\frac{e}{r}\right)^{1/2} \tag{4}$$

where $e^2=e_x^2+e_y^2$, with e being the eccentricity between the centers of mass and rigidity. The value of e/r will be small for an isolated building where the bearing stiffness is matched to the mass as mentioned earlier. The frequencies of the coupled response, therefore, can be approximated by

$$\omega_1 = \omega_0(1-\Delta), \quad \omega_2 = \omega_0, \quad \omega_3 = \omega_0(1+\Delta) \tag{5}$$

where $\Delta=e/2r$ is the shift of frequencies of the coupled system from the uncoupled system. In this analysis, Eq. (5) will be used instead of Eq. (4) for frequencies of the system. To the same order of

approximation, $O(\Delta)$, the orthonormal eigenvectors of the system are given by

$$[\phi_1\ ,\ \phi_2\ ,\ \phi_3] = \begin{bmatrix} \frac{e_y}{\sqrt{2}e} & \frac{e_x}{e} & -\frac{e_y}{\sqrt{2}e} \\ \frac{1}{\sqrt{2}} & 0 & \frac{1}{\sqrt{2}} \\ -\frac{e_x}{\sqrt{2}e} & \frac{e_y}{e} & \frac{e_x}{\sqrt{2}e} \end{bmatrix} \tag{6}$$

Damped Case

The damped displacement responses of the first order approximation, $O(\Delta)$, for the system take the form

$$u_x = \frac{-1}{\omega_0}\int_0^t e^{-\alpha\omega_0^2(t-\tau)}\ddot{u}_{gx}(\tau)\sin\omega_0(t-\tau)\left\{1-\left(\frac{e_y}{e}\right)^2\left[1-\cos\omega_0\Delta(t-\tau)\right]\right\}d\tau \tag{7a}$$

$$u_\theta = \frac{1}{\omega_0}\left(\frac{e_y}{e}\right)\int_0^t e^{-\alpha\omega_0^2(t-\tau)}\ddot{u}_{gx}(\tau)\cos\omega_0(t-\tau)\sin\omega_0\Delta(t-\tau)\,d\tau \tag{7b}$$

$$u_y = \frac{-1}{\omega_0}\left(\frac{e_x e_y}{e^2}\right)\int_0^t e^{-\alpha\omega_0^2(t-\tau)}\ddot{u}_{gx}(\tau)\sin\omega_0(t-\tau)\left[1-\cos\omega_0\Delta(t-\tau)\right]d\tau \tag{7c}$$

Undamped Case

The undamped displacement responses of the same order of approximation take the form

$$u_x = \frac{-1}{\omega_0}\int_0^t \ddot{u}_{gx}(\tau)\sin\omega_0(t-\tau)\left\{1-\left(\frac{e_y}{e}\right)^2\left[1-\cos\omega_0\Delta(t-\tau)\right]\right\}d\tau \tag{8a}$$

$$u_\theta = \frac{1}{\omega_0}\left(\frac{e_y}{e}\right)\int_0^t \ddot{u}_{gx}(\tau)\cos\omega_0(t-\tau)\sin\omega_0\Delta(t-\tau)\,d\tau \tag{8b}$$

$$u_y = \frac{-1}{\omega_0}\left(\frac{e_x e_y}{e^2}\right)\int_0^t \ddot{u}_{gx}(\tau)\sin\omega_0(t-\tau)\left[1-\cos\omega_0\Delta(t-\tau)\right]d\tau \tag{8c}$$

It is clear from Eqs. (7a) and (8a) that the response in the x direction, u_x, of the coupled system can never be greater than the corresponding response in the uncoupled system. The torsional response, u_θ, increases as e_y increases. However, for two-way torsionally coupled systems ($e_x \neq 0$ and $e_y \neq 0$) the eccentricity in the direction of the ground motion *reduces* the maximum torsional response. This is consistent with a result obtained in a recent study (Ref. 11). The response in the y-direction, u_y, vanishes when either e_x or e_y vanishes.

Green's Functions of Undamped Case

For undamped two-way torsionally coupled systems with equal eccentricities, $e_x = e_y$, the responses can be demonstrated as follows:

$$u_x = \frac{-1}{2\omega_0}\int_0^t \ddot{u}_{gx}(\tau)\sin\omega_0(t-\tau)\left[1-\cos\omega_0\Delta(t-\tau)\right]d\tau = \int_0^t \ddot{u}_{gx}(\tau)\,G_1(t,\tau)\,d\tau \tag{9a}$$

$$u_\theta = \frac{1}{\sqrt{2}\omega_0}\int_0^t \ddot{u}_{gx}(\tau)\cos\omega_0(t-\tau)\sin\omega_0\Delta(t-\tau)\,d\tau = \int_0^t \ddot{u}_{gx}(\tau)\,G_2(t,\tau)\,d\tau \tag{9b}$$

$$u_y = \frac{-1}{2\omega_0}\int_0^t \ddot{u}_{gx}(\tau)\sin\omega_0(t-\tau)\left[1+\cos\omega_0\Delta(t-\tau)\right]d\tau = \int_0^t \ddot{u}_{gx}(\tau)\,G_3(t,\tau)\,d\tau \qquad (9c)$$

in which $G_1(t,\tau), G_2(t,\tau)$, and $G_3(t,\tau)$ are the Green's functions with the slowly oscillating envelopes $(1-\cos\omega_0\Delta t)$, $\sin\omega_0\Delta t$, and $(1+\cos\omega_0\Delta t)$ for u_x, u_θ, and u_y, respectively.

The Green's functions of Eq. (9) for a particular case where $\Delta=0.01$ and $\omega_0=\pi$, which may be considered representative of a base-isolated structure, are shown in Figs. 2 and 3. These plots demonstrate the Green's functions of the undamped response of the system for one half the period of the envelope functions. The time lag between the maximum translational and torsional responses is clearly shown for the soft system with small eccentricity. The torsional coupling effects for such systems are negligible when a short duration transient input is involved. Figure 4 shows the response of a corner point located at a distance a away from the center of mass, Fig. 1. The corner point experiences a response of $U=u_x+u_\theta a/r$, for which a/r is taken as 1.5 in this example.

Figure 4 reveals the importance of damping in the response of a base-isolated structure. The maximum displacement at corners could exceed the maximum displacement at the center of mass due to the buildup of the torsional response in an undamped system. This could result in impact against adjacent structures if sufficient clearance is not provided.

Green's Functions of Damped Case

For damped two-way torsionally coupled systems with equal eccentricities, $e_x=e_y$, and a constant damping ratio, $\xi=\alpha\omega_0=0.05$, the displacement responses take the form

$$u_x = \frac{-1}{2\omega_0}\int_0^t e^{-\xi\omega_0(t-\tau)}\ddot{u}_{gx}(\tau)\sin\omega_0(t-\tau)\left[1-\cos\omega_0\Delta(t-\tau)\right]d\tau = \int_0^t \ddot{u}_{gx}(\tau)\,G_4(t,\tau)\,d\tau \qquad (10a)$$

$$u_\theta = \frac{1}{\sqrt{2}\omega_0}\int_0^t e^{-\xi\omega_0(t-\tau)}\ddot{u}_{gx}(\tau)\cos\omega_0(t-\tau)\sin\omega_0\Delta(t-\tau)\,d\tau = \int_0^t \ddot{u}_{gx}(\tau)\,G_5(t,\tau)\,d\tau \qquad (10b)$$

$$u_y = \frac{-1}{2\omega_0}\int_0^t e^{-\xi\omega_0(t-\tau)}\ddot{u}_{gx}(\tau)\sin\omega_0(t-\tau)\left[1+\cos\omega_0\Delta(t-\tau)\right]d\tau = \int_0^t \ddot{u}_{gx}(\tau)\,G_6(t,\tau)\,d\tau \qquad (10c)$$

where $G_4(t,\tau)$, $G_5(t,\tau)$, and $G_6(t,\tau)$ are the Green's functions with the slowly oscillating envelopes. The Green's function of these responses for the particular case where $\Delta=0.01$ and $\omega_0=\pi$ are shown in Figs. 5 and 6 and the corner motion, $U=u_x+u_\theta a/r$ with $a/r=1.5$, is shown in Fig. 7.

The torsional response, u_θ, Fig. 6, can not build up to significant values because of the exponentially decaying effect of the damping. The influence of the damping during the time lag between the maximum lateral and torsional responses causes the torsional coupling to become negligible for the system with small eccentricity. This is clearly demonstrated in the response of the corner point, Fig. 7, which has virtually the same response as the center of mass, Fig. 5. The results indicate that for typical base-isolated systems with small eccentricity and 5% equivalent viscous damping, the torsional coupling effects are negligible.

Large Eccentricity

An artificial eccentricity equal to 5% of the maximum plane dimension, a typical value required by various seismic codes, is considered as the large eccentricity in this analysis. Increasing the eccentricity on this order will reduce the time necessary for the torsional response to build up and, as a result, the effects of torsional coupling will increase. However, the maximum displacements at the corner point and the center of mass are not noticeably different (Ref. 13).

INTERACTION EQUATION

For the purpose of design, it is more appropriate to characterize the expected ground motion by a response spectrum. An idealized flat velocity spectrum will be used in formulating an interaction equation for normalized displacements. For a typical isolated building, fundamental period around 2 sec, design spectra will generally approximate the idealized spectrum.

An estimation of the maximum of a response quantity R may be obtained by combining the modal maxima R_1, R_2, and R_3 according to the Complete Quadratic Combination (CQC) method (Ref. 14),

$$R^2 = \sum_{n,m} \rho_{0,nm} R_n R_m \quad n,m = 1,2,3 \tag{11}$$

in which the cross-correlation coefficients are given by

$$\rho_{0,nm} = \frac{2(\xi_n \xi_m)^{1/2}[(\omega_n+\omega_m)^2(\xi_n+\xi_m)+(\omega_n^2-\omega_m^2)(\xi_n-\xi_m)]}{4(\omega_n-\omega_m)^2+(\omega_n+\omega_m)^2(\xi_n+\xi_m)^2} \tag{12}$$

where ξ_n and ξ_m are modal dampings for modes n and m, respectively. The cross-correlation terms can be important under certain conditions, in particular when the natural frequencies of the structure are closely spaced. As this is often the case for buildings on a rubber isolation system, these terms are included in this analysis.

The modal response quantities u_{xn}, $u_{\theta n}$, and u_{yn} can be expressed in their normalized forms:

$$\bar{u}_{xn}=\frac{u_{xn}}{u_{x0}} \quad , \quad \bar{u}_{\theta n}=\frac{u_{\theta n}}{u_{x0}} \quad , \quad \bar{u}_{yn}=\frac{u_{yn}}{u_{x0}} \qquad n = 1,2,3 \tag{13}$$

where $u_{x0}=S_d(\omega_0,\xi)=S_v(\omega_0,\xi)/\omega_0$ in which S_d and S_v are the spectral displacement and velocity of the uncoupled system , respectively.

For a flat velocity spectrum in the x-direction, Eq. (13) can be written as

$$\bar{u}_{xn} = \frac{\omega_0}{\omega_n}\phi_{xn}^2 \; , \quad \bar{u}_{\theta n} = \frac{\omega_0}{\omega_n}\phi_{xn}\phi_{\theta n} \; , \quad \bar{u}_{yn} = \frac{\omega_0}{\omega_n}\phi_{xn}\phi_{yn} \tag{14}$$

By substituting Eq. (14) into Eq. (11) as well as making use of the orthonormal properties of the eigenvectors, the estimated maximum responses $\bar{u}_x$, $\bar{u}_\theta$, and $\bar{u}_y$, can be shown to satisfy the following interaction equation:

$$\bar{u}_x^2 + \bar{u}_\theta^2 + \bar{u}_y^2 = 1 + \delta \approx 1 \tag{15}$$

in which $\delta=(e_y/r)^2/[1-(e/r)^2]$. The approximations made in Eq. (15) are consistent with those in the derivation of the equations of motion. The result is similar to that obtained in a previous study on elastic forces in torsionally coupled systems (Ref. 10).

For systems with small eccentricity, it is obvious from the interaction equation, Eq. (15), that u_x of the torsionally coupled system is not greater than u_{x0}, the displacement of the torsionally uncoupled system. This is consistent with the observation made for Eqs. (7a) and (8a) of u_x.

NUMERICAL EXAMPLE

In order to illustrate these analytical results, the previously mentioned building on an isolation system is analyzed. The system has a fundamental frequency of $\omega_0=\pi$ and the equivalent viscous damping is estimated to be 5% in the isolated modes. The El Centro earthquake record of May 18, 1940 and its corresponding response spectra are used as the input motion. Both the time history method and the response spectrum method using the modal superposition technique are implemented. For the small eccentricity case, the value of Δ is 0.01 and a/r is 1.5 for the corner point.

The results of the time history method are presented in Figs. 8 to 10. It can be seen that for Δ=0.01, the motion of the corner point, Fig. 10, is virtually the same as the motion at the center of mass, Fig. 8, and the torsional response is insignificant. It should, however, be noted that the 5% damping used is a conservative value, since elastomeric bearings can have an equivalent viscous damping ratio of up to 10%.

The results of the response spectrum method, along with the peak responses of the time history analysis, are presented in Table 1. The superiority of the CQC method over the conventional SRSS method is apparent. The SRSS method underestimates the corner motion and the response in the direction of the input motion, and overestimates the out-of-plane response. Hence, it is recommended that the CQC method be used in the response spectrum analysis for base-isolated buildings which are typically soft systems with small eccentricity and closely spaced frequencies.

CONCLUSIONS

As a result of this study the following conclusions can be drawn for a horizontal ground motion input in the x direction. They are confirmed by some general results obtained in previous studies using both deterministic and probabilistic approaches (Ref. 10,11).

1) Coupling induces the torsional response and reduces the translational response at the center of mass of the structure..

2) For two-way torsionally coupled systems where $e_x \neq 0$ and $e_y \neq 0$, the torsional response, u_θ, depends upon e_y/e, and the eccentricity in the direction of the ground motion, e_x, *reduces* the peak torsional response.

3) For one-way torsionally coupled systems where $e_x = 0$ or $e_y = 0$, the displacement response perpendicular to the direction of the ground motion, u_y, vanishes.

4) For a base-isolated structure with small eccentricity, the torsional coupling effect on the displacement response to transient loadings is negligible, due to both the time lag between the maximum lateral and torsional responses in the soft system and the influence of damping in the isolation system.

5) The displacements in a torsionally coupled system can be related to the displacements of the corresponding uncoupled system through an interaction equation when a flat velocity spectrum is used to characterize the ground motion. For the typical period range of isolated structures, *i.e.* 2.0 sec., many spectra, *e.g.* ATC-3-06, have this characteristic.

It is essential to obtain a reliable estimate of the maximum displacement response at the corner points of a base-isolated building. If sufficient clearance is not provided, impact against the adjacent structures may result. Because an isolated structure will inevitably have closely spaced frequencies, the CQC method should be used in the response spectrum analysis.

ACKNOWLEDGEMENTS

Partial support provided by the Malaysian Rubber Research and Development Board, Hertford, U.K. for this research is gratefully acknowledged. The authors would like to thank the Chief Civil/Structural engineer, F. E. Meyer, and Drs. F. J. W. Hsiu and K. M. S. Mark of NFO/Bechtel for their review of the paper. The first author is grateful to G. H. Borschel for her contribution. Excellent graphic work done by K. L. Dolan is acknowledged.

REFERENCES

[1] J. M. Kelly, "Aseismic Base Isolation," *The Shock and Vibration Digest,* **14,** 17-25 (1982).

[2] J. M. Kelly, J. M. Eidinger, and C. J. Derham, " A Practical Soft Story System," *Report No. UCB/EERC-77/27,* Earthquake Engineering Research Center, University of California, Berkeley (1977).

[3] J. M. Kelly, M. S. Skinner, and K. E. Beucke, "Experimental Testing of An Energy-Absorbing Base Isolation System," *Report No. UCB/EERC-80/35,* Earthquake Engineering Research Center, University of California, Berkeley (1980).

[4] J. M. Kelly and D. E. Chitty, "Control of Seismic Response of Piping Systems and Components in Power Plants by Base Isolation," *ASME Pressure Vessels and Piping Division,* 79-PVP-55 (1979).

[5] J. M. Kelly and K. E. Beucke, "A Friction Damped Base Isolation System with Fail-Safe Characteristics," *Earthquake Engineering and Structural Dynamics,* **11,** 33-56 (1983).

[6] R. I. Skinner, G. N. Bycroft, and G. H. McVerry, "A Practical System for Isolating Nuclear Power Plants from Earthquake Attack," *Nuclear Engineering and Design,* **36,** 287-297 (1976).

[7] L. M. Megget, "Analysis and Design of a Base-Isolated Reinforced Concrete Frame Building," *Bulletin of the New Zealand National Society for Earthquake Engineering,* **11,** 245-254 (1978).

[8] J. M. Kelly, "The Economic Feasibility of Seismic Rehabilitation of Buildings by Base Isolation," *Report No. UCB/EERC-83/01,* Earthquake Engineering Research Center, University of California, Berkeley (1983).

[9] R. S. Ayre, "Interconnection of Translational and Torsional Vibrations in Buildings," *Bulletin of the Seismological Society of America*, **28**, 89-130 (1938).

[10] C. L. Kan and A. K. Chopra, "Coupled Lateral Torsional Response of Buildings to Ground Shaking," *Report No. UCB/EERC-76/13*, Earthquake Engineering Research Center, University of California, Berkeley (1976).

[11] S.-Y. Kung and D. A. Pecknold, "Effect of Ground Motion Characteristics on the Seismic Response of Torsionally Coupled Elastic Systems," *Report No. UILU-ENG-82-2009*, University of Illinois, Urbana-Champaign (1982).

[12] J. Penzien, "Earthquake Response of Irregular Shaped Buildings," *Proceedings of Fourth World Conference on Earthquake Engineering*, **2**, A3-75-A3-89, Santiago, Chile (1969).

[13] T.-C. Pan and J. M. Kelly, "Seismic Response of Torsionally Coupled Base-Isolated Structures," *Earthquake Engineering and Structural Dynamics*, **11**, To appear (1983).

[14] E. L. Wilson, A. Der Kiureghian, and E. Bayo, "A Replacement for the SRSS method in Seismic Analysis," *Earthquake Engineering and Structural Dynamics*, **9**, 187-192 (1981).

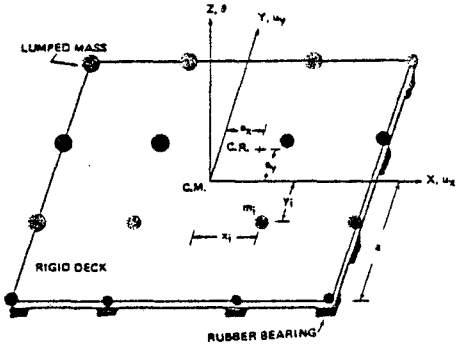

Fig. 1. Simplified 3-DOF System

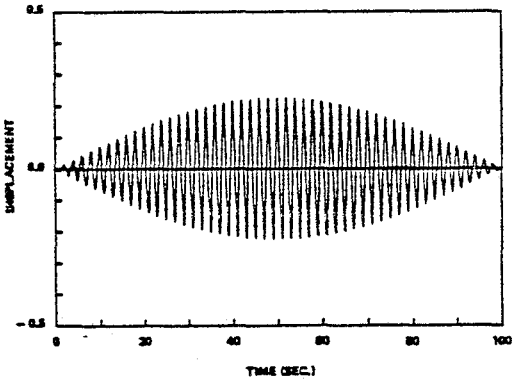

Fig. 3. Green's Function of u_θ (Undamped)

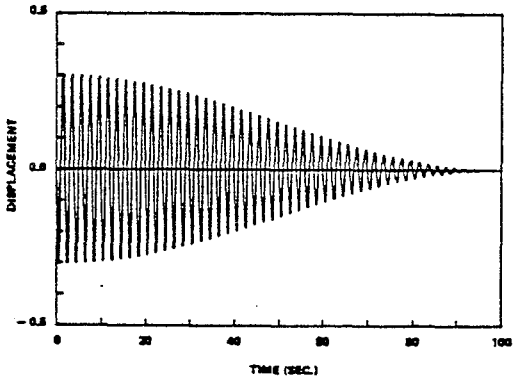

Fig. 2. Green's Function of u_x (Undamped)

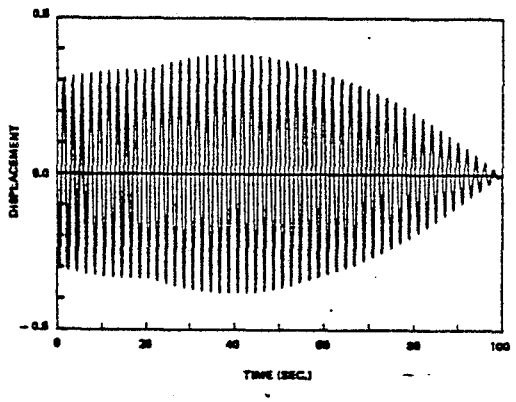

Fig. 4. Green's Function of U (Undamped)

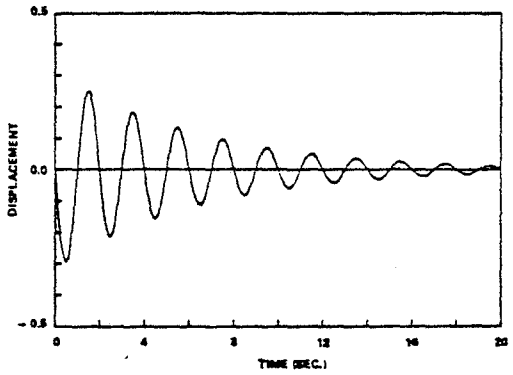

Fig. 5. Green's Function of u_x (Damped, ξ=0.05)

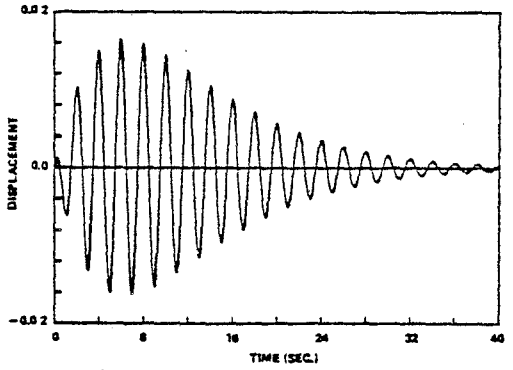

Fig. 6. Green's Function of u_θ (Damped, ξ=0.05)

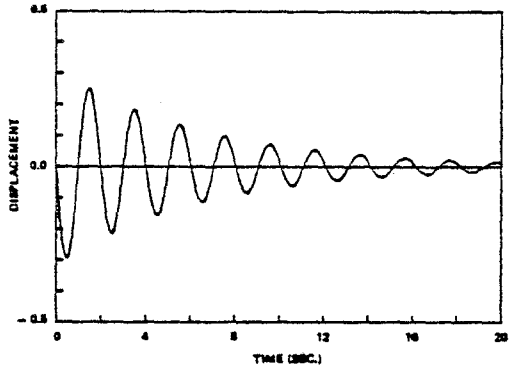

Fig. 7. Green's Function of U (Damped, ξ=0.05)

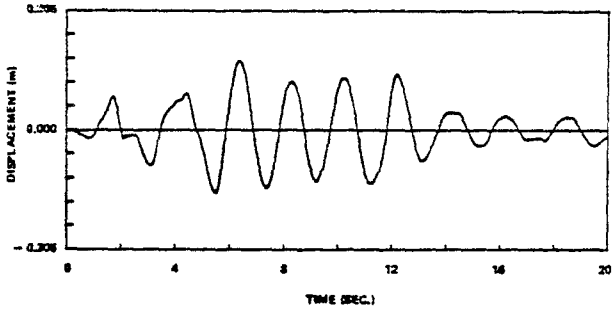

Fig. 8. Displacement Response, u_x, to the El Centro Earthquake, 1940

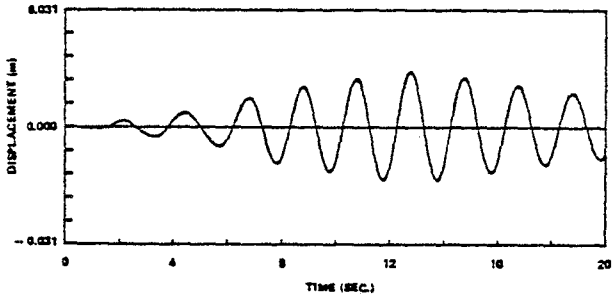

Fig. 9. Displacement Response, u_θ, to the El Centro Earthquake, 1940

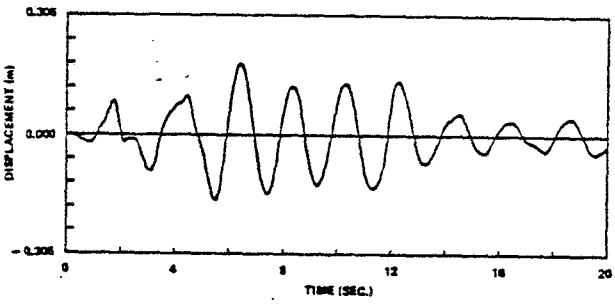

Fig. 10. Displacement Response, U, to the El Centro Earthquake, 1940

Table 1
Results of Time History and Response Spectrum Analysis; Unit: cm (in)

Small Eccentricity ($\Delta = 0.01$)			
Response	Time History	CQC	SRSS
u_x	17.78 (7.00)	17.58 (6.92)	10.82 (4.26)
u_θ	1.52 (0.60)	1.78 (0.70)	8.83 (3.48)
u_y	0.15 (0.06)	0.20 (0.08)	10.82 (4.26)
U	18.29 (7.20)	18.26 (7.19)	17.37 (6.84)

THE PERFORMANCE OF STAIRWAYS IN EARTHQUAKES

Catherine Roha (I)

SUMMARY

Stairways are essential building components serving critical functions of emergency access and egress following earthquakes and fires. Stairways also may significantly affect the seismic response of structural systems. Past earthquakes have exposed a wide variety of problems and failures related to stairway/structure interactions. Present architectural and structural engineering practices may not address these interactions adequately. A model code for seismic resistant design and construction of stairways is proposed. Directions for future research and recommendations for mitigation measures are outlined.

INTRODUCTION

Stairways play significant roles in building performance during earthquakes due to dynamic interactions with primary structural systems and the occurrence of unanticipated and undesirable responses. Damaged stairways adversely affect evacuation and rescue, fire fighting, salvage, and restoration. Severe earthquakes may require that building occupants rescue themselves, elevators may not be functional, and imminent secondary hazards such as fire or flooding may make immediate evacuation imperative.

Stairways are permanent, rigid, and frequently heavy elements often extending the full height of the building, connected directly or indirectly to the primary structure. In multi-story fire-resistive buildings, stairs are typically constructed of reinforced concrete, steel, or a combination of those materials. The stairway system includes stair flights and landings, enclosure walls, doors and windows, lighting, ventilating systems, standpipes, and other services. Stairways may be open monumental staircases, enclosed fire stairs, exterior fire escapes, or service stairs.

The main objective of this paper is to raise the issue of stairway interactions and hazards, summarizing studies conducted by the author and discussed in detail in Reference 1. This initiation study of stairway performance was based on discussions with architects and engineers practicing in the San Francisco area, and on extensive review of earthquake reconnaissance reports, engineering studies, handbooks, reference materials, and building codes. The report established groundwork for further investigations and analytical studies.

(I) Architect, Berkeley, California, USA

PAST PERFORMANCE

Although many stairways in multi-story buildings have withstood strong seismic shaking satisfactorily, other stairways have exhibited a wide range of significant damage. The most critical life safety issues are interference of stairway structural behavior with the building's overall seismic response which results in collapse, and interference of damage with emergency exiting and rescue. The typical diagonal brace-like configuration of stairways can, at one extreme, increase the overall lateral stiffness of the structure and significantly alter the dynamic character of the structure as a whole, or, at the other extreme, simply modify local response behavior of the structural element to which it is attached. The change in overall lateral and torsional stiffness often results in higher seismic force levels than would be anticipated by considering the primary structure alone and, in some cases, has jeopardized the stability of the whole structure. Damage to stairways can also result.

Stairway landings connected to columns at mid-height have added unexpected stiffness and created "short columns," resulting in brittle shear failures (Fig. 1). "Short beams" have been created by stair flight connections. High local shear stresses have occurred in floor diaphragms due to restraint by stair enclosure walls. Stairs and walls have introduced torsional eccentricities, causing local failures of primary structural elements (Fig. 2). Out-of-phase relative responses of stair towers and structures have caused pounding and damage to separation joints, and stair towers have overturned (Fig. 3).

Damage to stairways has included failures of brittle enclosure materials which have littered or broken treads (Fig. 4), cracking and spalling of concrete at landings and walls, jammed exit doors, broken glass, dislocation of non-structural components such as light fixtures or seismic joint coverplates, and disruption of building services. In some cases stairways have been inaccessible or unusable. Some stairways have been places of refuge during shaking; other stairways have caused injuries and fatalities.

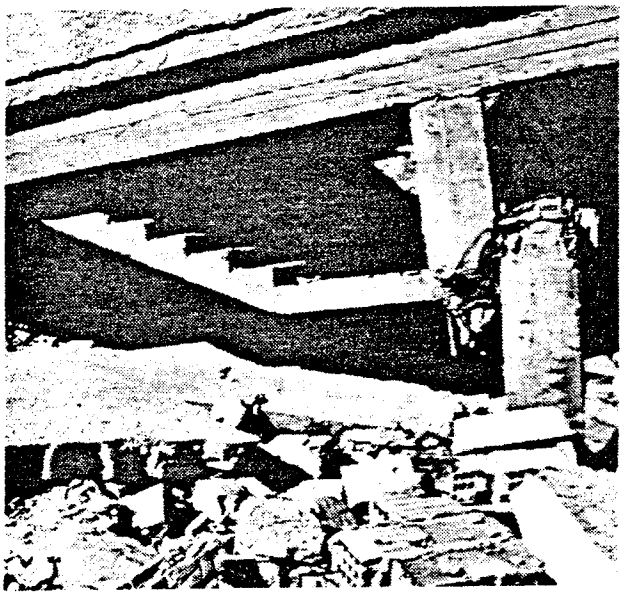

Fig. 1 Concrete column failure

Fig. 2 Torsional effects

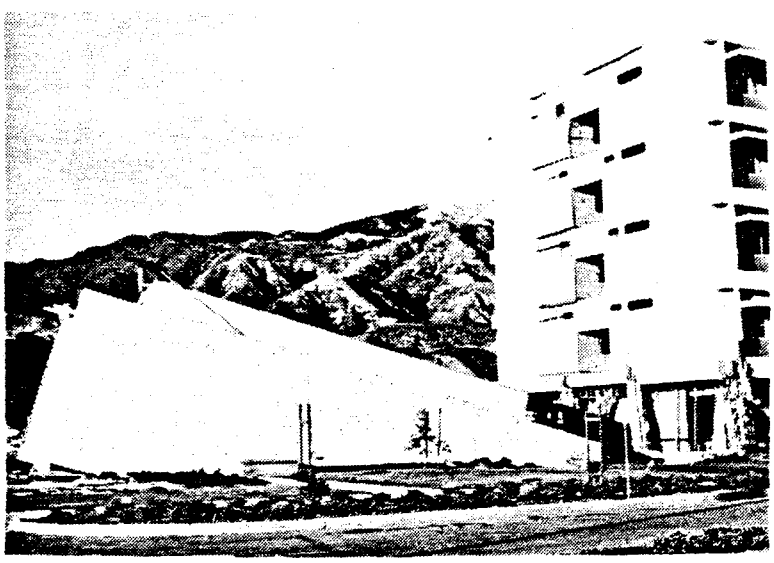

Fig. 3 Overturned stair tower

Fig. 4 Shattered wall

STAIRWAY PLANNING

Locations and arrangements of stairways result from design decisions on spatial organization and functional layout, internal circulation and emergency egress. For stairway systems intentionally designed to be part of the primary seismic resistant system, stairway shafts and other service cores are best distributed to avoid undesirable torsional effects, to balance the stiffness of the resistant elements with the mass. Especially problematic are stairway systems which act "unintentionally" as part of the primary structural system. These may significantly influence the initial elastic response of the building by their distribution and stiffness, and the inelastic response by their strength and ductility, producing unanticipated seismic behavior.

Movement characteristics of stairway structures must relate to those of the primary structural system. Stairways may be integrated in very stiff structures which protect them from damaging deformations. Stairways in ductile moment-resistant frame structures designed to stably dissipate seismic energy, may experience large deformations. These stairs may be isolated if stiff or integrated if having flexible enclosures and flights. Either structure deformations must be limited to those which the stair system can accommodate, or the stairways must be made tougher to withstand larger deformations. These deformations should be those which are expected in the actual building under real ground motions, not just those computed according to fictitious lateral forces defined by building codes.

Collaboration of architect and engineer in preliminary design phases can resolve basic configuration issues for stairways and establish the extent of stairway/structure interaction through selection of appropriate design strategies. Design proposals should be reviewed specifically to detect potential interactions and nonstructural elements which could cause undesired effects. When possible, the adequacy of the design should be verified through realistic analyses.

DESIGN STRATEGIES

Stairways can be structurally isolated as physically separate exterior towers, in enclosures mechanically isolated from the adjacent building frame, or as stairs with sliding joints at landings and walls. Isolation demands a clear understanding of the seismic response of the building and stairways in order to estimate with sufficient accuracy the necessary separations and appropriate interstory drift. By reducing interaction through carefully controlled connections or ductile isolators, damage and hazards could be considerably lessened, although the separated systems would still experience accelerations. Too small separations, because of the effects of impact (pounding), could worsen structural behavior rather than improve it. Separated stair tower foundations need special attention to withstand the large overturning forces which may be expected. Isolation strategies require consideration of materials, weatherproofing, fire and smoke infiltration, and maintenance to ensure effectiveness during the service life of the building.

Stairways may be integrated with the primary structural system to take advantage of the inherent stiffness characteristics of the stair as well as the enclosure walls. Stiffness contributions of some stair flights and landings may be assumed, but are usually not calculated, there being no easy method for this analysis. A stiff primary structure can protect stairways from damaging deformations. In a flexible system, integrated stairways can increase the stiffness of the structure substantially. This has advantages for controlling deformations, can result in an increase in overall lateral resistance, and may also lead to considerable increase in elastic strength. However, integration of stairway systems which lack sufficient strength to contribute usefully in a flexible primary structure, may create local problems and potential hazards.

STRUCTURAL ANALYSIS

For gravity load analysis a stairway is typically taken to be an independent system supported by the primary structural system in either a simple or a fixed manner. A single-flight stair is analyzed as if it were a simple beam, considering only flexural stresses. For lateral load analysis the initial elastic contribution of typical stairways to the behavior of the "total structure" could perhaps be approximately modeled as an equivalent assembly of rigidly connected beam or slab elements or as elements of a truss. But even if such an equivalent space frame approach provides sufficient accuracy, many stair/structure total systems would have to be modeled as complete three-dimensional assemblies to correctly analyze their interactions. Complications are added by openings, enclosures, complex stair geometries, and supports. The initial elastic detailed local behavior of a stairway system may be modeled using plate finite element analysis. Such detailed modeling of stairway systems within a "total" system offers an available, albeit cost-prohibitive, approach.

Rational design should be based upon analysis to predict the response of stairway systems to expected ground motions. The reliability of these analytical methods must be demonstrated experimentally, and the cost of analysis kept within practical limits. Simple methods are needed because complex studies may not be justified economically or technically. Structural engineers may need to decide for which stairway configurations costly analytical studies are warranted, and for which stairways standard details and provisions for construction and maintenance should be developed.

EXISTING SEISMIC CODES

Review of existing seismic code specifications (Ref. 2) reveals that few building codes directly refer to seismic design of stairways. Rather, stairways are implicitly included in provisions addressing the more general problems of seismic resistant design of architectural and nonstructural components, with primary emphasis on limiting interstory drift (or the effects thereof) of the primary structural system, and secondary emphasis on the actual seismic response of the component. These provisions, in effect, encourage analysis of the primary structural system without consideration of stairway/structure interactions. Furthermore, the actual response is estimated by an equivalent static lateral load that does not rationally account for interaction. In some codes a higher force factor is required for those elements (e.g., stairway enclosure walls) considered as part of the building's life safety system. These provisions may not be sufficiently specific for the important emergency functions of stairway system components.

MODEL CODE PROVISIONS FOR STAIRWAYS

In an ideal earthquake resistant design and construction code:

(a) The functions of stairways for regular service and emergency conditions should be stated, terms defined, and typical components identified.

(b) Conceptual guidelines for exit safety should be reviewed and modified to bring seismic safety issues forward. Structural guidelines should cover: advantages and disadvantages of integrating or isolating stairways; the effects of stairway distribution on the overall behavior of the primary structural system; selection of materials and construction to satisfy both fire and earthquake requirements; effects of stairways on the local behavior of structural and nonstructural components to which they are connected or come in contact during seismic excitation; selection and/or design guidelines for nonstructural components of stairways to control and limit damage.

(c) Minimum requirements should be established for structural analysis and design of stairways, considering both service load and extreme load conditions. For integrated stairway systems the code should refer directly to provisions for the primary structural system, clearly associating realistic load and load combination requirements with required deflection limitations, ductility requirements, and type of analysis (e.g., elastic or inelastic) to be used in evaluating member forces and deformations. Guidance on acceptable methods of analytically modeling the contribution of stairways to the total system response should be included. For isolated stairway systems the code should provide for analysis of the primary structural system to determine expected (realistic) system deformations that must be accommodated by the stairway system, and investigations needed to demonstrate that the proposed isolation technique will indeed accommodate the predicted deformations. The code should clearly establish acceptable means to model the seismic loadings and analytical methods to be used in evaluating the system response.

(d) The model code should set forth specific provisions regarding detailing and construction of the components of stairway systems, especially detailing between landings and their supports, and flights and landings.

(e) The model code should provide guidelines for identification of potentially hazardous stairways in existing structures, for evaluation of the degree of hazard, and for mitigation of these hazards.

GENERAL CONCLUSIONS

(a) Because stairways are the primary vertical emergency exit routes in multi-story buildings, they must be designed to ensure their use for safe egress and access during and after earthquakes.

(b) Jammed doors, debris-littered treads, detached components, and darkness are the most common hazards of stairway response to seismic shaking.

(c) Interactions of stairway structural systems with their nonstructural components and especially with the primary structural system have created much earthquake damage.

(d) Stair flights and enclosure walls have influenced, usually unintentionally, the dynamic characteristics and seismic responses of primary structures. Lack of attention to this problem has contributed to local structural damage and sometimes to structural collapse.

(e) Since stairways are often complex three-dimensional systems integrating a variety of architectural, structural, electrical, and mechanical components, their seismic behavior may involve complex interactions among these components.

(f) At present there exist no practical general analytical methods for predicting even the simplest aspects of stairway dynamic interaction with the primary structure. Few construction details for structural connections and assemblies have been experimentally evaluated for strong seismic shaking.

(g) Present U.S. seismic codes do not contain guidelines regarding stairway system selection, design or construction. Only a few foreign building codes specifically mention earthquake resistant stairway design.

(h) Current design practice relies upon prior projects and/or published recommendations which may not address seismic issues in a comprehensive manner. Yet the required high performance level for exitways makes stairway seismic design an important life safety concern.

RECOMMENDATIONS FOR IMMEDIATE IMPROVEMENTS

(a) Fuller understanding of stairway damage mechanisms requires more detailed information about, and analysis of, problems occurring in moderate and strong ground shaking. Reconnaissance and investigating teams should note stairway conditions, materials and construction, adjacent structural damage, possible interactions, and interference with evacuation. Post-earthquake studies should investigate human reactions and behaviors while exiting.

(b) Architectural design would benefit from consolidation of planning concepts for building configurations and stairway locations. Seismic implications of various architectural and structural plans should be studied and published so that designers may either avoid or consciously accommodate problematic schemes. Cost-benefit analyses of different design options should be considered in relation to seismic resistance, life safety, and property damage.

(c) The structural engineer in collaboration with the architect must consider the effects of stairway systems at early stages of the building design so that an appropriate structural strategy may be selected and applied. Professional handbooks and reference materials should be revised to include seismic implications of standard details.

(d) Seismic codes should include guidelines and comments about problems of interactions between stairways and primary structural systems. Omissions and ambiguities in specific requirements should be reduced so that designers using the code provisions could demonstrate the acceptability of their emergency egress schemes for earthquake hazards.

(e) Building officials should thoroughly review design calculations and drawings to ensure that proper design of stairways has been achieved.

(f) Development and dissemination of improved analytical methods will enable structural engineers to predict more accurately the stairway system response to be accommodated through proper selection of materials and detailing for stairways and their connections to the primary structure.

(g) Information about the anticipated stairway response must be communicated by the structural engineer to the architect, electrical engineer, mechanical engineer, and other consultants so that attachments, bracings, material assemblies, equipment characteristics, and damage limitations may be designed for expected displacements and accelerations.

(h) The concepts by which the exitways are designed should be communicated to the building owner, the occupants, and the maintenance staff so that expected building behavior during earthquakes may be anticipated, more comprehensive disaster response plans developed, and particular details or devices (such as separation joints) maintained as intended.

(i) Existing buildings should be inspected so that hazardous conditions in exitways can be removed or improved. This is especially important for any building which serves critical emergency functions or which has places of public assembly, high numbers of occupants, or hazardous contents.

RESEARCH NEEDS

(a) To improve the design and construction of new stairways and the repair and/or retrofit of existing stairways, a co-ordinated research program integrating literature and field surveys with analytical and experimental studies should be undertaken. This research program should (1) identify some stairway systems which show promising features for adequate fire and seismic performance; (2) initiate experimental studies to understand the behavior of stairway system components and assemblies and the interaction of specific stairway systems with primary structural systems; (3) devise experimental studies to improve methods and details of construction; (4) create matching analytical studies for rational mathematical idealizations of components and system behavior; and (5) develop simplified analysis and design procedures. The knowledge gained could lead to the development of new stairway systems as optimal solutions for specific building structural systems.

(b) Ideally, experimental studies of load-deformation behavior, carried into the inelastic range with load reversal, of typical stairway structural and enclosure components should be undertaken to develop analytical models that will serve as a basis for understanding real stairway system behavior. As the number and variety of even typical components are great, it may only be reasonable to investigate analytically the sensitivity of stairway seismic response to variations in the main parameters (components) by modeling the behavior of these components using available structural idealizations.

(c) Analytical studies should be undertaken to see if the initial elastic response of stairway structural systems alone and interacting with primary structures can be accurately modeled using available analytical techniques correlating predicted with measured behavior. Using plate finite elements, beam elements or a constraint approach might be considered. Studies should seek to develop methods of analysis, using existing techniques as much as possible, to model not only the behavior of isolated stairway systems but also the complete three-dimensional behavior of combined stairway/structural systems as well as detailed local behavior of stairway attachments to the primary structure.

(d) Because such elastic modeling techniques are of most use to the designer of stairway systems, the analytical studies should seek to develop simplified methods of analysis that may be implemented with available computer programs, and to produce design criteria (e.g., limit states for corresponding load conditions) for their application to practical problems of design.

(e) Analytical studies should be undertaken to see if aspects of nonlinear elastic and, particularly, nonlinear inelastic response behavior of stairway structural systems may be modeled with existing techniques. It is reasonable to initiate these studies after some experience with elastic modeling has been gained, using the nonlinear response studies to develop simplified practical methods that utilize linear elastic analysis techniques.

(f) Because stairway construction involves many nonstructural components which have suffered significant damage in past earthquakes, development of simplified methods of analysis and design of these components has become a pressing problem in recent years.

(g) The need to strengthen, demolish, or modify the use of existing hazardous buildings to improve life safety has been recognized as an important problem. Research efforts have been directed toward developing analytical methods to predict the behavior of existing buildings; consideration of stairway systems should be encouraged. Of special concern are unanticipated interactions and failures of brittle enclosure materials.

Finally, the main features and conclusions of research on the seismic performance of stairways should be compiled and made accessible to architects, engineers, and other design professionals. Design guidelines, structural strategy considerations, simple analytical methods, improved details, new construction techniques, and performance standards may reduce the amount of stairway damage encountered in future earthquakes and mitigate these hazards to human life.

ACKNOWLEDGMENTS

This paper summarizes research studies conducted with financial support from the National Science Foundation. Generous assistance in preparing this paper was provided by Professor Vitelmo V. Bertero, University of California at Berkeley, and Assistant Professor James W. Axley, University of Colorado at Boulder.

REFERENCES

1. Roha, C., J. W. Axley, and V. V. Bertero. The Performance of Stairways in Earthquakes. Report No. UCB/EERC-82/15. Berkeley: College of Engineering, University of California, September 1982.

2. International Association for Earthquake Engineering. Earthquake Resistant Regulations, A World List, 1980. Tokyo: Gakujutsu Bunken Fukyu-Kai, 1980.

EVALUATION OF ON-LINE COMPUTER CONTROL METHODS FOR SEISMIC PERFORMANCE TESTING

P. B. Shing (I), S. A. Mahin (II), and S. N. Dermitzakis (I)
Presenting Author: S. A. Mahin

SUMMARY

The seismic performance of structures that are too large, massive, or strong to be tested with available shaking tables can be efficiently studied by pseudodynamic testing. The pseudodynamic method, which utilizes a numerical algorithm in the on-line computer control of a test specimen, can realistically simulate the inelastic seismic response of a structural model. In spite of certain limitations, results of recent studies at Berkeley verify the practicality and reliability of the method.

INTRODUCTION

Shaking table testing is one of the most realistic experimental methods for studying the inelastic seismic performance of structural systems. Nevertheless, the weight and size of a structure which can be tested are significantly limited by the capacity of a table. Installing a new shaking table facility or increasing the capacity of an existing one is very costly. For this reason, on-line computer control (pseudodynamic) methods have been developed [1], which have the economy and versatility of conventional quasi-static testing, but achieve the realism of shaking table tests. In pseudodynamic testing, the seismic response of a structure is numerically evaluated by a computer, based on the direct experimental feedback of structural restoring forces, and is quasi-statically imposed on the structure through hydraulic actuators. This method has been successfully applied to tests of various structures by Japanese researchers [2]. As part of the U.S. - Japan Cooperative Earthquake Research Program, extensive analytical and experimental studies have been carried out at Berkeley to develop this method and to assess its capabilities and limitations. Some of the major findings are summarized in this paper.

THEORETICAL BACKGROUND

Numerical Formulation. The equations of motion of a discretized structural system can be expressed in terms of a family of second-order differential equations, which can be numerically solved by a direct step-by-step integration method for any arbitrary external excitations. This is a well-established numerical procedure in structural dynamics; and the mass, damping, and stiffness matrices of a discretized system can be formulated by the finite element method [3]. In pseudodynamic testing, the dynamic behavior of a structure is experimentally simulated by using the same numerical approach. However, instead of obtaining the stiffness matrix by finite element formulation, the restoring forces developed by structural deformations are directly measured from the test specimen during an experiment. Because of this, the inelastic dynamic response of a structure can be accurately simulated in a laboratory without the uncertainties associated with idealized inelastic mechanical properties of the structure.

Considering the dynamic response of a multiple-degree-of-freedom structure to an excitation of duration T, which is subdivided into N equal intervals Δt, i.e., $\Delta t = T/N$, we can write the equations of motion at time $(i+1)\Delta t$ as

$$\underline{m}\,\underline{a}_{i+1} + \underline{c}\,\underline{v}_{i+1} + \underline{k}\,\underline{d}_{i+1} = \underline{f}_{i+1} \qquad (1)$$

where $\underline{m}$, $\underline{c}$, and $\underline{k}$ are the mass, damping, and stiffness matrices of the structure; $\underline{a}_{i+1}$, $\underline{v}_{i+1}$, and $\underline{d}_{i+1}$ are the acceleration, velocity, and displacement vectors at $(i+1)\Delta t$; and $\underline{f}_{i+1}$ is the external force excitation vector. To solve the equations of motion during a pseudodynamic test, we can use an explicit

(I) Junior Specialist, Univ. of California, Berkeley, CA, USA
(II) Assoc. Prof. of Civil Engineering, Univ. of California, Berkeley, CA, USA

form of the Newmark integration method [4], which assumes that

$$\underline{v}_{i+1} = \underline{v}_i + \frac{\Delta t}{2}(\underline{a}_i + \underline{a}_{i+1}) \tag{2}$$

$$\underline{d}_{i+1} = \underline{d}_i + \Delta t\, \underline{v}_i + \frac{\Delta t^2}{2}\underline{a}_i \tag{3}$$

By substituting $\underline{v}_{i+1}$ in Eq. (1) with Eq. (2), we can solve for $\underline{a}_{i+1}$ in terms of $\underline{v}_i$, $\underline{a}_i$, and $\underline{k}\,\underline{d}_{i+1}$. Since the product $\underline{k}\cdot\underline{d}_i$ can be measured as the restoring-force vector $\underline{r}_i$ in every step of a test, the displacement response $\underline{d}_{i+1}$ can be readily computed and imposed on a test structure. However, the mass matrix $\underline{m}$ and viscous damping $\underline{c}$ have to be analytically modeled.

Structural Idealizations. During a pseudodynamic test, we have to idealize the test structure as a discrete-parameter system, of which the mass is concentrated at a limited number of degrees of freedom. In doing that, a lumped-mass matrix is usually constructed for the structure. This is exactly analogous to the discretization and static condensation procedures carried out in most dynamic analyses [3], in which the higher mode effects of a structure are neglected. The adequacy of a discrete-parameter model depends on the actual mass distribution of a structure as well as on the characteristics of excitations. In general, discrete-parameter idealizations are adequate for load carrying structures which have most of their masses located at the selected degrees of freedom [5], such as for building systems having heavy floor slabs.

Structural damping is most conveniently modeled by a viscous damping mechanism. However, other forms of energy-dissipation exist in real systems, such as Coulomb damping due to friction and hysteretic damping caused by inelastic material behavior. Both Coulomb and hysteretic damping mechanisms are automatically taken into account in pseudodynamic testing by using the actual restoring-force feedback in numerical computations; whereas, viscous damping coefficients have to be analytically specified. The damping property of an elastic structure can be easily measured by vibration tests. Based on these measurements, appropriate viscous damping coefficients can be selected for pseudodynamic testing. The damping characteristic can usually be realistically included in pseudodynamic testing since energy dissipation is eventually dominated by hysteretic damping during inelastic response. Furthermore, due to strain-rate effects, the inelastic behavior of a structure tested pseudodynamically may be different from that in an actual seismic response. However, the difference is usually insignificant for steel structures which generally have fundamental frequencies less than 10 Hz [5].

Numerical Stability and Accuracy. The stability and accuracy of numerical integration are major considerations in the selection of integration time interval Δt. The Newmark explicit method is stable (i.e., solution will not grow without bound for any arbitrary initial conditions) when $\omega_{\mathrm{M}}\Delta t \leqslant 2$, where ω_{M} is the highest angular frequency of a structure. Frequency distortion is usually observed in a numerical result. However, it is negligible when $\omega\Delta t$ is small (< 0.5) [5]. Although these properties are based on linear elastic systems, they are still valid for nonlinear systems by the fact that a nonlinear system can always be considered as piecewise linear. In addition, the Δt selected should be sufficiently small so that the nonlinear behavior of a system can be accurately traced by the discretized displacement increments. Otherwise, the stability and accuracy of an algorithm can be impaired [5].

EXPERIMENTAL ERROR PROPAGATION

Sources of Experimental Errors. In addition to the previously discussed problems, errors may also be introduced into pseudodynamic testing by experimental apparatus or improper instrumentation techniques. For example, the numerically computed displacements may not be exactly imposed on a test structure due to instability or lack of sensitivity of actuator-controller systems, miscalibrations of displacement transducers, or resolution errors in analog-to-digital (A/D) conversions of displacement control signals. The restoring forces measured from a test structure may be in error due to electrical noise or friction in actuator connections. Since the pseudodynamic response at any time depends on

experimental feedback from all previous steps and there may be hundreds or thousands of time steps in a single test, the experimental errors will have a significant cumulative effect. Because of this, test results may be rendered unreliable even though the errors introduced at any step might be small.

Error Propagation Effects. The error-propagation phenomenon in pseudodynamic testing can be mathematically modeled [6]. It can be shown that numerical results will be more accurate if the computed displacements are used instead of the measured ones in step-by-step computations. Even if this is done, displacement control errors are still introduced into the numerical computations through the resulting force feedback errors. Force feedback errors can have significant effects on experimental results depending on whether the errors are random or systematic in nature. Systematic errors, which often result from poor performance of experimental equipment or improper instrumentation techniques, can induce a significant cumulative error growth due to resonance-like effects. The cumulative growth of systematic errors within a fixed computational time span cannot be effectively reduced by decreasing Δt. Random errors may result from electrical noise or other less well-defined sources. Their effects are less severe and can be mitigated by reducing Δt. In both cases, the larger $\omega \Delta t$ is, the faster will be the rate of cumulative error growth with respect to the number of integration steps. Therefore, the higher modes of a multiple-degree-of-freedom system will be more sensitive to experimental errors than the lower modes. To illustrate this fact, analytical simulations were performed with a two-degree-of-freedom system shown in Fig. 1a. The exact response of the system to the El Centro ground motion was dominated by its fundamental frequency (see Fig. 1b). Random and systematic errors were then introduced into the computations by round-off and truncation, respectively, in the A/D conversions of displacement control signals. In both cases, the resulting cumulative errors were dominated by the second mode frequency (see Figs. 1c and 1d). In the case of systematic errors, the spurious second mode effect grew very rapidly. To assess error tolerance limits for a test, methods for establishing cumulative error bounds have been derived [6].

Error Correction Methods. Due to the error-propagation effects, experimental errors should always be eliminated or reduced to insignifcant levels in any test. This may not be always possible, especially in systems which have many degrees of freedom. In such systems, even small errors can propagate very rapidly in the higher modes. Under that circumstance, frequency-proportional numerical damping can be used to suppress the spurious higher mode effects. This numerical damping property can be introduced into the Newmark explicit algorithm by the following modification of the equilibrium equation (Eq. (1)):

$$\underline{m}\, a_{i+1} + \left[(1+\alpha)\, \underline{k} + \frac{\rho}{\Delta t^2}\, \underline{m}\right] \underline{d}_{i+1} = \underline{f}_{i+1} + \left[\alpha\, \underline{k} + \frac{\rho}{\Delta t^2}\, \underline{m}\right] \underline{d}_i \tag{4}$$

where α and ρ are parameters which control the damping characteristics (see Fig. 2). This method is applicable to inelastic systems. For example, a two-story shear building with inelastic inter-story force-deformation relations was numerically simulated. The results in Fig. 3 show that the spurious higher mode effect introduced by experimental errors was efficiently removed by numerical damping. A method based on conservation of energy has also been developed to compensate for the energy changes caused by systematic errors. Detailed discussions of these methods can be found in Reference 6.

VERIFICATION TESTS

A series of pseudodynamic tests were performed with simple one- and two-degree-of-freedom systems fabricated from steel columns. Tests involving 2000 time steps can be performed in less than 30 min. The results of these tests show good correlations with analytical predictions. Fig. 4a shows the pseudodynamic response of a two-degree-of-freedom system subjected to the El Centro 1940 (NS) earthquake excitation with 0.5g peak acceleration. The system had the configuration shown in Fig. 1a. It consisted of a 96 in. long, W6×20 steel cantilever column which carried two concentrated masses (m_1 and m_2 are 0.0054 and 0.0083 kip in/sec^2, respectively) at equal distances along its length. Significant yielding was developed at the fixed base of the column during the test. The results of this test

correlated well with an analytical simulation using inelastic beam elements, as shown in Fig. 4b. In addition, a tubular steel x-braced frame specimen previously tested on a shaking table [7] was repaired and tested pseudodynamically [8]. The correlations between the two experimental results are briefly discussed here.

Description of Tubular Frame Tests. The tubular frame specimen was a 5/48 scale planar model of a representative offshore platform constructed in Southern California. The shaking table test specimen was subjected to three levels of excitation based on the 1952 Taft (S69E) record. These corresponded to strength level (0.28g), ductility level (0.58g), and maximum credible (1.228g) events. The recorded motions of the table in these tests were used as the input for the pseudodynamic tests. Since 99% of the mass was concentrated at the top of the frame as service loads, the specimen could be considered as a single-degree-of-freedom system. A 1.5% viscous damping ratio, which was measured from the shaking table tests, was numerically specifed in the pseudodynamic tests. The pseudodynamic test setup is shown in Fig. 5.

Test Results. Due to the flexibilities of the specimen's base support and of the table itself, the frame stiffness measured on the table was 31% lower than that in the pseudodynamic tests. Because of this, the frame responses in the low level events were very different in the two experiments. However, the pseudodynamic response of the frame closely matched the analytical result in the elastic range, as shown in Fig. 6a, except that it had a slightly higher damping effect due to local nonlinearities. Excellent correlations were obtained for the inelastic responses as well. Furthermore, the inelastic seismic behaviors and the failure modes of the specimens in the two experiments were very similar. In the maximum credible event, the pseudodynamically tested frame had a deteriorated stiffness nearly identical to that of the shaking table specimen. Consequently, the two experimental results were almost identical during that event (see Fig. 6b). These results verify the reliability of the pseudodynamic method.

SUBSTRUCTURING METHODS

Based on the analytical formulation of the pseudodynamic method, it is possible to apply substructuring techniques to experimental testing, whereby part of a structure is tested pseudodynamically and the rest of it is modeled analytically. Computer software has been developed to incorporate a mathematically modeled system into a test specimen; and a mixed implicit-explicit integration method [9] is adopted to solve the resulting equations of motion. This program is capable of modeling three-dimensional structural systems. Additional efforts are currently devoted to improve the computational scheme and to expand modeling capabilities. By the substructuring methods, subassemblages of complete structural systems or equipment mounted in structures can be tested pseudodynamically, and the effects of soil-structure interaction can be analytically modeled and included in the testing as well.

CONCLUSIONS

The studies presented here indicate that the pseudodynamic method is a powerful and versatile experimental technique. However, as with all testing and analytical methods, users must have a clear understanding of its limitations and the factors which might influence its accuracy. To avoid severe experimental errors, particular attentions should be directed to the selection of appropriate test equipment and to instrumentation techniques. The accuracy of test results also depends on the mechanical properties of a structure and the numerical techniques used. In spite of that, it is possible to develop relatively error resistant systems using the methods discussed in this paper. In the future, the substructuring concepts should greatly expand the applicability of the method and permit testing of many types of structures not previously tested.

ACKNOWLEDGEMENTS

The financial support of the National Science Foundation in sponsoring this research is gratefully acknowledged. The assistance of C. Thewalt and A. Javadian-Gilani in this project is also appreciated.

REFERENCES

[1] Takanashi, K., et al., "Non-Linear Earthquake Response Analysis of Structures by a Computer-Actuator On-Line System," Bull. of Earthquake Resistant Structure Research Center, Inst. of Industrial Science, University of Tokyo, No. 8, 1975.

[2] Okada, T., et al., "A Simulation of Earthquake Response of Reinforced Concrete Building Frames To Bi-Directional Ground Motion By IIS Computer-Actuator On-Line System," Proceedings, 7th WCEE, Istanbul, Turkey, Sept. 1980.

[3] Clough, R. W. and Penzien, J., Dynamics of Structures, McGraw Hill, 1975.

[4] Newmark, N. M., "A Method of Computation for Structural Dynamics," Journal of the Engineering Mechanics Div., ASCE, No. EM3, Vol. 85, July 1959.

[5] Shing, P. B. and Mahin, S. A, "Pseudodynamic Test Method for Seismic Performance Evaluation: Theory and Implementation," Earthquake Engineering Research Center, University of California, Berkeley (in preparation).

[6] Shing, P. B. and Mahin, S. A., "Experimental Error Propagation in Pseudodynamic Testing," UCB/EERC-83/12, Earthquake Engineering Research Center, University of California, Berkeley, June 1983.

[7] Ghanaat, Y. and Clough, R. W., "Shaking Table Tests of A Tubular Steel Frame Model," UCB/EERC-82/02, Earthquake Engineering Research Center, University of California, Berkeley, Jan. 1982.

[8] Shing, P. B., Javadian-Gilani, A. S., and Mahin, S. A., "Evaluation of Seismic Behavior of a Braced Tubular Steel Structure by Pseudodynamic Testing," Proceedings, 3rd International Symposium on Offshore Mechanics and Arctic Engineering, New Orleans, LA., Feb 1984.

[9] Hughes, T. J. R. and Liu, W. K., "Implicit-Explicit Finite Elements in Transient Analysis: Implementation and Numerical Examples," ASME Journal of Applied Mechanics, Vol. 45, 1978.

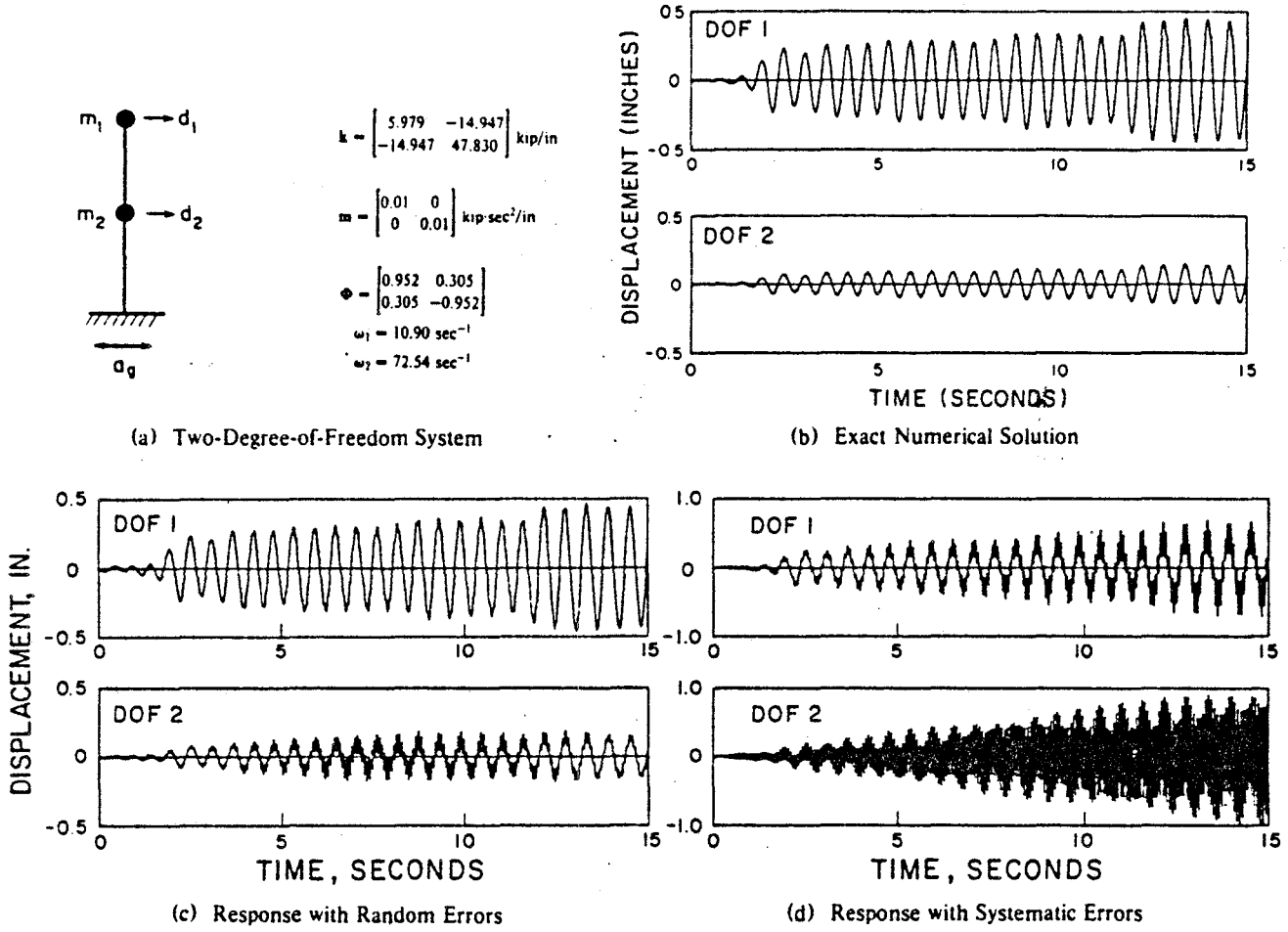

(a) Two-Degree-of-Freedom System

(b) Exact Numerical Solution

(c) Response with Random Errors

(d) Response with Systematic Errors

Fig. 1 Simulation of Experimental Error Effects using Newmark Explicit Method (Δt = 0.02 sec; a_g = 1940 El Centro (NS) with 0.02g Peak Acc.)

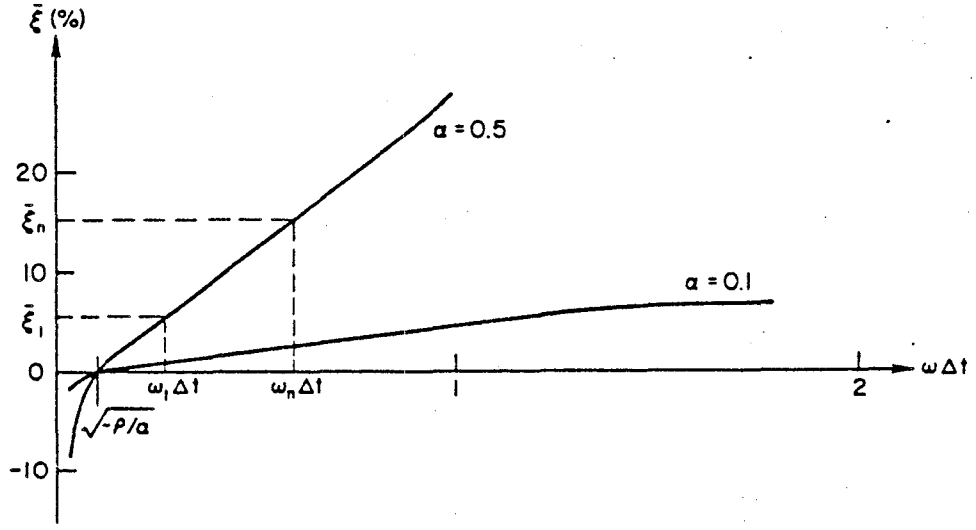

Fig. 2 Numerical Damping for the Modified Newmark Method

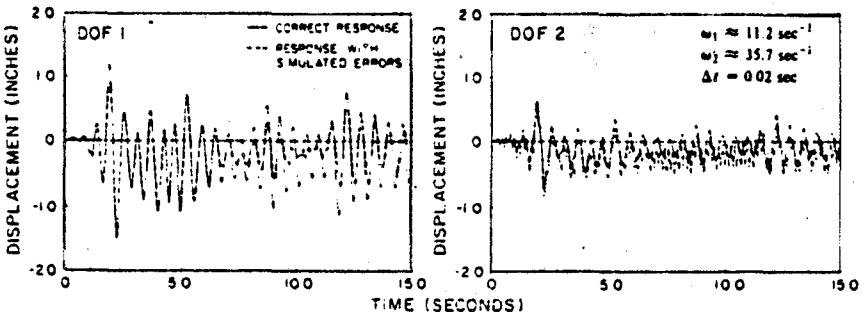

(a) Newmark Explicit Method
($\alpha = 0, \rho = 0$)

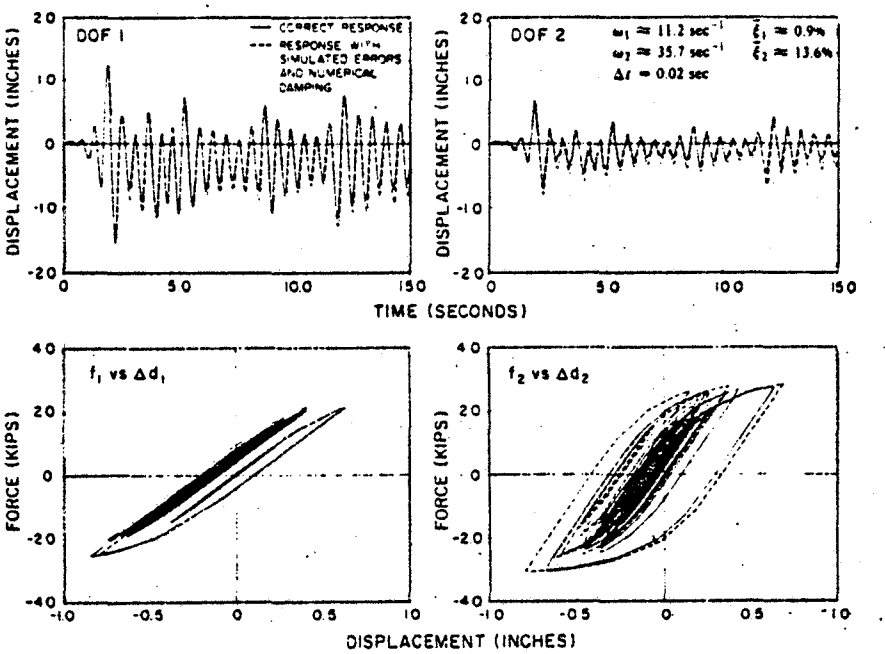

(b) Modified Newmark Method
($\alpha = 0.4, \rho = -0.016$)

Fig. 3 Removal of Experimental Errors by Numerical Damping for a Simulated Two-Degree-of-Freedom Inelastic Shear Building (1940 El Centro (NS) with 0.18g Peak Acc.)

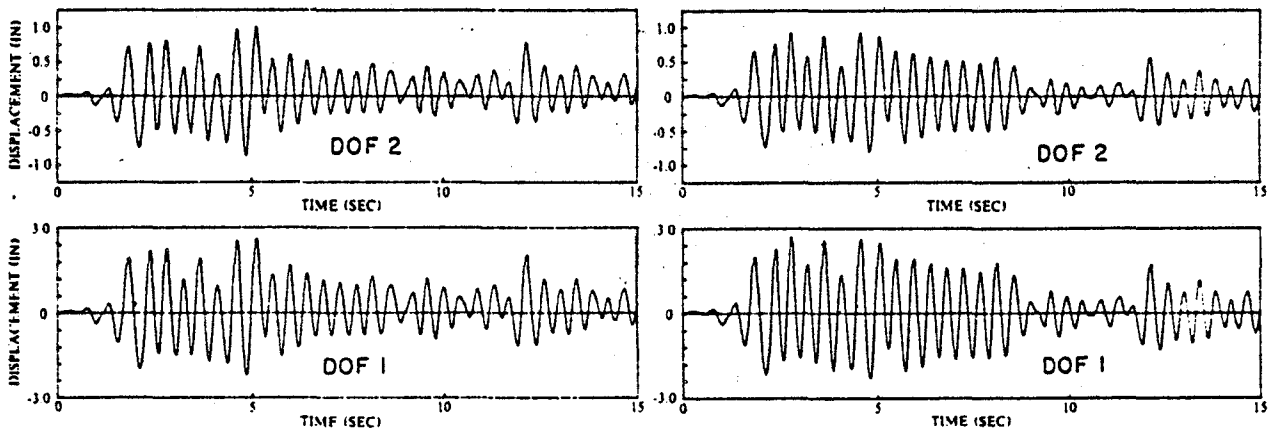

(a) Pseudodynamic Test Results

(b) Analytical Results

Fig. 4 Comparison of Pseudodynamic Test Results with Analytical Simulation for a Two-Degree-of-Freedom Inelastic System (1940 El Centro (NS) with 0.5g Peak Acc.)

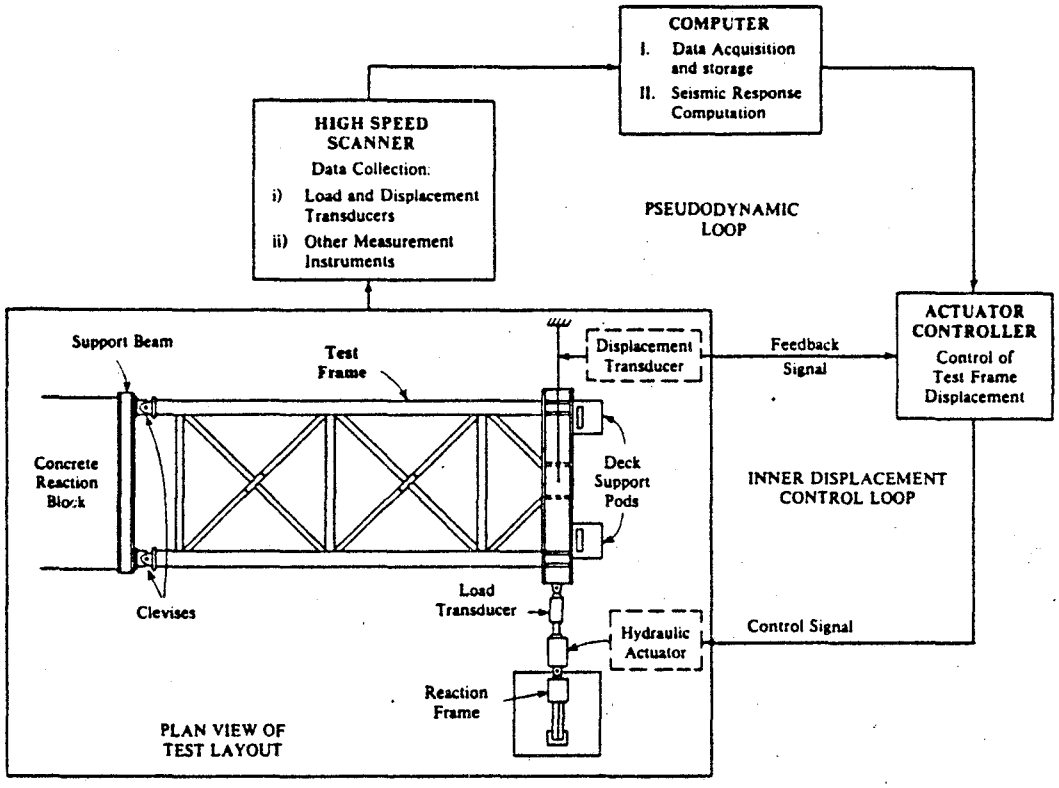

Fig. 5 Pseudodynamic Test Setup for a Tubular Steel Frame

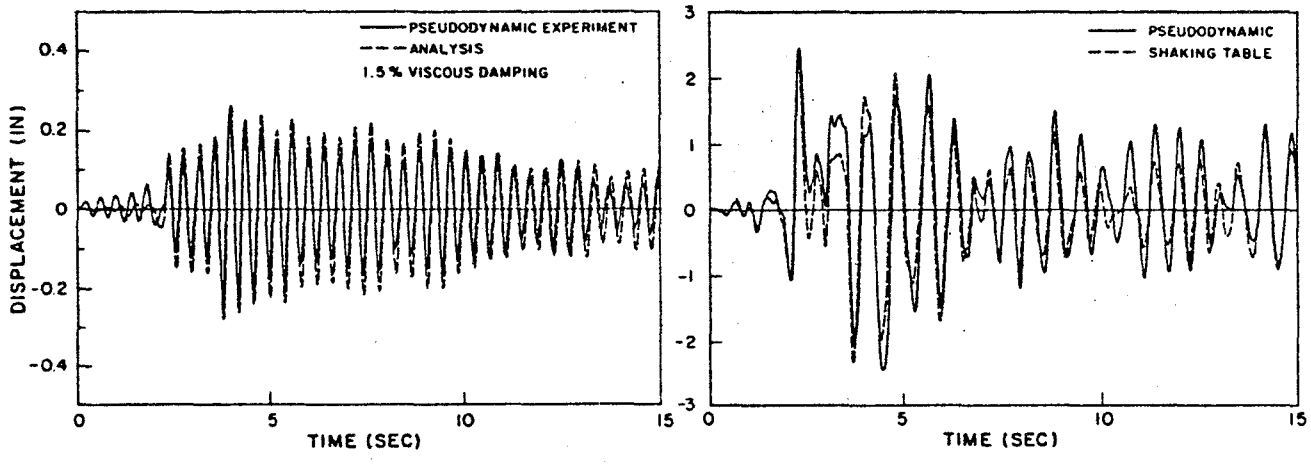

(a) Elastic Response at 0.069g Taft

(b) Inelastic Response at 1.228g Taft

Fig. 6 Comparison of Pseudodynamic Test Results with Analytical and Shaking Table Test Results for a Tubular Steel Frame (1952 Taft S69E)

DETERMINING MONETARY LOSSES AND CASUALTIES FOR USE IN EARTHQUAKE MITIGATION AND DISASTER RESPONSE PLANNING

Karl V. Steinbrugge (I)
S.T. Algermissen (II)
Henry J. Lagorio (III)
Presenting Author: S.T. Algermissen

SUMMARY

Estimates of the number of potential casualties and aggregate monetary losses are vital for selecting the most effective hazard mitigation measures as well as for post-earthquake disaster response planning. These are also very important in earthquake insurance. Major factors in these estimates are the casualty and monetary loss data by class of building construction, the appropriate building inventories, and the relevant geophysical parameters such as magnitude, focal depth, and probable recurrance intervals. This paper presents a summary of some of these major factors which have been applied to a number of seismic regions. Also summarized are the current advances in these methodologies. The loss estimation methods are intended for evaluating hundreds of buildings, or for a city, or for the entire shaken area. The algorithms given herein are not a substitute for site-specific investigations.

INTRODUCTION

The term "loss ratio" as used in this paper is defined as the mean percentage value of the monetary loss to a particular class of construction in the event of the maximum probable earthquake for buildings in the vicinity of the faulting. In California, the maximum probable earthquake is assumed to be magnitude 8.25 for the purposes of this paper. "Life-safety ratio" is the equivalent term to "loss ratio" for casualty estimates. Firm alluvial soil is assumed for building foundations, except where otherwise microzoned. An impersonal loss definition is used for monetary losses, namely, losses paid by the government or insurance company rather than by the owners or occupants. A parallel term to loss ratio used in earthquake insurance practice is "probable maximum loss (PML) which is defined in the same manner, except that 90% of the buildings will have losses not exceeding the PML. Transfer functions between loss ratio and PML can be easily developed.

Casualty life-safety ratios and monetary loss ratios by class of building construction along with relevant geophysical parameters constitute two of the most important inputs for quantifying casualties and monetary losses. These

---

(I) Consulting Engineer, El Cerrito, California, USA
(II) Geophysicist, U.S. Geological Survey, Denver, Colorado, USA
(III) Director, Center for Environmental Design Research, Univ. California, Berkeley, Calif., USA

ratios have commonalities throughout the world wherever similar construction is found. When these ratios are multiplied by the building inventories or population at risk, the results are the mean aggregate monetary losses and casualties.

Effective use of these ratios requires a careful examination of all of the other input parameters. These major inputs are:

1. A suitable building classification system.
2. Compilation of a building inventory and an inventory of population at risk in and adjacent to the buildings.
3. Selection of appropriate geophysical parameters, such as: magnitude, focal depth, fault rupture length, and probability of occurrence.
4. Appropriate loss ratios and life-safety ratios which have been carefully defined for intended uses and which include the damaging effects of long period ground motion.

The most costly aspect of applying the loss estimation algorithms is obtaining suitable inventories of buildings and populations at risk. Normally, appropriate inventories do not exist. Suitable building inventories must be divided into construction classes by damage vulnerability and must be segregated into small areas. It is also necessary to know story height (or an equivalent parameter for estimating long period effects), age, monetary values, and population at risk within these structures as a function of time of day. Provisions for local microzonation can be included when the individual areas are as small as a postal ZIP or census tract.

Area-specific hazards may also exist, such as hazardous upstream dams and fire following earthquake conditions. These are usually examined separately and the results added to those found by the general methodology.

Despite their importance, economics dictates that monetary loss ratios and casualty life-safety ratios must be developed in the context of cost-effective inventory methods. The entire process has been computerized using postal ZIPs for certain uses and census tracts for other uses.

BUILDING CLASSIFICATION SYSTEMS AND INVENTORIES

Excluding region-specific instances such as landslides and dam failures, life loss and monetary loss come from the failure of man-made structures such as buildings. It is therefore desirable to obtain building inventories based on a single classification system which is useable for developing casualty figures and monetary losses.

Every effort should be made to examine existing inventories for their applicability. The geographic distribution of buildings in the inventory must be known; unit areas in the United States may be postal ZIPs, census tracts, city blocks, political boundaries, or other small areas for which suitable inventories exist. The inventoried buildings must also be classed according to their relative vulnerabilities. Except for dwellings, it is usually incorrect to substitute occupancy inventories for construction class inventories. For example, a mercantile occupancy may be of wood frame construction (minimal vulnerability), or of non-earthquake-resistive unit masonry (highest vulnerability), or of anything between. The usual inventory prepared by or for governmental sources such as tax assessors and land use planners often

emphasizes occupancy, and therefore these inventories are usually inappropriate. Property insurance inventories held by private insurance companies are excellent resources; they are limited by not being commonly available and not necessarily including all privately owned buildings. Public buildings are usually not included. Federal, state, and local government inventories of their structures (owned or leased) are usually inadequate.

Building inventories may be adapted from various existing specialty inventories such as those prepared for real estate purposes. When suitable ones are not available as is the common case, field inspections by knowledgeable persons such as former building officials have been successful. These inspection may be supplemented (but not supplanted) by low-altitude air photography. Very important occupancy types, such as hospitals and fire stations, often require special inspections. These inspections may include a brief examination of the construction drawings, but normally do not include a mathematical analysis by engineers. (While desirable to obtain these dynamic analyses, costs have been prohibitive when hundreds of major structures have been involved.)

Table 1 is a summary description of a practical building classification system using construction materials. This table is based on experience gained over the past decade from the preparation of numerous vulnerability studies for governmental use in the United States. It also follows earthquake insurance practice. Experience has shown that not all earthquake resistive buildings can be placed into equivalent Classes 1 through 5, and Class 6 is therefore provided for these specialty cases. Each study area has regional construction variants which require minor revisions or interpretations to Table 1. It will be noted that Table 1 allows for further subdivision of Class 1C, if desired. Variants of the classification system are used by the private property insurance companies and by the California Department of Insurance. Only a summary description of a building classification system is given here, and Ref. 1 should be examined for further information on various classification systems.

ALTERNATIVE TO EARTHQUAKE INTENSITY

The authors have developed algorithms which minimize the use of intensity scales. Continued development of data for these algorithms will eventually bypass the use of intensity scales. In time, this change is expected to significantly improve the quality of the loss estimates.

The common approach to monetary loss estimates has been to group all kinds of damage, geologic effects, as well as human reactions into earthquake intensities, usually Modified Mercalli intensities. These commingled earthquake effects which include casualties and monetary losses are given as site or locality intensities. After plotting these intensities on a map, isoseismal lines are drawn which separate intensity grades. The isoseismal maps, or intensity-loss curves derived therefrom, can then relate intensity grades to casualties and/or monetary losses. Using an appropriate building inventory, the calculation of aggregate losses is readily achieved for any postulated seismic event using isoseismal maps (Ref. 2 and 3).

There are significant error potentials using these methods since intensity data on casualties and damage (and thereby monetary loss) are commingled with other earthquake effects which often are not compatible. There is no assurance

that monetary losses and casualties were the principal determinants when the site or regional intensity was established. The next step in this customary methodology is the reverse of the foregoing; the generalized intensities shown on the isoseismal maps are interpreted to obtain casualty and monetary loss information. Clearly, mixing incompatible data to obtain an intensity and then reversing the process may be a significant source of interpretational error.

The authors are minimizing this error potential through the use of distance-loss algorithms whenever the source data permit. Site-specific or region-specific monetary loss data or damage information is directly used or interpreted to provide the basis for distance-loss curves, thereby bypassing the intermediate determination of intensity. This does not presently eliminate the use of conventional isoseismal maps in the absence of building damage information. Summarizing, the algorithms are distance-loss relationships obtained directly from loss experience whenever known; intensity information becomes a secondary source in many situations.

DISTANCE - LOSS RELATIONSHIPS

Geophysical Parameters

Figure 1 is a diagrammatic crossection through the earth showing the model for the distance-loss relationships. A line source is assumed for the origin of the seismic energy. The assumed focal depth is that which is common for earthquakes in the region under study, being 10 km for California.

The earthquake magnitude may be selected on the basis of the most probable for a given recurrence interval. More often, however, the maximum probable earthquake is selected by governmental response planners to be in a "fail safe" position. It is also not an uncommon position for private financial organizations to take a similar position. Epicenters are assumed to be located at the rupture midpoint, and usually located to maximize losses.

The length of the fault rupture along the line source in Figure 1 may be approximated by using any one of the equations developed by various authorities (Ref. 4, 5, and 6). The length of rupture approximation may greatly vary, depending upon the user's choice among the the equations given in the references. The use of some of these equations may create a problem when simulating an earthquake on faults such as the San Andreas, San Fernando, or White Wolf. In these cases, the surface traces of past events have been well-mapped and the earthquake magnitudes are well-known. The rupture equations in the references may give results which are substantially different from those observed in past earthquakes. The authors tend to prefer past experience on the fault under consideration as the basis for estimating future rupture lengths. Special equations were developed for these cases. Depending upon the chosen equation, there can be significant differences in the shape and size of the shaken area. In turn, the aggregate monetary losses and total number of casualties may vary significantly.

Distance - Monetary Loss Curves

Certain aspects of the characteristic shape of the distance-loss curves shown in Figure 2 require explanation. It has been stated by a number of careful observers after many American earthquakes that damage near the surface

trace of the fault was not significantly different from that a few miles away when the structure was subjected only to ground shaking (and not from faulting or landsliding). The atlas to the thorough and classic Carnegie report on the 1906 San Francisco earthquake (Ref. 7) is often cited to the contrary, but see Louderback's observations in Ref. 8. It is also presumed that uniform soil conditions existed beneath all buildings for this uniform intensity. This observation of uniform damage is consistent with the model shown in Figure 1. However, one must also examine instrumental records from special instrumental arrays distributed at right angles to the fault. See, for example, the Parkfield earthquake of 1966 (Ref. 9) and the Imperial County earthquake of 1979 (Ref. 10). Little damage differential was noted among the few wood frame dwellings found near the strong motion instruments in the Imperial County earthquake. Tentatively, the portion of the distance-loss curve marked "A" is flat and represents observation-- certainly more investigation is necessary before this can be accepted as final.

The portion of the distance-loss curve marked "B" approaches the threshold of damage. This threshold varies with the building class as well as the kind of ground motion. Reported effects often include "imaginary" damage; imaginary damage is that which the owner/occupant believes to have occurred during the shock, but in fact it did not occur (or may have only partially occurred). It is most difficult for other than trained persons to distinguish between new and existing cracks; too often, cracks appear to be new to the untrained eye despite cobwebs or paint within the crack. When using the impersonal loss definition, the owner/tenant view is normally accepted. On that basis, the aggregate monetary losses become very inflated from the costs of patching pre-earthquake cracks and repainting many thousands of houses. The "B" portion of the curves will therefore vary with the definition of loss.

Long period effects are principally found as damage to high-rise buildings located at relatively long distances from the fault rupture. Human observation as well as seismographic records show that the short-period motions in the energy release region of an earthquake are damped and dispersed quickly, leaving the longer period motions dominant at large distances. Generally speaking, the greater the distance, the longer the ground motion period. At these greater distances, mostly the taller buildings with longer natural periods are adversely effected. Thus we can see the difficulty of assigning intensities to the multistory buildings in Anchorage after the 1964 Alaskan earthquake or after the 1967 Caracas earthquake. In each case, the "collapse hazard" types of one story buildings survived without damage but high-rise buildings were damaged (Refs. 11 and 12).

Figure 2 shows a family of characteristic distance-loss curves. From left to right, each curve represents a longer natural period of buildings. Computed or observed natural periods are not always available, and approximations based on story height are practical alternatives. Attenuation of seismic energy as a function of distance is a regional characteristic and therefore separate sets of curves are required for other seismic environments such as Puget Sound and eastern United States. Loss ratios at the fault trace for each building class listed in Table 1 are given in Table 2. Space does not allow a full presentation of the distance-loss algorithms, including consideration for long period effects.

Casualty Life-Safety Ratio

Life-safety ratio is used to estimate the number of deaths and injuries to persons within or adjacent to buildings. Its principal use to date has been to establish priorities for the strengthening or reconstruction of State of California buildings (Ref. 13). Its use can be expanded to follow the methods for distance-monetary loss curves discussed above.

For Table 3, the life-safety ratio is defined as the number of fatalities per 10,000 building occupants in the heaviest shaken areas of a great earthquake, being magnitude 8.25 in California. In Table 3, "large areas" implies auditoriums and other high occupancy loads.

CITED REFERENCES

1. Steinbrugge, K.V., "Earthquakes, Volcanoes, and Tsunamis: An Anatomy of Hazards", 1982, Skandia, New York City.
2. Algermissen, S.T., K.V. Steinbrugge, and H.J. Lagorio, "Estimation of Earthquake Losses to Buildings (Except Single Family Dwellings)", U.S.G.S. Open File Report 78-441, 1978.
3. Rinehart, W., S.T. Algermissen, and Mary Gibbons, "Estimation of Earthquake Losses to Single Family Dwellings", U.S.G.S. Open File Report 76-156, 1976.
4. Mark, R.K., "Application of Linear Statistical Models of Earthquake Magnitude Versus Fault Length in Estimating Maximum Expectable Earthquakes", Geology, 5:464/466(1977).
5. Mark, R.K., "Regression Analysis of Magnitude and Surface Fault Length Using the 1970 Data of Bonilla and Buchanan", U.S.G.S. Open File Report 77-614, 1977.
6. Algermissen, S.T., et al, "Probabilistic Estimates of Maximum Acceleration and Velocity in Rock in the Contiguous United States", U.S.G.S. Open File Report 82-1033, 1982.
7. California State Earthquake Investigation Commission, "The California Earthquake of April 18, 1906", 2 volumes plus atlas, Carnegie Institution of Washington, 1908.
8. Louderback, G.D., "Faults and Earthquakes", Bull. Seism. Soc. Am., 32:305/330. See particularly pages 317/319.
9. Harding, et al, "The Parkfield, California, Earthquake of June 27, 1966", Coast and Geodetic Survey, U.S. Department of Commerce, 1966.
10. ---, "The Imperial Valley, California, Earthquake of October 15, 1979", U.S.G.S. Professional Paper 1254, 2 volumes (text and plates), 1982.
11. Steinbrugge, K.V., J.H. Manning, and H.J. Degenkolb, "Building Damage in Anchorage", in volume II, part A, of The Prince William Sound, Alaska, Earthquake of 1964 and Aftershocks, U.S. Department of Commerce, 1967.
12. Steinbrugge, K.V., "Appendix A. Comparative Building Damage", in A Study of Soil Amplification Factors in Earthquake Damage Areas, Caracas, Venezuela", U.S. Department of Commerce, NOAA TR ERL 280-ESL 31, 1972.
13. Steinbrugge, K.V. (chairman), F.E. McClure, H.J. Degenkolb, "Evaluating the Seismic Hazard of State Owned Buildings", SSC 79-01, California Seismic Safety Commission, 1979.

TABLE 3
LIFE SAFETY RATIOS

Class	Summary Description of Building Class		Life Safety Ratios: Earthquake Resistive Buildings	Life Safety Ratios: Non-EQ Resistive Buildings
1A	1 to 4 family wood frame dwellings		2	4
1B	Mobile homes		2	4
1C	Large wood frame		5	10
2A	All-metal -- small		2	4
2B	All-metal -- large		8	15
3A	Steel frame, superior	-- small area	5	10
		-- large area	25	50
3AB	Steel frame, intermediate	-- small area	10	25
		-- large area	--	1500
3B	Steel frame, ordinary	-- small area	15	40
		-- large area	--	1500
3C	Steel frame, other	-- small area	25	50
		-- large area	--	1500
			Non-ductile Concrete	Ductile Concrete
4A	Reinf. conc., superior	-- small area	50	25 100
		-- large area	75	50 200
4AB	Reinf. conc., intermediate	-- small area	200	50 500
		-- large area	1000	200 2500
4B	Reinf. conc., ordinary	-- small area	300	75 1000
		-- large area	1000	200 2500
4C	Reinf. conc., precast		500	75 1500
4D	Reinf. conc., other		800	100 2000
5A	Mixed construction	-- small, such as dwellings	10	200
		-- superior tilt-up	15	800
		-- ordinary tilt-up	20	1000
		-- other	40	2000
5B	Mixed constr., unreinforced masonry		--	4000
5C	Mixed constr., adobe, hollow tile		--	5000

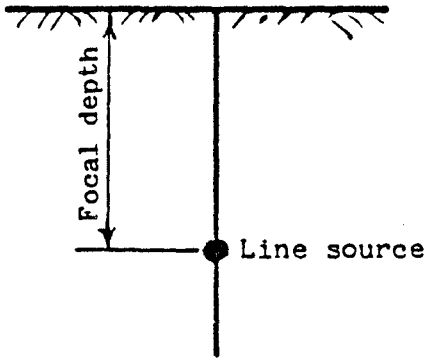

FIGURE 1

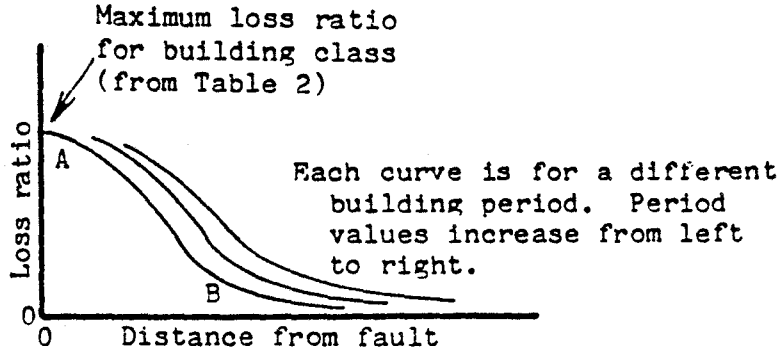

FIGURE 2

TABLE 1
SIMPLE IDENTIFICATION OF BUILDING CONSTRUCTION CLASSIFICATIONS

Building Construct. Class	Summary Description	Story Height Limit	Major Special Conditions
Wood Frame			
1A	1 to 4 family dwellings	-	Any height and area
1B	Mobile homes	-	
1C	Other habitational	2	
1C	Small non-habitational	3	Non-dwellings to 3,000 sq.ft.
1C	Wood frame -- other	-	Any height and area
All-Metal			
2A	Small	1	Up to 20,000 sq. ft. area
2B	Large	-	Any height and area
Steel Frame			
3A	Superior***	-	EQ resistive with damage control
3B	Ordinary	-	Poured R/C floors and roof**
3C	Other	-	Wood, metal, or precast R/C floors
Reinforced Concrete			
4A	Superior***	-	Superior EQ resistive with D/C**
4B	Ordinary	-	Poured R/C floors and roof**
4C	Precast, incl. lift slabs	-	Structural precast R/C, lift slabs
4D	Other	-	Wood or metal floors and roof
Mixed Construction			
5A	Reinforced concrete walls***	-	Superior earthquake resistive
5B	Non-reinforced walls*	-	Ordinary non-EQ resistive*
5C	Non-reinforced walls	-	Hollow masonry, adobe, tile
6	Special EQ resistive***	-	Special design for D/C

*Excluding hollow tile, hollow concrete block, hollow masonry, and adobe.
**Roof may be of any material if building is over 3 stories.
***Engineering review of existing inventories is recommended.
Abbreviations: EQ - earthquake; D/C - damage control; R/C - reinforced concrete

TABLE 2
MONETARY LOSS RATIOS

Class	Loss Ratio%	Class	Loss Ratio%
1A	8	4A	15
1B	10	4B	22.5
1C	9	4C	32.5
2A	7	4D	30
2B	9	5A	20.
3A	12.5	5B	100
3B	15	5C	100
3C	20	6	varies

EARTHQUAKE RESPONSE OF BUILDINGS ON WINKLER FOUNDATION ALLOWED TO UPLIFT

Solomon C. S. Yim (I)
Anil K. Chopra (II)
Presenting Author: Solomon C. S. Yim

SUMMARY

The effects of transient foundation uplift on the earthquake response of flexible structures attached to a rigid foundation mat supported on Winkler foundation with spring-damper elements distributed over the entire width of the mat are investigated. Based on the response spectra presented, the effects of foundation-mat uplift on the maximum response of structures are identified, and the accuracy of an equivalent two spring-damper-element foundation system are explored.

INTRODUCTION

The earthquake induced lateral forces on a structure, computed by dynamic analysis under the assumption that the foundation and soil are firmly bonded, will often produce a base overturning moment that exceeds the available overturning resistance due to gravity loads. The computed overload implies that a portion of the foundation mat or some of the individual column footings, as the case may be, would intermittently uplift during an earthquake. The effects of foundation uplift on the earthquake response of flexible structures have been investigated in recent analytical studies (Ref. 1-3). Whereas the flexibility and damping of the supporting soil were not incorporated in Refs. 1 and 2, they were modeled by two spring-damper elements, one at each edge of the foundation mat, in the most recent work (Ref. 3). Because the Winkler foundation model leads to considerable complication in the analysis, an equivalent two-element supporting system was developed based on the dynamics of rigid blocks (Ref. 3). Without resorting to this approximation in modeling the foundation, this paper aims to develop a better understanding of the effects of transient foundation uplift on building response. It is based on a report (Ref. 4) prepared under a research grant from the National Science Foundation.

SYSTEM CONSIDERED

The structural system considered, is a linear structure of mass m, lateral stiffness k and lateral damping c, which is supported through the

---

(I) Assistant Research Engineer, University of California, Berkeley, California, USA

(II) Professor of Civil Engineering, University of California, Berkeley, California, USA

foundation mat of mass m_o resting on a Winkler foundation, with spring-damper elements distributed over the entire width of the foundation mat, connected to the base which is assumed to be rigid (Fig. 1). If the dampers are absent in the Winkler foundation, the relation between the displacement and reaction force per unit width of the foundation mat is shown in Fig. 2a. The relation between the static moment M applied at the c.g and the resulting foundation-mat rotation θ, is shown in Fig. 2b where p is a static force acting in the downward direction at its center of gravity. If the mat is not bonded to the supporting elements the M-θ relation is linear, implying constant rotational stiffness, until one edge of the foundation mat uplifts from the supporting elements; thereafter the rotational stiffness decreases monotonically with increasing θ, which implies an expanding foundation-mat width over which uplift occurs. Uplift is initiated when the rotation reaches $\theta_u = p/2k_w b^2$ with the corresponding moment $M_u = pb/3$. The M-θ curve asymptotically approaches the critical moment, $M_c = pb$, corresponding to the physically unrealizable condition of uplift of the entire foundation mat from the supporting elements except for one edge. The downward force is $p = (m + m_o)g$, the combined weight of the superstructure and foundation mat, prior to any dynamic excitation, but would vary with time during vibration.

Next consider the entire structural system with a gradually increasing force f_s applied at the lumped mass m in the lateral direction. If the foundation mat is bonded to the supporting elements, which along with the structure have linear properties, the lateral force can increase without limit if the overturning effects of gravity forces are neglected. However, if the mat is not bonded to the supporting elements, one edge of the foundation mat is at incipient uplift when the lateral force reaches $f_{su} = (m + m_o)gb/3h$. Thus the corresponding base shear at incipient uplift under the action of static force is

$$V_u = (m + m_o)g\,\frac{b}{3h} \tag{1a}$$

The structural deformation u_u associated with this base shear and the foundation-mat rotation θ_u at incipient uplift are

$$u_u = \frac{(m + m_o)g}{k}\,\frac{b}{3h}; \quad \theta_u = \frac{(m + m_o)g}{2k_w b^2} \tag{1b}$$

As the lateral force continues to increase beyond f_{su}, the foundation mat separates over increasing width from its supporting elements. The lateral force $f_{sc} = (m + m_o)gb/h$ corresponds to the physically unrealizable condition of uplift of the entire foundation mat from the supporting elements except for one edge. Thus the limiting value for base shear under the action of static forces is

$$V_c = (m + m_o)g\frac{b}{h} \tag{1c}$$

The structural deformation due to this base shear is

$$u_c = \frac{(m + m_o)g}{k} \frac{b}{h} \tag{1d}$$

EQUATIONS OF MOTION

The differential equations governing the small-amplitude motion of the system of Fig. 1 due to horizontal ground acceleration $\ddot{u}_g(t)$ can be expressed as

$$m\ddot{u} + m(h\ddot{\theta}) + c\dot{u} + ku = - m\ddot{u}_g(t) + \frac{m(u + h\theta)}{h}(\ddot{v} + g) \tag{2a}$$

$$\frac{m_o b^2}{3h^2}(h\ddot{\theta}) - c\dot{u} + (1 + \varepsilon_1^3)c_w \frac{b^3}{3h^2}(h\dot{\theta}) + (1 - \varepsilon_1^2)\varepsilon_2 c_w \frac{b^2}{2h}\dot{v}$$

$$- ku + (1 + \varepsilon_1^3)k_w \frac{b^3}{3h^2}(h\theta) + (1 - \varepsilon_1^2)\varepsilon_2 k_w \frac{b^2}{2h} v = 0 \tag{2b}$$

$$(m + m_o)\ddot{v} + (1 + \varepsilon_1)c_w b\dot{v} + (1 - \varepsilon_1^2)\varepsilon_2 c_w \frac{b^2}{2h}(h\dot{\theta})$$

$$+ (1 + \varepsilon_1)k_w bv + (1 - \varepsilon_1^2)\varepsilon_2 k_w \frac{b^2}{2h}(h\theta) = - (m + m_o)g \tag{2c}$$

where contact coefficient ε_1 is equal to unity during full contact but depends continuously on foundation-mat rotation θ and vertical displacement v during partial uplift as follows:

$$\varepsilon_1 = \begin{cases} 1 & \text{contact at both edges} \\ \varepsilon_2 v/b\theta & \text{left or right edge uplifted} \end{cases} \tag{3a}$$

and contact coefficient ε_2 depends on whether one or both edges of the foundation mat are in contact with the supporting elements:

$$\varepsilon_1 = \begin{cases} -1 & \text{left edge uplifted} \\ 0 & \text{contact at both edges} \\ 1 & \text{right edge uplifted} \end{cases} \tag{3b}$$

The vertical displacements at the edges of the foundation mat, measured from the initial unstressed position, are

$$v_i = v \pm b\theta(t) \qquad i = 1,r \tag{4a}$$

Because the Winkler foundation cannot extend above its initial unstressed position an edge of the foundation mat would uplift at the time instant when

$$v_i(t) > 0 \qquad i = 1,r \tag{4b}$$

The equations of motion for the system of Fig. 1 are nonlinear as indicated by the dependence of the coefficients ε_1 and ε_2 on whether the foundation mat is in full or partial contact with the supporting system; and on the contact width.

EQUIVALENT TWO-ELEMENT FOUNDATION SYSTEM

The solution of the nonlinear equations of motion is complicated by the fact that after lift off these equations depend continuously on the varying degree of contact between the mat and its supporting elements. In contrast, the equations of motion are relatively simple for a system with foundation mat resting on two spring-damper elements, one at each edge of the foundation mat. In the latter case, the nonlinear equations of motion depend on three discrete contact conditions -- both edges of foundation mat are in contact with supporting elements, the left edge is uplifted, or the right edge is uplifted -- but for each contact condition the governing equations are linear. Because of the relative simplicity of the two-element supporting system, it is of interest to define its properties in such a way that it can model the more complicated Winkler foundation.

The equations of motion for the idealized one-story structure supported through a foundation mat resting on a Winkler foundation were presented in the preceding section and those for a two-element foundation in Chapter 2 of Ref. 4. If the foundation mat is bonded to the supporting elements the equations of motion for the structure supported on Winkler foundation are identical to those for the same structure on a two-element foundation with the following properties: $k_f = bk_w$, $c_f = bc_w$ and half base-width = $b/\sqrt{3}$. This two-element foundation is exactly equivalent to the Winkler foundation if uplift is not permitted.

If the mat is not bonded to the supporting elements, the relation between the static moment M applied at the c.g and the resulting foundation-mat rotation is shown in Fig. 3 for the two systems. The M-θ relation is linear with the same rotational stiffness for the two systems until θ reaches $\theta_u = p/2k_w b^2$ when one edge of the foundation mat on Winkler foundation is at incipient uplift. For larger rotation angles the M-θ relation for the two systems are different. The constant rotational stiffness implied by the linear M-θ relation continues to apply for the equivalent two-element supporting system until θ reaches

$\theta_u\sqrt{3}$ when one edge of the foundation mat uplifts from one of the supporting elements; thereafter no additional moment can be developed. On the other hand the M-θ relation for the Winkler supporting system is nonlinear for $\theta > \theta_u$ with the rotational stiffness decreasing monotonically with increasing θ. The M-θ curve asymptotically approaches the critical moment $M_c = pb$. Whereas the equivalent two-element supporting system is an exact representation of the Winkler foundation system for rotation angles $\theta < \theta_u$, it is only an approximation if the ground motion is intense enough to cause significant uplift. The accuracy of this approximation is explored by comparing the earthquake response of structures supported on the two foundations.

PRESENTATION AND DISCUSSION OF RESULTS

The response of a structural system to the north-south component of the El Centro, 1940 ground motion, computed by the special numerical procedures developed for the solution of the equations of motion (Ref. 4), is presented in Fig. 4. During the initial phase of the ground shaking, the foundation mat remains in contact with the supporting elements over its entire width. As the ground motion intensity builds up, the two edges of the foundation mat alternately uplift in a vibration cycle, including partial separation of the mat from the supporting elements. In this example the foundation mat uplifts over a significant portion of its width in every vibration cycle during the strong phase of ground shaking, with the duration of uplift depending on the amplitudes of foundation-mat rotation. As the intensity of ground motion decays toward the later phase of the earthquake, the foundation-mat uplift becomes negligible and full contact is maintained for long durations.

The base shear coefficient $V_{max} = V_{max}/w$, where V_{max} is the maximum base shear, and w is the weight of the superstructure, is plotted as a function of the natural vibration period of the corresponding rigidly supported structure. Also presented are the results for the corresponding rigidly supported structure not allowed to uplift, which is simply the standard pseudo-acceleration response spectrum, normalized with respect to gravitational acceleration. Included in the response spectra plots is V_u, the base shear coefficient associated with the value of base shear, V_u, at which uplift of an edge of the foundation mat is initiated (Equation 1a): $V_u = V_u/w$. Also included is V_c, the critical base shear coefficient associated with the static asymptotic base shear, V_c (Equation 1d) which corresponds to the uplift of the foundation mat from its supporting springs over the entire width, i.e., the foundation mat is standing on its edge: $V_c = V_c/w$. These base shear coefficients depend on the mass ratio m_o/m and slenderness-ratio parameter h/b, but are independent of the vibration period T. The differences between the response spectra for the two linear systems, the structure with foundation mat bonded to the supporting elements and the corresponding rigidly supported structure, are due to the change in period and damping resulting from support flexibility (Ref. 4). The base shear developed in structures with relatively long vibration periods is below the static value at incipient uplift and throughout the earthquake the foundation mat remains in contact over its entire width with the supporting elements. If foundation mat uplift is prevented, the maximum base shear at some vibration periods may exceed the incipient-uplift value. For the selected system parameters and ground motion, Fig. 5 indicates that this occurs for all vibration periods shorter than the period where the linear spectrum first attains the incipient-uplift value. If the foundation mat of such a structure rests on the Winkler spring-damper

elements only through gravity and is not bonded to these elements, partial separation occurs and this has the effect of reducing the base shear. However, the base shear exceeds the value at incipient-uplift because even under static forces the base moment, and hence base shear, continue to increase considerably beyond this value (Fig. 2b). Furthermore the base shear is not reduced to as low as the critical value based on static considerations. Although this asymptotic value can never be exceeded under static forces, depending on the state -- displacement, velocity and acceleration -- of the system, the deformation and base shear may exceed the critical values during dynamic response, as seen in Fig. 5. Because the base shear developed in linear structures (foundation-mat uplift prevented) tends to exceed the incipient-uplift value by increasing margins as the vibration period decreases, the foundation mat of a shorter-period structure has a greater tendency to uplift over a greater portion of its width, which in turn results in the incipient-uplift base shear being exceeded by a greater margin although it remains well below the linear response.

Also shown in Fig. 5 is the response spectrum for the equivalent two-element system defined earlier. This response spectrum is identical to that for the Winkler system for the relatively long periods because the base shear developed is below the incipient-uplift value and the foundation mat does not uplift from its supporting elements and for this condition the two-element supporting system is exactly equivalent to the Winkler supporting system. Uplift occurs for any structure if the corresponding ordinate of the linear response spectrum exceeds the static base shear coefficient at incipient uplift, which is $1/3\alpha$ for a Winkler system and $1/\sqrt{3}\alpha$ for the equivalent two-element system. Because the base shear developed in linear structures tends to increase as the vibration period decreases, uplift in a Winkler system is initiated at a longer period compared to the two-element system. However, because the uplift is limited in extent and duration in the range of periods bounded on the low side by the period at which uplift is initiated in a two-element system and on the high side by the period at which uplift is initiated in a Winkler system, the difference between the response spectra for the two systems is small in this period range. For shorter vibration periods outside this range the equivalent two-element system consistently underestimates the maximum response because, as shown in Fig. 3, the equivalent two-element system does not adequately represent the moment-rotation relation for larger rotation angles. Overall, the equivalent two-element system is successful in displaying the main effects of foundation uplift on maximum structural response, and it provides results that are reasonably close to those for a Winkler system over a wide range of vibration periods, excluding the very short periods.

REFERENCES

1. Meek, J.W., J. Struct. Div., ASCE, 101, ST7, pp. 1297-1311, 1975
2. Meek, J.W., Earthq. Eng. Struct. Dyn., 6, pp 437-454, 1978.
3. Psycharis, Report No. EERL 81-02, Calif. Inst. Tech., Pasadena, 1981; Earthq. Eng. Struct. Dyn. 11, pp. 57-76 and 501-521 (1983).
4. Yim, C.S., and Chopra, A.K., Report No. UCB/EERC 83-09, Univ. of Calif., Berkeley, 1983.

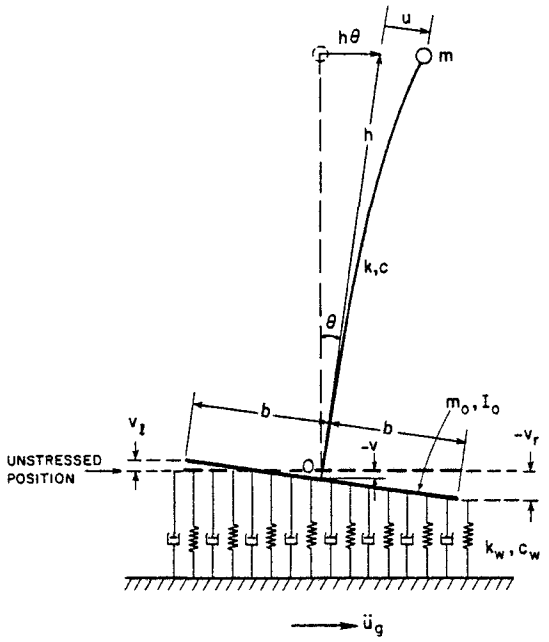

Fig. 1 Flexible Structure on Winkler Foundation.

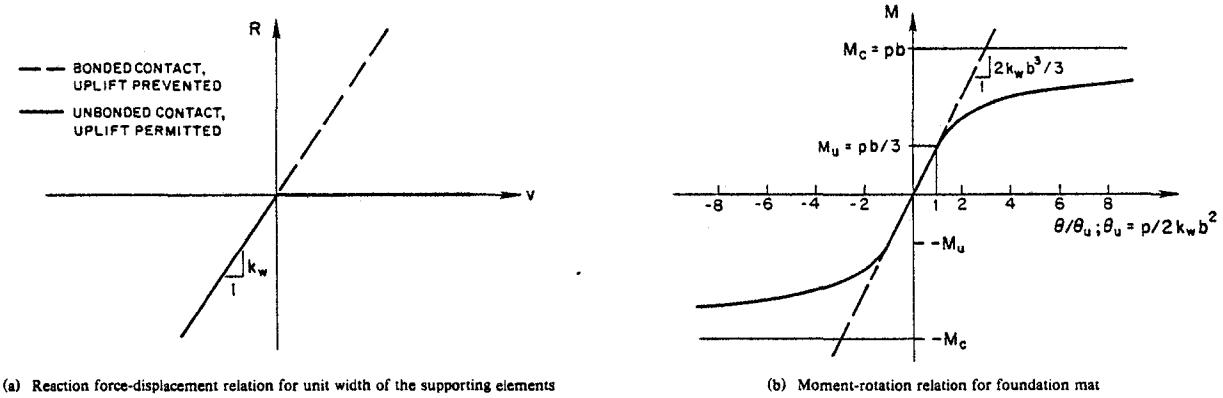

(a) Reaction force-displacement relation for unit width of the supporting elements

(b) Moment-rotation relation for foundation mat

Fig. 2 Properties of Winkler Foundation.

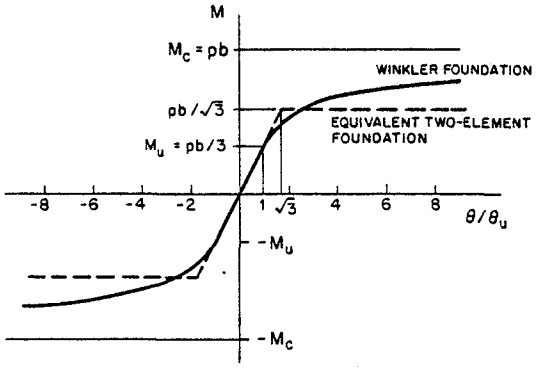

Fig. 3 Moment-rotation Relations for Foundation Mat on Winkler Foundation and on Equivalent Two-element Foundation.

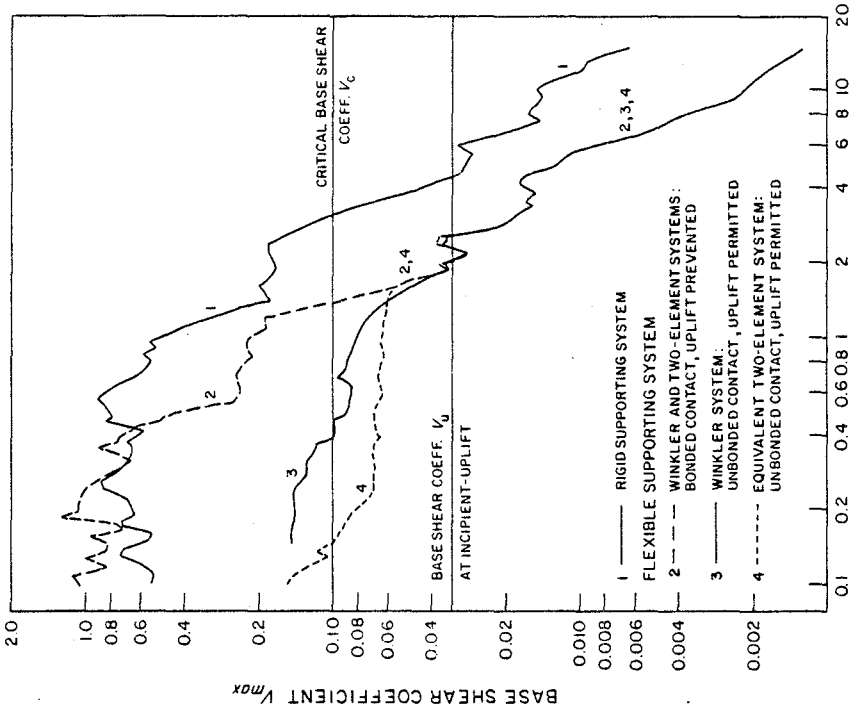

Fig. 5 Response Spectra for Structures Subjected to El Centro Ground Motion for Four Support Conditions.

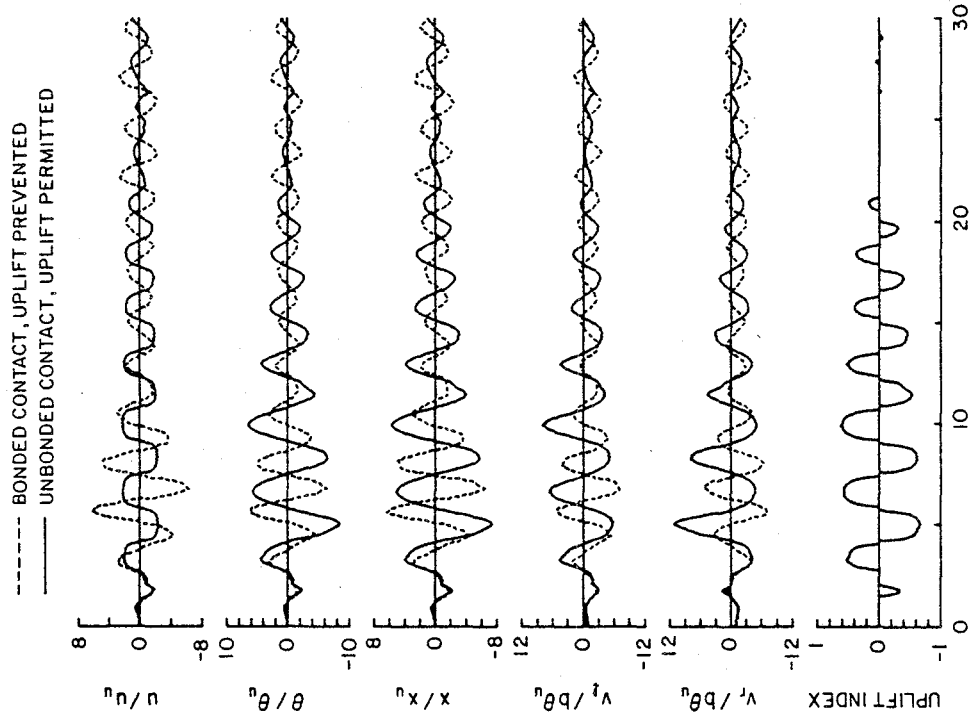

Fig. 4 Response of a Structure to El Centro Ground Motion for Two Conditions of Contact Between the Foundation Mat and the Supporting Elements.

IMPLICATIONS OF DAMAGES TO THE IMPERIAL COUNTY SERVICES BUILDING FOR EARTHQUAKE-RESISTANT DESIGN

Christos A. Zeris (I)
Rodrigo Altmann (II)
Presenting Author:Christos A. Zeris

SUMMARY

The Imperial County Services Building located in El Centro, California was severely damaged during the 6.6 Richter magnitude Imperial Valley earthquake of October 15, 1979. Considerable information was recovered from sixteen accelerographs located in and near the building providing a unique opportunity for evaluating the reliability of present methods for predicting the seismic response of this type of buildings as well as for assessing the soundness of modern code seismic provisions. Correlation studies conducted for this purpose are briefly presented and the main results obtained are examined.

INTRODUCTION

The Imperial County Services Building (ICSB) was a modern six story, reinforced concrete office structure severely damaged during the 1979 Imperial Valley earthquake. The severity of the damage and the availability of reliable acceleration response records (Ref.1) motivated researchers at the University of California, Berkeley to initiate a comprehensive program of field, laboratory experimental and analytical investigations. The main objectives of this paper are to report some of the results of this investigation related to an assessement of (a) the reliability of analytical means for predicting the response of this type of buildings, (b) the suitability of the particular system used in resisting motions similar to those recorded and (c) the adequacy of the seismic provisions used in the design, as well as those of present codes. In order to achieve these objectives different stuctural models are analyzed with a linear analysis program and the results are compared to those obtained from the recorded accelerations.

DESCRIPTION OF THE BUILDING AND STRUCTURAL RESPONSE

The ICSB was rectangular in plan, having five bays in the East-West (EW) and three bays in the North-South (NS) direction (Fig.1,14). It was designed according to the Uniform Building Code (UBC) 1967. The lateral force resisting system consisted of moment resisting frames in the EW direction and shear walls in the NS direction. A characteristic feature of this structure was that the shear walls provided at the East and West ends (over the full width) were discontinued; lateral resistance in the ground story was provided by four narrower walls (Fig.2, Ref.2). For the design a base shear coefficient (C) of 0.059 was used in conjunction with three K factors: 1.33 for the NS shear wall system, 1.00 for the EW exterior frames (non-ductile) and 0.67 for the EW interior frames (ductile). Other important features were the use of deep

(I) Research Assistant, University of California, Berkeley
(II) Structural Engineer,San Jose,Costa Rica

"nonstructural" reinforced concrete panels above the beams on the N and S facades and the bar offset detailing in the ground story columns (Fig.5). The building was founded on pile groups.

Primary damages to the structure consisted of: (a) spalling of the cover (with buckling of the longitudinal reinforcement also observed) above the base of most ground story columns, accentuated at those in line G. The crushing of these regions led to shortening of these columns by one foot (Fig.4,9). (b) Formation of yield lines along the width of the building at lines F and G (Fig.1) due to the G column shortening. (c) Flexural cracking of the exterior beams mainly in the lower floors. (d) Non-structural damage with separation of the nonstructural elements from the structure especially near lines F and G. (e) Diagonal and horizontal cracking of the walls at ground level, those at frames F and E being more heavily damaged than at B and D (Fig.1).

The building was instrumented with thirteen accelerometers (Fig.2), with an additional triaxial recorder 300' away to monitor the free field response; four instruments located at ground level were used to deduce two translational and a torsional component of input motion. The peak ground acceleration was 0.32g. However one special characteristic of the record was a 0.23g pulse of more than one second duration (Fig.3), influencing significantly the building response.

EXPERIMENTAL AND ANALYTICAL INVESTIGATIONS

Tests performed on steel and concrete samples removed from the building revealed that materials (particularly the concrete) were stronger than nominally specified (Table 1 and Ref.3). Based on the measured material mechanical characteristics, realistic member nonlinear characteristics and capacities were determined. Cracked flexural beam stiffnesses were about 50% of the gross section stiffnesses. However, in the case of the exterior beams, the cracked flexural stiffness was doubled if the contribution of the nonstructural elements was included; consideration also of the slab reinforcement increased significantly the beam flexural capacities (Fig.6). Motivated by the localized damage of the ground columns above the recess (Fig.4,5,9), the effect of detailing on the flexural characteristics of the columns were estimated (Ref.4) - namely the reductions in confinement (Fig.7) and in load bearing capacity of the offset reinforcing bar due to buckling (Fig. 7,8).

Three dimensional models of the ICSB were formulated and analyzed elastically using ETABS (Ref.5), extended so that two translational and one torsional components of earthquake could be prescribed independently. Two additional stories were added to the models to account for the rocking of the building. Beam,column and panel elements were used. An inherent assumption of the program is the use of in plane rigid diaphragms. However analysis (Ref.6) of the building using flexible floors showed that as a result of this simplification the dynamic characteristics of the model significantly differed from those determined by the ambient vibration tests. It is believed that this assumption is acceptable for the small amplitude phase of the motion, for which the elastic analysis is valid.

By comparing (a) the model periods of vibration to the ambient test results before the earthquake (Ref.7) and (b) the predicted and recorded responses, the reliability of the model was evaluated. The sensitivity of the

response to the modeling assumptions of using gross versus cracked member properties, true versus nominal strengths of the materials and including the effects of the nonstructural elements was investigated (Table 2,Ref.4). The variability observed is typical of moment resisting frames (Ref.8). From this analysis it was concluded that the most reliable model was the one based on the use of the cracked flexural properties for the elements and included the contribution of the deep nonstructural beams (Model 3, Table 2); the periods for the first three modes correlate well to those obtained by inspection of the records (Ref.1,9) or by frequency domain analysis of the response (Ref.10), but do not correlate well to those obtained from ambient tests; small amplitude ambient tests may overestimate the stiffness of concrete structures relative to their resistance after cracking. The model (No 3, Table 2) was analyzed separately for two different combinations of site recorded ground motions: (a) the two translational and the rotational component applied simultaneously and (b) the EW translational component, to evaluate the significance of the NS and torsional components (Ref.4).

As illustrated in Fig.(10), the correlation of the recorded and the predicted displacements is satisfactory until 6.20 seconds, with minor deviations until the 6.90 sec., when a change in the recorded response is observed; subsequent peaks exceed the elastically predicted ones by a factor of two. By comparing the true member capacities with the predicted demands the sequence of failure is estimated to be: (a) separation of the "nonstructural" elements from the frames around 6.0 seconds and subsequent yielding of the exterior beams in bending at the second and third floor at 6.40 seconds (Fig.10). (b) Probable yielding of the interior second floor beams, between 6.40 and 6.90 seconds. (c) Yielding of the ground level columns at their base (Fig.12) and subsequent large displacements above the second story.

CONCLUSIONS AND RECOMMENDATIONS

From the results of the studies conducted on the ICSB the following conclusions can be drawn, regarding the building's response during the earthquake and its compliance to codes:

The concrete strengths obtained from the tests were considerably higher than the specified especially for the lower strength concrete. The only exception being the concrete at the ground level columns on line G which was significantly weaker than the other columns' concrete. (Table 1,Ref.3,11).

The design calculations were checked and found in essential agreement with the the UBC 1967 used in design (Ref.3). The detailing of the building was consistent with the system adopted; some additional details were implemented in design to provide limited ductility in the outer frames. Design details not in accordance with present UBC (1982) requirements were: (a) the use of non-uniform tie distribution with spacing larger than code requirements at the ground story columns supporting discontinuous walls, (b) the use of non-ductile perimeter frames in moment-resisting frame systems, (c) the amount of vertical reinforcement used in the end walls above the second story is smaller than the required minimum and (d) reduced ultimate moment capacities were used to estimate maximum shear demands in flexural members.

Although the analysis showed that recorded ground motions exceeded those for which the building was designed to remain elastic, most of the damage was

a consequence of poor conceptual design, the main drawbacks being:

(a) The character of the ground motion was such that all ground columns yielded irrespective of applied axial force, in EW response. However, post-yield behavior for the corner columns in particular was adversely affected by the wall discontinuity which introduced high compressive axial forces due to the overturning of the supported walls in the NS direction. This simultaneous action demanded from these columns a ductility they could not provide due to the poor detailing.

(b) Specifying offset reinforcement and a reduced confinement in the columns at ground level (Fig.5), reduced their deformability under maximum axial strength considerably. The observed localized damage at the ground story was further enhanced by: (1) significant strengthening of the second floor beams not accounted in code design, accentuated by the presence of the heavily reinforced slab; (2) the presence of the concrete ground slab between lines 2 and 3 (Fig.1) at ground level restraining the columns above the analytically assumed column bases reducing their effective clear height. On the whole, the high rigidity of the structure above the second story due to the presence of the deep nonstructural girders, and the absence of EW shear walls at ground level tended to concentrate the lateral displacements at the ground story enhancing the behavior of a soft story structure, a system that has proved inadequate in similar near-field earthquakes (Ref.12).

(c) The absence of a shear wall at ground floor in G in the NS direction resulted in the one foot shortening of the East end and the formation of a yield line mechanism at F and G (Fig.1). As determined analytically, the West end columns (B, Fig.1) were equally heavily loaded axially as the columns at G; however, one of the reasons they did not suffer the extensive damage of the latter was because of the presence of the wall in the center span of bay B.

(d) The analysis revealed a prominent contribution of torsion, which due to the structural layout was coupled to the NS translational response. This torsional motion, together with the imposed rotational component of the ground motion induced in the East end ground walls higher shear forces than those at the West end (Fig.12), as well as significant biaxial bending to all four corner columns, reducing even further their resistance.

(e) The presence of the nonstructural elements affected the dynamic characteristics and the performance of the EW system. Analytical studies showed that the lateral stiffness and therefore the periods of the building were very sensitive to the interaction of the frames with these elements. From correlations of displacement and force time histories, the nonstructural elements were believed to significantly contribute up to about 6.0 seconds, when their connections with the structure weakened considerably.

Based on the observed performance of the building, and the analytically predicted response the following are recommended:

1) The use of non-continuous shear walls supported on columns, especially for columns positioned at the edges of the structure should be discouraged. If this particular system is used, well-confined columns especially by closely spaced spiral reinforcement should be employed, to ensure ductile behavior.

2) Stringer detailing requirements and rational design of perimeter members should be implemented, accounting for all factors such as material overstrength, boundary condition restraints and biaxial bending.

3) In column design the effects of all components of the ground motion

acting simultaneously should be taken into account.

4) More severe restrictions on the detailing and careful field inspection during construction of reinforcement offsets and similar details are encouraged.

5) The use of structural systems consisting of frames with different ability of ductile deformation, acting in the same direction of lateral resistance should be discouraged. As was observed in this particular case, since the response of the building required all EW frames to displace equally, the exterior semiductile and stiffer frames had to supply more ductility than the interior ductile frames; this additional ductility they were unable to provide, leading to the system's overall nonductile failure observed.

ACKNOWLEDGEMENTS

The authors are grateful to Project Supervisors S.A. Mahin and V.V. Bertero, Professors of Civil Engineering at the University of California, Berkeley, for their valuable assistance throughout this study. The funding by the National Science Foundation is gratefully acknowledged. We are also indebted to C. Rojahn and P. Mork for the ground motions, and to Structural Software Development for providing part of the software.

REFERENCES

[1] Rojahn C. and Mork P.N.,"An Analysis of Strong Motion Data From a Severely Damaged Structure,the ICSB,El Centro,California",U.S.G.S., Rep.81-194,Menlo Park,California.
[2] Altmann R.,"Elastic Time History Analysis of the ICSB Seismic Performance", Grad. Res. Rep.,Univ. of California,Berkeley,July 1982.
[3] Allawh N.,"A Study of the Behavior of the ICSB During the 1979 Imperial Valley Earthquake",Grad. Res. Rep.,Univ. of California,Berkeley,1981.
[4] Zeris C.A.,Altmann R.,Mahin S.A. and Bertero V.V.,"Response of the ICSB During the Imperial Valley Earthquake",EERC Rep. in preparation,Univ.of Calif.,Berkeley.
[5] Wilson E.L.,Hollings J.P. and Dovey H.H.,"Three Dimensional Analysis of Building Systems",Rep. No EERC 75-13,Univ. of Calif.,Berkeley,1975.
[6] Jain S.K.,"Analytical Models for the Dynamics of Buildings",Rep. No EERL 83-02, California Institute of Technology,Pasadena Calif.,May 1983.
[7] Pardoen G.,"ICSB. Ambient Vibration Test Results",Res. Rep. No 79-14,Univ. of Canterburry,New Zealand,Dec. 1979.
[8] Brokken S. and Bertero V.V.,"Studies on Effects of Infills in Seismic Resistant Reinforced Concrete Construction",Rep. No EERC 81-12,Univ. of Calif.,Berkeley,Sept.1981.
[9] Housner G.W. and Jennings P.C.,"Earthquake Design Criteria",Earth. Eng. Res. Inst., Engineering Monographs,vol.4,Sept. 1982,pp.112-118.
[10] Pauschke J.M. et al.,"A Preliminary Investigation of the Dynamic Behavior of the ICSB During the October 15, 1979 Imperial Valley Earthquake", Stanford Univ.,Rep. No 49,Jan. 1981.
[11] Selna L.G. and Boyens R.D.,"Performance of the ICSB, El Centro",Proc.,Ann. Conv. of SEAOC,Monterey 1980,pp. 37-68.
[12] Mahin S.A.,Bertero V.V.,Chopra A.K. and Collins R.G.,"Response of the Olive View Hospital Main Building During the San Fernando Earthquake",Rep. No EERC 76-22, Univ. of Calif.,Berkeley, Oct. 1976.

TABLE 1. ICSB Concrete Test Results			
Specified Nominal f_c,psi	Location	Measured f_c,psi	
		at 28 Days	after EQ
3000	Tie Beams, Ground Slab	-	8820
4000	Beams, Joists	4656	5950
5000	All columns	5695	7020
	G Line, Ground Level		5630

TABLE 2. Sensitivity of Model Periods							
Case	Properties	Material	Non Str.	Columns	Periods,sec.		
					EW	NS	Rot.
1	Gross Section 100%	Nominal	Yes	Elastic	0.66	0.39	0.33
2	Gross Section 70%	Nominal	No	Elastic	0.88	0.40	0.32
3	Gross Section 70%	Nominal	No	Pinned	0.99	0.46	0.38
4	Cracked Section	True	Yes	Elastic	0.94	0.44	0.37
5	Cracked Section	True	Yes (Wall)	Elastic	0.83	0.44	0.36
6	Cracked Section	True	No	Pinned	1.16	0.45	0.39
7	Cracked Section	True	Yes (Wall)	Pinned	0.78	0.48	0.37
8	Averaged	Average	Yes (Wall)	Elastic	0.72	0.44	0.36
9	Ambient(Ref.6) Pre Earthquake Post Earthquake				 0.65 0.83	 0.45 0.52	 0.36 -
10	Observed (Ref.1,9)				1.00	0.50	-

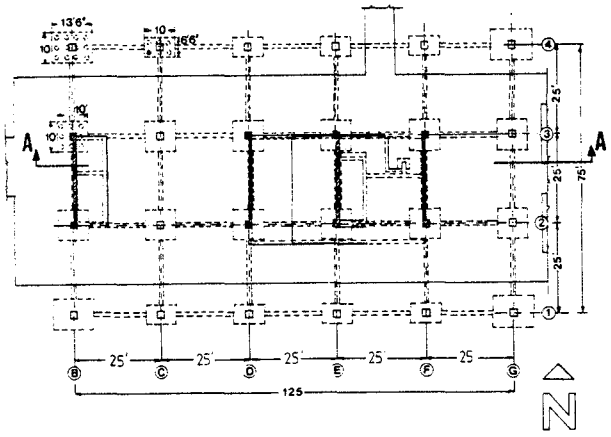

Fig. 1 ICSB Ground Level and Foundation Plan

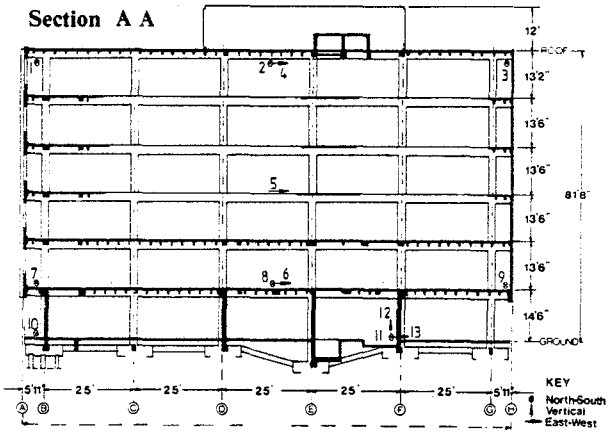

Fig. 2 Elevation and Instrument Location

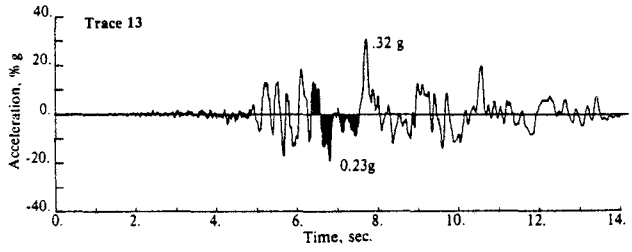

Fig. 3 Ground Motion, EW Direction

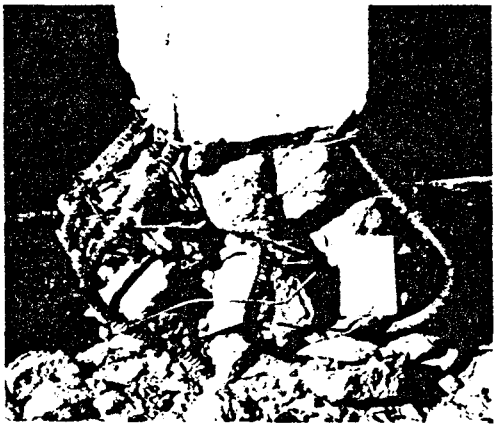

Fig. 4 Detail of Column G4 Failure

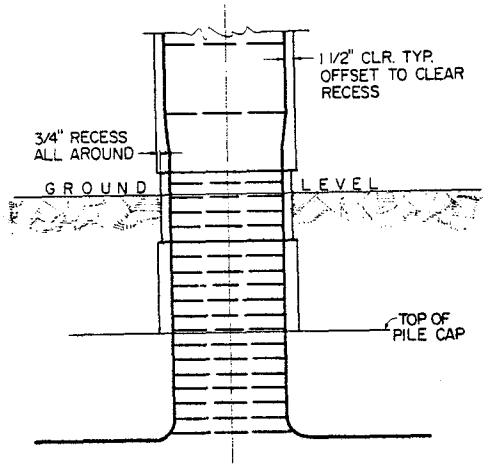

Fig. 5 Typical Ground Corner Column Detail

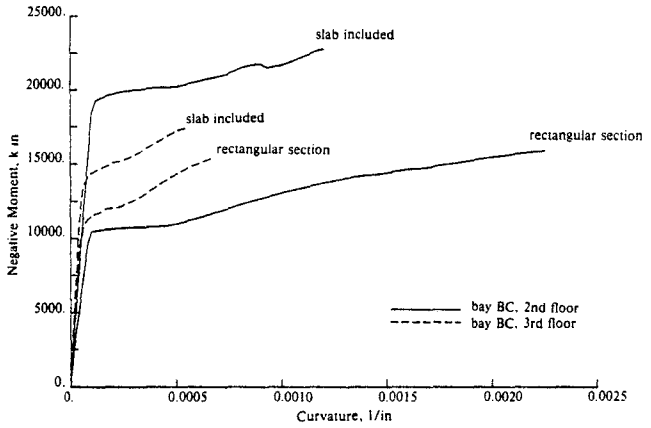

Fig. 6 Typical Exterior Beam Nonlinear Characteristics

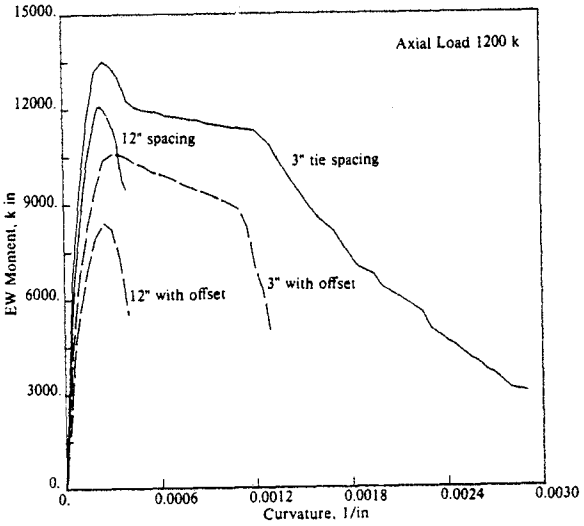

Fig. 7 Influence of Ground Column Detailing

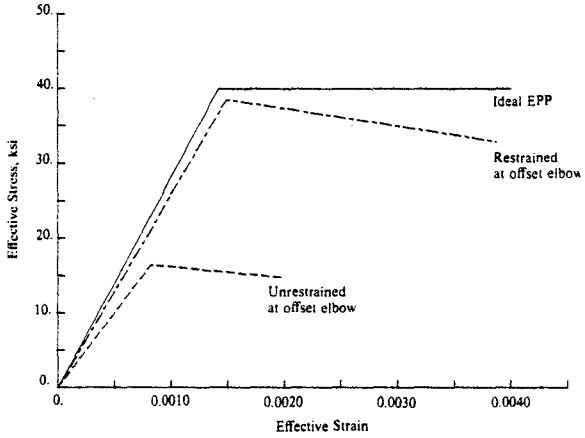

Fig. 8 Offset Bar Behavior

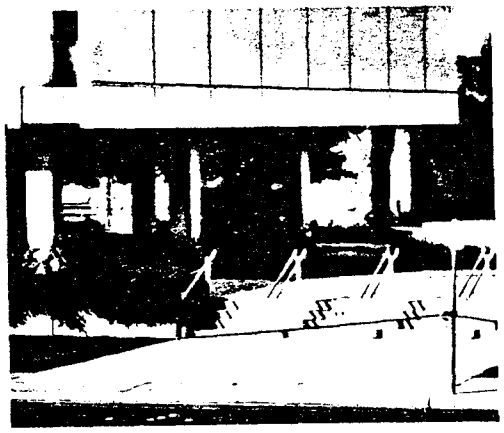

Fig. 9 Damage of G Column Line, Ground Level

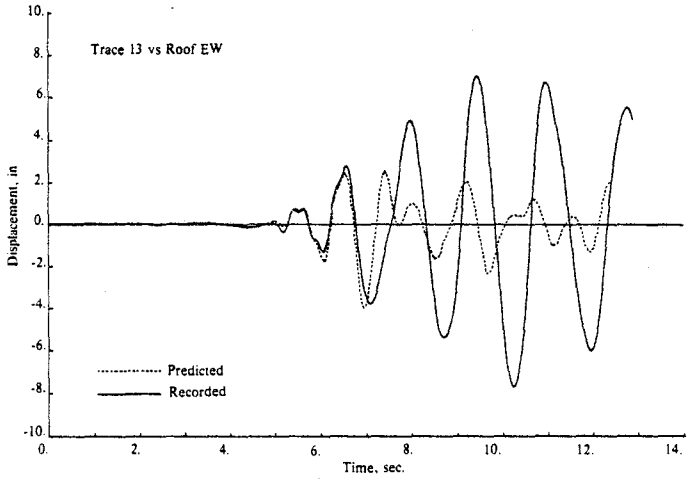

Fig.10 Comparison of Predicted and Recorded Displacements

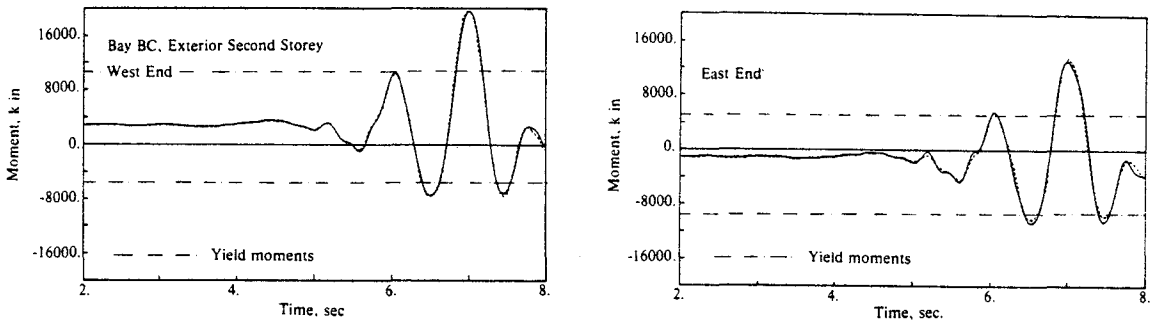

Fig. 11 Typical Beam Moment History

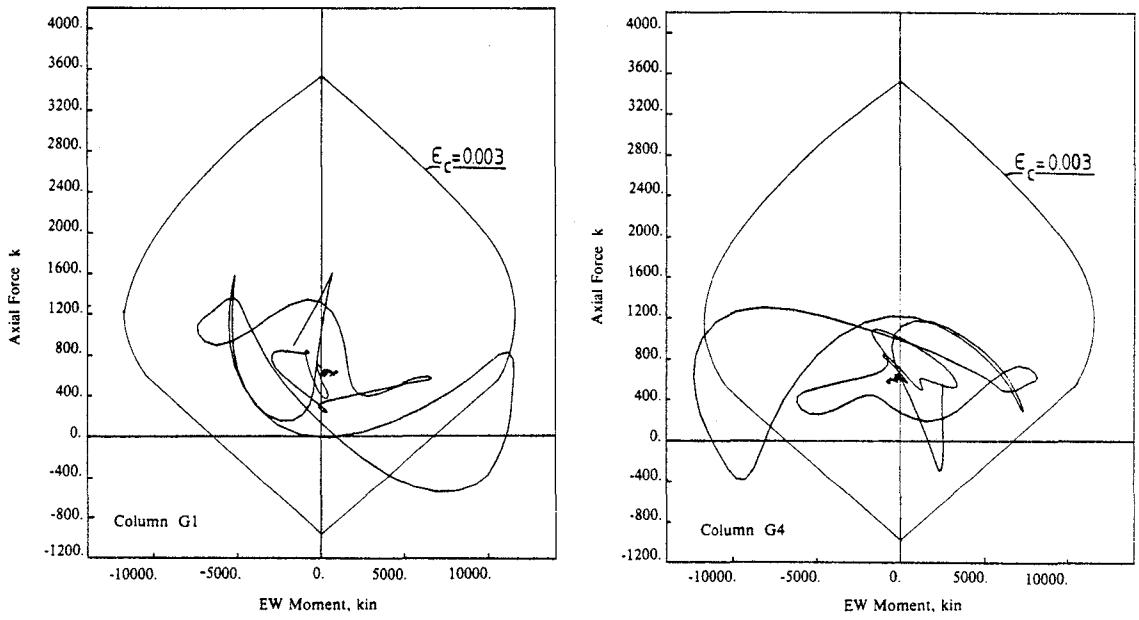

Fig. 12 Predicted Load Paths of Ground Corner Columns

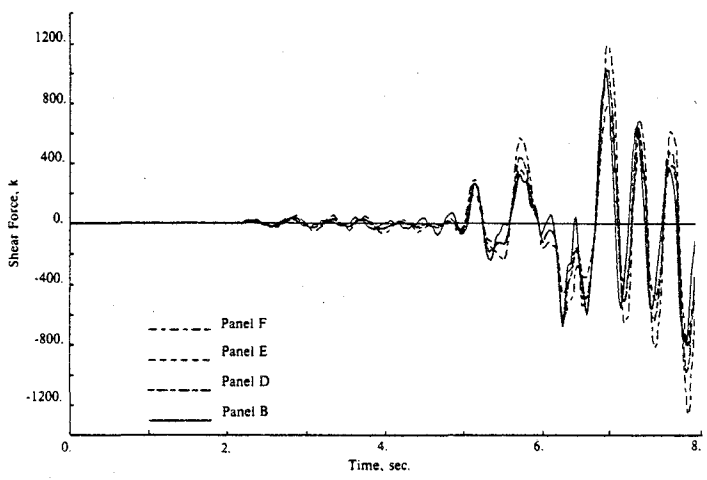

Fig. 13 Ground Walls Shear Force History

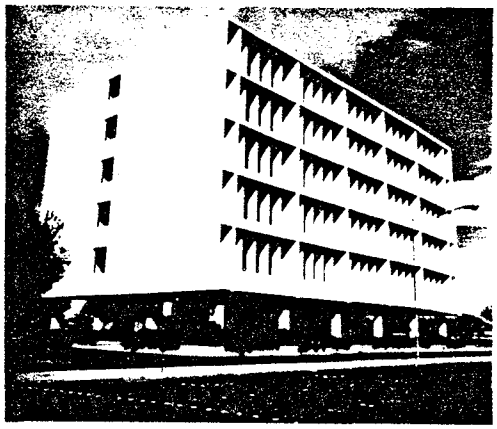

Fig. 14 View of the Imperial County Services Building, from SW

EARTHQUAKE ENGINEERING RESEARCH CENTER REPORTS

NOTE: Numbers in parenthesis are Accession Numbers assigned by the National Technical Information Service; these are followed by a price code. Copies of the reports may be ordered from the National Technical Information Service, 5285 Port Royal Road, Springfield, Virginia, 22161. Accession Numbers should be quoted on orders for reports (PB --- ---) and remittance must accompany each order. Reports without this information were not available at time of printing. Upon request, EERC will mail inquirers this information when it becomes available.

EERC 67-1 "Feasibility Study Large-Scale Earthquake Simulator Facility," by J. Penzien, J.G. Bouwkamp, R.W. Clough and D. Rea - 1967 (PB 187 905)A07

EERC 68-1 Unassigned

EERC 68-2 "Inelastic Behavior of Beam-to-Column Subassemblages Under Repeated Loading," by V.V. Bertero - 1968 (PB 184 888)A05

EERC 68-3 "A Graphical Method for Solving the Wave Reflection-Refraction Problem," by H.D. McNiven and Y. Mengi - 1968 (PB 187 943)A03

EERC 68-4 "Dynamic Properties of McKinley School Buildings," by D. Rea, J.G. Bouwkamp and R.W. Clough - 1968 (PB 187 902)A07

EERC 68-5 "Characteristics of Rock Motions During Earthquakes," by H.B. Seed, I.M. Idriss and F.W. Kiefer - 1968 (PB 188 338)A03

EERC 69-1 "Earthquake Engineering Research at Berkeley," - 1969 (PB 187 906)A11

EERC 69-2 "Nonlinear Seismic Response of Earth Structures," by M. Dibaj and J. Penzien - 1969 (PB 187 904)A08

EERC 69-3 "Probabilistic Study of the Behavior of Structures During Earthquakes," by R. Ruiz and J. Penzien - 1969 (PB 187 886)A06

EERC 69-4 "Numerical Solution of Boundary Value Problems in Structural Mechanics by Reduction to an Initial Value Formulation," by N. Distefano and J. Schujman - 1969 (PB 187 942)A02

EERC 69-5 "Dynamic Programming and the Solution of the Biharmonic Equation," by N. Distefano - 1969 (PB 187 941)A03

EERC 69-6 "Stochastic Analysis of Offshore Tower Structures," by A.K. Malhotra and J. Penzien - 1969 (PB 187 903)A09

EERC 69-7 "Rock Motion Accelerograms for High Magnitude Earthquakes," by H.B. Seed and I.M. Idriss - 1969 (PB 187 940)A02

EERC 69-8 "Structural Dynamics Testing Facilities at the University of California, Berkeley," by R.M. Stephen, J.G. Bouwkamp, R.W. Clough and J. Penzien - 1969 (PB 189 111)A04

EERC 69-9 "Seismic Response of Soil Deposits Underlain by Sloping Rock Boundaries," by H. Dezfulian and H.B. Seed 1969 (PB 189 114)A03

EERC 69-10 "Dynamic Stress Analysis of Axisymmetric Structures Under Arbitrary Loading," by S. Ghosh and E.L. Wilson 1969 (PB 189 026)A10

EERC 69-11 "Seismic Behavior of Multistory Frames Designed by Different Philosophies," by J.C. Anderson and V. V. Bertero - 1969 (PB 190 662)A10

EERC 69-12 "Stiffness Degradation of Reinforcing Concrete Members Subjected to Cyclic Flexural Moments," by V.V. Bertero, B. Bresler and H. Ming Liao - 1969 (PB 202 942)A07

EERC 69-13 "Response of Non-Uniform Soil Deposits to Travelling Seismic Waves," by H. Dezfulian and H.B. Seed - 1969 (PB 191 023)A03

EERC 69-14 "Damping Capacity of a Model Steel Structure," by D. Rea, R.W. Clough and J.G. Bouwkamp - 1969 (PB 190 663)A06

EERC 69-15 "Influence of Local Soil Conditions on Building Damage Potential during Earthquakes," by H.B. Seed and I.M. Idriss - 1969 (PB 191 036)A03

EERC 69-16 "The Behavior of Sands Under Seismic Loading Conditions," by M.L. Silver and H.B. Seed - 1969 (AD 714 982)A07

EERC 70-1 "Earthquake Response of Gravity Dams," by A.K. Chopra - 1970 (AD 709 640)A03

EERC 70-2 "Relationships between Soil Conditions and Building Damage in the Caracas Earthquake of July 29, 1967," by H.B. Seed, I.M. Idriss and H. Dezfulian - 1970 (PB 195 762)A05

EERC 70-3 "Cyclic Loading of Full Size Steel Connections," by E.P. Popov and R.M. Stephen - 1970 (PB 213 545)A04

EERC 70-4 "Seismic Analysis of the Charaima Building, Caraballeda, Venezuela," by Subcommittee of the SEAONC Research Committee: V.V. Bertero, P.F. Fratessa, S.A. Mahin, J.H. Sexton, A.C. Scordelis, E.L. Wilson, L.A. Wyllie, H.B. Seed and J. Penzien, Chairman - 1970 (PB 201 455)A06

EERC 70-5 "A Computer Program for Earthquake Analysis of Dams," by A.K. Chopra and P. Chakrabarti - 1970 (AD 723 994)A05

EERC 70-6 "The Propagation of Love Waves Across Non-Horizontally Layered Structures," by J. Lysmer and L.A. Drake 1970 (PB 197 896)A03

EERC 70-7 "Influence of Base Rock Characteristics on Ground Response," by J. Lysmer, H.B. Seed and P.B. Schnabel 1970 (PB 197 897)A03

EERC 70-8 "Applicability of Laboratory Test Procedures for Measuring Soil Liquefaction Characteristics under Cyclic Loading," by H.B. Seed and W.H. Peacock - 1970 (PB 198 016)A03

EERC 70-9 "A Simplified Procedure for Evaluating Soil Liquefaction Potential," by H.B. Seed and I.M. Idriss - 1970 (PB 198 009)A03

EERC 70-10 "Soil Moduli and Damping Factors for Dynamic Response Analysis," by H.B. Seed and I.M. Idriss - 1970 (PB 197 869)A03

EERC 71-1 "Koyna Earthquake of December 11, 1967 and the Performance of Koyna Dam," by A.K. Chopra and P. Chakrabarti 1971 (AD 731 496)A06

EERC 71-2 "Preliminary In-Situ Measurements of Anelastic Absorption in Soils Using a Prototype Earthquake Simulator," by R.D. Borcherdt and P.W. Rodgers - 1971 (PB 201 454)A03

EERC 71-3 "Static and Dynamic Analysis of Inelastic Frame Structures," by F.L. Porter and G.H. Powell - 1971 (PB 210 135)A06

EERC 71-4 "Research Needs in Limit Design of Reinforced Concrete Structures," by V.V. Bertero - 1971 (PB 202 943)A04

EERC 71-5 "Dynamic Behavior of a High-Rise Diagonally Braced Steel Building," by D. Rea, A.A. Shah and J.G. Bouwkamp 1971 (PB 203 584)A06

EERC 71-6 "Dynamic Stress Analysis of Porous Elastic Solids Saturated with Compressible Fluids," by J. Ghaboussi and E. L. Wilson - 1971 (PB 211 396)A06

EERC 71-7 "Inelastic Behavior of Steel Beam-to-Column Subassemblages," by H. Krawinkler, V.V. Bertero and E.P. Popov 1971 (PB 211 335)A14

EERC 71-8 "Modification of Seismograph Records for Effects of Local Soil Conditions," by P. Schnabel, H.B. Seed and J. Lysmer - 1971 (PB 214 450)A03

EERC 72-1 "Static and Earthquake Analysis of Three Dimensional Frame and Shear Wall Buildings," by E.L. Wilson and H.H. Dovey - 1972 (PB 212 904)A05

EERC 72-2 "Accelerations in Rock for Earthquakes in the Western United States," by P.B. Schnabel and H.B. Seed - 1972 (PB 213 100)A03

EERC 72-3 "Elastic-Plastic Earthquake Response of Soil-Building Systems," by T. Minami - 1972 (PB 214 868)A08

EERC 72-4 "Stochastic Inelastic Response of Offshore Towers to Strong Motion Earthquakes," by M.K. Kaul - 1972 (PB 215 713)A05

EERC 72-5 "Cyclic Behavior of Three Reinforced Concrete Flexural Members with High Shear," by E.P. Popov, V.V. Bertero and H. Krawinkler - 1972 (PB 214 555)A05

EERC 72-6 "Earthquake Response of Gravity Dams Including Reservoir Interaction Effects," by P. Chakrabarti and A.K. Chopra - 1972 (AD 762 330)A08

EERC 72-7 "Dynamic Properties of Pine Flat Dam," by D. Rea, C.Y. Liaw and A.K. Chopra - 1972 (AD 763 928)A05

EERC 72-8 "Three Dimensional Analysis of Building Systems," by E.L. Wilson and H.H. Dovey - 1972 (PB 222 438)A06

EERC 72-9 "Rate of Loading Effects on Uncracked and Repaired Reinforced Concrete Members," by S. Mahin, V.V. Bertero, D. Rea and M. Atalay - 1972 (PB 224 520)A08

EERC 72-10 "Computer Program for Static and Dynamic Analysis of Linear Structural Systems," by E.L. Wilson, K.-J. Bathe, J.E. Peterson and H.H.Dovey - 1972 (PB 220 437)A04

EERC 72-11 "Literature Survey - Seismic Effects on Highway Bridges," by T. Iwasaki, J. Penzien and R.W. Clough - 1972 (PB 215 613)A19

EERC 72-12 "SHAKE-A Computer Program for Earthquake Response Analysis of Horizontally Layered Sites," by P.B. Schnabel and J. Lysmer - 1972 (PB 220 207)A06

EERC 73-1 Unassigned

EERC 73-2 "Analysis of the Slides in the San Fernando Dams During the Earthquake of February 9, 1971," by H.B. Seed, K.L. Lee, I.M. Idriss and F. Makdisi - 1973 (PB 223 402)A14

EERC 73-3 "Computer Aided Ultimate Load Design of Unbraced Multistory Steel Frames," by M.B. El-Hafez and G.H. Powell 1973 (PB 248 315)A09

EERC 73-4 "Experimental Investigation into the Seismic Behavior of Critical Regions of Reinforced Concrete Components as Influenced by Moment and Shear," by M. Celebi and J. Penzien - 1973 (PB 215 884)A09

EERC 73-5 "Hysteretic Behavior of Epoxy-Repaired Reinforced Concrete Beams," by M. Celebi and J. Penzien - 1973 (PB 239 568)A03

EERC 73-6 "General Purpose Computer Program for Inelastic Dynamic Response of Plane Structures," by A. Kanaan and G.H. Powell - 1973 (PB 221 260)A08

EERC 73-7 "A Computer Program for Earthquake Analysis of Gravity Dams Including Reservoir Interaction," by P. Chakrabarti and A.K. Chopra - 1973 (AD 766 271)A04

EERC 73-8 "Behavior of Reinforced Concrete Deep Beam-Column Subassemblages Under Cyclic Loads," by O. Küstü and J.G. Bouwkamp - 1973 (PB 246 117)A12

EERC 73-9 "Earthquake Analysis of Structure-Foundation Systems," by A.K. Vaish and A.K. Chopra - 1973 (AD 766 272)A07

EERC 73-10 "Deconvolution of Seismic Response for Linear Systems," by R.B. Reimer - 1973 (PB 227 179)A08

EERC 73-11 "SAP IV: A Structural Analysis Program for Static and Dynamic Response of Linear Systems," by K.-J. Bathe, E.L. Wilson and F.E. Peterson - 1973 (PB 221 967)A09

EERC 73-12 "Analytical Investigations of the Seismic Response of Long, Multiple Span Highway Bridges," by W.S. Tseng and J. Penzien - 1973 (PB 227 816)A10

EERC 73-13 "Earthquake Analysis of Multi-Story Buildings Including Foundation Interaction," by A.K. Chopra and J.A. Gutierrez - 1973 (PB 222 970)A03

EERC 73-14 "ADAP: A Computer Program for Static and Dynamic Analysis of Arch Dams," by R.W. Clough, J.M. Raphael and S. Mojtahedi - 1973 (PB 223 763)A09

EERC 73-15 "Cyclic Plastic Analysis of Structural Steel Joints," by R.B. Pinkney and R.W. Clough - 1973 (PB 226 843)A08

EERC 73-16 "QUAD-4: A Computer Program for Evaluating the Seismic Response of Soil Structures by Variable Damping Finite Element Procedures," by I.M. Idriss, J. Lysmer, R. Hwang and H.B. Seed - 1973 (PB 229 424)A05

EERC 73-17 "Dynamic Behavior of a Multi-Story Pyramid Shaped Building," by R.M. Stephen, J.P. Hollings and J.G. Bouwkamp - 1973 (PB 240 718)A06

EERC 73-18 Unassigned

EERC 73-19 "Olive View Medical Center Materials Studies, Phase I," by B. Bresler and V.V. Bertero - 1973 (PB 235 986)A06

EERC 73-20 Unassigned

EERC 73-21 "Constitutive Models for Cyclic Plastic Deformation of Engineering Materials," by J.M. Kelly and P.P. Gillis 1973 (PB 226 024)A03

EERC 73-22 "DRAIN - 2D User's Guide," by G.H. Powell - 1973 (PB 227 016)A05

EERC 73-23 "Earthquake Engineering at Berkeley - 1973," (PB 226 033)A11

EERC 73-24 Unassigned

EERC 73-25 "Earthquake Response of Axisymmetric Tower Structures Surrounded by Water," by C.Y. Liaw and A.K. Chopra 1973 (AD 773 052)A09

EERC 73-26 "Investigation of the Failures of the Olive View Stairtowers During the San Fernando Earthquake and Their Implications on Seismic Design," by V.V. Bertero and R.G. Collins - 1973 (PB 235 106)A13

EERC 73-27 "Further Studies on Seismic Behavior of Steel Beam-Column Subassemblages," by V.V. Bertero, H. Krawinkler and E.P. Popov - 1973 (PB 234 172)A06

EERC 74-1 "Seismic Risk Analysis," by C.S. Oliveira - 1974 (PB 235 920)A06

EERC 74-2 "Settlement and Liquefaction of Sands Under Multi-Directional Shaking," by R. Pyke, C.K. Chan and H.B. Seed 1974

EERC 74-3 "Optimum Design of Earthquake Resistant Shear Buildings," by D. Ray, K.S. Pister and A.K. Chopra - 1974 (PB 231 172)A06

EERC 74-4 "LUSH - A Computer Program for Complex Response Analysis of Soil-Structure Systems," by J. Lysmer, T. Udaka, H.B. Seed and R. Hwang - 1974 (PB 236 796)A05

EERC 74-5 "Sensitivity Analysis for Hysteretic Dynamic Systems: Applications to Earthquake Engineering," by D. Ray 1974 (PB 233 213)A06

EERC 74-6 "Soil Structure Interaction Analyses for Evaluating Seismic Response," by H.B. Seed, J. Lysmer and R. Hwang 1974 (PB 236 519)A04

EERC 74-7 Unassigned

EERC 74-8 "Shaking Table Tests of a Steel Frame - A Progress Report," by R.W. Clough and D. Tang - 1974 (PB 240 869)A03

EERC 74-9 "Hysteretic Behavior of Reinforced Concrete Flexural Members with Special Web Reinforcement," by V.V. Bertero, E.P. Popov and T.Y. Wang - 1974 (PB 236 797)A07

EERC 74-10 "Applications of Reliability-Based, Global Cost Optimization to Design of Earthquake Resistant Structures," by E. Vitiello and K.S. Pister - 1974 (PB 237 231)A06

EERC 74-11 "Liquefaction of Gravelly Soils Under Cyclic Loading Conditions," by R.T. Wong, H.B. Seed and C.K. Chan 1974 (PB 242 042)A03

EERC 74-12 "Site-Dependent Spectra for Earthquake-Resistant Design," by H.B. Seed, C. Ugas and J. Lysmer - 1974 (PB 240 953)A03

EERC 74-13 "Earthquake Simulator Study of a Reinforced Concrete Frame," by P. Hidalgo and R.W. Clough - 1974 (PB 241 944)A13

EERC 74-14 "Nonlinear Earthquake Response of Concrete Gravity Dams," by N. Pal - 1974 (AD/A 006 583)A06

EERC 74-15 "Modeling and Identification in Nonlinear Structural Dynamics - I. One Degree of Freedom Models," by N. Distefano and A. Rath - 1974 (PB 241 548)A06

EERC 75-1 "Determination of Seismic Design Criteria for the Dumbarton Bridge Replacement Structure, Vol. I: Description, Theory and Analytical Modeling of Bridge and Parameters," by F. Baron and S.-H. Pang - 1975 (PB 259 407)A15

EERC 75-2 "Determination of Seismic Design Criteria for the Dumbarton Bridge Replacement Structure, Vol. II: Numerical Studies and Establishment of Seismic Design Criteria," by F. Baron and S.-H. Pang - 1975 (PB 259 408)A11 (For set of EERC 75-1 and 75-2 (PB 259 406) A25)NA

EERC 75-3 "Seismic Risk Analysis for a Site and a Metropolitan Area," by C.S. Oliveira - 1975 (PB 248 134)A09

EERC 75-4 "Analytical Investigations of Seismic Response of Short, Single or Multiple-Span Highway Bridges," by M.-C. Chen and J. Penzien - 1975 (PB 241 454)A09

EERC 75-5 "An Evaluation of Some Methods for Predicting Seismic Behavior of Reinforced Concrete Buildings," by S.A. Mahin and V.V. Bertero - 1975 (PB 246 306)A16

EERC 75-6 "Earthquake Simulator Study of a Steel Frame Structure, Vol. I: Experimental Results," by R.W. Clough and D.T. Tang - 1975 (PB 243 981)A13

EERC 75-7 "Dynamic Properties of San Bernardino Intake Tower," by D. Rea, C.-Y. Liaw and A.K. Chopra - 1975 (AD/A008 406) A05

EERC 75-8 "Seismic Studies of the Articulation for the Dumbarton Bridge Replacement Structure, Vol. I: Description, Theory and Analytical Modeling of Bridge Components," by F. Baron and R.E. Hamati - 1975 (PB 251 539)A07

EERC 75-9 "Seismic Studies of the Articulation for the Dumbarton Bridge Replacement Structure, Vol. 2: Numerical Studies of Steel and Concrete Girder Alternates," by F. Baron and R.E. Hamati - 1975 (PB 251 540)A10

EERC 75-10 "Static and Dynamic Analysis of Nonlinear Structures," by D.P. Mondkar and G.H. Powell - 1975 (PB 242 434)A08

EERC 75-11 "Hysteretic Behavior of Steel Columns," by E.P. Popov, V.V. Bertero and S. Chandramouli - 1975 (PB 252 365)A11

EERC 75-12 "Earthquake Engineering Research Center Library Printed Catalog," - 1975 (PB 243 711)A26

EERC 75-13 "Three Dimensional Analysis of Building Systems (Extended Version)," by E.L. Wilson, J.P. Hollings and H.H. Dovey - 1975 (PB 243 989)A07

EERC 75-14 "Determination of Soil Liquefaction Characteristics by Large-Scale Laboratory Tests," by P. De Alba, C.K. Chan and H.B. Seed - 1975 (NUREG 0027)A08

EERC 75-15 "A Literature Survey - Compressive, Tensile, Bond and Shear Strength of Masonry," by R.L. Mayes and R.W. Clough - 1975 (PB 246 292)A10

EERC 75-16 "Hysteretic Behavior of Ductile Moment Resisting Reinforced Concrete Frame Components," by V.V. Bertero and E.P. Popov - 1975 (PB 246 388)A05

EERC 75-17 "Relationships Between Maximum Acceleration, Maximum Velocity, Distance from Source, Local Site Conditions for Moderately Strong Earthquakes," by H.B. Seed, R. Murarka, J. Lysmer and I.M. Idriss - 1975 (PB 248 172)A03

EERC 75-18 "The Effects of Method of Sample Preparation on the Cyclic Stress-Strain Behavior of Sands," by J. Mulilis, C.K. Chan and H.B. Seed - 1975 (Summarized in EERC 75-28)

EERC 75-19 "The Seismic Behavior of Critical Regions of Reinforced Concrete Components as Influenced by Moment, Shear and Axial Force," by M.B. Atalay and J. Penzien - 1975 (PB 258 842)A11

EERC 75-20 "Dynamic Properties of an Eleven Story Masonry Building," by R.M. Stephen, J.P. Hollings, J.G. Bouwkamp and D. Jurukovski - 1975 (PB 246 945)A04

EERC 75-21 "State-of-the-Art in Seismic Strength of Masonry - An Evaluation and Review," by R.L. Mayes and R.W. Clough 1975 (PB 249 040)A07

EERC 75-22 "Frequency Dependent Stiffness Matrices for Viscoelastic Half-Plane Foundations," by A.K. Chopra, P. Chakrabarti and G. Dasgupta - 1975 (PB 248 121)A07

EERC 75-23 "Hysteretic Behavior of Reinforced Concrete Framed Walls," by T.Y. Wang, V.V. Bertero and E.P. Popov - 1975 (PB 267 298)A17

EERC 75-24 Unassigned

EERC 75-25 "Influence of Seismic History on the Liquefaction Characteristics of Sands," by H.B. Seed, K. Mori and C.K. Chan - 1975 (Summarized in EERC 75-28)

EERC 75-26 "The Generation and Dissipation of Pore Water Pressures during Soil Liquefaction," by H.B. Seed, P.P. Martin and J. Lysmer - 1975 (PB 252 648)A03

EERC 75-27 "Identification of Research Needs for Improving Aseismic Design of Building Structures," by V.V. Bertero 1975 (PB 248 136)A05

EERC 75-28 "Evaluation of Soil Liquefaction Potential during Earthquakes," by H.B. Seed, I. Arango and C.K. Chan - 1975 (NUREG 0026)A13

EERC 75-29 "Representation of Irregular Stress Time Histories by Equivalent Uniform Stress Series in Liquefaction Analyses," by H.B. Seed, I.M. Idriss, F. Makdisi and N. Banerjee - 1975 (PB 252 635)A03

EERC 75-30 "FLUSH - A Computer Program for Approximate 3-D Analysis of Soil-Structure Interaction Problems," by J. Lysmer, T. Udaka, C.-F. Tsai and H. B. Seed - 1975 (PB 259 332)A07

EERC 75-31 Unassigned

EERC 75-32 Unassigned

EERC 75-33 "Predicting the Performance of Structures in Regions of High Seismicity," by J. Penzien - 1975 (PB 248 130)A03

EERC 75-34 "Efficient Finite Element Analysis of Seismic Structure - Soil - Direction," by J. Lysmer, H.B. Seed, T. Udaka, R.N. Hwang and C.-F. Tsai - 1975 (PB 253 570)A03

EERC 75-35 "The Dynamic Behavior of a First Story Girder of a Three-Story Steel Frame Subjected to Earthquake Loading," by R.W. Clough and L.-Y. Li - 1975 (PB 248 841)A05

EERC 75-36 "Earthquake Simulator Study of a Steel Frame Structure, Volume II - Analytical Results," by D.T. Tang - 1975 (PB 252 926)A10

EERC 75-37 "ANSR-I General Purpose Computer Program for Analysis of Non-Linear Structural Response," by D.P. Mondkar and G.H. Powell - 1975 (PB 252 386)A08

EERC 75-38 "Nonlinear Response Spectra for Probabilistic Seismic Design and Damage Assessment of Reinforced Concrete Structures," by M. Murakami and J. Penzien - 1975 (PB 259 530)A05

EERC 75-39 "Study of a Method of Feasible Directions for Optimal Elastic Design of Frame Structures Subjected to Earthquake Loading," by N.D. Walker and K.S. Pister - 1975 (PB 257 781)A06

EERC 75-40 "An Alternative Representation of the Elastic-Viscoelastic Analogy," by G. Dasgupta and J.L. Sackman - 1975 (PB 252 173)A03

EERC 75-41 "Effect of Multi-Directional Shaking on Liquefaction of Sands," by H.B. Seed, R. Pyke and G.R. Martin - 1975 (PB 258 781)A03

EERC 76-1 "Strength and Ductility Evaluation of Existing Low-Rise Reinforced Concrete Buildings - Screening Method," by T. Okada and B. Bresler - 1976 (PB 257 906)A11

EERC 76-2 "Experimental and Analytical Studies on the Hysteretic Behavior of Reinforced Concrete Rectangular and T-Beams," by S.-Y.M. Ma, E.P. Popov and V.V. Bertero - 1976 (PB 260 843)A12

EERC 76-3 "Dynamic Behavior of a Multistory Triangular-Shaped Building," by J. Petrovski, R.M. Stephen, E. Gartenbaum and J.G. Bouwkamp - 1976 (PB 273 279)A07

EERC 76-4 "Earthquake Induced Deformations of Earth Dams," by N. Serff, H.B. Seed, F.I. Makdisi & C.-Y. Chang - 1976 (PB 292 065)A08

EERC 76-5 "Analysis and Design of Tube-Type Tall Building Structures," by H. de Clercq and G.H. Powell - 1976 (PB 252 220) A10

EERC 76-6 "Time and Frequency Domain Analysis of Three-Dimensional Ground Motions, San Fernando Earthquake," by T. Kubo and J. Penzien (PB 260 556)A11

EERC 76-7 "Expected Performance of Uniform Building Code Design Masonry Structures," by R.L. Mayes, Y. Omote, S.W. Chen and R.W. Clough - 1976 (PB 270 098)A05

EERC 76-8 "Cyclic Shear Tests of Masonry Piers, Volume 1 - Test Results," by R.L. Mayes, Y. Omote, R.W. Clough - 1976 (PB 264 424)A06

EERC 76-9 "A Substructure Method for Earthquake Analysis of Structure - Soil Interaction," by J.A. Gutierrez and A.K. Chopra - 1976 (PB 257 783)A08

EERC 76-10 "Stabilization of Potentially Liquefiable Sand Deposits using Gravel Drain Systems," by H.B. Seed and J.R. Booker - 1976 (PB 258 820)A04

EERC 76-11 "Influence of Design and Analysis Assumptions on Computed Inelastic Response of Moderately Tall Frames," by G.H. Powell and D.G. Row - 1976 (PB 271 409)A06

EERC 76-12 "Sensitivity Analysis for Hysteretic Dynamic Systems: Theory and Applications," by D. Ray, K.S. Pister and E. Polak - 1976 (PB 262 859)A04

EERC 76-13 "Coupled Lateral Torsional Response of Buildings to Ground Shaking," by C.L. Kan and A.K. Chopra - 1976 (PB 257 907)A09

EERC 76-14 Unassigned

EERC 76-15 "Reinforced Concrete Frame 2: Seismic Testing and Analytical Correlation," by R.W. Clough and J. Gidwani - 1976 (PB 261 323)A08

EERC 76-16 "Cyclic Shear Tests of Masonry Piers, Volume 2 - Analysis of Test Results," by R.L. Mayes, Y. Omote and R.W. Clough - 1976 (PB 297 158)A05

EERC 76-17 "Structural Steel Bracing Systems: Behavior Under Cyclic Loading," by E.P. Popov, K. Takanashi and C.W. Roeder - 1976 (PB 260 715)A05

EERC 76-18 "Experimental Model Studies on Seismic Response of High Curved Overcrossings," by D. Williams and W.G. Godden - 1976 (PB 269 548)A08

EERC 76-19 "Effects of Non-Uniform Seismic Disturbances on the Dumbarton Bridge Replacement Structure," by F. Baron and R.E. Hamati - 1976 (PB 282 981)A16

EERC 76-20 "Investigation of the Inelastic Characteristics of a Single Story Steel Structure Using System Identification and Shaking Table Experiments," by V.C. Matzen and H.D. McNiven - 1976 (PB 258 453)A07

EERC 76-21 "Capacity of Columns with Splice Imperfections," by E.P. Popov, R.M. Stephen and R. Philbrick - 1976 (PB 260 378)A04

EERC 76-22 "Response of the Olive View Hospital Main Building during the San Fernando Earthquake," by S. A. Mahin, V.V. Bertero, A.K. Chopra and R. Collins - 1976 (PB 271 425)A14

EERC 76-23 "A Study on the Major Factors Influencing the Strength of Masonry Prisms," by N.M. Mostaghel, R.L. Mayes, R. W. Clough and S.W. Chen - 1976 (Not published)

EERC 76-24 "GADFLEA - A Computer Program for the Analysis of Pore Pressure Generation and Dissipation during Cyclic or Earthquake Loading," by J.R. Booker, M.S. Rahman and H.B. Seed - 1976 (PB 263 947)A04

EERC 76-25 Unassigned

EERC 76-26 "Correlative Investigations on Theoretical and Experimental Dynamic Behavior of a Model Bridge Structure," by K. Kawashima and J. Penzien - 1976 (PB 263 388)A11

EERC 76-27 "Earthquake Response of Coupled Shear Wall Buildings," by T. Srichatrapimuk - 1976 (PB 265 157)A07

EERC 76-28 "Tensile Capacity of Partial Penetration Welds," by E.P. Popov and R.M. Stephen - 1976 (PB 262 899)A03

EERC 76-29 "Analysis and Design of Numerical Integration Methods in Structural Dynamics," by H.M. Hilber - 1976 (PB 264 410)A06

EERC 76-30 "Contribution of a Floor System to the Dynamic Characteristics of Reinforced Concrete Buildings," by L.E. Malik and V.V. Bertero - 1976 (PB 272 247)A13

EERC 76-31 "The Effects of Seismic Disturbances on the Golden Gate Bridge," by F. Baron, M. Arikan and R.E. Hamati - 1976 (PB 272 279)A09

EERC 76-32 "Infilled Frames in Earthquake Resistant Construction," by R.E. Klingner and V.V. Bertero - 1976 (PB 265 892)A13

UCB/EERC-77/01 "PLUSH - A Computer Program for Probabilistic Finite Element Analysis of Seismic Soil-Structure Interaction," by M.P. Romo Organista, J. Lysmer and H.B. Seed - 1977 (PB81 177 651)A05

UCB/EERC-77/02 "Soil-Structure Interaction Effects at the Humboldt Bay Power Plant in the Ferndale Earthquake of June 7, 1975," by J.E. Valera, H.B. Seed, C.F. Tsai and J. Lysmer - 1977 (PB 265 795)A04

UCB/EERC-77/03 "Influence of Sample Disturbance on Sand Response to Cyclic Loading," by K. Mori, H.B. Seed and C.K. Chan - 1977 (PB 267 352)A04

UCB/EERC-77/04 "Seismological Studies of Strong Motion Records," by J. Shoja-Taheri - 1977 (PB 269 655)A10

UCB/EERC-77/05 Unassigned

UCB/EERC-77/06 "Developing Methodologies for Evaluating the Earthquake Safety of Existing Buildings," by No. 1 - B. Bresler; No. 2 - B. Bresler, T. Okada and D. Zisling; No. 3 - T. Okada and B. Bresler; No. 4 - V.V. Bertero and B. Bresler - 1977 (PB 267 354)A08

UCB/EERC-77/07 "A Literature Survey - Transverse Strength of Masonry Walls," by Y. Omote, R.L. Mayes, S.W. Chen and R.W. Clough - 1977 (PB 277 933)A07

UCB/EERC-77/08 "DRAIN-TABS: A Computer Program for Inelastic Earthquake Response of Three Dimensional Buildings," by R. Guendelman-Israel and G.H. Powell - 1977 (PB 270 693)A07

UCB/EERC-77/09 "SUBWALL: A Special Purpose Finite Element Computer Program for Practical Elastic Analysis and Design of Structural Walls with Substructure Option," by D.Q. Le, H. Peterson and E.P. Popov - 1977 (PB 270 567)A05

UCB/EERC-77/10 "Experimental Evaluation of Seismic Design Methods for Broad Cylindrical Tanks," by D.P. Clough (PB 272 280)A13

UCB/EERC-77/11 "Earthquake Engineering Research at Berkeley - 1976," - 1977 (PB 273 507)A09

UCB/EERC-77/12 "Automated Design of Earthquake Resistant Multistory Steel Building Frames," by N.D. Walker, Jr. - 1977 (PB 276 526)A09

UCB/EERC-77/13 "Concrete Confined by Rectangular Hoops Subjected to Axial Loads," by J. Vallenas, V.V. Bertero and E.P. Popov - 1977 (PB 275 165)A06

UCB/EERC-77/14 "Seismic Strain Induced in the Ground During Earthquakes," by Y. Sugimura - 1977 (PB 284 201)A04

UCB/EERC-77/15 Unassigned

UCB/EERC-77/16 "Computer Aided Optimum Design of Ductile Reinforced Concrete Moment Resisting Frames," by S.W. Zagajeski and V.V. Bertero - 1977 (PB 280 137)A07

UCB/EERC-77/17 "Earthquake Simulation Testing of a Stepping Frame with Energy-Absorbing Devices," by J.M. Kelly and D.F. Tsztoo - 1977 (PB 273 506)A04

UCB/EERC-77/18 "Inelastic Behavior of Eccentrically Braced Steel Frames under Cyclic Loadings," by C.W. Roeder and E.P. Popov - 1977 (PB 275 526)A15

UCB/EERC-77/19 "A Simplified Procedure for Estimating Earthquake-Induced Deformations in Dams and Embankments," by F.I. Makdisi and H.B. Seed - 1977 (PB 276 820)A04

UCB/EERC-77/20 "The Performance of Earth Dams during Earthquakes," by H.B. Seed, F.I. Makdisi and P. de Alba - 1977 (PB 276 821)A04

UCB/EERC-77/21 "Dynamic Plastic Analysis Using Stress Resultant Finite Element Formulation," by P. Lukkunapvasit and J.M. Kelly - 1977 (PB 275 453)A04

UCB/EERC-77/22 "Preliminary Experimental Study of Seismic Uplift of a Steel Frame," by R.W. Clough and A.A. Huckelbridge 1977 (PB 278 769)A08

UCB/EERC-77/23 "Earthquake Simulator Tests of a Nine-Story Steel Frame with Columns Allowed to Uplift," by A.A. Huckelbridge - 1977 (PB 277 944)A09

UCB/EERC-77/24 "Nonlinear Soil-Structure Interaction of Skew Highway Bridges," by M.-C. Chen and J. Penzien - 1977 (PB 276 176)A07

UCB/EERC-77/25 "Seismic Analysis of an Offshore Structure Supported on Pile Foundations," by D.D.-N. Liou and J. Penzien 1977 (PB 283 180)A06

UCB/EERC-77/26 "Dynamic Stiffness Matrices for Homogeneous Viscoelastic Half-Planes," by G. Dasgupta and A.K. Chopra - 1977 (PB 279 654)A06

UCB/EERC-77/27 "A Practical Soft Story Earthquake Isolation System," by J.M. Kelly, J.M. Eidinger and C.J. Derham - 1977 (PB 276 814)A07

UCB/EERC-77/28 "Seismic Safety of Existing Buildings and Incentives for Hazard Mitigation in San Francisco: An Exploratory Study," by A.J. Meltsner - 1977 (PB 281 970)A05

UCB/EERC-77/29 "Dynamic Analysis of Electrohydraulic Shaking Tables," by D. Rea, S. Abedi-Hayati and Y. Takahashi 1977 (PB 282 569)A04

UCB/EERC-77/30 "An Approach for Improving Seismic - Resistant Behavior of Reinforced Concrete Interior Joints," by B. Galunic, V.V. Bertero and E.P. Popov - 1977 (PB 290 870)A06

UCB/EERC-78/01 "The Development of Energy-Absorbing Devices for Aseismic Base Isolation Systems," by J.M. Kelly and D.F. Tsztoo - 1978 (PB 284 978)A04

UCB/EERC-78/02 "Effect of Tensile Prestrain on the Cyclic Response of Structural Steel Connections, by J.G. Bouwkamp and A. Mukhopadhyay - 1978

UCB/EERC-78/03 "Experimental Results of an Earthquake Isolation System using Natural Rubber Bearings," by J.M. Eidinger and J.M. Kelly - 1978 (PB 281 686)A04

UCB/EERC-78/04 "Seismic Behavior of Tall Liquid Storage Tanks," by A. Niwa - 1978 (PB 284 017)A14

UCB/EERC-78/05 "Hysteretic Behavior of Reinforced Concrete Columns Subjected to High Axial and Cyclic Shear Forces," by S.W. Zagajeski, V.V. Bertero and J.G. Bouwkamp - 1978 (PB 283 858)A13

UCB/EERC-78/06 "Three Dimensional Inelastic Frame Elements for the ANSR-I Program," by A. Riahi, D.G. Row and G.H. Powell - 1978 (PB 295 755)A04

UCB/EERC-78/07 "Studies of Structural Response to Earthquake Ground Motion," by O.A. Lopez and A.K. Chopra - 1978 (PB 282 790)A05

UCB/EERC-78/08 "A Laboratory Study of the Fluid-Structure Interaction of Submerged Tanks and Caissons in Earthquakes," by R.C. Byrd - 1978 (PB 284 957)A08

UCB/EERC-78/09 Unassigned

UCB/EERC-78/10 "Seismic Performance of Nonstructural and Secondary Structural Elements," by I. Sakamoto - 1978 (PB81 154 593)A05

UCB/EERC-78/11 "Mathematical Modelling of Hysteresis Loops for Reinforced Concrete Columns," by S. Nakata, T. Sproul and J. Penzien - 1978 (PB 298 274)A05

UCB/EERC-78/12 "Damageability in Existing Buildings," by T. Blejwas and B. Bresler - 1978 (PB 80 166 978)A05

UCB/EERC-78/13 "Dynamic Behavior of a Pedestal Base Multistory Building," by R.M. Stephen, E.L. Wilson, J.G. Bouwkamp and M. Button - 1978 (PB 286 650)A08

UCB/EERC-78/14 "Seismic Response of Bridges - Case Studies," by R.A. Imbsen, V. Nutt and J. Penzien - 1978 (PB 286 503)A10

UCB/EERC-78/15 "A Substructure Technique for Nonlinear Static and Dynamic Analysis," by D.G. Row and G.H. Powell - 1978 (PB 288 077)A10

UCB/EERC-78/16 "Seismic Risk Studies for San Francisco and for the Greater San Francisco Bay Area," by C.S. Oliveira - 1978 (PB 81 120 115)A07

UCB/EERC-78/17 "Strength of Timber Roof Connections Subjected to Cyclic Loads," by P. Gülkan, R.L. Mayes and R.W. Clough - 1978 (HUD-000 1491)A07

UCB/EERC-78/18 "Response of K-Braced Steel Frame Models to Lateral Loads," by J.G. Bouwkamp, R.M. Stephen and E.P. Popov - 1978

UCB/EERC-78/19 "Rational Design Methods for Light Equipment in Structures Subjected to Ground Motion," by J.L. Sackman and J.M. Kelly - 1978 (PB 292 357)A04

UCB/EERC-78/20 "Testing of a Wind Restraint for Aseismic Base Isolation," by J.M. Kelly and D.E. Chitty - 1978 (PB 292 833)A03

UCB/EERC-78/21 "APOLLO - A Computer Program for the Analysis of Pore Pressure Generation and Dissipation in Horizontal Sand Layers During Cyclic or Earthquake Loading," by P.P. Martin and H.B. Seed - 1978 (PB 292 835)A04

UCB/EERC-78/22 "Optimal Design of an Earthquake Isolation System," by M.A. Bhatti, K.S. Pister and E. Polak - 1978 (PB 294 735)A06

UCB/EERC-78/23 "MASH - A Computer Program for the Non-Linear Analysis of Vertically Propagating Shear Waves in Horizontally Layered Deposits," by P.P. Martin and H.B. Seed - 1978 (PB 293 101)A05

UCB/EERC-78/24 "Investigation of the Elastic Characteristics of a Three Story Steel Frame Using System Identification," by I. Kaya and H.D. McNiven - 1978 (PB 296 225)A06

UCB/EERC-78/25 "Investigation of the Nonlinear Characteristics of a Three-Story Steel Frame Using System Identification," by I. Kaya and H.D. McNiven - 1978 (PB 301 363)A05

UCB/EERC-78/26 "Studies of Strong Ground Motion in Taiwan," by Y.M. Hsiung, B.A. Bolt and J. Penzien - 1978 (PB 298 436)A06

UCB/EERC-78/27 "Cyclic Loading Tests of Masonry Single Piers: Volume 1 - Height to Width Ratio of 2," by P.A. Hidalgo, R.L. Mayes, H.D. McNiven and R.W. Clough - 1978 (PB 296 211)A07

UCB/EERC-78/28 "Cyclic Loading Tests of Masonry Single Piers: Volume 2 - Height to Width Ratio of 1," by S.-W.J. Chen, P.A. Hidalgo, R.L. Mayes, R.W. Clough and H.D. McNiven - 1978 (PB 296 212)A09

UCB/EERC-78/29 "Analytical Procedures in Soil Dynamics," by J. Lysmer - 1978 (PB 298 445)A06

UCB/EERC-79/01 "Hysteretic Behavior of Lightweight Reinforced Concrete Beam-Column Subassemblages," by B. Forzani, E.P. Popov and V.V. Bertero - April 1979(PB 298 267)A06

UCB/EERC-79/02 "The Development of a Mathematical Model to Predict the Flexural Response of Reinforced Concrete Beams to Cyclic Loads, Using System Identification," by J. Stanton & H. McNiven - Jan. 1979(PB 295 875)A10

UCB/EERC-79/03 "Linear and Nonlinear Earthquake Response of Simple Torsionally Coupled Systems," by C.L. Kan and A.K. Chopra - Feb. 1979(PB 298 262)A06

UCB/EERC-79/04 "A Mathematical Model of Masonry for Predicting its Linear Seismic Response Characteristics," by Y. Mengi and H.D. McNiven - Feb. 1979(PB 298 266)A06

UCB/EERC-79/05 "Mechanical Behavior of Lightweight Concrete Confined by Different Types of Lateral Reinforcement," by M.A. Manrique, V.V. Bertero and E.P. Popov - May 1979(PB 301 114)A06

UCB/EERC-79/06 "Static Tilt Tests of a Tall Cylindrical Liquid Storage Tank," by R.W. Clough and A. Niwa - Feb. 1979 (PB 301 167)A06

UCB/EERC-79/07 "The Design of Steel Energy Absorbing Restrainers and Their Incorporation into Nuclear Power Plants for Enhanced Safety: Volume 1 - Summary Report," by P.N. Spencer, V.F. Zackay, and E.R. Parker - Feb. 1979(UCB/EERC-79/07)A09

UCB/EERC-79/08 "The Design of Steel Energy Absorbing Restrainers and Their Incorporation into Nuclear Power Plants for Enhanced Safety: Volume 2 - The Development of Analyses for Reactor System Piping,""Simple Systems" by M.C. Lee, J. Penzien, A.K. Chopra and K, Suzuki "Complex Systems" by G.H. Powell, E.L. Wilson, R.W. Clough and D.G. Row - Feb. 1979(UCB/EERC-79/08)A10

UCB/EERC-79/09 "The Design of Steel Energy Absorbing Restrainers and Their Incorporation into Nuclear Power Plants for Enhanced Safety: Volume 3 - Evaluation of Commercial Steels," by W.S. Owen, R.M.N. Pelloux, R.O. Ritchie, M. Faral, T. Ohhashi, J. Toplosky, S.J. Hartman, V.F. Zackay and E.R. Parker - Feb. 1979(UCB/EERC-79/09)A04

UCB/EERC-79/10 "The Design of Steel Energy Absorbing Restrainers and Their Incorporation into Nuclear Power Plants for Enhanced Safety: Volume 4 - A Review of Energy-Absorbing Devices," by J.M. Kelly and M.S. Skinner - Feb. 1979(UCB/EERC-79/10)A04

UCB/EERC-79/11 "Conservatism In Summation Rules for Closely Spaced Modes," by J.M. Kelly and J.L. Sackman - May 1979(PB 301 328)A03

UCB/EERC-79/12 "Cyclic Loading Tests of Masonry Single Piers; Volume 3 - Height to Width Ratio of 0.5," by P.A. Hidalgo, R.L. Mayes, H.D. McNiven and R.W. Clough - May 1979(PB 301 321)A08

UCB/EERC-79/13 "Cyclic Behavior of Dense Course-Grained Materials in Relation to the Seismic Stability of Dams," by N.G. Banerjee, H.B. Seed and C.K. Chan - June 1979(PB 301 373)A13

UCB/EERC-79/14 "Seismic Behavior of Reinforced Concrete Interior Beam-Column Subassemblages," by S. Viwathanatepa, E.P. Popov and V.V. Bertero - June 1979(PB 301 326)A10

UCB/EERC-79/15 "Optimal Design of Localized Nonlinear Systems with Dual Performance Criteria Under Earthquake Excitations," by M.A. Bhatti - July 1979(PB 80 167 109)A06

UCB/EERC-79/16 "OPTDYN - A General Purpose Optimization Program for Problems with or without Dynamic Constraints," by M.A. Bhatti, E. Polak and K.S. Pister - July 1979(PB 80 167 091)A05

UCB/EERC-79/17 "ANSR-II, Analysis of Nonlinear Structural Response, Users Manual," by D.P. Mondkar and G.H. Powell July 1979(PB 80 113 301)A05

UCB/EERC-79/18 "Soil Structure Interaction in Different Seismic Environments," A. Gomez-Masso, J. Lysmer, J.-C. Chen and H.B. Seed - August 1979(PB 80 101 520)A04

UCB/EERC-79/19 "ARMA Models for Earthquake Ground Motions," by M.K. Chang, J.W. Kwiatkowski, R.F. Nau, R.M. Oliver and K.S. Pister - July 1979(PB 301 166)A05

UCB/EERC-79/20 "Hysteretic Behavior of Reinforced Concrete Structural Walls," by J.M. Vallenas, V.V. Bertero and E.P. Popov - August 1979(PB 80 165 905)A12

UCB/EERC-79/21 "Studies on High-Frequency Vibrations of Buildings - 1: The Column Effect," by J. Lubliner - August 1979 (PB 80 158 553)A03

UCB/EERC-79/22 "Effects of Generalized Loadings on Bond Reinforcing Bars Embedded in Confined Concrete Blocks," by S. Viwathanatepa, E.P. Popov and V.V. Bertero - August 1979(PB 81 124 018)A14

UCB/EERC-79/23 "Shaking Table Study of Single-Story Masonry Houses, Volume 1: Test Structures 1 and 2," by P. Gülkan, R.L. Mayes and R.W. Clough - Sept. 1979 (HUD-000 1763)A12

UCB/EERC-79/24 "Shaking Table Study of Single-Story Masonry Houses, Volume 2: Test Structures 3 and 4," by P. Gülkan, R.L. Mayes and R.W. Clough - Sept. 1979 (HUD-000 1836)A12

UCB/EERC-79/25 "Shaking Table Study of Single-Story Masonry Houses, Volume 3: Summary, Conclusions and Recommendations," by R.W. Clough, R.L. Mayes and P. Gülkan - Sept. 1979 (HUD-000 1837)A06

UCB/EERC-79/26 "Recommendations for a U.S.-Japan Cooperative Research Program Utilizing Large-Scale Testing Facilities," by U.S.-Japan Planning Group - Sept. 1979(PB 301 407)A06

UCB/EERC-79/27 "Earthquake-Induced Liquefaction Near Lake Amatitlan, Guatemala," by H.B. Seed, I. Arango, C.K. Chan, A. Gomez-Masso and R. Grant de Ascoli - Sept. 1979(NUREG-CR1341)A03

UCB/EERC-79/28 "Infill Panels: Their Influence on Seismic Response of Buildings," by J.W. Axley and V.V. Bertero Sept. 1979(PB 80 163 371)A10

UCB/EERC-79/29 "3D Truss Bar Element (Type 1) for the ANSR-II Program," by D.P. Mondkar and G.H. Powell - Nov. 1979 (PB 80 169 709)A02

UCB/EERC-79/30 "2D Beam-Column Element (Type 5 - Parallel Element Theory) for the ANSR-II Program," by D.G. Row, G.H. Powell and D.P. Mondkar - Dec. 1979(PB 80 167 224)A03

UCB/EERC-79/31 "3D Beam-Column Element (Type 2 - Parallel Element Theory) for the ANSR-II Program," by A. Riahi, G.H. Powell and D.P. Mondkar - Dec. 1979(PB 80 167 216)A03

UCB/EERC-79/32 "On Response of Structures to Stationary Excitation," by A. Der Kiureghian - Dec. 1979(PB 80166 929)A03

UCB/EERC-79/33 "Undisturbed Sampling and Cyclic Load Testing of Sands," by S. Singh, H.B. Seed and C.K. Chan Dec. 1979(ADA 087 298)A07

UCB/EERC-79/34 "Interaction Effects of Simultaneous Torsional and Compressional Cyclic Loading of Sand," by P.M. Griffin and W.N. Houston - Dec. 1979(ADA 092 352)A15

UCB/EERC-80/01 "Earthquake Response of Concrete Gravity Dams Including Hydrodynamic and Foundation Interaction Effects," by A.K. Chopra, P. Chakrabarti and S. Gupta - Jan. 1980(AD-A087297)A10

UCB/EERC-80/02 "Rocking Response of Rigid Blocks to Earthquakes," by C.S. Yim, A.K. Chopra and J. Penzien - Jan. 1980 (PB80 166 002)A04

UCB/EERC-80/03 "Optimum Inelastic Design of Seismic-Resistant Reinforced Concrete Frame Structures," by S.W. Zagajeski and V.V. Bertero - Jan. 1980(PB80 164 635)A06

UCB/EERC-80/04 "Effects of Amount and Arrangement of Wall-Panel Reinforcement on Hysteretic Behavior of Reinforced Concrete Walls," by R. Iliya and V.V. Bertero - Feb. 1980(PB81 122 525)A09

UCB/EERC-80/05 "Shaking Table Research on Concrete Dam Models," by A. Niwa and R.W. Clough - Sept. 1980(PB81 122 368)A06

UCB/EERC-80/06 "The Design of Steel Energy-Absorbing Restrainers and their Incorporation into Nuclear Power Plants for Enhanced Safety (Vol 1A): Piping with Energy Absorbing Restrainers: Parameter Study on Small Systems," by G.H. Powell, C. Oughourlian and J. Simons - June 1980 (UCB-EERC-80-06)A05

UCB/EERC-80/07 "Inelastic Torsional Response of Structures Subjected to Earthquake Ground Motions," by Y. Yamazaki April 1980(PB81 122 327)A08

UCB/EERC-80/08 "Study of X-Braced Steel Frame Structures Under Earthquake Simulation," by Y. Ghanaat - April 1980 (PB81 122 335)A11

UCB/EERC-80/09 "Hybrid Modelling of Soil-Structure Interaction," by S. Gupta, T.W. Lin, J. Penzien and C.S. Yeh May 1980(PB81 122 319)A07

UCB/EERC-80/10 "General Applicability of a Nonlinear Model of a One Story Steel Frame," by B.I. Sveinsson and H.D. McNiven - May 1980(PB81 124 877)A06

UCB/EERC-80/11 "A Green-Function Method for Wave Interaction with a Submerged Body," by W. Kioka - April 1980 (PB81 122 269)A07

UCB/EERC-80/12 "Hydrodynamic Pressure and Added Mass for Axisymmetric Bodies," by F. Nilrat - May 1980(PB81 122 343)A08

UCB/EERC-80/13 "Treatment of Non-Linear Drag Forces Acting on Offshore Platforms," by B.V. Dao and J. Penzien May 1980(PB81 153 413)A07

UCB/EERC-80/14 "2D Plane/Axisymmetric Solid Element (Type 3 - Elastic or Elastic-Perfectly Plastic) for the ANSR-II Program," by D.P. Mondkar and G.H. Powell - July 1980(PB81 122 350)A03

UCB/EERC-80/15 "A Response Spectrum Method for Random Vibrations," by A. Der Kiureghian - June 1980(PB81 122 301)A03

UCB/EERC-80/16 "Cyclic Inelastic Buckling of Tubular Steel Braces," by V.A. Zayas, E.P. Popov and S.A. Mahin June 1980(PB81 124 885)A10

UCB/EERC-80/17 "Dynamic Response of Simple Arch Dams Including Hydrodynamic Interaction," by C.S. Porter and A.K. Chopra - July 1980(PB81 124 000)A13

UCB/EERC-80/18 "Experimental Testing of a Friction Damped Aseismic Base Isolation System with Fail-Safe Characteristics," by J.M. Kelly, K.E. Beucke and M.S. Skinner - July 1980(PB81 148 595)A04

UCB/EERC-80/19 "The Design of Steel Energy-Absorbing Restrainers and their Incorporation into Nuclear Power Plants for Enhanced Safety (Vol 1B): Stochastic Seismic Analyses of Nuclear Power Plant Structures and Piping Systems Subjected to Multiple Support Excitations," by M.C. Lee and J. Penzien - June 1980 (PB82 201 872)A08

UCB/EERC-80/20 "The Design of Steel Energy-Absorbing Restrainers and their Incorporation into Nuclear Power Plants for Enhanced Safety (Vol 1C): Numerical Method for Dynamic Substructure Analysis," by J.M. Dickens and E.L. Wilson - June 1980 (UCB-EERC-80-20)A10

UCB/EERC-80/21 "The Design of Steel Energy-Absorbing Restrainers and their Incorporation into Nuclear Power Plants for Enhanced Safety (Vol 2): Development and Testing of Restraints for Nuclear Piping Systems," by J.M. Kelly and M.S. Skinner - June 1980 (UCB-EERC-80-21)A05

UCB/EERC-80/22 "3D Solid Element (Type 4-Elastic or Elastic-Perfectly-Plastic) for the ANSR-II Program," by D.P. Mondkar and G.H. Powell - July 1980(PB81 123 242)A03

UCB/EERC-80/23 "Gap-Friction Element (Type 5) for the ANSR-II Program," by D.P. Mondkar and G.H. Powell - July 1980 (PB81 122 285)A03

UCB/EERC-80/24 "U-Bar Restraint Element (Type 11) for the ANSR-II Program," by C. Oughourlian and G.H. Powell July 1980(PB81 122 293)A03

UCB/EERC-80/25 "Testing of a Natural Rubber Base Isolation System by an Explosively Simulated Earthquake," by J.M. Kelly - August 1980(PB81 201 360)A04

UCB/EERC-80/26 "Input Identification from Structural Vibrational Response," by Y. Hu - August 1980(PB81 152 308)A05

UCB/EERC-80/27 "Cyclic Inelastic Behavior of Steel Offshore Structures," by V.A. Zayas, S.A. Mahin and E.P. Popov August 1980(PB81 196 180)A15

UCB/EERC-80/28 "Shaking Table Testing of a Reinforced Concrete Frame with Biaxial Response," by M.G. Oliva October 1980(PB81 154 304)A10

UCB/EERC-80/29 "Dynamic Properties of a Twelve-Story Prefabricated Panel Building," by J.G. Bouwkamp, J.P. Kollegger and R.M. Stephen - October 1980(PB82 117 128)A06

UCB/EERC-80/30 "Dynamic Properties of an Eight-Story Prefabricated Panel Building," by J.G. Bouwkamp, J.P. Kollegger and R.M. Stephen - October 1980(PB81 200 313)A05

UCB/EERC-80/31 "Predictive Dynamic Response of Panel Type Structures Under Earthquakes," by J.P. Kollegger and J.G. Bouwkamp - October 1980(PB81 152 316)A04

UCB/EERC-80/32 "The Design of Steel Energy-Absorbing Restrainers and their Incorporation into Nuclear Power Plants for Enhanced Safety (Vol 3): Testing of Commercial Steels in Low-Cycle Torsional Fatigue," by P. Spencer, E.R. Parker, E. Jongewaard and M. Drory

UCB/EERC-80/33 "The Design of Steel Energy-Absorbing Restrainers and their Incorporation into Nuclear Power Plants for Enhanced Safety (Vol 4): Shaking Table Tests of Piping Systems with Energy-Absorbing Restrainers," by S.F. Stiemer and W.G. Godden - Sept. 1980(PB82 201 880)A05

UCB/EERC-80/34 "The Design of Steel Energy-Absorbing Restrainers and their Incorporation into Nuclear Power Plants for Enhanced Safety (Vol 5): Summary Report," by P. Spencer

UCB/EERC-80/35 "Experimental Testing of an Energy-Absorbing Base Isolation System," by J.M. Kelly, M.S. Skinner and K.E. Beucke - October 1980(PB81 154 072)A04

UCB/EERC-80/36 "Simulating and Analyzing Artificial Non-Stationary Earthquake Ground Motions," by R.F. Nau, R.M. Oliver and K.S. Pister - October 1980(PB81 153 397)A04

UCB/EERC-80/37 "Earthquake Engineering at Berkeley - 1980," - Sept. 1980(PB81 205 874)A09

UCB/EERC-80/38 "Inelastic Seismic Analysis of Large Panel Buildings," by V. Schricker and G.H. Powell - Sept. 1980 (PB81 154 338)A13

UCB/EERC-80/39 "Dynamic Response of Embankment, Concrete-Gravity and Arch Dams Including Hydrodynamic Interaction," by J.F. Hall and A.K. Chopra - October 1980(PB81 152 324)A11

UCB/EERC-80/40 "Inelastic Buckling of Steel Struts Under Cyclic Load Reversal," by R.G. Black, W.A. Wenger and E.P. Popov - October 1980(PB81 154 312)A08

UCB/EERC-80/41 "Influence of Site Characteristics on Building Damage During the October 3, 1974 Lima Earthquake," by P. Repetto, I. Arango and H.B. Seed - Sept. 1980(PB81 161 739)A05

UCB/EERC-80/42 "Evaluation of a Shaking Table Test Program on Response Behavior of a Two Story Reinforced Concrete Frame," by J.M. Blondet, R.W. Clough and S.A. Mahin(PB82 196 544)A11

UCB/EERC-80/43 "Modelling of Soil-Structure Interaction by Finite and Infinite Elements," by F. Medina - December 1980(PB81 229 270)A04

UCB/EERC-81/01 "Control of Seismic Response of Piping Systems and Other Structures by Base Isolation," edited by J.M. Kelly - January 1981 (PB81 200 735)A05

UCB/EERC-81/02 "OPTNSR - An Interactive Software System for Optimal Design of Statically and Dynamically Loaded Structures with Nonlinear Response," by M.A. Bhatti, V. Ciampi and K.S. Pister - January 1981 (PB81 218 851)A09

UCB/EERC-81/03 "Analysis of Local Variations in Free Field Seismic Ground Motions," by J.-C. Chen, J. Lysmer and H.B. Seed - January 1981 (AD-A099508)A13

UCB/EERC-81/04 "Inelastic Structural Modeling of Braced Offshore Platforms for Seismic Loading," by V.A. Zayas, P.-S.B. Shing, S.A. Mahin and E.P. Popov - January 1981(PB82 138 777)A07

UCB/EERC-81/05 "Dynamic Response of Light Equipment in Structures," by A. Der Kiureghian, J.L. Sackman and B. Nour-Omid - April 1981 (PB81 218 497)A04

UCB/EERC-81/06 "Preliminary Experimental Investigation of a Broad Base Liquid Storage Tank," by J.G. Bouwkamp, J.P. Kollegger and R.M. Stephen - May 1981(PB82 140 385)A03

UCB/EERC-81/07 "The Seismic Resistant Design of Reinforced Concrete Coupled Structural Walls," by A.E. Aktan and V.V. Bertero - June 1981(PB82 113 358)A11

UCB/EERC-81/08 "The Undrained Shearing Resistance of Cohesive Soils at Large Deformations," by M.R. Pyles and H.B. Seed - August 1981

UCB/EERC-81/09 "Experimental Behavior of a Spatial Piping System with Steel Energy Absorbers Subjected to a Simulated Differential Seismic Input," by S.F. Stiemer, W.G. Godden and J.M. Kelly - July 1981(PB82 201 898)A04

UCB/EERC-81/10 "Evaluation of Seismic Design Provisions for Masonry in the United States," by B.I. Sveinsson, R.L. Mayes and H.D. McNiven - August 1981 (PB82 166 075)A08

UCB/EERC-81/11 "Two-Dimensional Hybrid Modelling of Soil-Structure Interaction," by T.-J. Tzong, S. Gupta and J. Penzien - August 1981(PB82 142 118)A04

UCB/EERC-81/12 "Studies on Effects of Infills in Seismic Resistant R/C Construction," by S. Brokken and V.V. Bertero - October 1981(PB82 166 190)A09

UCB/EERC-81/13 "Linear Models to Predict the Nonlinear Seismic Behavior of a One-Story Steel Frame," by H. Valdimarsson, A.H. Shah and H.D. McNiven - September 1981(PB82 138 793)A07

UCB/EERC-81/14 "TLUSH: A Computer Program for the Three-Dimensional Dynamic Analysis of Earth Dams," by T. Kagawa, L.H. Mejia, H.B. Seed and J. Lysmer - September 1981(PB82 139 940)A06

UCB/EERC-81/15 "Three Dimensional Dynamic Response Analysis of Earth Dams," by L.H. Mejia and H.B. Seed - September 1981 (PB82 137 274)A12

UCB/EERC-81/16 "Experimental Study of Lead and Elastomeric Dampers for Base Isolation Systems," by J.M. Kelly and S.B. Hodder - October 1981 (PB82 166 182)A05

UCB/EERC-81/17 "The Influence of Base Isolation on the Seismic Response of Light Secondary Equipment," by J.M. Kelly - April 1981 (PB82 255 266)A04

UCB/EERC-81/18 "Studies on Evaluation of Shaking Table Response Analysis Procedures," by J. Marcial Blondet - November 1981 (PB82 197 278)A10

UCB/EERC-81/19 "DELIGHT.STRUCT: A Computer-Aided Design Environment for Structural Engineering," by R.J. Balling, K.S. Pister and E. Polak - December 1981 (PB82 218 496)A07

UCB/EERC-81/20 "Optimal Design of Seismic-Resistant Planar Steel Frames," by R.J. Balling, V. Ciampi, K.S. Pister and E. Polak - December 1981 (PB82 220 179)A07

UCB/EERC-82/01 "Dynamic Behavior of Ground for Seismic Analysis of Lifeline Systems," by T. Sato and A. Der Kiureghian - January 1982 (PB82 218 926)A05

UCB/EERC-82/02 "Shaking Table Tests of a Tubular Steel Frame Model," by Y. Ghanaat and R. W. Clough - January 1982 (PB82 220 161)A07

UCB/EERC-82/03 "Behavior of a Piping System under Seismic Excitation: Experimental Investigations of a Spatial Piping System supported by Mechanical Shock Arrestors and Steel Energy Absorbing Devices under Seismic Excitation," by S. Schneider, H.-M. Lee and W. G. Godden - May 1982 (PB83 172 544)A09

UCB/EERC-82/04 "New Approaches for the Dynamic Analysis of Large Structural Systems," by E. L. Wilson - June 1982 (PB83 148 080)A05

UCB/EERC-82/05 "Model Study of Effects of Damage on the Vibration Properties of Steel Offshore Platforms," by F. Shahrivar and J. G. Bouwkamp - June 1982 (PB83 148 742)A10

UCB/EERC-82/06 "States of the Art and Practice in the Optimum Seismic Design and Analytical Response Prediction of R/C Frame-Wall Structures," by A. E. Aktan and V. V. Bertero - July 1982 (PB83 147 736)A05

UCB/EERC-82/07 "Further Study of the Earthquake Response of a Broad Cylindrical Liquid-Storage Tank Model," by G. C. Manos and R. W. Clough - July 1982 (PB83 147 744)A11

UCB/EERC-82/08 "An Evaluation of the Design and Analytical Seismic Response of a Seven Story Reinforced Concrete Frame - Wall Structure," by F. A. Charney and V. V. Bertero - July 1982(PB83 157 628)A09

UCB/EERC-82/09 "Fluid-Structure Interactions: Added Mass Computations for Incompressible Fluid," by J. S.-H. Kuo - August 1982 (PB83 156 281)A07

UCB/EERC-82/10 "Joint-Opening Nonlinear Mechanism: Interface Smeared Crack Model," by J. S.-H. Kuo - August 1982 (PB83 149 195)A05

UCB/EERC-82/11 "Dynamic Response Analysis of Techi Dam," by R. W. Clough, R. M. Stephen and J. S.-H. Kuo - August 1982 (PB83 147 496)A06

UCB/EERC-82/12 "Prediction of the Seismic Responses of R/C Frame-Coupled Wall Structures," by A. E. Aktan, V. V. Bertero and M. Piazza - August 1982 (PB83 149 203)A09

UCB/EERC-82/13 "Preliminary Report on the SMART 1 Strong Motion Array in Taiwan," by B. A. Bolt, C. H. Loh, J. Penzien, Y. B. Tsai and Y. T. Yeh - August 1982 (PB83 159 400)A10

UCB/EERC-82/14 "Shaking-Table Studies of an Eccentrically X-Braced Steel Structure," by M. S. Yang - September 1982 (PB83 260 778)A12

UCB/EERC-82/15 "The Performance of Stairways in Earthquakes," by C. Roha, J. W. Axley and V. V. Bertero - September 1982 (PB83 157 693)A07

UCB/EERC-82/16 "The Behavior of Submerged Multiple Bodies in Earthquakes," by W.-G. Liao - Sept. 1982 (PB83 158 709)A07

UCB/EERC-82/17 "Effects of Concrete Types and Loading Conditions on Local Bond-Slip Relationships," by A. D. Cowell, E. P. Popov and V. V. Bertero - September 1982 (PB83 153 577)A04

UCB/EERC-82/18 "Mechanical Behavior of Shear Wall Vertical Boundary Members: An Experimental Investigation," by M. T. Wagner and V. V. Bertero - October 1982 (PB83 159 764)A05

UCB/EERC-82/19 "Experimental Studies of Multi-support Seismic Loading on Piping Systems," by J. M. Kelly and A. D. Cowell - November 1982

UCB/EERC-82/20 "Generalized Plastic Hinge Concepts for 3D Beam-Column Elements," by P. F.-S. Chen and G. H. Powell - November 1982 (PB83 247 981)A13

UCB/EERC-82/21 "ANSR-III: General Purpose Computer Program for Nonlinear Structural Analysis," by C. V. Oughourlian and G. H. Powell - November 1982 (PB83 251 330)A12

UCB/EERC-82/22 "Solution Strategies for Statically Loaded Nonlinear Structures," by J. W. Simons and G. H. Powell - November 1982 (PB83 197 970)A06

UCB/EERC-82/23 "Analytical Model of Deformed Bar Anchorages under Generalized Excitations," by V. Ciampi, R. Eligehausen, V. V. Bertero and E. P. Popov - November 1982 (PB83 169 532)A06

UCB/EERC-82/24 "A Mathematical Model for the Response of Masonry Walls to Dynamic Excitations," by H. Sucuoğlu, Y. Mengi and H. D. McNiven - November 1982 (PB83 169 011)A07

UCB/EERC-82/25 "Earthquake Response Considerations of Broad Liquid Storage Tanks," by F. J. Cambra - November 1982 (PB83 251 215)A09

UCB/EERC-82/26 "Computational Models for Cyclic Plasticity, Rate Dependence and Creep," by B. Mosaddad and G. H. Powell - November 1982 (PB83 245 829)A08

UCB/EERC-82/27 "Inelastic Analysis of Piping and Tubular Structures," by M. Mahasuverachai and G. H. Powell - November 1982 (PB83 249 987)A07

UCB/EERC-83/01 "The Economic Feasibility of Seismic Rehabilitation of Buildings by Base Isolation," by J. M. Kelly - January 1983 (PB83 197 988)A05

UCB/EERC-83/02 "Seismic Moment Connections for Moment-Resisting Steel Frames," by E. P. Popov - January 1983 (PB83 195 412)A04

UCB/EERC-83/03 "Design of Links and Beam-to-Column Connections for Eccentrically Braced Steel Frames," by E. P. Popov and J. O. Malley - January 1983 (PB83 194 811)A04

UCB/EERC-83/04 "Numerical Techniques for the Evaluation of Soil-Structure Interaction Effects in the Time Domain," by E. Bayo and E. L. Wilson - February 1983 (PB83 245 605)A09

UCB/EERC-83/05 "A Transducer for Measuring the Internal Forces in the Columns of a Frame-Wall Reinforced Concrete Structure," by R. Sause and V. V. Bertero - May 1983 (PB84 119 494)A06

UCB/EERC-83/06 "Dynamic Interactions between Floating Ice and Offshore Structures," by P. Croteau - May 1983 (PB84 119 486)A16

UCB/EERC-83/07 "Dynamic Analysis of Multiply Tuned and Arbitrarily Supported Secondary Systems," by T. Igusa and A. Der Kiureghian - June 1983 (PB84 118 272)A11

UCB/EERC-83/08 "A Laboratory Study of Submerged Multi-body Systems in Earthquakes," by G. R. Ansari - June 1983 (PB83 261 842)A17

UCB/EERC-83/09 "Effects of Transient Foundation Uplift on Earthquake Response of Structures," by C.-S. Yim and A. K. Chopra - June 1983 (PB83 261 396)A07

UCB/EERC-83/10 "Optimal Design of Friction-Braced Frames under Seismic Loading," by M. A. Austin and K. S. Pister - June 1983 (PB84 119 288)A06

UCB/EERC-83/11 "Shaking Table Study of Single-Story Masonry Houses: Dynamic Performance under Three Component Seismic Input and Recommendations," by G. C. Manos, R. W. Clough and R. L. Mayes - June 1983

UCB/EERC-83/12 "Experimental Error Propagation in Pseudodynamic Testing," by P. B. Shing and S. A. Mahin - June 1983 (PB84 119 270)A09

UCB/EERC-83/13 "Experimental and Analytical Predictions of the Mechanical Characteristics of a 1/5-scale Model of a 7-story R/C Frame-Wall Building Structure," by A. E. Aktan, V. V. Bertero, A. A. Chowdhury and T. Nagashima - August 1983 (PB84 119 213)A07

UCB/EERC-83/14 "Shaking Table Tests of Large-Panel Precast Concrete Building System Assemblages," by M. G. Oliva and R. W. Clough - August 1983

UCB/EERC-83/15 "Seismic Behavior of Active Beam Links in Eccentrically Braced Frames," by K. D. Hjelmstad and E. P. Popov - July 1983 (PB84 119 676)A09

UCB/EERC-83/16 "System Identification of Structures with Joint Rotation," by J. S. Dimsdale July 1983 (PB84 192 210)A06

UCB/EERC-83/17 "Construction of Inelastic Response Spectra for Single-Degree-of-Freedom Systems," by S. Mahin and J. Lin - July 1983 (PB84 208 834)A05

UCB/EERC-83/18 "Interactive Computer Analysis Methods for Predicting the Inelastic Cyclic Behaviour of Structural Sections," by S. Kaba and S. Mahin - July 1983 (PB84 192 012) A06

UCB/EERC-83/19 "Effects of Bond Deterioration on Hysteretic Behavior of Reinforced Concrete Joints," by F.C. Filippou, E.P. Popov and V.V. Bertero - August 1983 (PB84 192 020) A10

UCB/EERC-83/20 "Analytical and Experimental Correlation of Large-Panel Precast Building System Performance," by M.G. Oliva, R.W. Clough, M. Velkov, P. Gavrilovic and J. Petrovski - November 1983

UCB/EERC-83/21 "Mechanical Characteristics of Materials Used in a 1/5 Scale Model of a 7-Story Reinforced Concrete Test Structure," by V.V. Bertero, A.E. Aktan, H.G. Harris and A.A. Chowdhury - September 1983 (PB84 193 697) A05

UCB/EERC-83/22 "Hybrid Modelling of Soil-Structure Interaction in Layered Media," by T.-J. Tzong and J. Penzien - October 1983 (PB84 192 178) A08

UCB/EERC-83/23 "Local Bond Stress-Slip Relationships of Deformed Bars under Generalized Excitations," by R. Eligehausen, E.P. Popov and V.V. Bertero - October 1983 (PB84 192 848) A09

UCB/EERC-83/24 "Design Considerations for Shear Links in Eccentrically Braced Frames," by J.O. Malley and E.P. Popov - November 1983 (PB84 192 186) A07

UCB/EERC-84/01 "Pseudodynamic Test Method for Seismic Performance Evaluation: Theory and Implementation," by P.-S. B. Shing and S. A. Mahin - January 1984 (PB84 190 644) A08

UCB/EERC-84/02 "Dynamic Response Behavior of Xiang Hong Dian Dam," by R.W. Clough, K.-T. Chang, H.-Q. Chen, R.M. Stephen, G.-L. Wang, and Y. Ghanaat - April 1984

UCB/EERC-84/03 "Refined Modelling of Reinforced Concrete Columns for Seismic Analysis," by S.A. Kaba and S.A. Mahin - April, 1984

UCB/EERC-84/04 "A New Floor Response Spectrum Method for Seismic Analysis of Multiply Supported Secondary Systems," by A. Asfura and A. Der Kiureghian - June 1984

UCB/EERC-84/05 "Earthquake Simulation Test and Associated Studies of a 1/5th-scale Model of a 7-Story R/C Frame-Wall Test Structure," by V.V. Bertero, A.E. Aktan, F.A. Charney and R. Sause - June 1984

UCB/EERC-84/06 "R/C Structural Walls: Seismic Design for Shear," by A.E. Aktan and V.V. Bertero

UCB/EERC-84/07 "Behavior of Interior and Exterior Flat-Plate Connections subjected to Inelastic Load Reversals," by H.L. Zee and J.P. Moehle

UCB/EERC-84/08 "Experimental Study of the Seismic Behavior of a two-story Flat-Plate Structure," by J.W. Diebold and J.P. Moehle

UCB/EERC-84/09 "Phenonomenological Modeling of Steel Braces under Cyclic Loading," by K. Ikeda, S. A. Mahin and S. N. Dermitzakis

UCB/EERC-84/10 "A Refined Physical Theory Model for Predicting the Seismic Behavior of Braced Steel Frames," by K. Ikeda and S. A. Mahin

UCB/EERC-84/11 "Earthquake Analysis and Response of Concrete Gravity Dams," by G. Fenves and A. Chopra

UCB/EERC-84/12 "EAGD-84: A Computer Program for Earthquake Analysis of Concrete Gravity Dams," by G. Fenves and A. Chopra

UCB/EERC-84/13 "Earthquake Engineering Research at Berkeley - 1984"